

F. W. Klaiber T. J. Wipf K. F. Dunker R. B. Abu-Kishk S. M. Planck

Alternate Methods of Bridge Strengthening

Part 1: Providing Partial End Restraint

Part 2: Post-Compression of Stringers

Sponsored by the Iowa Department of Transportation,
Highway Division, and the Iowa Highway Research Board

February 1989

Iowa DOT Project HR-302
ISU-ERI-Ames-89262



report

College of
Engineering
Iowa State University

The opinions, findings, and conclusions expressed in this publication are those of the authors and not necessarily those of the Highway Division of the Iowa Department of Transportation.

F. W. Klaiber T. J. Wipf K. F. Dunker R. B. Abu-Kishk S. M. Plonck

Alternate Methods of Bridge Strengthening

Part 1: Providing Partial End Restraint

Part 2: Post-Compression of Stringers

Sponsored by the Iowa Department of Transportation,
Highway Division, and the Iowa Highway Research Board

February 1989

Iowa DOT Project HR-302
ISU-ERI-Ames-89262



engineering
research institute
iowa state university

TABLE OF CONTENTS

	<u>Page</u>
ACKNOWLEDGMENTS	1
ABSTRACT	3
GENERAL INTRODUCTION	5
Strengthening Technique 1: Providing Partial End Restraint	7
Strengthening Technique 2: Post-Compression of Stringers	7
Structure of the Report	8
PART 1: PROVIDING PARTIAL END RESTRAINT	13
(Full Table of Contents appears on page 15)	
PART 2: POST-COMPRESSION OF STRINGERS	171
(Full Table of Contents appears on page 173)	

ACKNOWLEDGMENTS

The study presented in this report was conducted by the Bridge Engineering Center under the auspices of the Engineering Research Institute of Iowa State University. The research was sponsored by the Highway Division, Iowa Department of Transportation, and the Iowa Highway Research Board under Research Project HR-302.

The authors extend sincere appreciation to the engineers of the Iowa DOT for their support, cooperation, and counseling. A special thanks is extended to William A. Lundquist, Bridge Engineer, and John P. Harkin, Chief Structural Engineer.

Special thanks are accorded Douglas L. Wood, Structures Laboratory supervisor; graduate students William E. Wiley and Lam H. Ng; and undergraduates Jeff A. Bales, Bret M. Farmer, Gerald C. Franklin, Robert J. Freiburger, Mamta Israni, Darin N. Johnson, Deborah M. McAuley, and Chris D. Maskrey for their contributions to the project.

ABSTRACT

The need for upgrading a large number of understrength and obsolete bridges in the United States has been well documented in the literature. Through the performance of several Iowa DOT projects, the concept of strengthening bridges (simple and continuous spans) by post-tensioning has been developed. The purpose of this project was to investigate two additional strengthening alternatives that may be more efficient than post-tensioning in certain situations. The research program for each strengthening scheme included a literature review, laboratory testing of the strengthening scheme, and a finite-element analysis of the scheme. For clarity the two strengthening schemes are presented separately in the following paragraphs.

In Part 1 of this report, the strengthening of existing steel stringers in composite steel-beam concrete-deck bridges by providing partial end restraint was shown to be feasible. Various degrees of end restraint were investigated on a full-scale bridge stringer as well as on an existing 1/3-scale bridge model. By varying the amount of restraint, different amounts of strain reduction can be obtained. The finite-element analysis developed for verification of the experimental results can be used in determining the degree and location of end restraint required to strengthen a particular bridge.

Part 2 of this report summarizes the research that was undertaken to strengthen the negative moment regions of continuous, composite bridges. Two schemes were investigated: post-compression of stringers and superimposed trusses within the stringers. Both schemes were designed to apply positive moment to the negative moment regions of continuous stringers and thus reduce the stresses resulting from service loads. Each of the strengthening schemes was service load tested on a full-scale mockup of a negative moment region of a bridge stringer. After completion of the service load tests, the full-scale mockup was loaded to failure with the superimposed truss in place. Both schemes were effective in reducing bottom flange stresses; however, the post-compression scheme slightly increased the top flange stresses because of the tension applied to the section. The superimposed truss was very effective in reducing both the top and bottom flange stresses as it applied only positive moment to the mockup. Finite-element analysis verified the experimental results; thus, the finite-element model developed can be used in the analysis of actual bridges.

GENERAL INTRODUCTION

About one-half of the approximately 600,000 highway bridges in the United States were built before 1940, and many have not been adequately maintained. Most of these bridges were designed for lower traffic volumes, smaller vehicles, slower speeds, and lighter loads than are common today. In addition, deterioration caused by environmental factors is a growing problem. According to the Federal Highway Administration (FHWA), almost 40% of the nation's bridges are classified as deficient and in need of rehabilitation or replacement. Many of these bridges are deficient because their load-carrying capacity is inadequate for today's traffic. Strengthening can often be used as a cost-effective alternative to replacement or posting.

Many different methods exist for increasing the live load-carrying capacity of the various types of bridges. Through Iowa Department of Transportation (Iowa DOT) Projects HR-214 [22] and HR-238 [6,8,20], the concept of strengthening simple-span, composite steel beam and concrete deck bridges by post-tensioning was developed. These projects took the concept from the feasibility phase through the implementation and design methodology phase. Results of these projects verified that strengthening of simple-span bridges by post-tensioning is a viable and economical strengthening technique. The design methodology developed by Dunker et al. [8] provided a procedure by which the required post-tensioning force could be determined relatively easily. This design methodology has since been used successfully by the Iowa DOT and other agencies for the strengthening of simple-span composite bridges.

As a result of the success in strengthening simple-span bridges by post-tensioning, a laboratory investigation, Iowa DOT project HR-287 [7], was undertaken to examine the feasibility of strengthening continuous, composite steel beam and concrete deck bridges. This research program indicated that the strengthening of continuous composite bridges is feasible. Longitudinal as well as transverse distribution of post-tensioning must be considered if only exterior or only interior stringers are post-tensioned. Laboratory testing of the 1/3-scale model bridge and finite element analysis showed that post-tensioning of positive moment regions with straight tendons was more effective than post-tensioning negative movement regions with straight tendons. It was also determined that changes in the tension in tendons may either be beneficial or detrimental when live loads are applied to strengthened bridges; this must be carefully considered in design.

On the basis of the success of laboratory investigation of strengthening continuous composite bridges by post-tensioning, Iowa DOT project HR-308 was undertaken. In the summer of 1988, a three-span, continuous bridge close to Fonda on N28 was strengthened by post-tensioning the positive movement regions of all twelve beams. The bridge was load-tested before and after post-tensioning to determine the effectiveness of the post-tensioning. This bridge is scheduled for retesting during the summer of 1989. As this project is still in progress, no references are available.

At the same time that several of the previously described strengthening projects sponsored by the Iowa DOT were in progress, several members of the research team working on this particular project were involved in a National Cooperative Highway Research Program research project NCHRP 12-28(4), "Methods of Strengthening Existing Highway Bridges" [21]. The main objectives of this project were to compile, evaluate, and improve existing strengthening procedures as well as develop new procedures, equipment, and materials for increasing or restoring the load capacity of existing bridges.

In this project, more than 375 references were reviewed to determine the bridge strengthening methods being used worldwide. The methods reviewed can be broadly categorized as member replacement, stiffness modification, member additions, and post-stressing.

As a result of work on the NCHRP 12-28(4) project, several other concepts for strengthening bridges have been conceived. These, coupled with the difficulties encountered in HR-287 in post-tensioning the negative movement regions of continuous beams, led to this project. Two of the more promising strength concepts were investigated in this project, Iowa DOT project HR-302. One advantage of investigating these strengthening techniques while work was still in progress on the post-tensioning of continuous bridges (HR-308) was the availability of the 1/3-scale, three-span model bridge and the full-scale composite beam, which were fabricated and tested in HR-287. These two laboratory test specimens were both used in this investigation, saving both time and money. It is believed that the work completed in this project will provide engineers with strengthening alternatives that may be more efficient than post-tensioning in certain situations.

The two strengthening concepts investigated in this project are presented in the following sections. For clarity, the two concepts are presented separately. For each concept, the overall objectives and scope are presented. Later in this report, detailed objectives as well as the research plan employed will be presented.

Strengthening Technique 1: Providing Partial End Restraint

The primary objective of this portion of the investigation was to determine the feasibility of strengthening stringer bridges by the addition of partial end restraint, thus reducing the existing positive moment at the midspan of the stringers. As the end restraint is increased, larger stress reductions at midspan will be realized. The investigation was broken into the following steps:

- Determine the feasibility of utilizing partial end restraint to strengthen simple-span bridges as well as continuous bridges.
- Design several methods of developing end restraint. These methods should provide a range of rotational stiffnesses, thus making it possible to reduce the stress in a given stringer by the desired amount.
- Determine the most efficient location for the end-restraint brackets on simple-span and continuous stringer bridges.
- Determine the effect of end restraint on the existing supports (i.e., abutments or piers).

In addition to employing the end-restraint schemes on the bridge model from HR-287, several different brackets were also tested on an individual test beam. All systems tested in the laboratory were also analyzed by finite-element analysis.

Strengthening Technique 2: Post-Compression of Stringers

In Iowa DOT project HR-287, it was found that by post-tensioning the positive moment regions of continuous bridges, stress reduction can also be obtained in the negative moment regions. However, in certain instances, additional stress reduction is required in the negative moment region, which obviously requires additional post-tensioning force. Due to the proximity of the bridge deck in the negative moment region, the required connections in most instances would require removal of a portion of the bridge deck. One method of avoiding this problem is to apply tension to the lower flange rather than compression to the upper flange. Thus, the primary objective of this portion of the investigation was to develop a scheme for applying tension stresses to the lower flange area of the stringer in negative moment regions. The investigation was broken into the following steps:

- Design the compression strut and provide adequate lateral support if such is required.

- Determine the best method of attaching the compression struts to the beams.
- Determine the distribution of post-compression force(s) in the various regions of a given bridge.

In the process of developing compression tubes for applying tensile stress to the lower flange regions of stringers, the investigators conceived the idea of using superimposed trusses to strengthen negative moment regions of stringers. Thus, in addition to the post-compression system, two different configurations of trusses were fabricated and tested on the full-scale mockup fabricated for testing post-tensioning systems in HR-287.

Structure of the Report

For the ease of the reader, the two strengthening procedures investigated in this study are presented separately. Part 1 presents the portion of the project involving providing partial end restraint; henceforth, this strengthening technique will be referred to as ST1. In Part 2, the portion of the project involving post-compression of stringers is presented. Thus, that strengthening technique will be referenced as ST2.1, while the techniques involving the use of the two superimposed trusses will be referenced as ST2.2 and ST2.3. A more definitive description of this identification scheme will be presented in Part 2.

Each part (Parts 1 and 2) of this final report is written independently. Thus, the reader may read one part without knowledge of what has been presented in the other part. To further assist readers in their review of this final report:

- Each part (i.e., Part 1 and 2) has an abstract, a summary and conclusions chapter, and recommendations for continued studies, which is pertinent to that particular part of the report. A general abstract summarizing the entire project is presented at the beginning of this report. Thus, the report has three abstracts.
- A bibliography has been developed that includes all citations in Parts 1 and 2, as well as those in the introduction of the report. For easy reference, the bibliography has been included in both parts of the report.
- Tables and figures in Parts 1 and 2 have been given a double number, (e.g., Table 1.6, Table 2.3, Fig. 2.7, etc.). The first number indicates the part of the report in which the figure or table is located, while the second number identifies the number of the table or figure.

As verification of the pertinence of this strengthening project as well as the others recently completed, one need only review the data from the National Bridge Inventory (NBI) for the state of Iowa. The accuracy of this analysis is obviously a function of the reliability of the data. An initial review of the bridge records revealed few obvious coding errors; however, there were numerous blanks. To avoid misinterpretation of the bridge records, all computer sort runs were programmed to reject any records containing blanks or unauthorized characters in items being examined. Overall, the NBI data are relatively free of obvious errors. Though there are some definite and some probable coding errors, those errors did not exceed 5% and often were less than 1% for the NBI items utilized. In order to analyze the NBI records most accurately, researchers rejected records having obvious errors or significant omissions. Based on data from the NBI, the 14 most common bridge types in Iowa are listed in order in Table 1. The 14 bridge types represent approximately 90% of the more than 26,000 bridges in Iowa.

To show the urgency of the strengthening needs, the number of anticipated bridge retirements was examined for all the 14 common bridge types. In Fig. 1 the number of steel-stringer bridges constructed in each 5-year period is plotted. The first point in the figure is for the number of bridges constructed in 1900 or in previous years, and the other points connected by the dotted line are for the numbers constructed during five-year periods such as 1901 to 1905.

For steel-stringer bridges the average life was computed from NBI data by adding the age computed from year built and the estimated remaining life. The solid line was plotted by using the numbers of bridges for the construction points but extending it into the future by the average life; thus the solid line represents bridge retirements. Although the average life has some inaccuracy because it is based on surviving bridges and remaining life estimates, it is the best available statistic for predicting bridge life. For those bridge types having large numbers of anticipated retirements in the near future, strengthening may extend the useful service life. A review of Fig. 1 indicates that the number of anticipated retirements of steel-stringer bridges is at a high level and is projected to increase significantly in the near future.

An analysis similar to this one including data from all states may be found in Ref. [21]. Results from this analysis are similar to the one that uses only Iowa data in that in both analyses steel-stringer bridges lead the list of bridges for which strengthening may be required.

Table 1. Fourteen common bridge types in Iowa (NBI).

NBI Item 43	Main Structure Type	Number of Bridges	Percentage of Bridges
302	Steel stringer	6,761	26.0
702	Timber stringer	4,946	19.0
310	Steel through-truss	2,983	11.5
201	Continuous concrete slab	2,000	7.7
502	Prestressed concrete stringer	1,903	7.3
402	Continuous steel stringer	1,860	7.1
101	Concrete slab	1,237	4.7
504	Prestressed concrete tee	414	1.6
102	Concrete stringer	393	1.6
104	Concrete tee	387	1.5
303	Steel-girder floor beam	289	1.1
111	Concrete-deck arch	141	0.5
204	Continuous concrete tee	51	0.2
501	Prestressed concrete slab	36	0.1
	Total	23,412	89.9

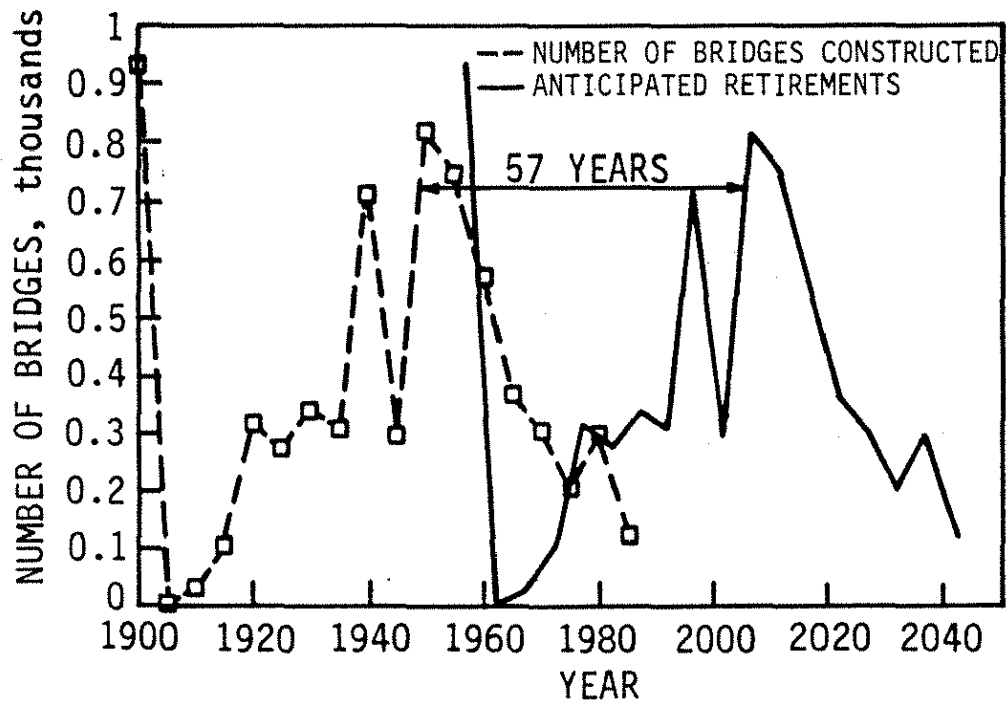


Fig. 1. Number of steel stringer bridges constructed and anticipated retirements by 5-year periods (NBI).

Part 1: Providing Partial End Restraint

T. J. Wipf, F. W. Klaiber, and R. B. Abu-Kishk

	<u>Page</u>
3.2. Model Bridge	66
3.2.1. Model Bridge Instrumentation	66
3.2.2. Model Bridge Tests	68
3.2.2.1. Vertical Load Tests with One Concentrated Load	72
3.2.2.2. Vertical Load Tests with Two Concentrated Loads	73
4. FINITE-ELEMENT ANALYSIS	75
4.1. Finite-Element Software: ANSYS	75
4.1.1. Bottom Flange Bracket Model	75
4.1.2. Test Beam Model	81
4.2. Finite-Element Software: SAP IV	83
4.2.1. Bridge Model	83
5. TEST RESULTS AND ANALYSIS	89
5.1. Test Beam Analysis and Test Results	89
5.1.1. Presentation of Test Data	93
5.1.1.1. Test 1	93
5.1.1.2. Tests 2 through 7	93
5.1.2. Analysis and Comparison of Test Beam Results	98
5.1.2.1. Tests 1, 2, and 3	98
5.1.2.2. Bottom Flange Bracket Tests—Tests 2, 4, and 6	105
5.1.2.3. Bottom Flange and Web Restrained—Tests 3, 5, and 7	110
5.1.2.4. Determination of Bracket Stiffness	114
5.2. Model Bridge Analysis and Test Results	119
5.2.1. Experimental Results	119
5.2.1.1. One Concentrated Load	119
5.2.1.2. Two Concentrated Loads	122
5.2.2. Analytical Results	127
5.2.2.1. Comparison of Analytical and Experimental Results	127
5.2.2.2. Sensitivity Study	132
6. SUMMARY AND CONCLUSIONS	141
6.1. Summary	141
6.2. Conclusions	143

	<u>Page</u>
7. RECOMMENDED FURTHER RESEARCH	145
8. BIBLIOGRAPHY	147
9. APPENDIX A. DETAILS OF REINFORCEMENT FOR ABUTMENT 1	151
10. APPENDIX B. TEST BEAM DATA	155
11. APPENDIX C. STRAIN REDUCTION TABLES FOR MODEL BRIDGE	165

LIST OF TABLES

	<u>Page</u>
Table 1.1. Description of beam tests.	66
Table 1.2. Restraint provided in various bridge tests.	72
Table 1.3. Location of vertical load for tests of model bridge.	74
Table 1.4. Comparison of various bracket alterations.	76
Table 1.5. Effectiveness of restraint brackets.	100
Table 1.6. Effects of reduction in bottom flange stiffness.	109
Table 1.7. Percent reductions due to full restraint conditions.	114
Table 1.8. Comparison of analytical and experimental midspan moments.	117
Table 1.9. Bracket stiffnesses.	118
Table 1.10. Results of study to obtain 10% strain reduction.	137
Table B.1. Linear-regression analysis results of beam tests 1-7.	156
Table B.2. Forces transferred to abutment from finite-element analysis.	157
Table C.1. Strain reductions at Section 1 with symmetric restraint conditions (one concentrated load).	167
Table C.2. Strain reductions at Section 1 with asymmetric restraint conditions (one concentrated load).	168
Table C.3. Strain reductions at Section 1 with symmetric restraint conditions (two concentrated loads).	169
Table C.4. Strain reductions at Section 1 with asymmetric restraint conditions (two concentrated loads).	170

LIST OF FIGURES

	<u>Page</u>
Fig. 1.1. Test beam setup.	38
Fig. 1.2. Details of Abutment 1.	39
a. Section A-A	
b. Front view of Abutment 1	
Fig. 1.3. Photographs of Abutment 1.	41
a. After removal of formwork	
b. Location of horizontal holes	
Fig. 1.4. Bottom flange bracket (Bracket 1).	43
a. Front view	
b. Side view	
c. Axonometric view	
Fig. 1.5. Attachment of bottom flange bracket .	44
Fig. 1.6. Photographs of Bracket 1 in place.	45
a. Prior to post-tensioning	
b. After post-tensioning	
Fig. 1.7. Web bracket (Bracket 2).	47
a. Front view	
b. Side view	
c. Axonometric view	
Fig. 1.8. Attachment of Bracket 2.	48
a. Side view	
b. Front view	
Fig. 1.9. Photographs of Bracket 1 and Bracket 2 in place.	49
a. Closeup view	
b. Overall view	
Fig. 1.10. Bracket 3.	50
a. Side view	
b. Axonometric view	
Fig. 1.11. Bracket 4.	51
a. Side view	
b. Axonometric view	

	<u>Page</u>
Fig. 1.12. Model bridge.	52
a. Cross section at midspan (Section A-A)	
b. Plan view	
c. Section B-B	
d. Section C-C	
Fig. 1.13. Restraint brackets on bridge stringers.	54
a. Top view	
b. Section A-A	
Fig. 1.14. Side view of bridge brackets in place.	56
Fig. 1.15. Front view of bridge brackets in place.	57
Fig. 1.16. Photographs of bridge brackets.	58
a. View of simulated back wall	
b. Front view of abutment	
Fig. 1.17. Test beam instrumentation.	60
Fig. 1.18. Determination of rotation at the supports.	62
Fig. 1.19. Loading of test beam.	63
Fig. 1.20. Photographs of loading scheme.	64
a. General view of beam	
b. Closeup view of loading apparatus.	
Fig. 1.21. Locations of strain-gage sections.	67
Fig. 1.22. Location of DCDTs.	69
Fig. 1.23. Concrete dead weight.	70
a. Elevation view	
b. Section A-A	
Fig. 1.24. Locations of vertical load points.	71
Fig. 1.25. Finite-element model of Bracket 1.	77
Fig. 1.26. Different finite-element idealizations of Bracket 1.	78
a. Configuration A	
b. Configuration B	
c. Configuration C	
Fig. 1.27. Alterations of Bracket 1.	79
a. Reduction 1	
b. Reduction 2	

	<u>Page</u>
c. Reduction 3	
d. Reduction 4	
e. Reduction 5	
f. Reduction 6	
g. Reduction 7	
Fig. 1.28. Representation of actual to idealized test setup.	82
a. Finite-element idealization	
b. Actual setup	
Fig. 1.29. Grillage mesh for laboratory model bridge.	84
Fig. 1.30. Plot of transverse strain at Section 1 for one concentrated load for no end restraint—model vs. experimental at various load points (see Fig. 1.24).	86
a. LP 1	
b. LP 2	
c. LP 3	
d. LP 4	
Fig. 1.31. Plot of transverse strain at Section 1 for two concentrated loads for no end restraint—model vs. experimental at various load points.	87
a. LPs 3 & 17	
b. LPs 4 & 18	
c. LPs 5 & 19	
d. LPs 6 & 20	
Fig. 1.32. Photographs of test-beam bracing system.	91
a. At midspan	
b. At abutment 1	
Fig. 1.33. Configuration of a typical test-beam brace.	92
a. Front view	
b. Side view	
Fig. 1.34. Test 1 data.	94
a. Strain distribution at midspan	
b. Midspan deflection	
c. Transit deflection	
Fig. 1.35. Initial end restraint: Test 1.	95

	<u>Page</u>
Fig. 1.36. Comparison of theoretical and experimental results at midspan for fixed simple support conditions.	97
Fig. 1.37. Strain distribution vs. load for theoretical and experimental results.	99
Fig. 1.38. Representation of maximum restraint conditions.	101
a. Midspan strains	
b. Midspan deflection	
c. Transit deflection	
Fig. 1.39. Comparison of results from tests 1, 2, 4, 6.	106
a. Midspan strains	
b. Midspan deflection	
c. Transit deflection	
Fig. 1.40. Comparison of results from tests 1, 3, 5, 7.	111
a. Midspan strains	
b. Midspan deflection	
c. Transit deflection	
Fig. 1.41. Effects of end restraint in beams.	115
a. Assumed simply supported beam	
b. Simple beam moment distribution	
c. Beam with restraining end connection	
d. Moment distribution with end restraint included	
Fig. 1.42. Determination of restraining moment.	116
a. Simple support conditions	
b. Rotational restraint provided	
c. Moment fraction	
Fig. 1.43. Plot of longitudinal strain distribution for Beam 2; load at LP 5.	120
Fig. 1.44. Plot of transverse strain at Section 1 for one concentrated load (symmetrical restraint) at various load points.	123
Fig. 1.45. Plot of transverse strain at Section 1 for one concentrated load (asymmetrical restraint) at various load points.	124
a. LP 1	
b. LP 3	
Fig. 1.46. Plot of transverse strain at Section 1 for two concentrated loads (symmetrical restraint) at various load points.	126

	<u>Page</u>
a. LPs 3 & 17	
b. LPs 4 & 18	
c. LPs 5 & 19	
d. LPs 6 & 20	
Fig. 1.47. Plot of transverse strain at Section 1 for two concentrated loads (asymmetrical restraint); load at LPs 3 & 17.	128
Fig. 1.48. Plot of transverse strain at Section 1 for one concentrated load for all flanges restrained—model vs. experimental at various load points.	129
a. LP 1	
b. LP 2	
c. LP 3	
d. LP 4	
Fig. 1.49. Plot of transverse strain at Section 1 for two concentrated loads for all flanges restrained—model vs. experimental at various load points.	130
a. LPs 3 & 17	
b. LPs 4 & 18	
c. LPs 5 & 19	
d. LPs 6 & 20	
Fig. 1.50. Plot of transverse deflection at Section 1 for two concentrated loads at LPs 3 & 17 for all flanges restrained—model vs. experimental.	131
Fig. 1.51. Plot of analytical transverse strains at Section 1 for one concentrated load at various load points for various conditions of end restraint.	133
a. LP 1	
b. LP 3	
c. LP 4	

	<u>Page</u>
Fig. 1.52. Plot of analytical transverse deflections at Section 1 for one concentrated load at various load points for various conditions of end restraint.	134
a. LP 1	
b. LP 3	
c. LP 4	
Fig. 1.53. Plot of analytical transverse strains at Section 1 for two concentrated loads at various load points for various conditions of end restraint.	135
a. LPs 3 & 17	
b. LPs 4 & 18	
c. LPs 5 & 19	
Fig. 1.54. Plot of analytical deflections at Section 1 for two concentrated loads at various load points for various conditions of end restraint.	136
a. LPs 3 & 17	
b. LPs 4 & 18	
c. LPs 5 & 19	
Fig. 1.55. Plot of transverse strain at Section 1 for one concentrated load at various load points—exterior flanges only restrained.	139
a. LPs 3 & 10	
b. LPs 4 & 11	
Fig. 1.56. Plot of transverse strain at Section 1 for two concentrated loads at various load points—exterior flanges only restrained.	139
a. LPs 3 & 17	
b. LPs 6 & 20	
APPENDIX	
Fig. A.1. Reinforcement details for Abutment I.	152
a. Side view	
b. Front view	
c. Section A-A	
d. Section B-B	
e. Section C-C	
Fig. B.1. Test 2 data.	158
a. Strain distribution at midspan	

	<u>Page</u>
b. Midspan deflection	
c. Transit deflection	
Fig. B.2. Test 3 data.	159
a. Strain distribution at midspan	
b. Midspan deflection	
c. Transit deflection	
Fig. B.3. Test 4 data.	160
a. Strain distribution at midspan	
b. Midspan deflection	
c. Transit deflection	
Fig. B.4. Test 5 data.	161
a. Strain distribution at midspan	
b. Midspan deflection	
c. Transit deflection	
Fig. B.5. Test 6 data.	162
a. Strain distribution at midspan	
b. Midspan deflection	
c. Transit deflection	
Fig. B.6. Test 7 data.	163
a. Strain distribution at midspan	
b. Midspan deflection	
c. Transit deflection	

ABSTRACT

Strengthening existing steel stringers in composite steel-beam concrete-deck bridges by providing partial end restraint is shown to be feasible. The purpose of the study is to determine a technique for increasing the capacity of bridges to accommodate today's increase in loading. The research program included a review of existing literature, testing of a full-scale bridge beam and testing of a 1/3-scale bridge model, and finite-element analyses of the restraint brackets, the test beam, and the model bridge.

Results pertaining to the analytical and experimental aspects of this investigation, in addition to theoretical expectations when various degrees of end restraint are provided, are presented. Six different degrees of end restraint were examined. The percent reductions achieved ranged from 12% to 26% for midspan strains, 20% to 30% for midspan deflections, and 10% to 32% for beam rotation. The correlation between the analytical and experimental results verified the basic design assumptions; hence, the analytical models can be used for determining the degree of end restraint required and its location for strengthening existing bridges.

1. INTRODUCTION

1.1. General Background

A problem confronting the majority of states in the United States is the inadequacy of hundreds of their existing bridges, both on the primary and secondary road networks. Many of these bridges were constructed more than 25 years ago and, for the most part, have deteriorated to the point where they are inadequate for original design loads or have been rendered inadequate by changes in design or maintenance standards and design loads. Most of these bridges were designed for lower traffic volumes, slower speeds, and lighter loads than are common today. In response to this problem, numerous research projects have been undertaken at Iowa State University (ISU) to determine the feasibility of strengthening existing bridges.

Earlier research work focused on the concept of strengthening bridges (simple and continuous spans) by post-tensioning. The performance of these Iowa DOT projects—namely, HR-214, HR-238, and HR-287—laid the foundation for investigating additional strengthening concepts. One of the more promising strengthening concepts, providing partial end restraint, is addressed in Part 1 of this report.

Information pertaining to this concept (end restraint) was minimal, and of the information found, essentially none dealt with bridges. This study, therefore, is an effort to correlate existing information, theoretical approaches, and experimental data. Based on the outcome of this study, the investigators believe that a second phase of the study should be undertaken in which one or more bridges in Iowa are strengthened by procedures developed in this investigation.

1.2. Objectives

The overall objective of this study was to determine the feasibility of strengthening stringer bridges by the addition of partial end restraint. Providing end restraint to one end of a stringer will obviously reduce the live-load positive moment along the entire length of the stringer. Live loading on a given simple-span bridge will produce maximum stress near midspan; thus this research program only investigated the reduction of stresses at the

midspan of the stringers. As end restraint is increased, larger stress reductions at midspan will be achieved.

In line with the overall objective of this study, the following secondary objectives were established:

- Determine the feasibility of using partial end restraint to strengthen simple-span bridges, as well as continuous bridges.
- Design several methods for developing end restraint.
- Determine the most efficient location for providing end restraint.
- Determine the effects of various end-restraint mechanisms on stress reduction.

These objectives were pursued by the research team through a comprehensive review of existing literature, testing of a full-scale bridge beam, and testing of a 1/3-scale model bridge in the ISU Structural Engineering Research Laboratory. In addition to the experimental work, a finite-element analysis of the laboratory beam model and the bridge model with various end-restraint conditions, as well as a finite-element analysis of the individual restraining brackets, was performed.

1.3. Research Program

The research program consisted of several distinct parts with a strong emphasis on the laboratory testing. Initially, a review of existing literature was conducted; however, the information available cited the presence of end restraint but provided no means of qualifying it. The fact that no previous work had been performed in this area was both a source of interest and challenge for the researchers.

At the onset of the previous laboratory testing program, Iowa DOT project HR-287, the researchers consulted the Iowa DOT Office of Bridge Design to obtain plans for standard continuous, composite bridges. From the various sets of plans, the V12 (1957) series of composite, three-span bridges was selected. The prototype bridge chosen was used in modeling the 1/3-scale bridge in the laboratory. All the testing in this project was in the elastic range; thus the model bridge was undamaged and provided an excellent model for testing end restraint. To eliminate the size effects, a full-scale beam with cross-sectional properties similar to the interior and exterior stringers of the V12 series bridges was chosen for testing. This test setup was constructed to simulate a typical one-span bridge. During the

testing of both the test beam and the model bridge, strains and deflections at various locations were monitored.

Two finite element software packages, ANSYS and SAP IV, were used in conducting the analytical work. These were chosen primarily because of user familiarity and their adaptability to the research work. ANSYS was used in modeling the end restraint brackets and also in modeling the test beam. Several of the preprocessing and postprocessing computer programs from earlier research projects were adapted for use with continuous bridges such as the three-span prototype bridge. Those programs were utilized with SAP IV in order to analyze the laboratory model bridge. The three finite-element models were all interrelated. For instance, modeling of the end-restraint bracket was required prior to the modeling of the test beam in order to determine the type of brackets that would provide the greatest restraint. From the various configurations analyzed, three brackets were chosen to be modeled with the test beam. Based on the results of the test beam and bracket analysis, the stiffness of each of the three restraining brackets was determined. These stiffnesses were then used in the analysis of the effects of end restraint on the model bridge. The results of the experimental and the analytical work on the model bridge were then compared. The agreement in their values verified that previous modeling assumptions were correct.

The results from the various parts of the research program are presented in this report. The literature review follows in Section 1.4. Chapter 2 describes the end-restraint mechanisms investigated, as well as the test beam and the bridge model tested in the laboratory. Test procedures employed are described in Chapter 3 and the finite-element work in Chapter 4. Results from the laboratory testing program and the finite-element analyses are summarized and presented in Chapter 5. Following the results are the summary and conclusions in Chapter 6 and the recommendations for further research in Chapter 7.

1.4. Literature Review

A review of existing literature on end-restraint connections for bridge stringers revealed that no such work had taken place. Several cases cited the effects of natural end restraint on the behavior of a bridge but went no further in trying to quantify it. A considerable amount of literature related to general connection behavior, especially building connections, was found. This information, which related to the methods of characterizing

connection behavior, was useful. However, it served only as general background information and was not used in the actual experimental work for this particular research project.

As previously mentioned, end restraint has been determined in various structural systems. This literature review provides some of the historical development of the concept of end restraint and corroborates the reasons for conducting this research at ISU.

The importance of end restraint was realized over 50 years ago when researchers measured the relationship between end moments and the relative rotation between the members in various beam-to-column joints [16]. Experimental investigations of actual joint behavior found that typical simple connections do possess a certain amount of rotational rigidity. Extensive studies of the influence of end restraint on the strength and behavior of columns have been conducted by Jones et al. and Lui and Chen, among others [15, 26]. These investigations have examined different aspects of restraint on member behavior, specifically determining the influence of

- type of beam-to-column connection
- column length
- magnitude and distribution of residual stresses
- initial out-of-straightness.

Among the observations made with regard to the previously noted variables are (1) for the same deflection, the column with end restraint can carry more load than the corresponding pin-ended column, and (2) for the same load, the midheight deflection of the end-restrained column is considerably less than that of the hinge-ended column.

In an actual framework, columns are connected to other structural members and thus their ends are restrained [5]. It is believed that the behavior and strength of columns in actual building frames will be affected significantly by the presence of these unavoidable end restraints and must therefore be included in the determination of their load-carrying capacity. On the basis of such findings, the Structural Stability Research Council (SSRC) in 1979 assigned Task Group 23, "Effects of End Restraint on Initially Crooked Columns," to study the combined effects of residual stresses, initial out-of-straightness, and end restraints on column strength [26]. In that same year, SSRC adopted the Technical Memorandum No. 5, "General Principles for the Stability Design of Metal Structures." In the case of columns, the memorandum requires explicitly the inclusion of the following three main factors in the determination of the load-carrying capacity: (1) residual stresses, (2) initial geometric imperfections, and (3) end restraints. Since then, it has become obvious that residual stresses

and initial crookedness have a destabilizing effect on columns, whereas end restraint can provide a stabilizing effect.

In the same manner that end restraint can be taken into account in the design of compression members, it could probably be used in the design of beams. It has been well established that beam connections considered to be simple, nonrestraining connections have some predictable amount of rotational restraint. Lindsey et al. [25] collected many of the moment-rotation ($M-\theta$) curves for simple connections and derived expressions for prediction of the $M-\theta$ characteristics. It was demonstrated that using the natural restraint of the so-called simple connection can reduce the size and deflection of a simply supported purlin. Although this work focused on the design of roof purlins, the analysis is general and can be applied to any set of beams. Making use of the fact that any connection that possesses rotational restraint will reduce the positive moments in the beam, this reduction can be applied to the governing positive-bending moments.

Up to this point, several researchers have noted the presence of end restraint, but to the authors' knowledge no work has been undertaken to determine how to take advantage of this natural restraint. Based on this, and the fact that in previous projects (HR-238, HR-287, HR-308) considerable end restraint has been determined in several bridges in the field, the researchers at ISU undertook the task of testing a simply supported beam with restraining brackets of various stiffnesses as an initial step toward a better comprehension of end restraint on bridge stringers.

The presence of end restraint in bridges is becoming more evident as more bridges are being tested in the field. Somewhat unexpectedly, Klaiber et al. [20] found, while testing a post-tensioning scheme on an existing single-span steel beam and composite concrete deck bridge, that field-measured strains and deflections for the bridge were less than those computed on the basis of orthotropic plate theory and simple-span end conditions. The field results obtained were, however, bracketed by simple-span and fixed end conditions. It was then concluded that end restraint at bridge abutments was greater than might be expected. Also, through various theoretical investigations, end restraint and the differences in end restraint among bridge beams were determined to affect load distribution and the performance of a given bridge.

Beal [3], in the testing to failure of a jack-arch bridge in 1984, found that all the collected data supported the conclusion that a significant amount of end restraint was present in this nominally simply supported structure. This 47-ft bridge was loaded to failure to determine the degree of composite action between the steel beams and their concrete

encasements. At service loads the structure behaved like a fixed-ended structure. Service-load testing produced values for live-load distribution coefficients that differed from design values. It was concluded that the restraint was a consequence of the bearing details and soil pressure against the end diaphragm, but no theory was available to calculate its magnitude.

As a result of many field tests, Bakht and Jaeger [1] concluded in 1988 that slab-on-girder bridges are usually stiffer in flexure than is predicted by normal deflection analysis. The main reason for this enhanced stiffness, they concluded, was restraint to horizontal movement at girder supports. They derived expressions that account for this beneficial effect of girder support restraint. These expressions relate to girder deflections, moments, and bottom flange stresses of the girders. All of these were found to respond differently as a consequence of bearing restraint.

The literature review shows that natural end restraint is an inherent aspect of any type of structure. However, no research to date has focused on a method of determining this restraint in beams, bridges, and so forth. The lack of a rational procedure for predicting its magnitude prevents use of the enhanced strength in load-rating calculations. On the basis of these observations, strengthening of existing bridges by providing partial end restraint is not only viable but should not be difficult to develop because of the existence of some natural end restraint already present in most connections.

2. DESCRIPTION OF TEST SPECIMENS

This chapter presents the details of the test beam and model bridge used in the investigation. In this chapter, as in all subsequent chapters, the material has been subdivided into two sections: The first section pertains to the test beam, and the second section pertains to the model bridge. In each case test specimens, testing procedures, and instrumentation are described.

2.1. Test Beam

2.1.1. Description

In the development of the laboratory testing program, the researchers consulted with the Iowa DOT Office of Bridge Design and obtained plans for standard continuous, composite bridges. In selecting a standard series for a prototype bridge, the researchers of HR-287 considered the following factors. The bridge series must have a roadway wide enough for two 12-ft traffic lanes. The number of bridges constructed in Iowa from the standard plans should be large enough that if strengthening is applied to a bridge as part of another phase of research, a suitable bridge will be available in central Iowa. The shortest bridge in the standard series, at a scale no less than 1/3 full size, must fit the space available in the ISU Structural Engineering Research Laboratory. In light of these factors and the advice of the Office of Bridge Design, the V12 (1957) series of bridges was selected. After examination of the V12 series and the Iowa DOT list of surplus beams, the authors decided that a $W24 \times 84 \times 32$ -ft long beam would be suitable for the proposed testing program. This decision was reached because the section properties of a $W24 \times 84$ are akin to some of the exterior and interior beams of the V12 series.

The beam setup was constructed to be simply supported and rested on two abutments, as illustrated in Fig. 1.1. The abutments will be referred to as Abutment 1 and Abutment 2 from this point on. Abutment 1 (see Fig. 1.2) was designed specifically to accommodate various restraint mechanisms. The location of holes for attachment of the various restraint mechanisms is shown in this figure. Vertical holes (formed with 1 1/2-in.-diameter PVC pipe) were for connecting the abutment to the structural tie-down floor. This was done in an attempt to represent the situation found in the field; however, the amount of restraint present in the field is a function of pile size, arrangement, and number as well as soil conditions, and

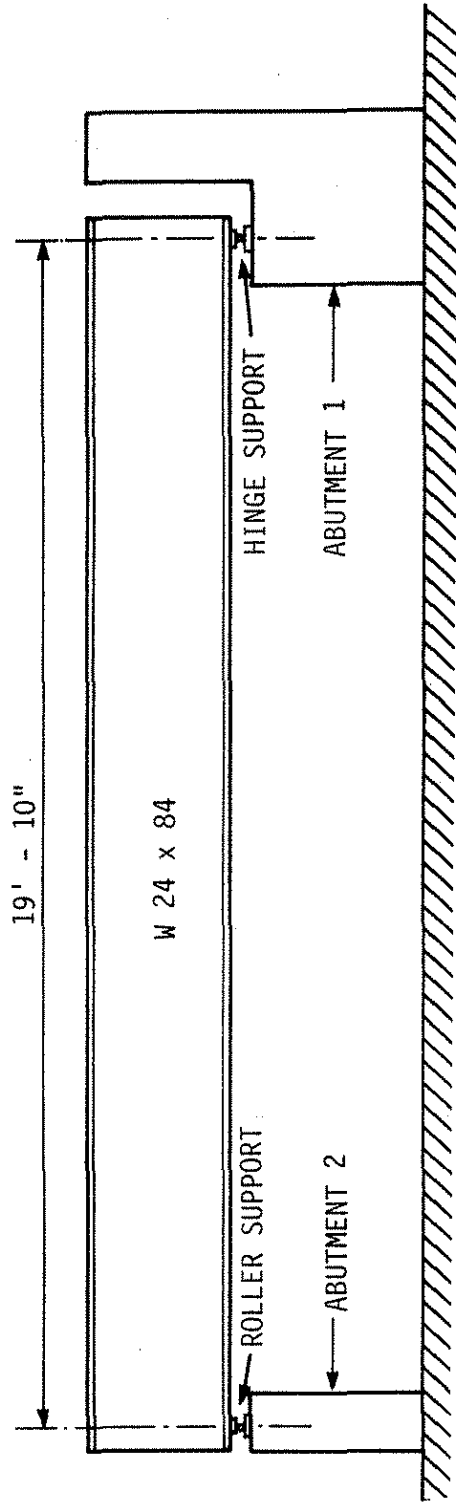
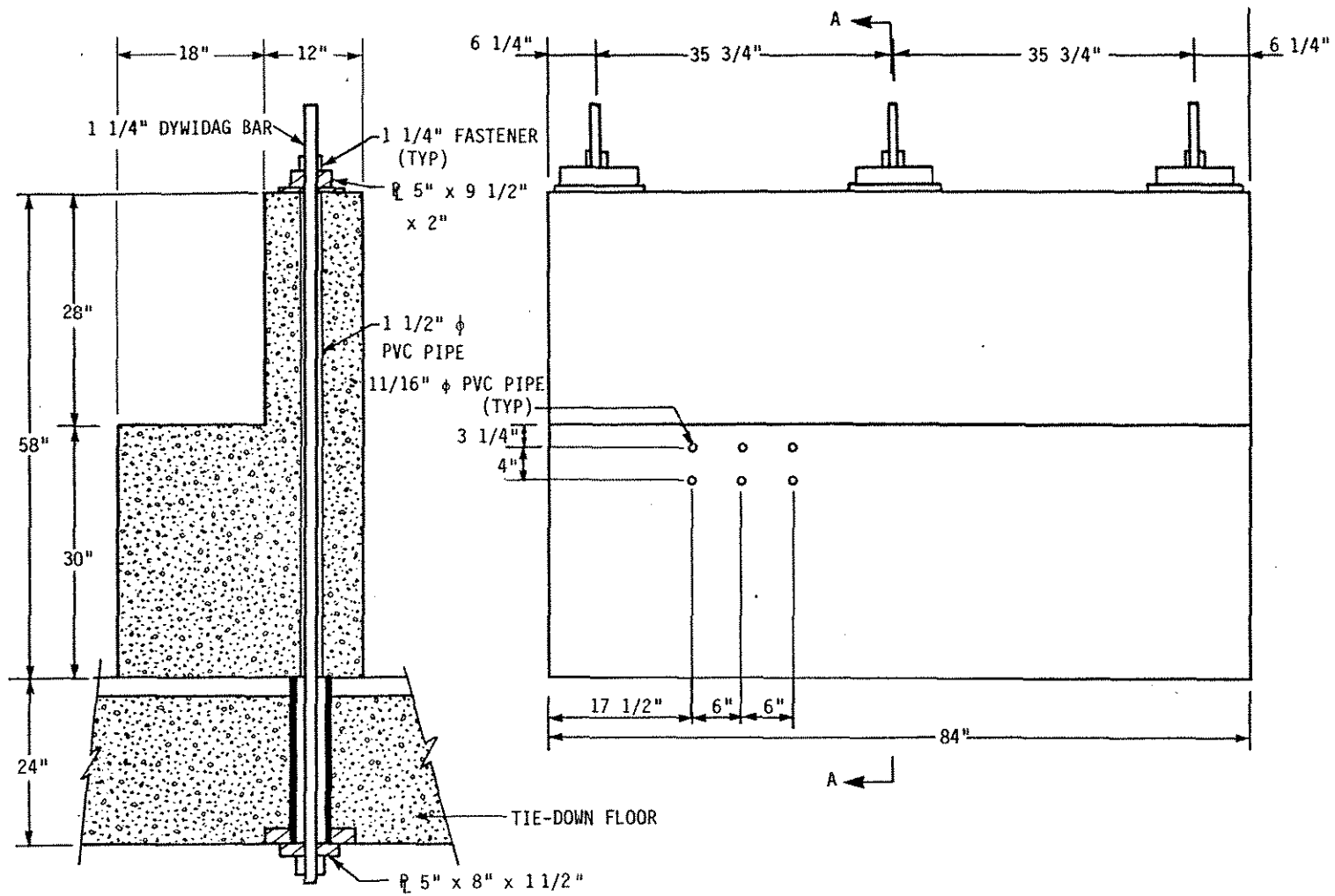


Fig. 1.1. Test beam setup.



a. SECTION A-A

b. FRONT VIEW OF ABUTMENT 1

Fig. 1.2. Details of Abutment 1.

thus varies from one site to another. Figure 1.3a is a photograph of Abutment 1 after the formwork was removed. Horizontal holes (formed with 1 1/16-in.-diameter PVC pipe) were for attaching the restraint mechanisms and are shown in Fig. 1.3b. The arrangement of the steel reinforcement used in this abutment is shown in Fig. A.1 (Appendix A). Abutment 2 was designed and constructed for the convenience of the laboratory testing program, because its design would not significantly affect the performance of the beam. This abutment is basically a stub reinforced-concrete wall, 2 ft 6 in. high \times 1 ft wide \times 4 ft long.

In the field, bridge standards specify the use of bridge bearings at the supports. A number of bearing types are available for use in bridge structures, ranging from steel rockers to fabric pad slide bearings. Because there are various types of bearings in the field and (due to the lack of proper maintenance) many of them are completely or partially "frozen," the authors decided to use a simple roller or hinge support in the laboratory testing. The use of a simple roller or hinge support will lead to conservative results because these support conditions provide essentially no restraint. Therefore, it is anticipated that field conditions will produce higher moment reductions as a result of the additional restraint provided by the bearings. Hence, the support conditions were fabricated so that a hinge existed at Abutment 1 and a roller existed at Abutment 2.

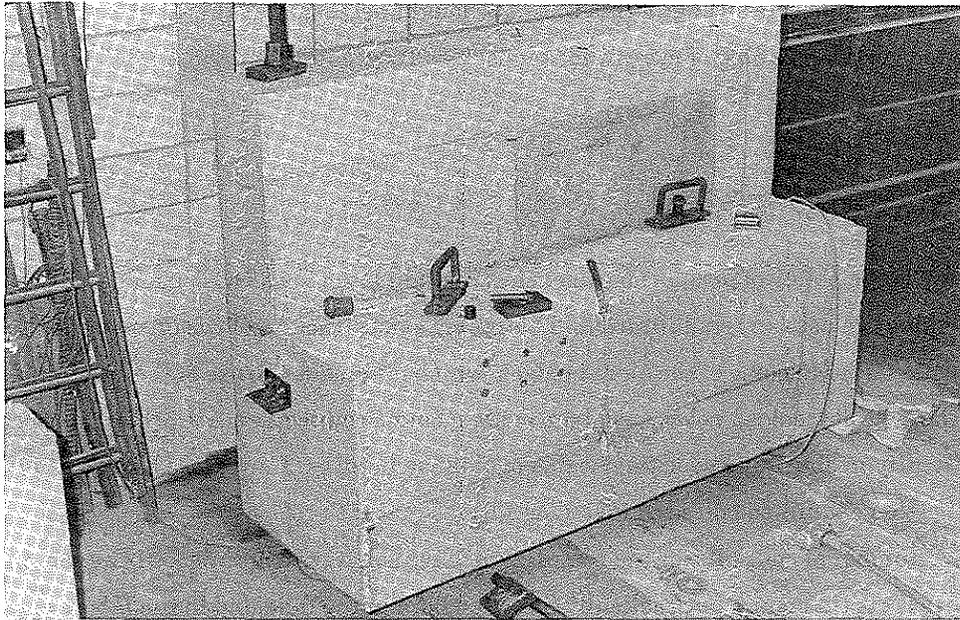
2.1.2. Physical Properties

2.1.2.1. Steel

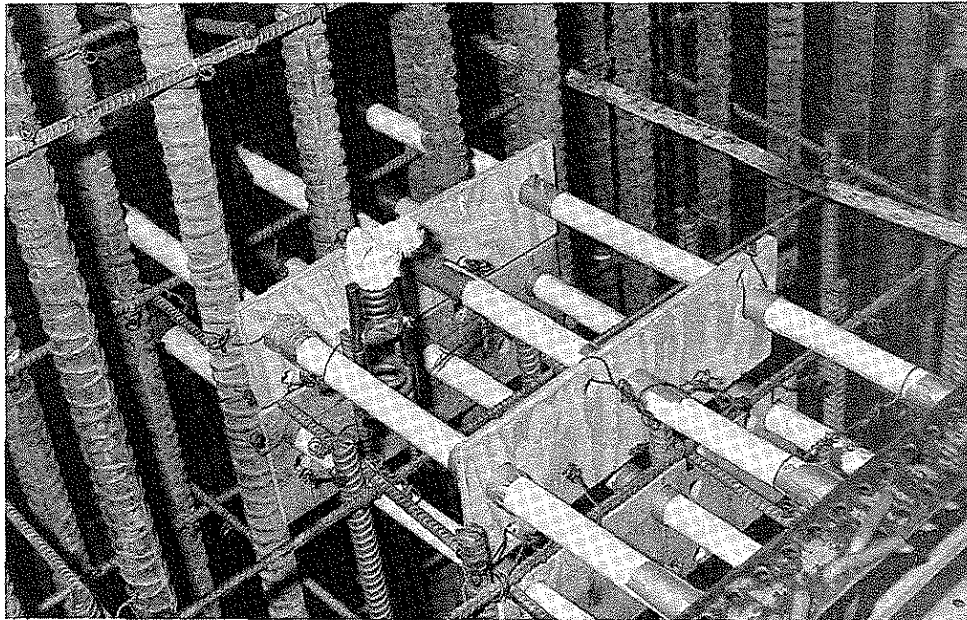
Because steel strength was not one of the variables being studied in the investigation, and because the bridge model and simulated bridge stringer were tested within the steel elastic-stress range, no tension tests were performed on any of the steel used in this testing program. In the analysis presented in Chapter 5, nominal values of the modulus of elasticity of the steel beams and Dywidag tendons were assumed to be 29,000 ksi and 24,000 ksi, respectively. These assumed values were based on steel tension tests made in previous research projects.

2.1.2.2. Concrete

Three standard cylinders (6 in. diameter \times 12 in. long) were made during the placing of concrete for Abutment 1. The average 28-day compressive strength, f'_c , was determined to be 6761 psi. As Abutment 2 was one that had been in the laboratory for some time, its compressive strength was not readily available. Although cores could have been taken to



a. AFTER REMOVAL OF FORMWORK



b. LOCATION OF HORIZONTAL HOLES

Fig. 1.3. Photographs of Abutment 1.

determine the concrete strength, this was not thought necessary as this abutment had supported vertical loading of magnitudes considerably greater than those applied in this project.

2.1.3. Bracket Configuration

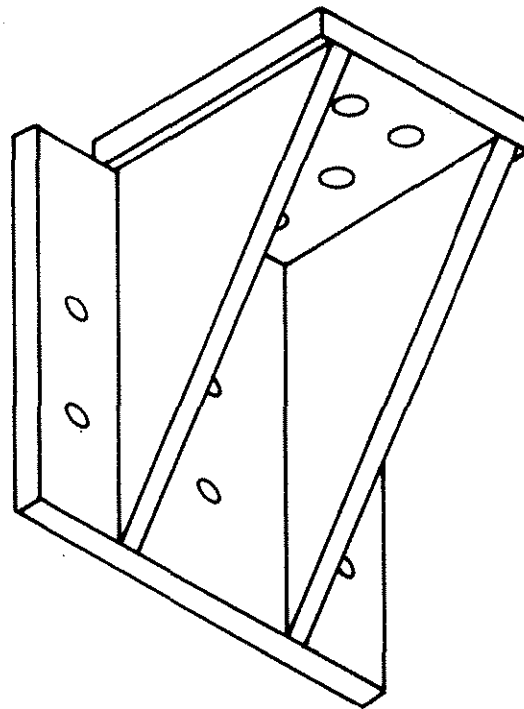
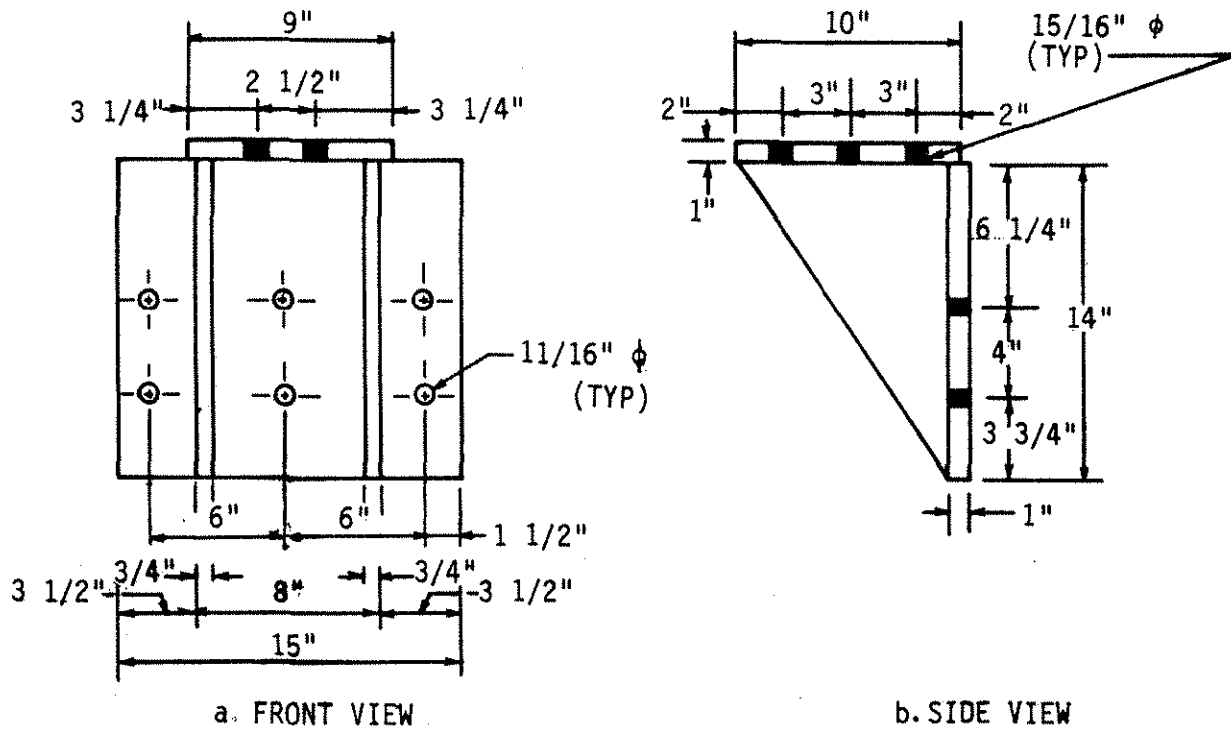
As is the policy of most bridge agencies, including the Iowa DOT, usually only bolted connections are used in rehabilitation. This policy exists because of the uncertainty about the type of steel used in some of the older bridges, which precludes the use of field welding. Even when the type of steel is known in a given bridge, bolted connections are preferred, because of the difficulty in obtaining good field welds in older structures. For these reasons, this investigation examined bolted connections only.

A number of concepts for the restraint mechanism were examined. However, only those brackets that could be practically installed both in the field and in the laboratory were given additional consideration. On the basis of these criteria, two types of brackets were chosen.

In addition to the above, it was desired to determine the effect of bracket stiffness on strain reduction. The initial bracket configurations were altered to achieve this objective (see Section 2.1.3.3).

2.1.3.1. Bottom Flange Bracket (Bracket 1)

The configuration of the bottom flange bracket, referred to as Bracket 1, is illustrated in Fig. 1.4. This bracket was designed to carry a vertical load of 50 kips, approximately twice the magnitude of a vertical reaction at Abutment 1 assuming a fixed-end support condition. As shown in the figure, the bracket consisted of a 14 in. \times 15 in. \times 1-in. back steel plate welded to a 9 in. \times 10 in. \times 1-in. top plate, forming an angle-shaped connection. The bracket was then stiffened with two 14 in. \times 10 in. \times 3/4-in. stiffener plates welded in position as shown. When used, Bracket 1 was bolted to the bottom beam flange with six A325 bolts 7/8 in. in diameter and post-tensioned to the abutment with six 5/8-in.-diameter Dywidag threadbars (see Fig. 1.5). Each of the six Dywidag threadbars was post-tensioned with a force of 34 kips, which is the maximum allowable for this size of bar. The use of Dywidag bars was easily accommodated in the laboratory; however, field conditions would dictate the use of some type of expansion anchor bolts. This bracket was later modified, as will be discussed in Section 2.1.3.3. A photograph of this bracket in place is shown in Fig. 1.6.



c. AXONOMETRIC VIEW.

Fig. 1.4. Bottom flange bracket(Bracket 1).

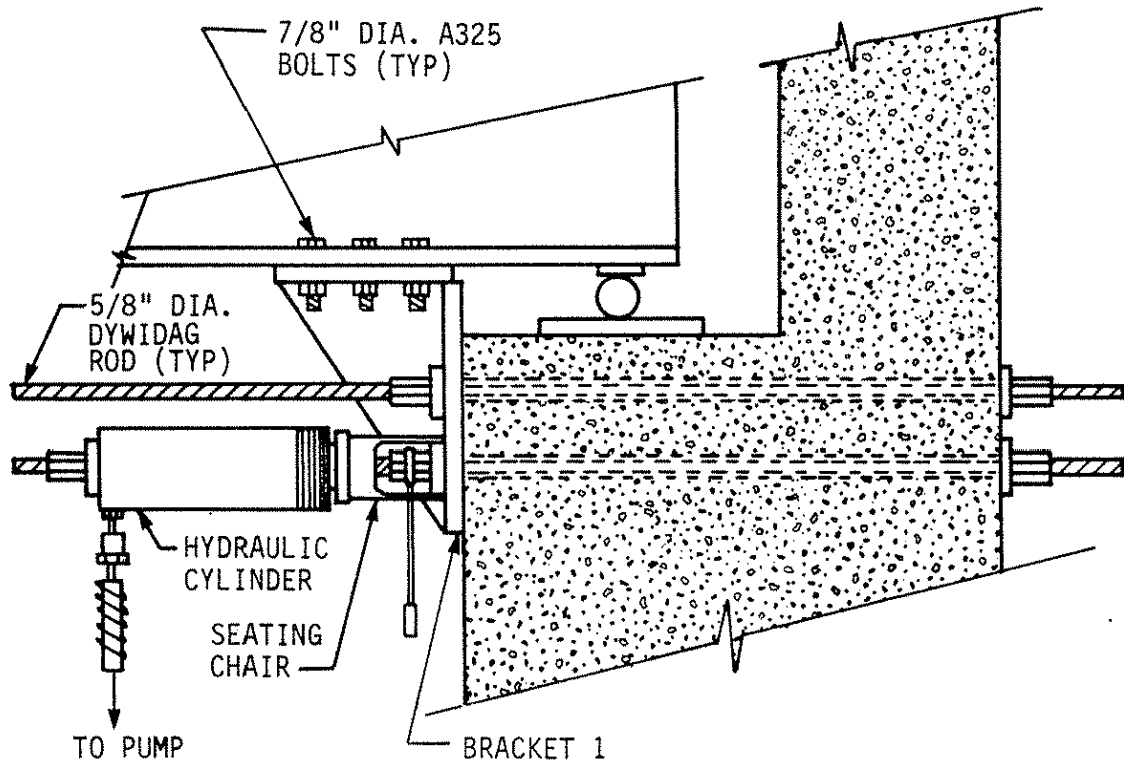
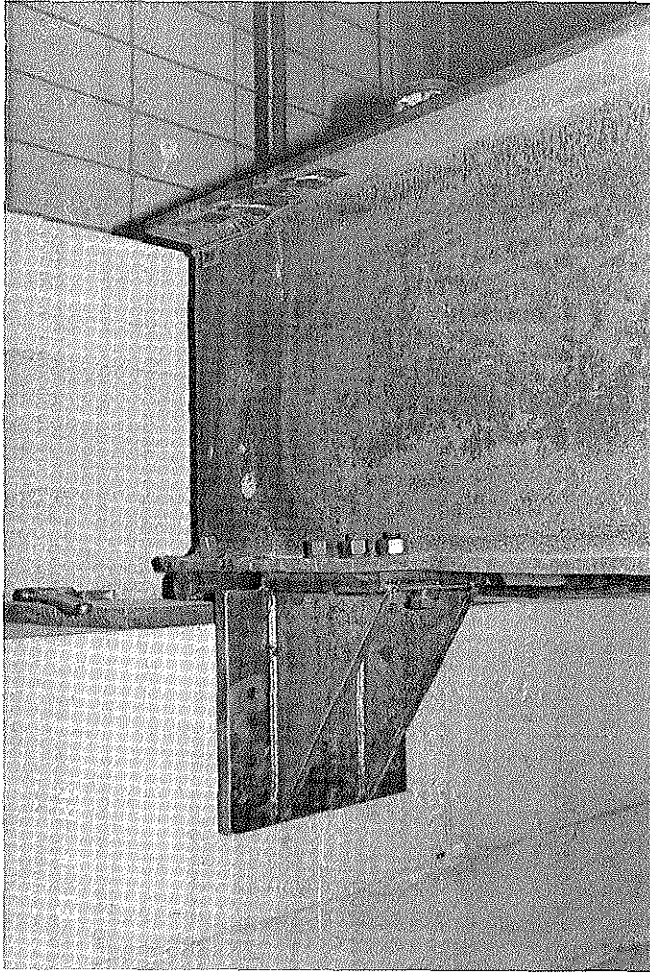
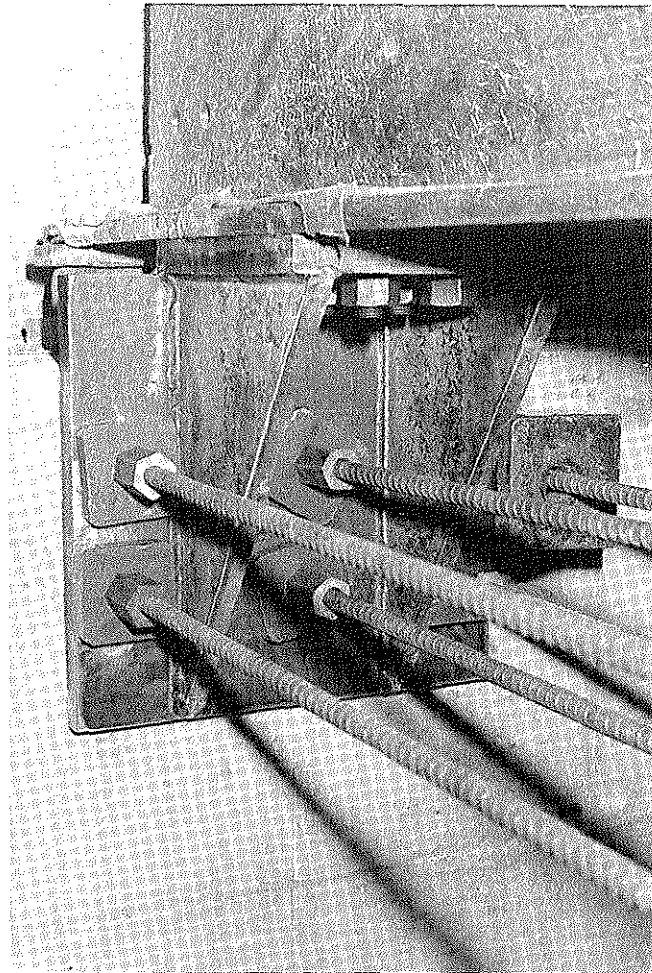


Fig. 1.5. Attachment of bottom flange bracket.



a. PRIOR TO POST-TENSIONING



b. AFTER POST-TENSIONING

Fig. 1.6. Photographs of Bracket 1 in place.

2.1.3.2. Web Bracket (Bracket 2)

Throughout the report, the web bracket will be referred to as Bracket 2; this bracket is illustrated in Fig. 1.7. This bracket consists of two angles with each angle formed by welding one 23 in. \times 13 1/2 in. \times 3/4-in. plate to a 21 in. \times 13 in. \times 3/4-in. plate. Bracket 2 was attached to the beam web with eight 7/8-in.-diameter bolts. The attachment to the abutment was facilitated through the use of WEJ-IT anchor bolts (see Fig. 1.8). A total of eight WEJ-IT anchor bolts (1 1/8-in. diameter and 12 in. in length) were needed per angle to achieve the required strength capacity. The bolts were embedded seven inches into the abutment in order to achieve their maximum tensile and shear strength of 34.8 and 34 kips, respectively. Bracket 2 acting in conjunction with Bracket 1 was designed to resist a 200 ft-kip moment, maintaining a safety factor of approximately four. This factor of safety is recommended by the manufacturers of WEJ-IT anchor bolts and ensures against any pullout or shear failures. A photograph of the bracket attachment in place is shown in Fig. 1.9.

2.1.3.3. Bracket 3 and Bracket 4

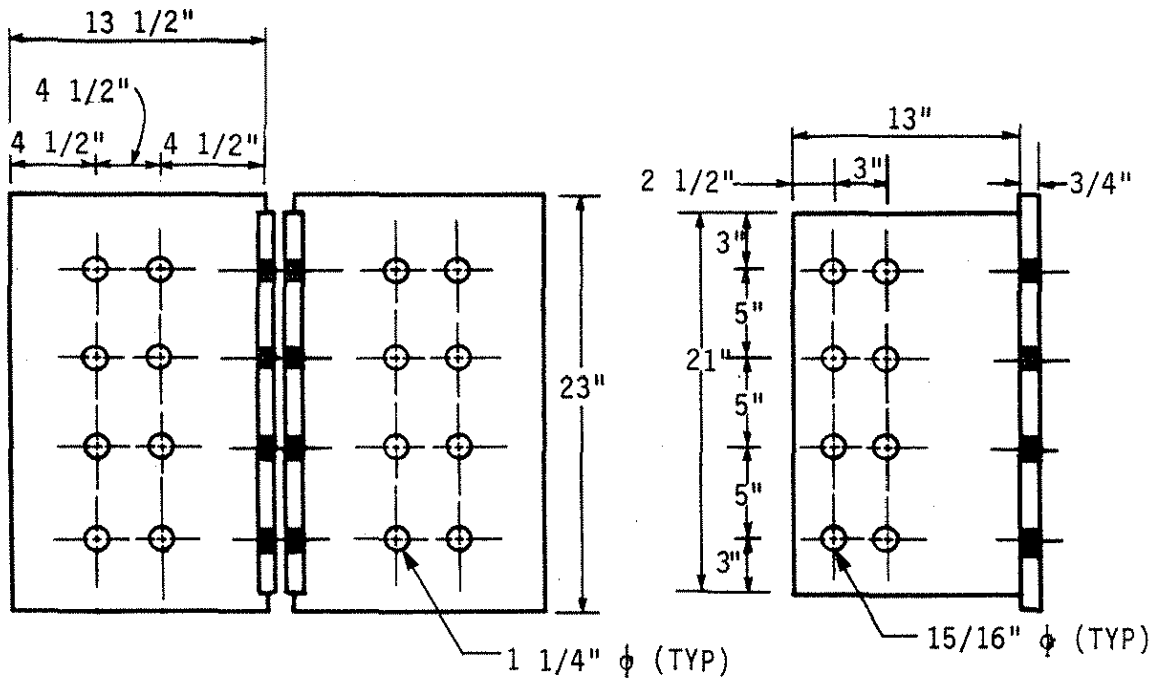
These brackets, seen in Figs 1.10 and 1.11, respectively, are a result of modifications on Bracket 1. As can be seen, approximately 50% of the area of the stiffener plates was removed from Bracket 1 to make Bracket 3, and approximately 66% of the area of the stiffener plates was removed from Bracket 1 to make Bracket 4. The amount and location of material removed was determined by a finite-element analysis of the bracket. Additional information and the results of this analysis will be presented in Section 4.1.1.

2.2. Model Bridge

2.2.1. Description

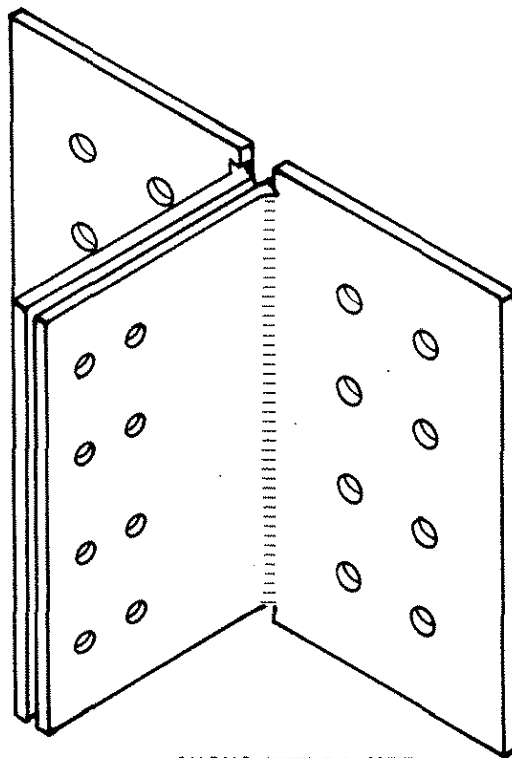
The model bridge (see Fig. 1.12) was constructed to be, as nearly as possible, a 1/3-scale replica of a three-span V12 (1957) bridge. The scale was selected to make the model as large as possible, yet capable of fitting within the confines of the laboratory.

As shown in Fig. 1.12, the steel frame is composed of four longitudinal beams connected transversely by 24 diaphragms. As previously noted, this model was originally fabricated for the testing programs of HR-287; thus, additional information on the framing and structural details can be found in Ref. 7. Note that the exterior stringers are 1 in. shallower than the interior stringers, which correctly models the 3 in. difference in stringer height found in the



a. FRONT VIEW

b. SIDE VIEW



c. AXONOMETRIC VIEW

Fig. 1.7. Web bracket (Bracket 2).

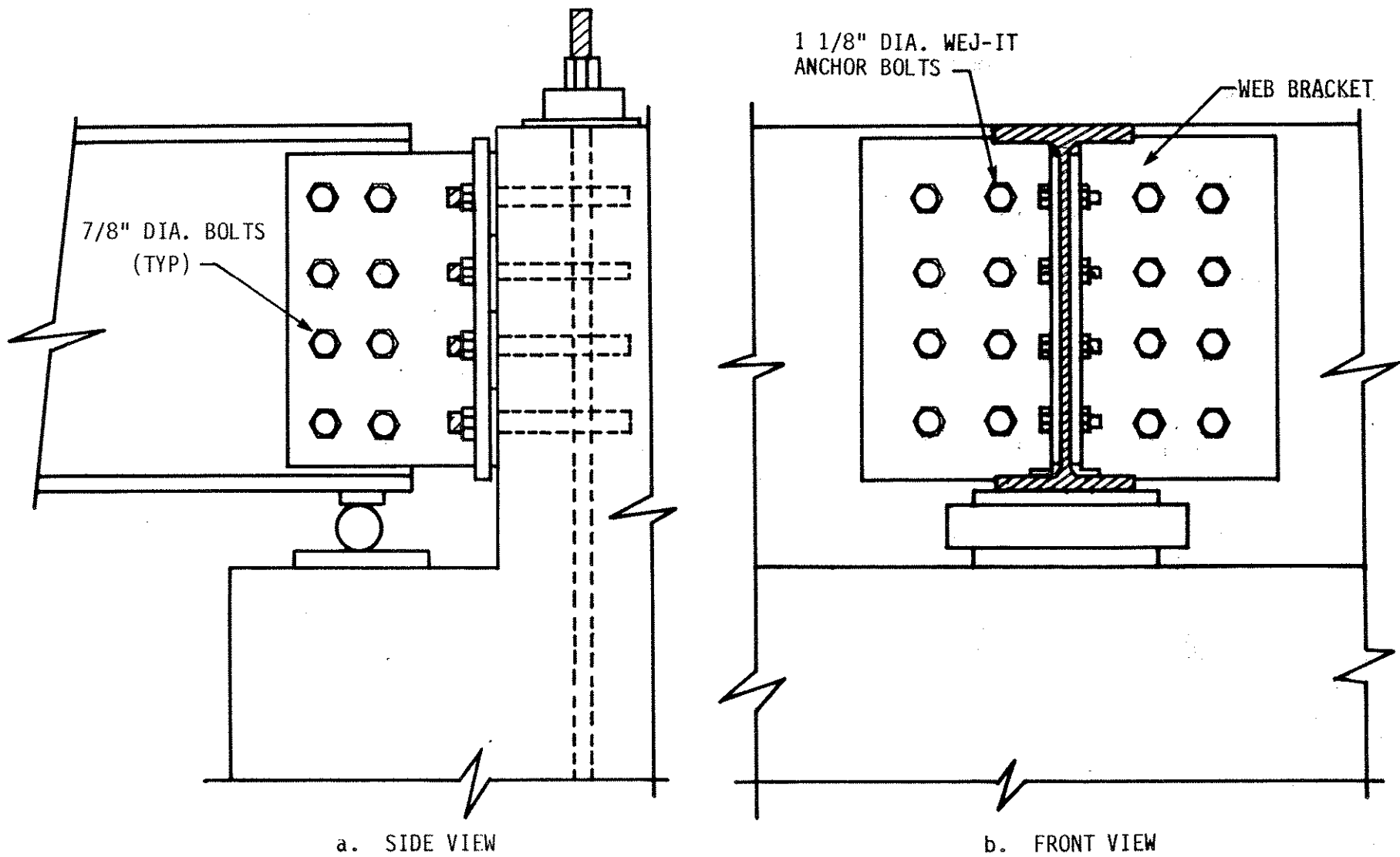
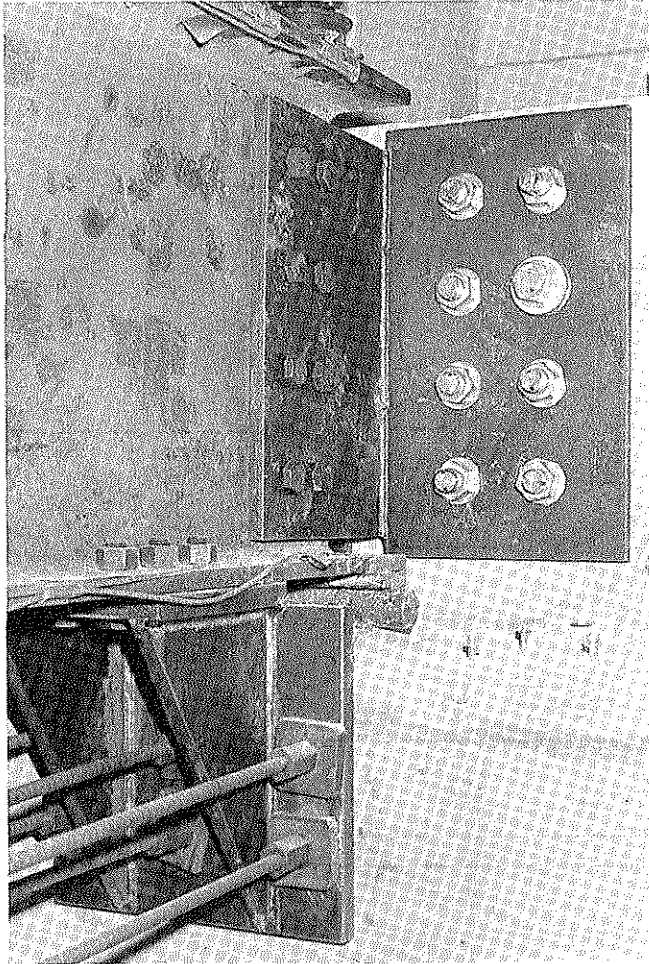
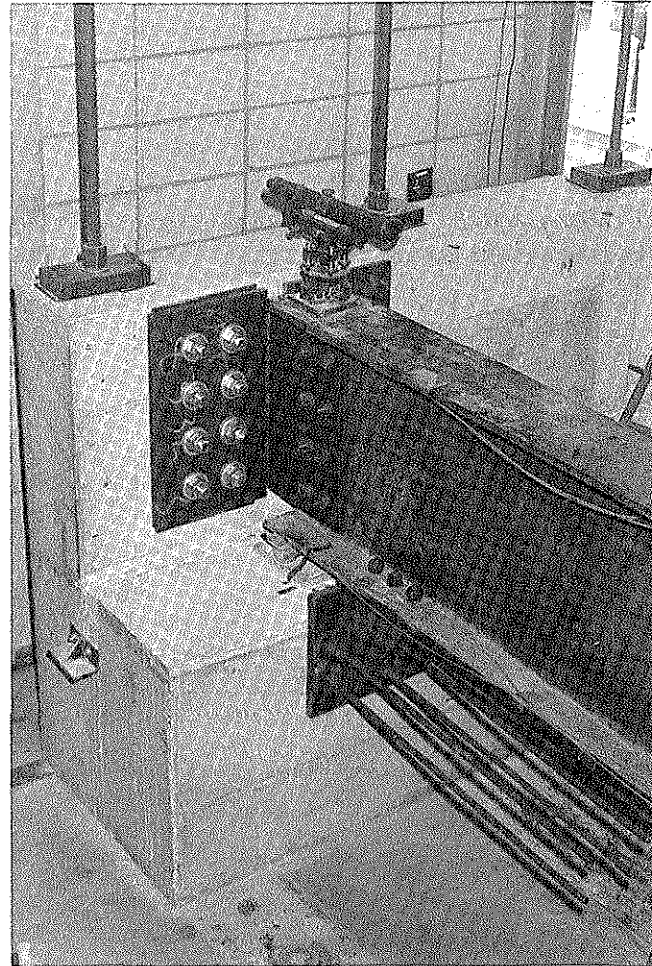


Fig. 1.8. Attachment of Bracket 2.

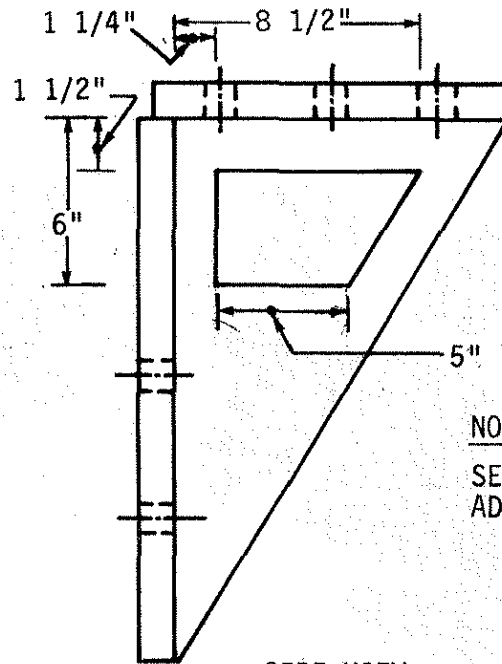


a. CLOSEUP VIEW



b. OVERALL VIEW

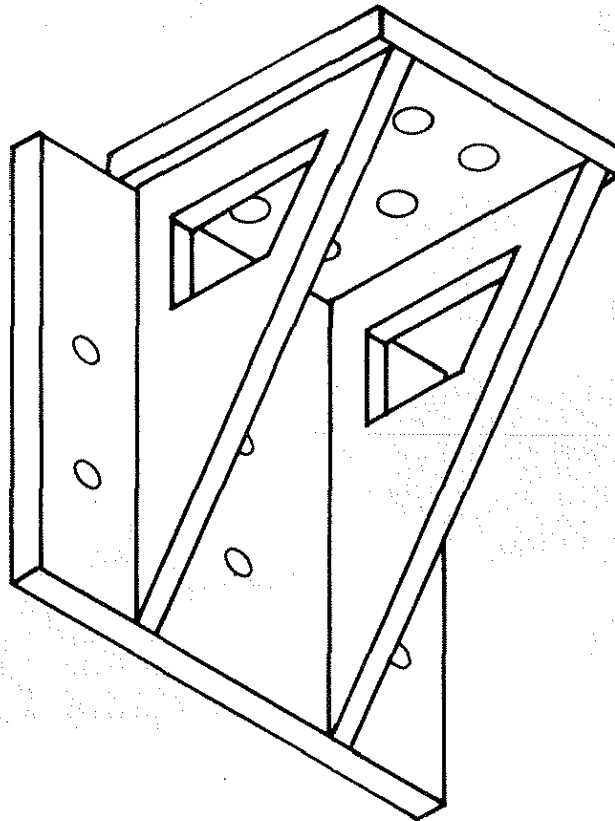
Fig. 1.9. Photographs of Bracket 1 and Bracket 2 in place.



NOTE:

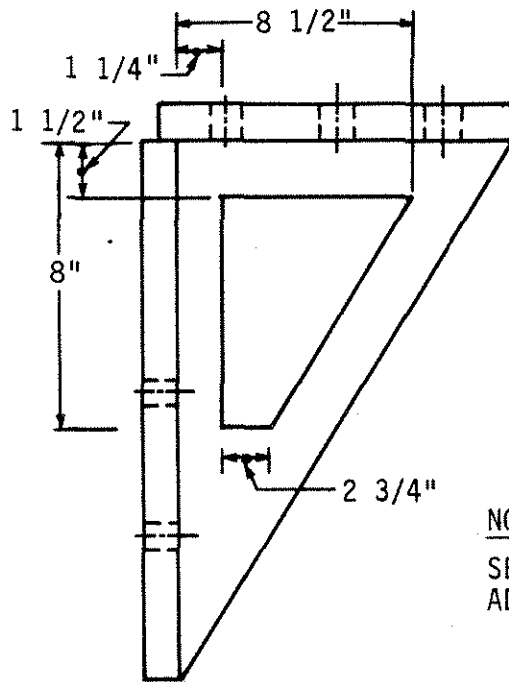
SEE FIG. 1.4 FOR
ADDITIONAL DIMENSIONS

a. SIDE VIEW



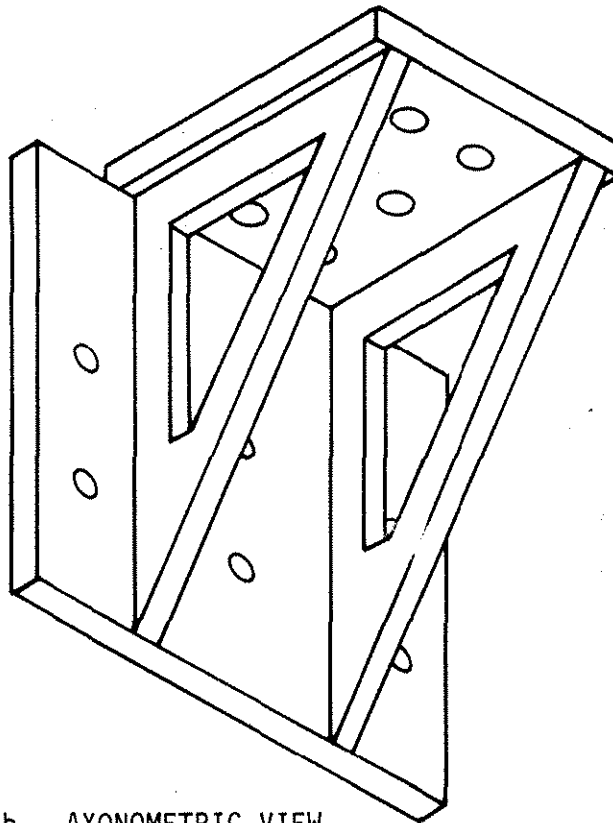
b. AXONOMETRIC VIEW

Fig. 1.10. Bracket 3.



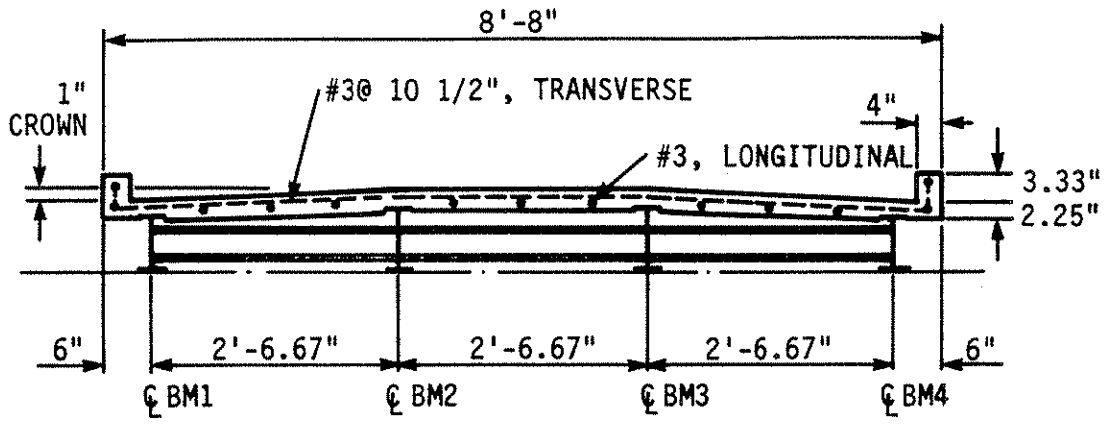
NOTE:
SEE FIG.1.4 FOR
ADDITIONAL DIMENSIONS

a. SIDE VIEW

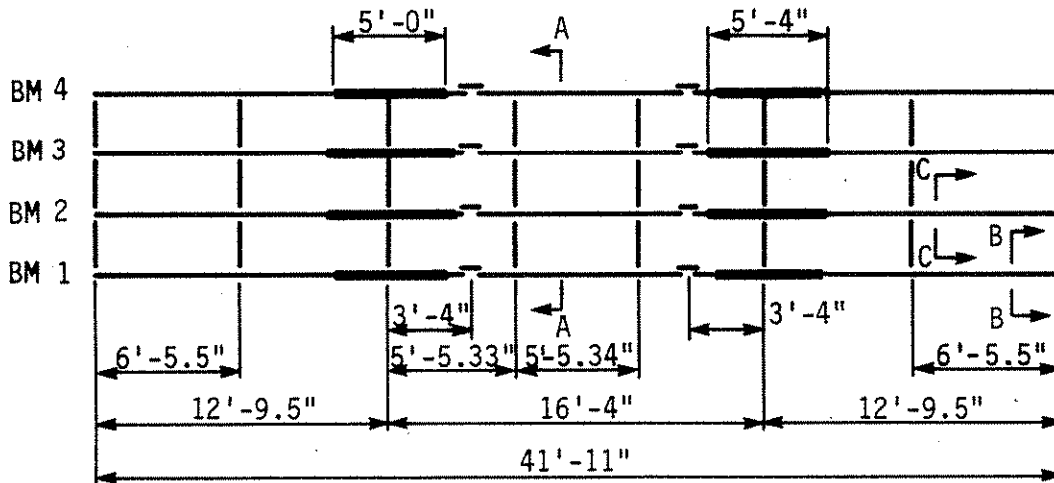


b. AXONOMETRIC VIEW

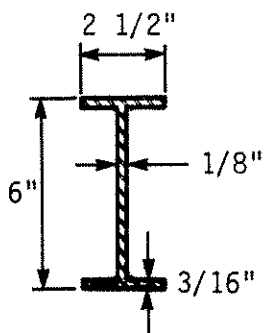
Fig. 1.11. Bracket 4.



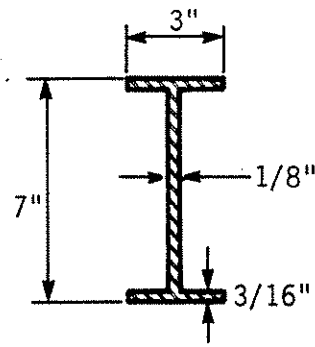
a. CROSS SECTION AT MIDSPAN (SEC A-A)



b. PLAN VIEW



c. SECTION B-B



d. SECTION C-C

Fig. 1.12. Model bridge.

prototype. The dimensioning of the bridge model follows the principles of similitude; hence it will respond to loading essentially in the same manner as the prototype.

The model bridge is supported on four reinforced concrete walls 10 in. wide, 3 ft high, and 12 ft 6 in. long. At each abutment or pier, each longitudinal girder is supported on a roller that is placed on a 1/2-in. steel plate that was grouted on the abutment or pier.

As is the general case when a bridge is modeled, the bridge weight is not adequately represented. Because of the insufficient amount of dead weight on the bridge, there was concern that the bridge would lift off the supports. In order to prevent uplift of the model bridge caused by various end restraint and vertical loading conditions, tiedowns were fabricated and placed at each stringer support. These tiedowns were designed to prevent uplift, but to permit horizontal movements.

2.2.2. Physical Properties

A complete summary of the concrete and steel properties can be found in the final report for HR-287 [7]. However, the material properties that are of relevance to this project are the compressive strength of concrete and the modulus of elasticity of steel. The compressive strength of the deck and curb are 3450 psi and 3355 psi, respectively. The modulus of elasticity of the steel beams and Dywidag tendons are assumed to be 29,000 ksi and 24,000 ksi, respectively.

2.2.3. Bracket Configurations

The brackets used on the model bridge are a 1/3-size replica of Brackets 1 and 2 used on the test beam (see Figs. 1.4 and 1.6). Due to the size of the model bridge, certain adjustments had to be made with respect to how the brackets were to be attached to the abutments; these modifications are illustrated in Fig. 1.13. For instance, instead of post-tensioning the individual bottom flange brackets to the abutment, they were welded onto a 21 3/4-in. \times 122 1/2-in. \times 1/4-in. thick steel plate. The plate extended along the full length of the abutment and was epoxied to it. This plate was post-tensioned with four 5/8-in.-diameter Dywidag bars at each corner of the four bottom flange brackets, and one Dywidag bar through the middle of each bracket. This had to be done because the smallest diameter Dywidag bar was 5/8 in. and the minimum spacing requirements to develop its full capacity exceeded the confines of the brackets. The back wall of Abutment 1 to which the web bracket was anchored

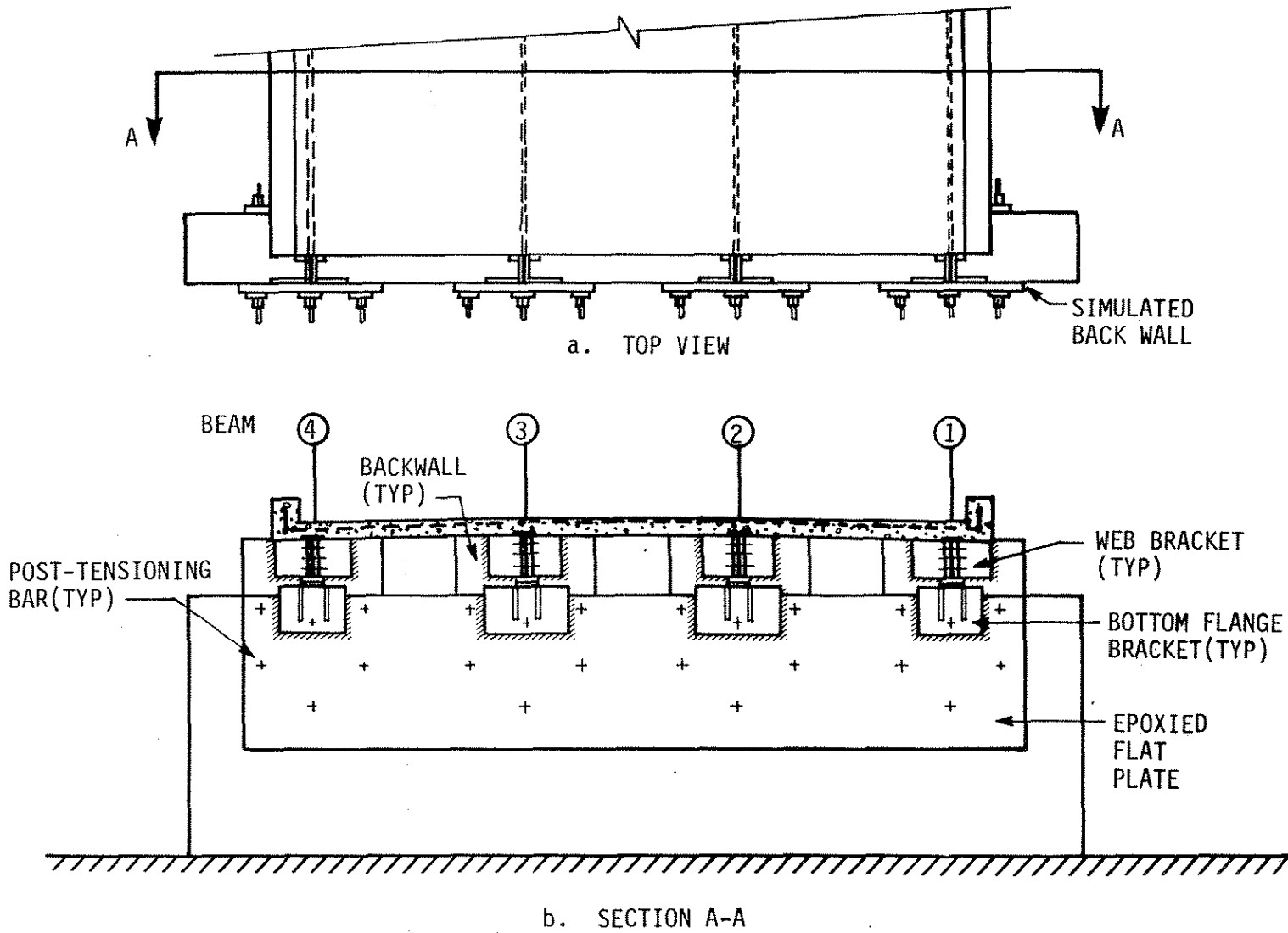


Fig. 1.13. Restraint brackets on bridge stringers.

was built up by using steel plates on the model bridge abutment. The thickness of the built-up backwall is 1 in., resulting in a stiffness proportionally equivalent to the stiffness of Abutment 1 used with the test beam. The web connections were then bolted to the beam webs with 1/2-in.-diameter A449 bolts and welded to the back plates. Figures 1.14 and 1.15 show the details of the bridge connections, which are typical for both interior and exterior beams. Due to the small scale of the model, it was necessary to remove the abutment diaphragms at the restrained end. This would probably not be the case in the field because of the larger surfaces available for attaching the brackets. A photograph of the bridge brackets in place is shown in Fig. 1.16.

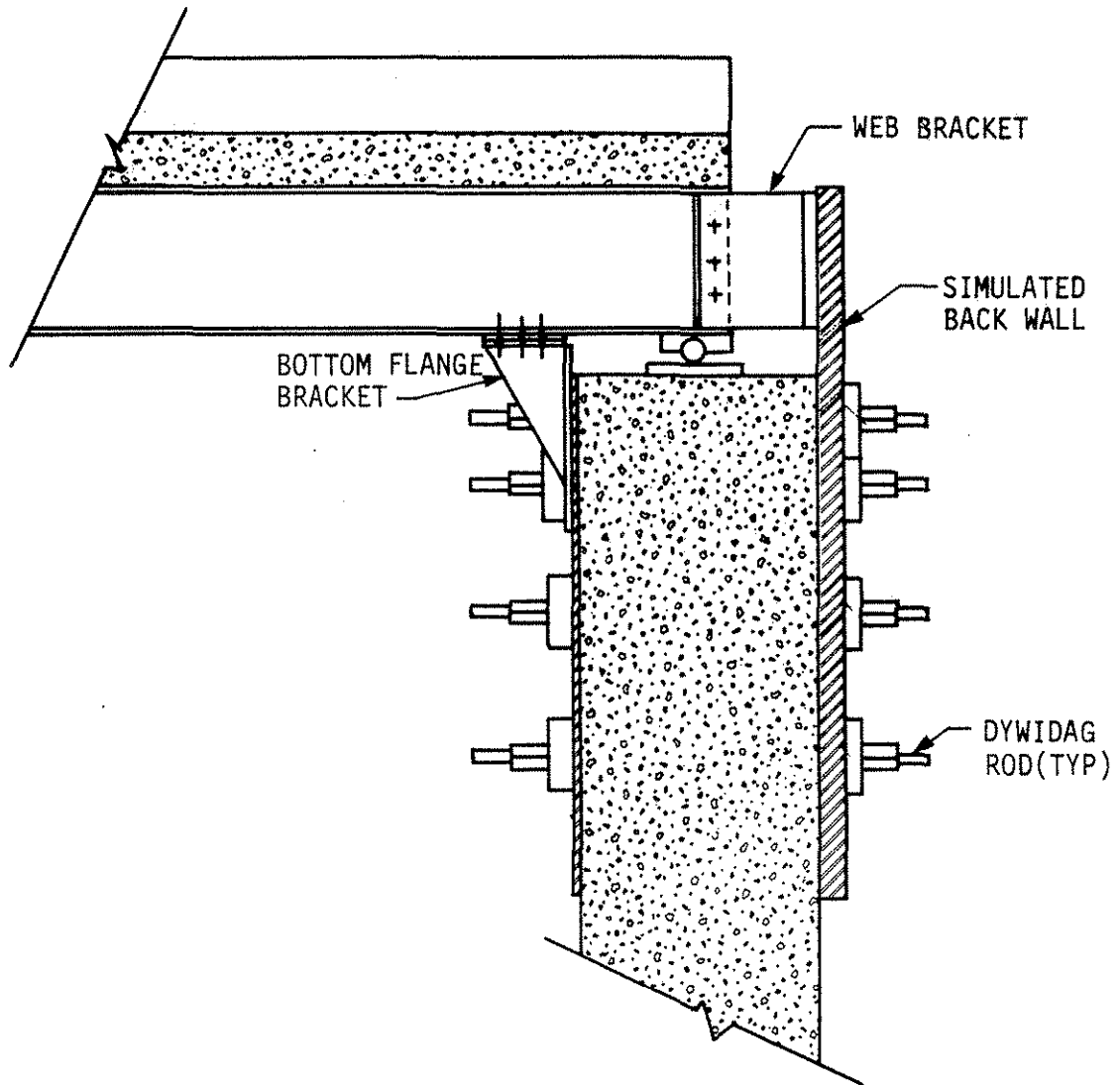


Fig. 1.14. Side view of bridge brackets in place.

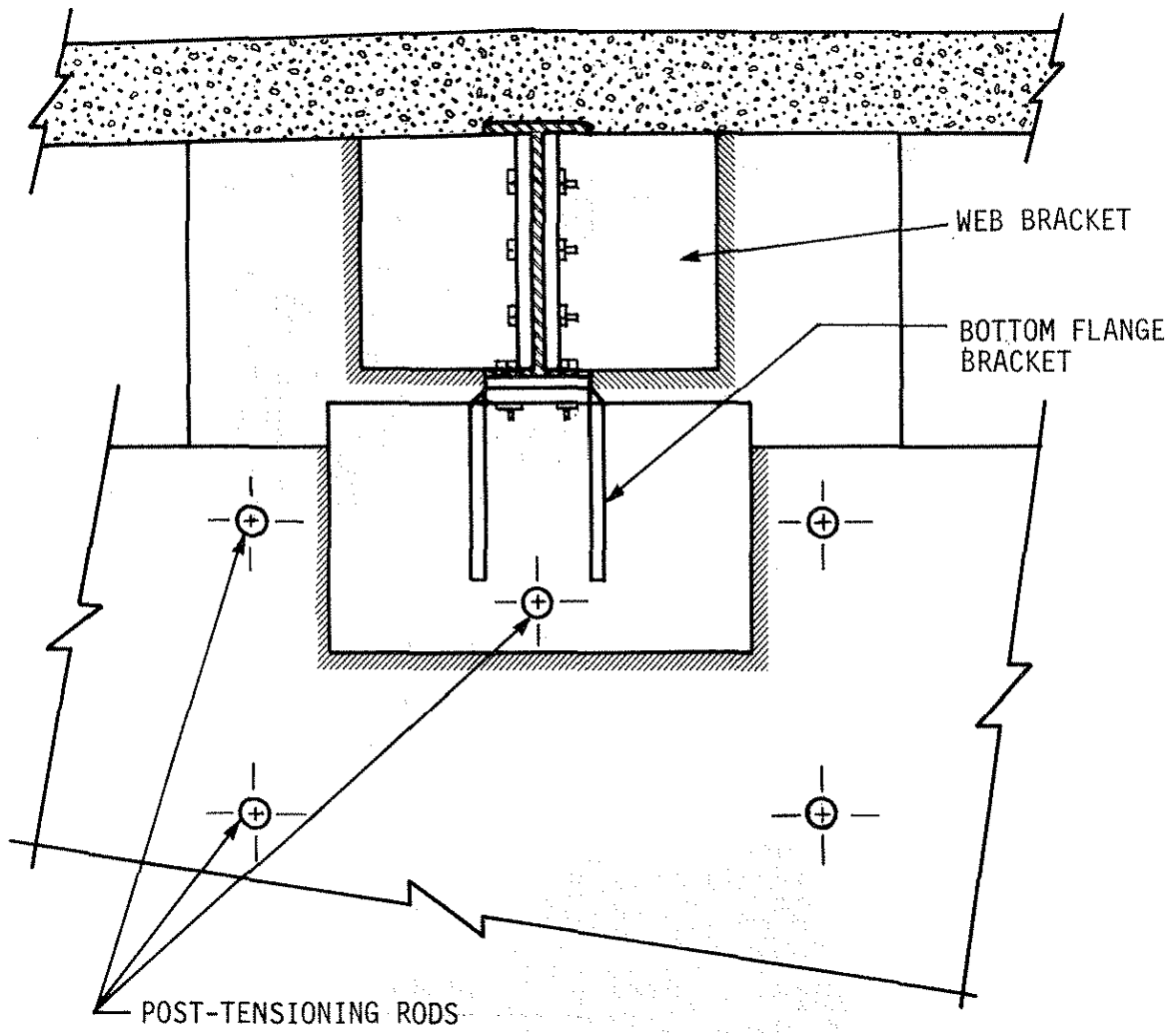
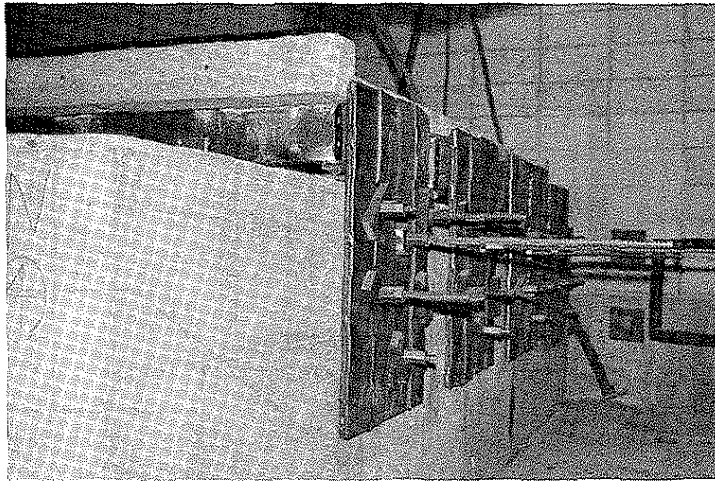
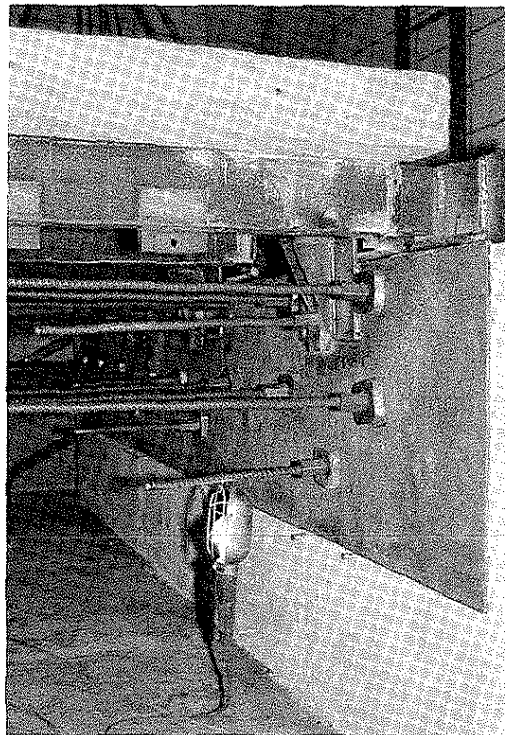


Fig. 1.15. Front view of bridge brackets in place.



a. VIEW OF SIMULATED BACK WALL



b. FRONT VIEW OF ABUTMENT

Fig. 1.16. Photographs of bridge brackets.

3. TESTS AND TEST PROCEDURES

This section outlines the details of the specific tests and events that occurred during the course of the experimental portion of this investigation. In this section, only test setups, instrumentation, and procedures will be outlined; discussion and analysis of the results as well as the behavior of the test beam and model bridge will be presented in Chapter 5.

The instrumentation for all tests consisted of electrical-resistance strain gages (strain gages) and direct current displacement transducers (DCDTs). In addition to this instrumentation, a mechanical displacement dial gage (deflection dial) and a transit to measure beam rotations were employed in the testing of the test beam.

The temperature-compensated strain gages were attached to the specimens by recommended surface preparation and adhesives. Three-wire leads were used to minimize the effect of the long lead wires and temperature changes. All strain gages were waterproofed with a minimum of two layers of protective coatings. Strain gages and DCDTs on the test beam and bridge model were monitored and recorded with a computerized data acquisition system (DAS). Deflections measured by the deflection dial and transit were read and recorded by hand in all tests.

3.1. Test Beam

3.1.1. Test Beam Instrumentation

Tests conducted on the beam focused on providing insight into the effects of end restraint on end rotations, beam deflections, and strain distribution. To accomplish this, a total of 20 strain gages were mounted on the beam. Figure 1.17 indicates the location of the strain gages; at each of the five sections instrumented, four strain gages were oriented with their axes parallel to the axis of the beam. Two of the four were on the bottom surface of the top flange of the beam and two were on the top surface of the bottom flange. All strain gages were placed 5/8 in. in from the flange edge.

Three DCDTs were utilized to measure the vertical displacements along the beam. As shown in Fig. 1.17, these DCDTs were placed at the quarter points.

Alternate methods of measuring beam rotations at the restrained end were researched. These included the use of various combinations of displacement transducers and strain gages. However, many of the systems reviewed were still in the developmental stages and thus

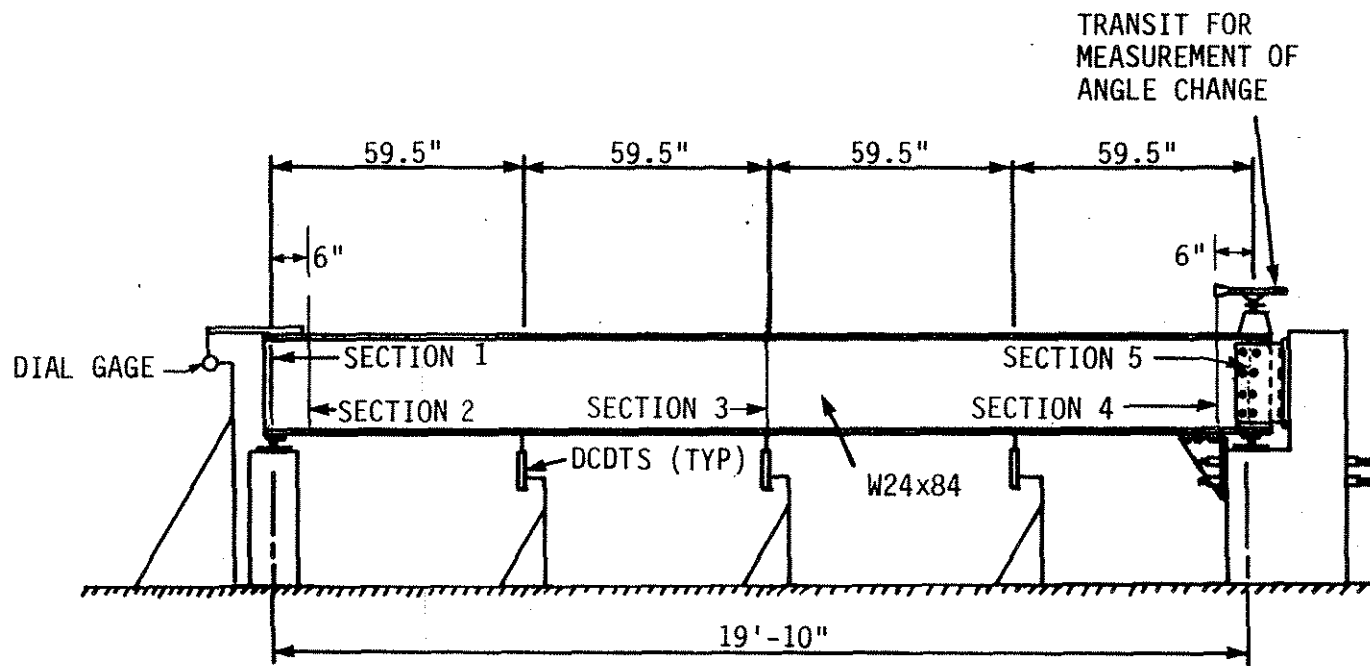


Fig. 1.17. Test beam instrumentation.

sufficient information was not available. After considering the various options, researchers decided to use a transit for two main reasons: first, data could be read and recorded directly and second, the Department of Engineering Science and Mechanics at ISU has had great success in measuring rotations with a transit. By sighting through the transit one can determine the rotation that the axis of the transit experiences as the beam is loaded by noting the changes in readings on a distant calibrated scale; in this case the scale was mounted on the far wall of the laboratory. The transit was mounted on the top flange of the beam to measure the rotation at the restrained end. An illustration of this technique is shown in Fig. 1.18. The smallest division that could be read on the scale was 1/16 in. As the distance from the transit to the wall was 876 in., it was possible to detect changes in rotation at the restrained end as small as 7×10^{-5} rad.

The rotation at the unrestrained end was also measured. A steel rectangular plate was clamped to the top flange of the beam and a deflection dial was placed 12 in. from the centerline of support (see Fig. 1.18). Hence, the rotation was determined by dividing the deflection of the plate by the lever arm distance. With this arrangement it was possible to measure angles as small as 8×10^{-5} rad. A transit could not be used at this end because of sighting restrictions. However, after several tests no significant change in this rotation was noticed; therefore, these results will not be discussed.

Figure 1.19 illustrates the method in which the beam was loaded. A load cell centered on the spreader beam monitored the 5-kip load increments that were desired. A hydraulic cylinder attached to the test frame supplied the desired vertical force. The spreader beam produced a two-point loading on the beam. A photograph of the loading scheme can be seen in Fig. 1.20. Two-point loading rather than one-point loading was chosen in an attempt to provide a region of pure bending moment and to avoid large stress concentrations due to the presence of a concentrated load at midspan, thus resulting in unrealistic strain readings at midspan. The spreader beam had to have a tubular cross section in order to permit sighting through it to the far wall for taking deflection readings. The beam was stiffened to prevent any lateral buckling and had a capacity of 35 kips. Therefore, the test beam was loaded to only 35 kips. This load produced a sufficient magnitude of strains, deflections, and rotations in the test beam.

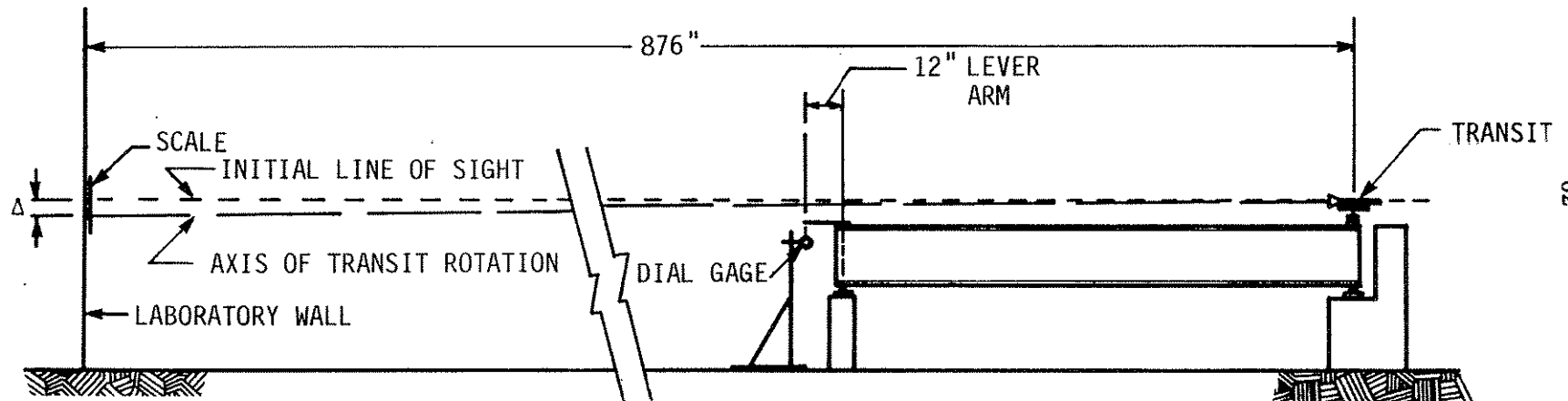


Fig. 1.18. Determination of rotation at the supports.

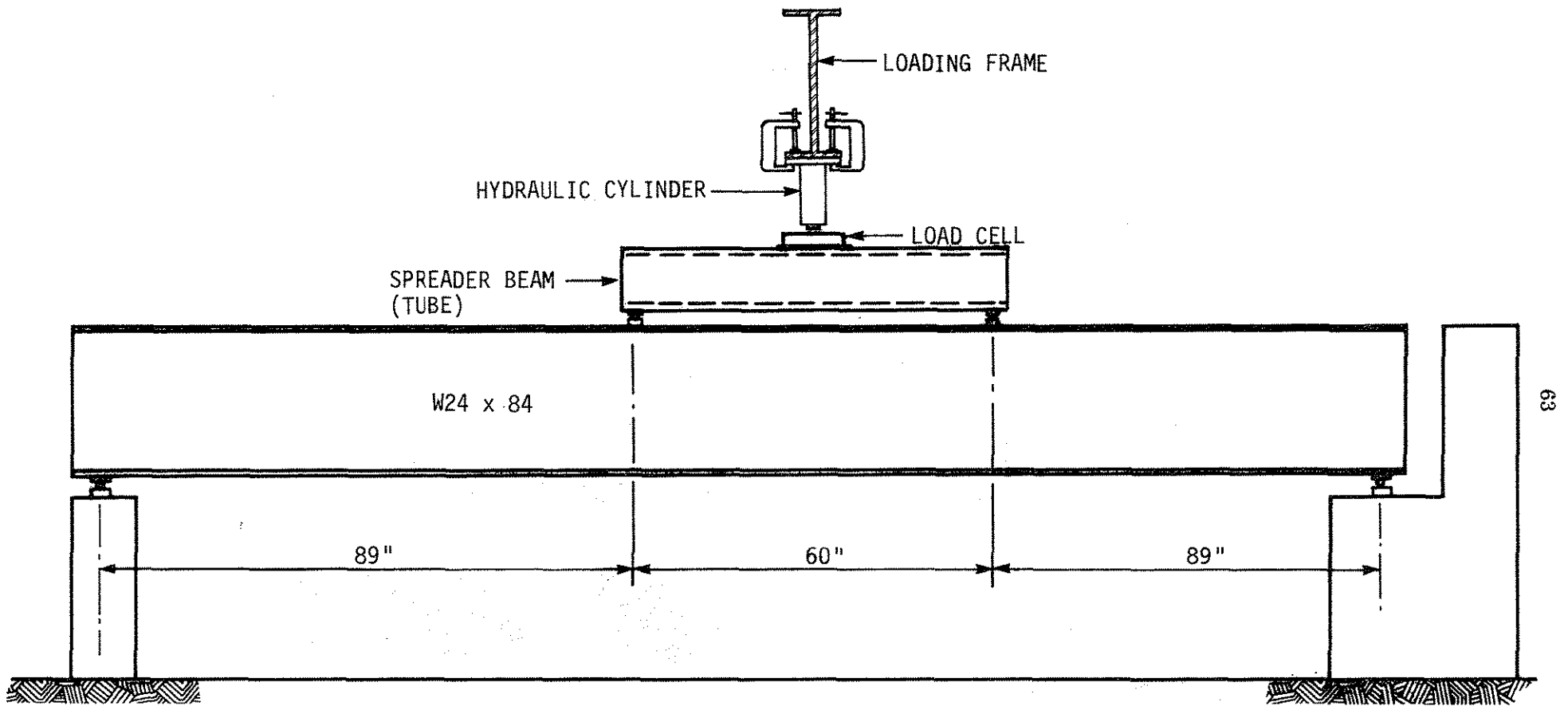
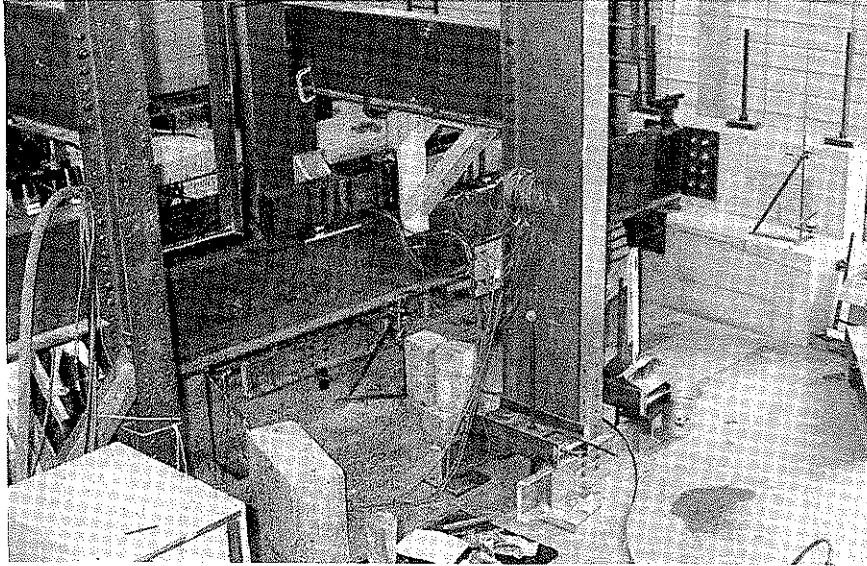
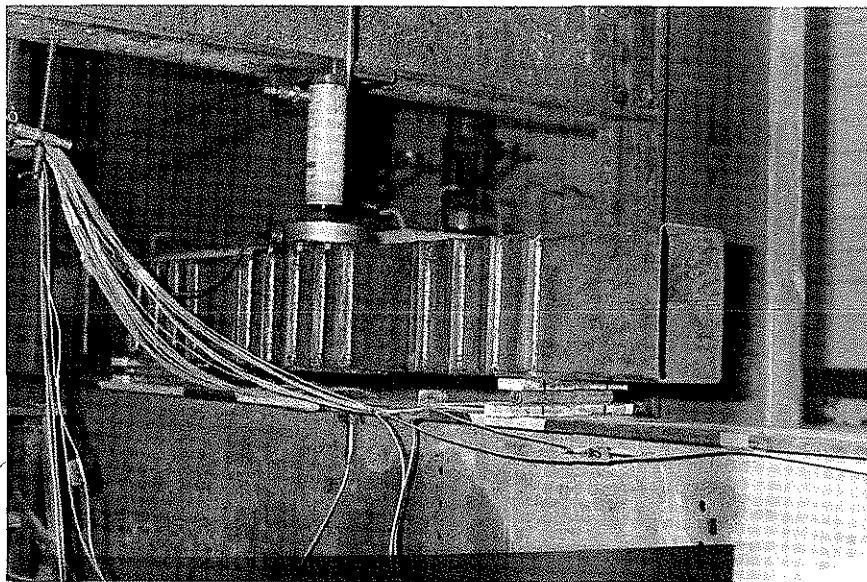


Fig. 1.19. Loading of test beam.



a. GENERAL VIEW OF BEAM



b. CLOSEUP VIEW OF LOADING APPARATUS

Fig. 1.20. Photographs of loading scheme.

3.1.2. Beam Tests

A series of seven tests was performed; each test used a different end-restraint mechanism. The general procedure in each of the tests followed several steps:

1. Record "zero" strain readings and "zero" deflection readings with the DAS. Level the transit and "zero" the deflection dial.
2. Apply the predetermined increment of force.
3. Take strain gage and DCDT readings as in Step 1. Record the transit reading and the deflection dial reading.
4. Repeat Steps 2 and 3 until the desired load is reached. The total applied load is 35 kips, which is the magnitude of load used in the analysis.
5. Release force slowly.
6. Take a final reading for strains and deflections.

3.1.2.1. Test 1 - No Restraint Provided

The objective of this test was to obtain base data on the behavior of the beam under no restraint conditions. The results of this test, along with the results of the other tests, will be presented and discussed in Chapter 5. However, it is noteworthy to mention at this point that some restraint did initially exist because a perfect hinge or roller did not exist at the supports; that is, some restraint was present.

3.1.2.2. Tests 2 through 7 - Variations in the Degree of Restraint Provided

As previously mentioned, all tests followed essentially the same procedure; the only variable was the restraint configuration. The various tests with the restraint condition used are listed in Table 1.1.

Test 1 was repeated after all testing was completed in order to make sure that the same base data could be reproduced. The reason for this is that testing was conducted over a period of several months and the researchers wanted to check the replication of the initial data.

A review of the seven tests presented in Table 1.1 reveals that seven different degrees of restraint were investigated. These ranged from initially no restraint (Test 1) to an approximation of complete fixity (Test 3). The restraint used in the other five tests fell between these two limits.

Table 1.1. Description of beam tests.

Test No.	Restraint Condition			
	Web Bracket 2	Flange Brackets		
		1	3	4
1*				
2		X		
3**	X	X		
4			X	
5	X		X	
6				X
7	X			X

*Test 1 depicted the case of a simply supported beam.

X Refers to brackets that are acting (see descriptions in Sections 2.1.3.1 through 2.1.3.3).

**Figure 1.9 illustrates the maximum restraint condition.

3.2. Model Bridge

3.2.1. Model Bridge Instrumentation

A total of 64 strain gages were mounted on the four beams in the bridge model. Figure 1.21 indicates the location of the strain gages; at each of the 16 sections instrumented, four strain gages were oriented with their axes parallel to the axis of the beam. Two of the four strain gages were on the top surface of the top flange of the beam and two were on the bottom surface of the bottom flange. All strain gages were placed at a distance equal to one-sixth the flange width from the flange edge, approximately 1/2 in. Since the strain gages had been mounted for a previous research project (HR-287 [7]), and some had suffered mistreatment in the interim period, approximately ten of them did not give stable output readings. These

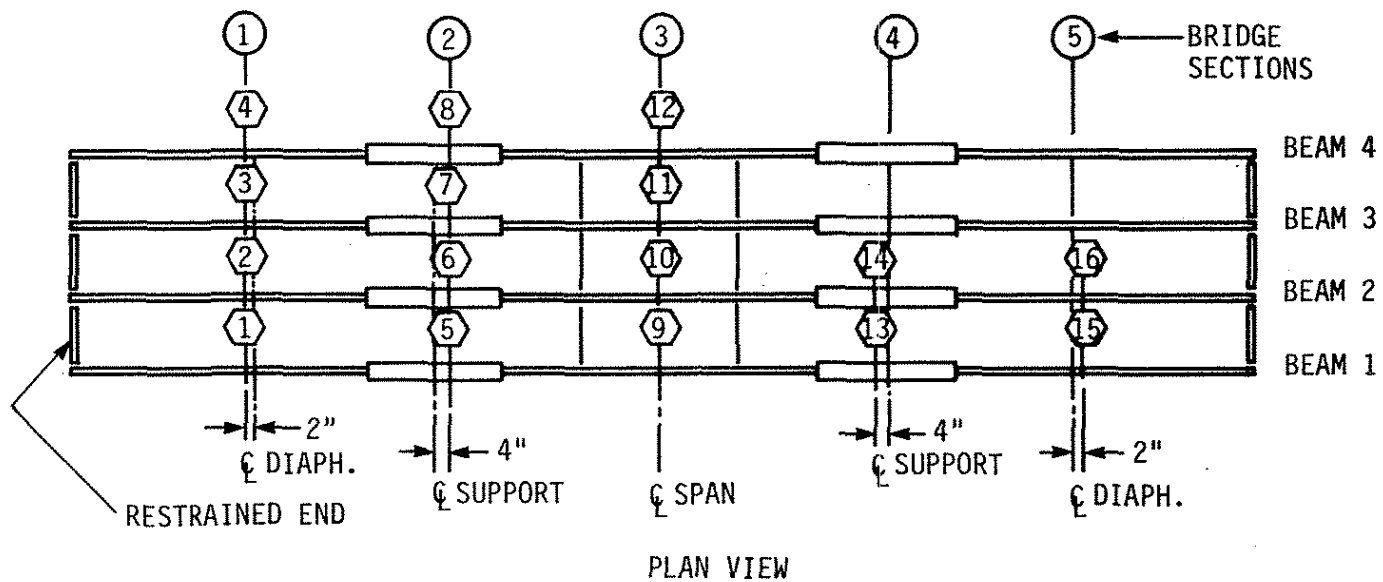


Fig. 1.21. Locations of strain-gage sections.

gages were not replaced either because they were at a location that was not considered critical to this project or because, given the symmetry of the bridge, gages on other beams provided the desired readings. As may be seen in Fig. 1.21, the majority of the instrumentation was on Beams 1 and 2; however, sufficient instrumentation was placed on Beams 3 and 4 so that symmetry could be verified.

Twelve DCDTs were utilized to measure the vertical displacements of the beams. These DCDTs were placed at the center of each beam in each span (see Fig. 1.22).

As shown in Fig. 1.21, longitudinal beams of this bridge were identified as Beams 1 through 4 and the strain gage sections were sections 1 through 16; thus, a particular region of a given beam can be identified by beam and section number.

3.2.2. Model Bridge Tests

For clarity, the bridge testing program has been subdivided into two parts according to the type of loading used. Each part involved seven different tests conducted on the bridge, providing a total of 14 tests on the bridge model. The individual tests represent various end-restraint conditions.

The following procedure (similar to that used in the beam tests) was used in each of the tests:

1. Record "zero" strain and "zero" deflection readings with the DAS.
2. Place the load(s) at the desired location(s).
3. Take strain gage and DCDT readings as in Step 1. Record any behavioral changes.
4. Repeat Steps 2 and 3 until the load(s) have been positioned at all desired locations.

Loading for the model consisted of a 3-ft \times 3-ft \times 4-ft-8-in. concrete block that has a 1-ft \times 1-ft. \times 4-in. concrete block integral with its base. This approximates a concentrated load and simplifies placing the weight on the bridge (see Fig. 1.23). Two such concrete weights were constructed in the laboratory. The actual weights of the blocks were 6020 lbs and 6010 lbs; however they will be referred to as 6-kip loads in the remainder of this report. The various tests and restraint conditions are shown in Table 1.2. These loads were positioned at various locations; these are shown in Fig. 1.24.

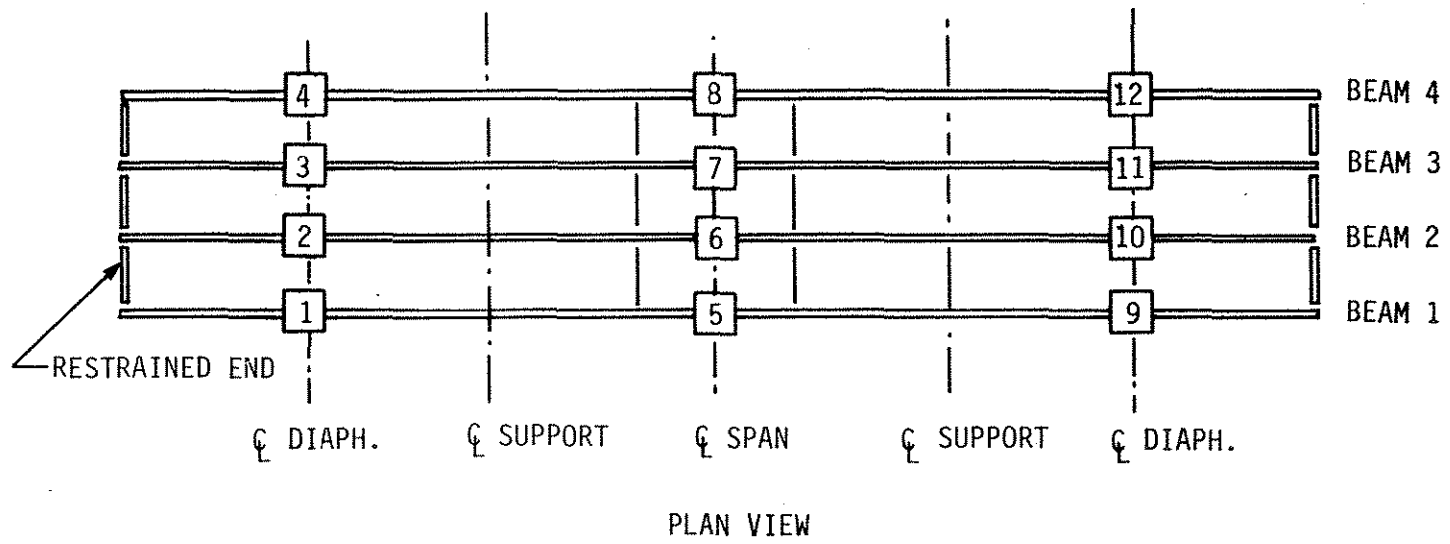


Fig. 1.22. Location of DCDTs.

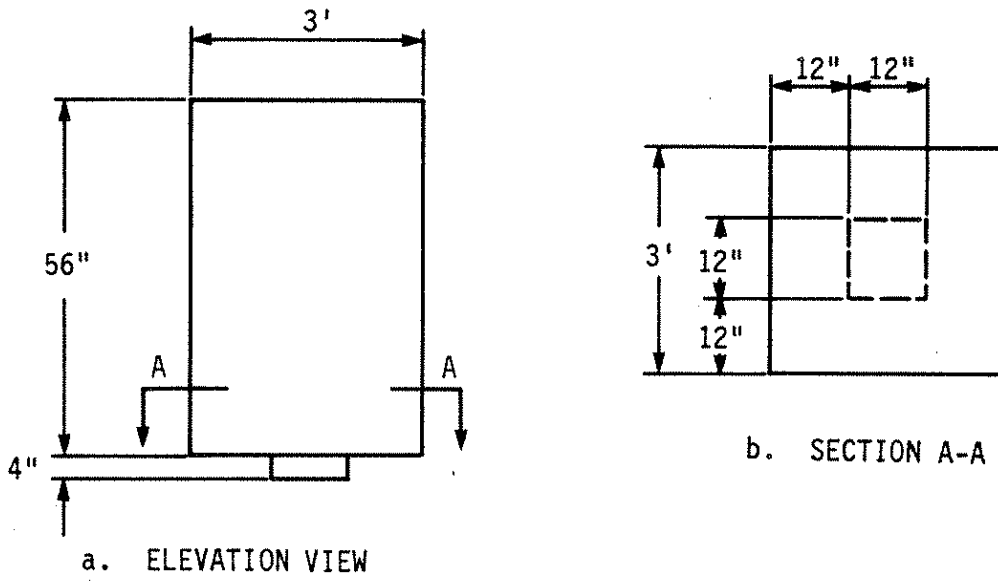


Fig. 1.23. Concrete dead weight.

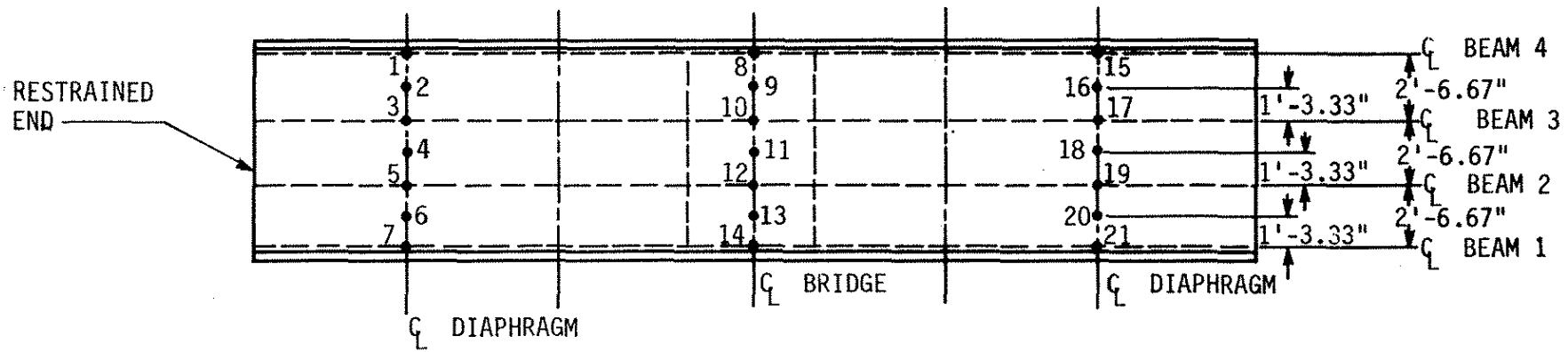


Fig. 1.24. Locations of vertical load points.

Table 1.2. Restraint provided in various bridge tests.

Test No.	Beams							
	1		2		3		4	
	Bottom Flange	Web						
1								
2	X						X	
3	X		X		X		X	
4	X	X	X	X	X	X	X	X
5							X	X
6					X	X		
7			X		X			

X Restraint provided.

3.2.2.1. Vertical Load Tests with One Concentrated Load

For these tests, one 6-kip load was placed on a 12-in. × 12-in. × 1-in. neoprene pad at the various loading points. As indicated in Table 1.3, the load was applied at ten points (1–6 and 10–13). The other points were not loaded for either of two reasons: One, the crane was unable to reach these points because of their proximity to the laboratory walls, as was the case with Points 7, 14, and 21. Otherwise, the effects of restraint were considered to be minimal, as was the case with load points 15 through 20 located in the span farthest from the restraint. The effects of restraint became evident after the preliminary test results were examined, which indicated that the magnitude of strains in the middle span compared to the magnitude of strains in the adjacent restrained end span where the load was applied were much smaller (see Section 6.1). Thus, it was concluded that it would not be beneficial to load the span farthest from the restrained end.

3.2.2.2. Vertical Load Tests with Two Concentrated Loads

These tests involved placing two 6-kip loads simultaneously at various loading points on the bridge. The various combinations investigated are given in Table 1.3. These load combinations were chosen based on pattern loading arrangements to produce maximum positive moments along the bridge and maximum negative moments over the supports. For these tests, all three spans were loaded at various times with the two weights depending on the desired effects.

Table 1.3. Location of vertical load for tests of model bridge.

Loads	Vertical Loading Points*																			
	1	2	3	4	5	6	7	8	9	10	11	12	13	14	15	16	17	18	19	20
One Conc.	X	X	X	X	X	X				X	X	X	X							
Two Conc.			X X	X X	X X	X X				X	X	X	X				X	X	X	X

X = Loaded

* See Fig. 1.24 for location of load points.

4. FINITE-ELEMENT ANALYSIS

This chapter describes the analytical investigation of the behavior of the bottom flange bracket, test beam, and bridge model previously discussed in Chapter 2. One of the objectives of this work was to validate the experimental results obtained; however, with this model, other structures can be analyzed. This analytical work is organized into two sections; each section describes a different finite-element software program used in the analysis. The finite-element software used in analyzing the bottom flange bracket and test beam was ANSYS, while SAP IV was used for the analysis of the model bridge. SAP IV, rather than ANSYS, was chosen to model the bridge because it had been used successfully on continuous bridges investigated in other research projects.

4.1. Finite-Element Software: ANSYS

ANSYS—a large-scale, user-oriented, general purpose finite-element program for linear and nonlinear systems—has a wide range of analysis capabilities. The program contains a library of more than 70 elements. One of the main advantages of ANSYS is the integration of the three phases of finite element analysis: preprocessing (i.e., data input), solution, and postprocessing (i.e., formulated results). Preprocessing routines in ANSYS define the model, boundary conditions, and loadings. Displays may be created interactively on a graphics terminal as the data are input to assist with model verification. Postprocessing routines may be used to retrieve analysis results in a variety of ways. In addition to providing the results in tabular form, plots of the structure's deformed shape and stress or strain contours can be obtained at this stage.

4.1.1. Bottom Flange Bracket Model

The main purpose of modeling the bracket was to determine the effect that removing material from the stiffener plates of Bracket 1 would have on the overall behavior of the bracket. In addition to this, the magnitude of forces and stress levels in the bracket could be examined. Information obtained from this analysis would then be used in modeling the test beam and bottom flange bracket setup. This objective was achieved by developing a model that was flexible, thereby permitting convenient additions or removal of material. Because of symmetry conditions, it was necessary to model only one-half of the bracket in the finite-

element analysis. Symmetry boundary conditions were imposed on the two edges shown in Fig. 1.25. The bracket was initially analyzed by using three different meshes consisting of quadrilateral shell elements, as shown in Fig. 1.26. The results of these analyses were compared, and the model in Fig. 1.26c was chosen for further analysis because its configuration was easier to alter, it saved on computer time, and the results were essentially the same as those obtained from the finer meshes.

With the most adaptable configuration of the bracket idealized, emphases shifted toward analyzing the effects of material reduction on bracket behavior. To obtain information on the bracket response to removing material, a total of seven bracket alterations were analyzed. These are illustrated in Fig. 1.27. For all bracket configurations, the maximum displacement occurred at the same location (see Fig. 1.25); therefore, this displacement was chosen as a basis for comparison of bracket behavior. The results of the analysis are shown in Table 1.4.

Table 1.4. Comparison of various bracket alterations.

Bracket Type	Deflection in.	% Increase in Deflection
No reduction (Bracket 1)	0.151	-
Reduction 1	0.167	10.13
Reduction 2	0.177	16.62
Reduction 3	0.190	25.42
Reduction 4	0.160	5.47
Reduction 5	0.187	23.23
Reduction 6	0.229	50.64
Reduction 7	0.252	66.06

According to the above, the most significant increase in bracket deflection occurred with the sixth and seventh material reductions. Hence, Bracket 1 was modified to conform to the shape resulting from Reductions 6 and 7. Based on these Reductions, Bracket 1 was altered to become Brackets 3 and 4 (see Section 2.1.3.3), respectively.

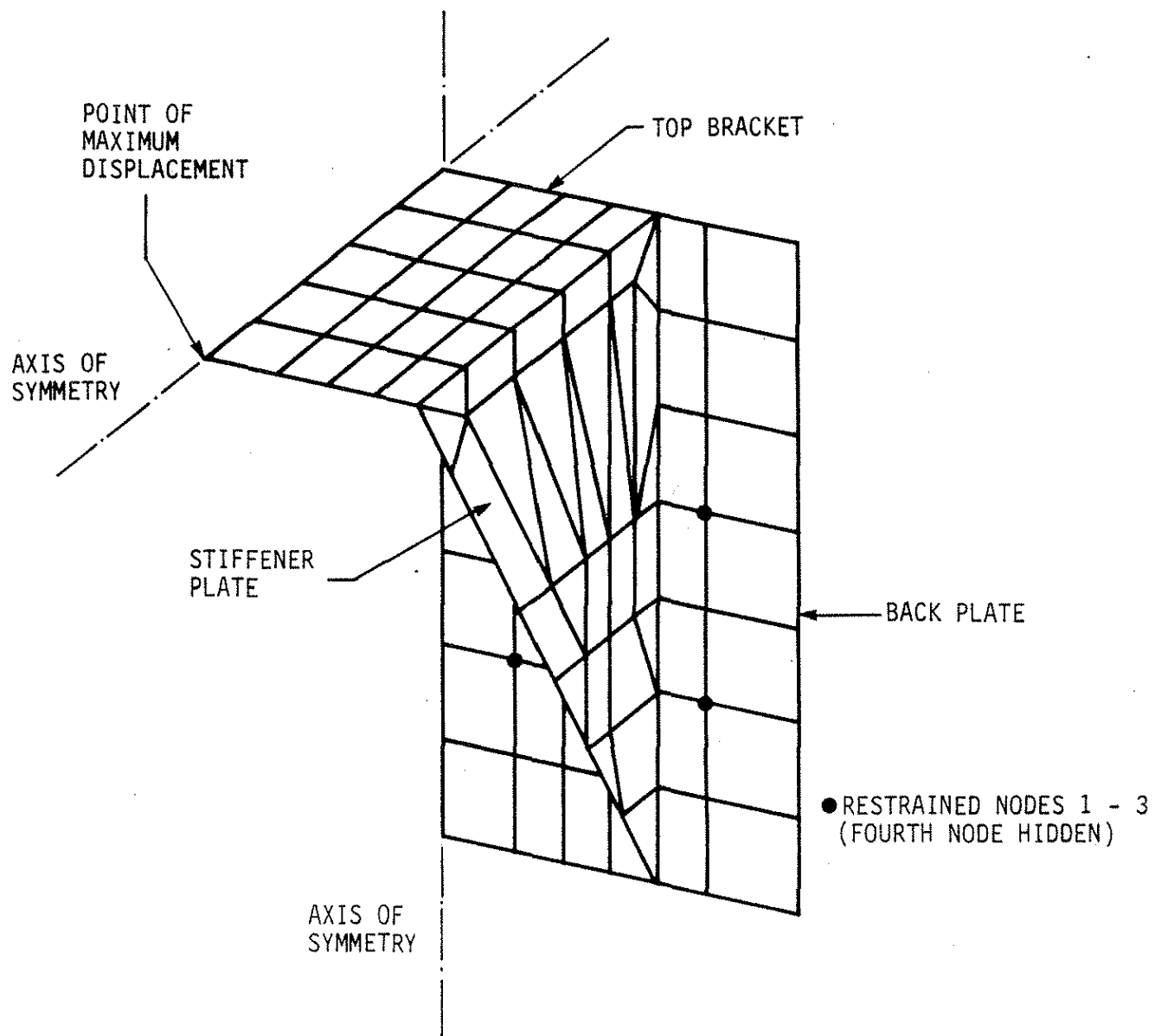


Fig. 1.25. Finite-element model of Bracket 1.

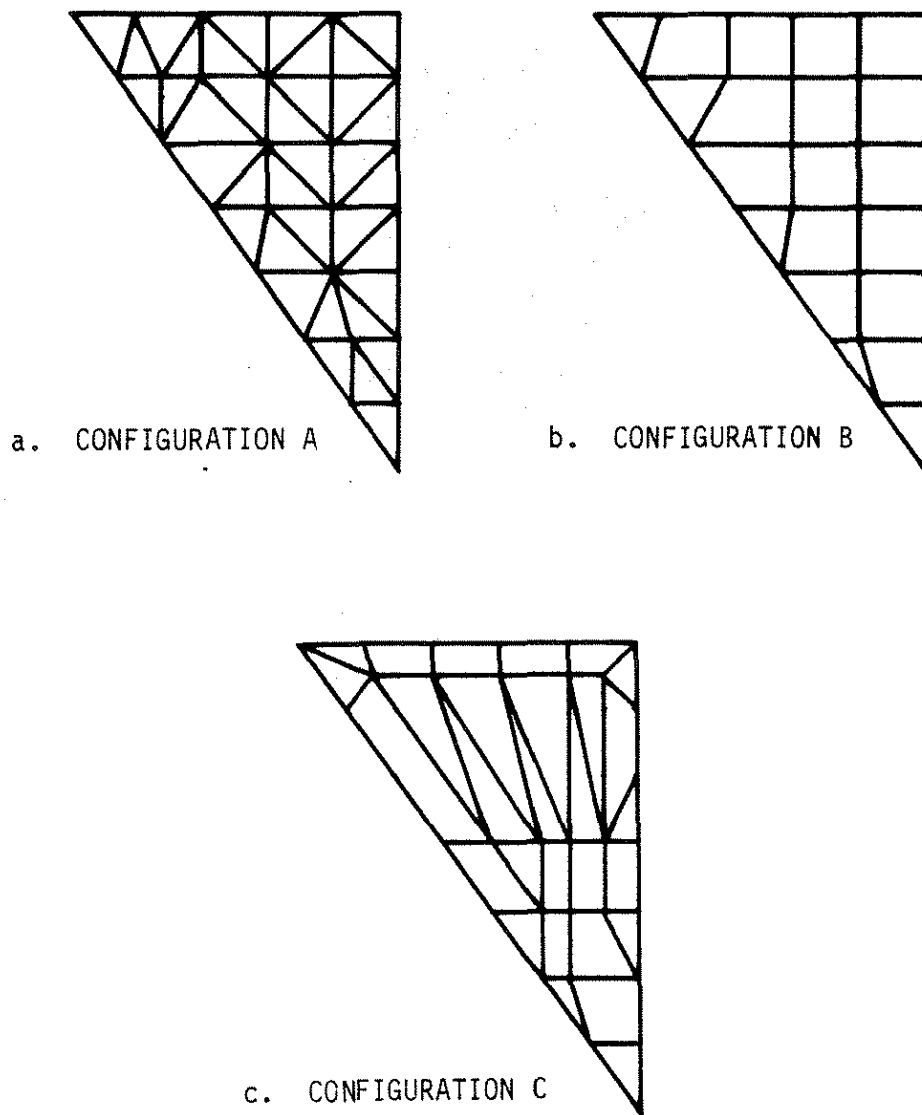


Fig. 1.26. Different finite-element idealizations of Bracket 1.

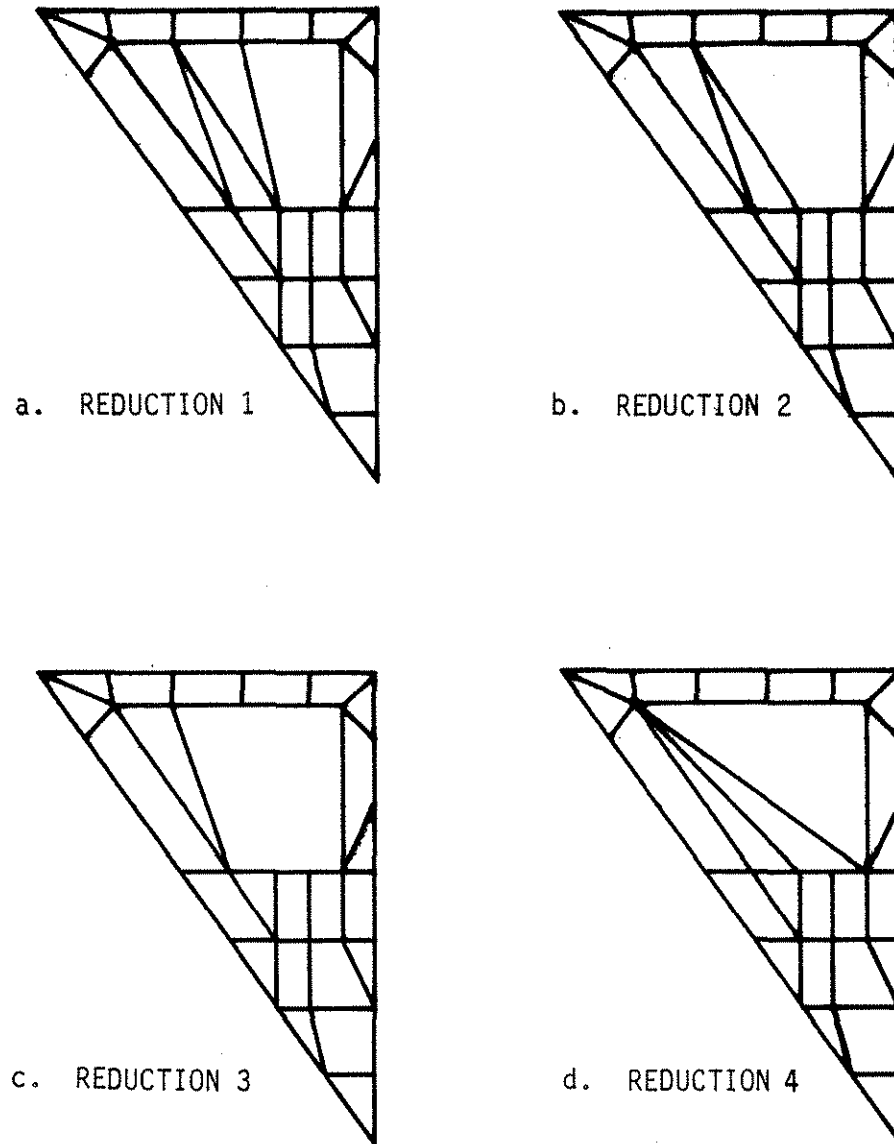
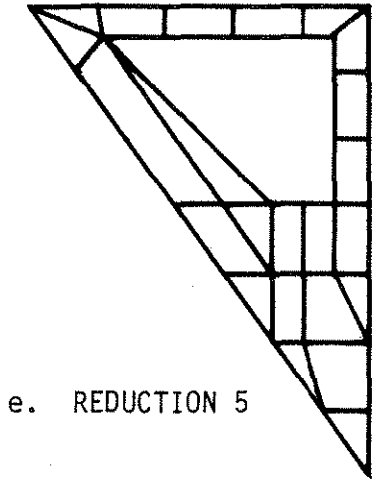
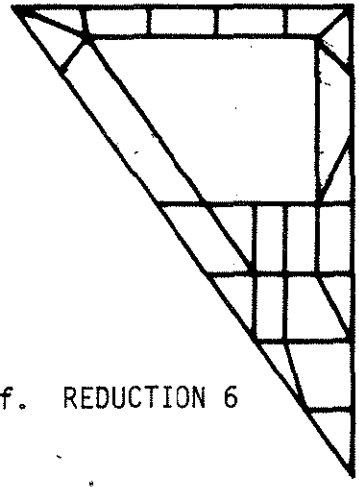


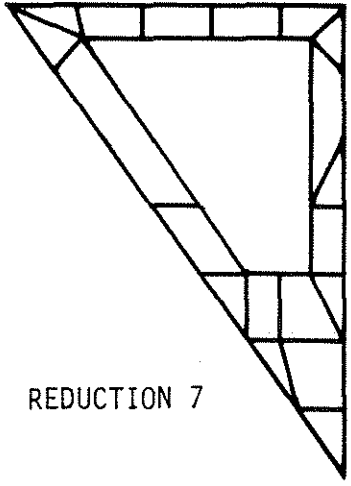
Fig. 1.27. Alterations of Bracket 1.



e. REDUCTION 5



f. REDUCTION 6



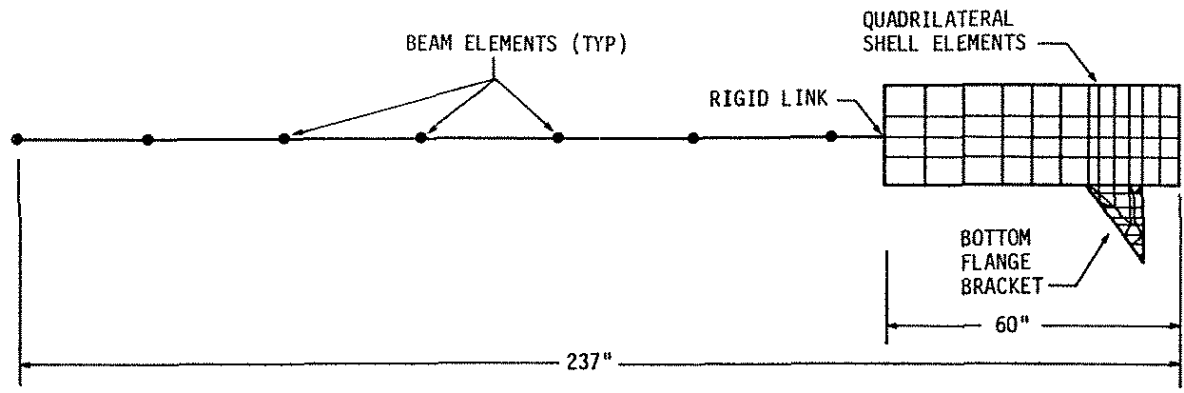
g. REDUCTION 7

Fig. 1.27. Continued.

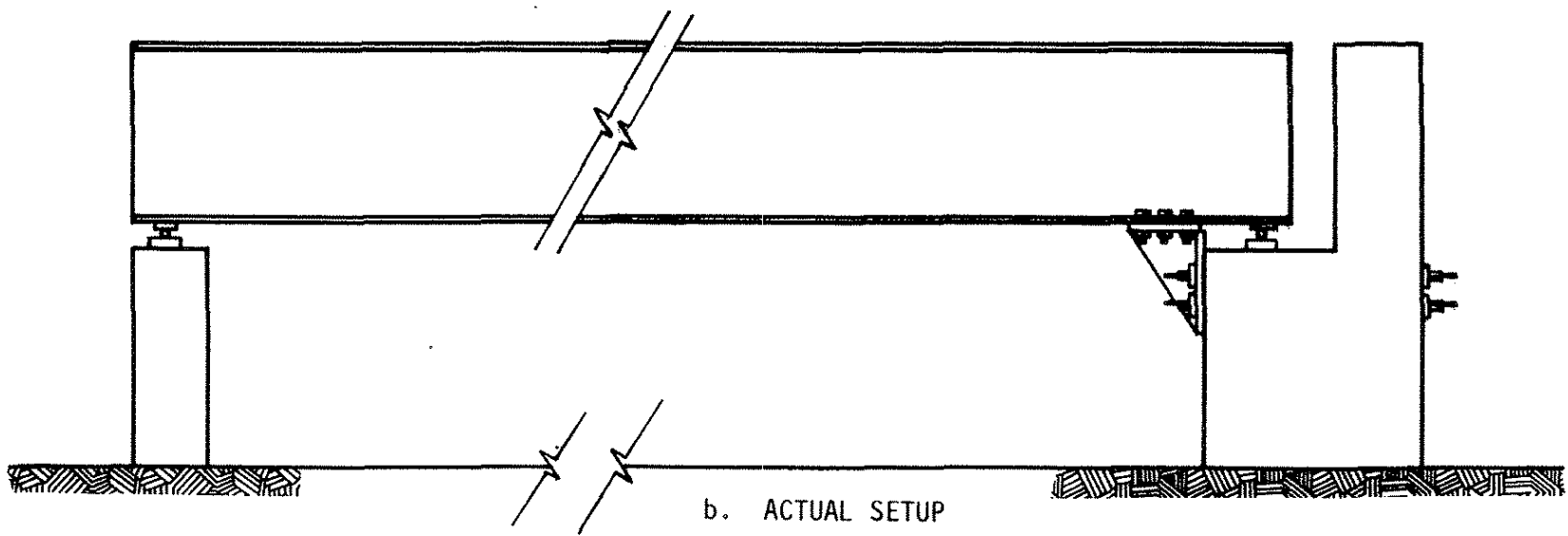
4.1.2. Test Beam Model

The primary purpose of modeling the test beam with the bottom flange bracket was to determine the effects of different brackets on the end restraint and thus the strain reduction near midspan. Modeling of the test beam by using finite elements focused on generating a model that both accurately represented the test setup and did not require excessive computation time. This was complicated by the large size of the actual test beam. In general, this idealization involved choosing the type of elements to be used, then determining the element size and a rational scheme to connect the individual elements. The model used in the finite-element work along with the actual test beam setup is illustrated in Fig. 1.28.

Because of symmetry, only one-half of the beam and bracket setup had to be modeled (see Fig 1.28). As shown in Fig. 1.28a, only the first 60 in. of the model were generated by using discrete quadrilateral shell elements. This length, which is approximately three times the depth of the beam, was the region of interest. The reason for this is that within this region, the behavior of the bottom flange bracket would not be affected by the sudden change of element type. The remainder of the beam was modeled by using three-dimensional beam elements. In order to ensure continuity of the structure, the two element types were idealized such that the midsurface of both was connected at the same node as depicted in Fig. 1.28a. Moreover, since the behavior of the shell elements differs from that of the beam elements, constraint equations were required at this node to prevent any distortions. The behavior of these equations in three dimensions is as follows. If Point A is required to move relatively to Point B, a set of six equations is needed to represent this movement. Three of these equations relate the relative linear displacement between points A and B to the global displacement system. The other three equations relate the rotation of A about the three axes. The six equations are established relative to the six degrees of freedom at B. The constraint equations were thus used to define mathematically the displacements of selected nodal points called slave nodes (Point A in this discussion), with respect to some master nodes (Point B in this discussion) on structure. The slave nodes move following the motion described by the required constraint equations. In this work, all nodes used to define the beam web (composed of quadrilateral shell elements) at the interface of shell and beam elements were constrained to the beam node (master). To model the test setup, the beam supports were idealized as a hinge support at Abutment 1 and a roller support at Abutment 2. Loads placed on the finite element model were the same as those used in the actual testing, except at half the magnitude because of the symmetry previously noted.



a. FINITE-ELEMENT IDEALIZATION



b. ACTUAL SETUP

Fig. 1.28. Representation of actual to idealized test setup.

The main purpose of the tests involving the test beam model was to aid the researchers in determining the rotational stiffness of the various restraining brackets. The method in which the stiffness was determined will be discussed in Section 5.1.2.4. As previously noted, the bracket was then modified to result in configurations akin to those of Brackets 3 and 4. These also were analyzed to determine their respective stiffnesses. The three stiffnesses obtained were then used in the modeling of the connections used on the bridge model.

4.2. Finite-Element Software: SAP IV

Several finite element programs for elastic, static analysis are available at ISU, including SAP IV, SAP 6, ANSYS, ADINA, and NASTRAN. SAP IV [2] was selected for the finite-element analysis of the scale-model bridge, primarily because of investigators' prior experience with the program for similar bridge modeling.

SAP IV—a large-scale, general purpose finite-element program—is capable of performing linear analyses of structural systems subjected to static or dynamic loadings. The program library contains nine element types. Because no graphics programs were available for SAP IV at ISU, several FORTRAN programs were written during previous research projects for plotting the generated model, deflection shape, and stress diagrams.

4.2.1. Bridge Model

The laboratory bridge was idealized by using the grillage method. The grillage method and its applicability to modeling bridges has been well documented [1,13,34,37]. Bridge components (slab, stringer, and diaphragm) are idealized as three-dimensional flexural members and are assigned flexural and torsional properties consistent with their geometric and material properties. The concrete deck and stringer were constructed compositely, and the composite stiffness properties were calculated as if the concrete and steel were elastic. Past research has shown that considering the concrete as an elastic material for analyses in the working stress range leads to accurate results. The corresponding mesh developed from these idealizations was subsequently analyzed by using the SAP IV program.

The mesh representing the bridge model is shown in Fig. 1.29. The stiffness of the four stringers is represented by the longitudinal elements (elements A). The transverse elements

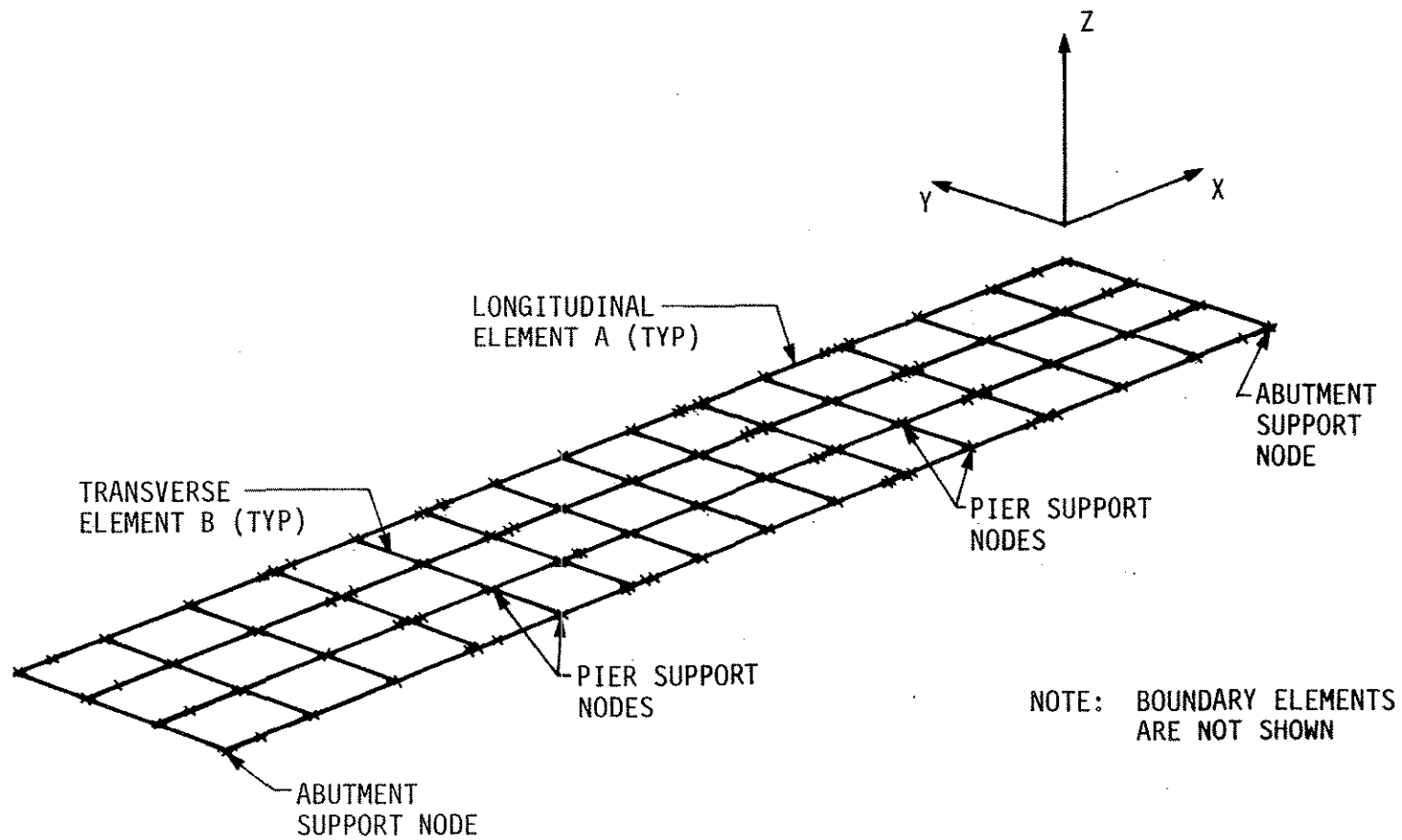
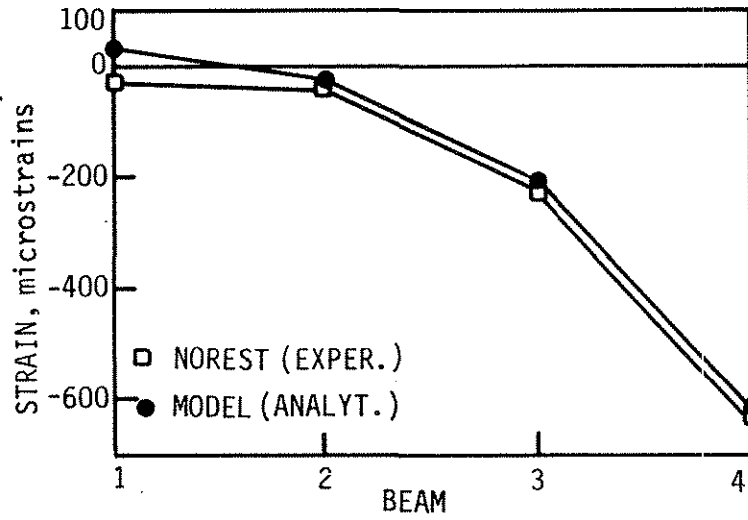


Fig. 1.29. Grillage mesh for laboratory model bridge.

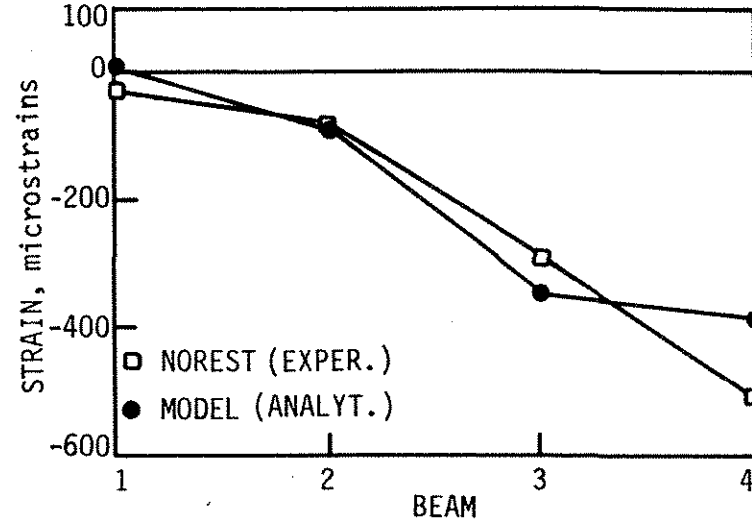
(elements B) in the mesh simulate both the diaphragms and the transverse stiffness of the concrete deck. The steel stringers were considered to be composite with the deck. The section property change in the width and thickness of the stringer flanges (which simulated cover plates) dictated the spacing of the beam elements in the longitudinal direction. These locations are referenced by the X-symbol in Fig. 1.29 (not including locations of transverse elements).

The sensitivity and accuracy of idealization of stringer bridges relative to the grillage mesh size has been discussed previously [13,14]. The model used in this study was initially developed for simulating a full-scale three-span continuous bridge. Since the model bridge is 1/3 scale, the corresponding longitudinal mesh size is 1/3 of that used for a full-scale bridge. A validation of this model was performed by using experimental data, and the accuracy of solution was deemed to be within limits of acceptability. Figures 1.30 and 1.31 show comparison plots of strains for the analytical and experimental results. In these plots LP designates the location of the vertical load (see Fig. 1.24) and NOREST indicates no end restraint was provided. It is noted from these comparisons that the analytical model is stiffer than the experimental model in the transverse direction, although the extreme differences in the resulting strain do not exceed 20%. In fact, in most cases the comparisons are very good. Using a coarser-than-ideal mesh is one of the reasons for a stiffer analytical model, but the effects are also due to the fact that the experimental loads are not "ideal" point loads, as idealized in the analytical model.

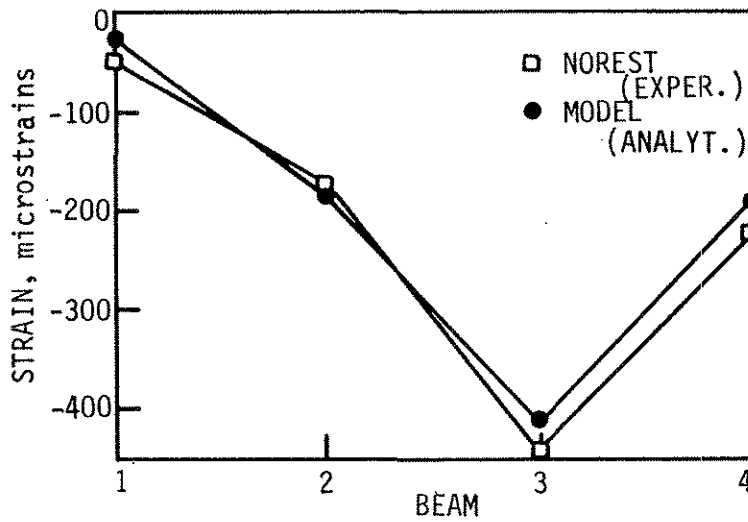
The SAP IV program library contained the elements needed for the bridge model, including three-dimensional beam and boundary elements. The three-dimensional beams simulated all of the elements shown in the mesh in Fig. 1.29. The boundary elements were used to simulate partial, rotational end restraint on the stringers at the abutment for computer analyses performed with the end brackets in place. The boundary element is defined at the abutment nodes and is assigned a finite rotational stiffness to simulate the end restraint.



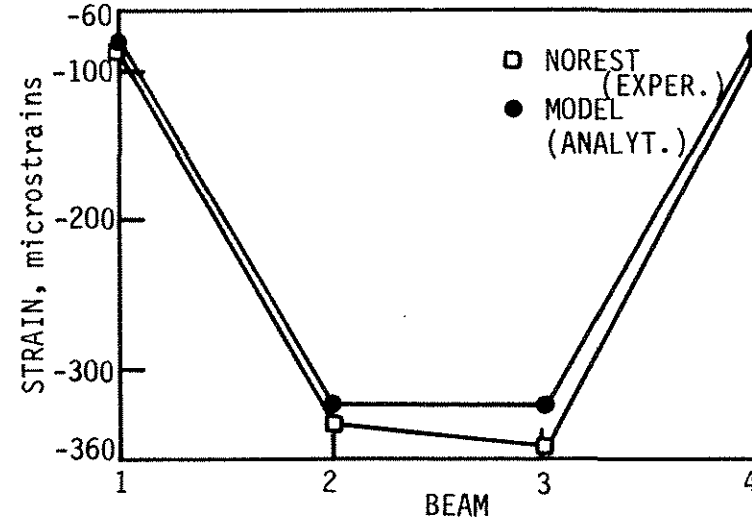
a. LP1



b. LP2

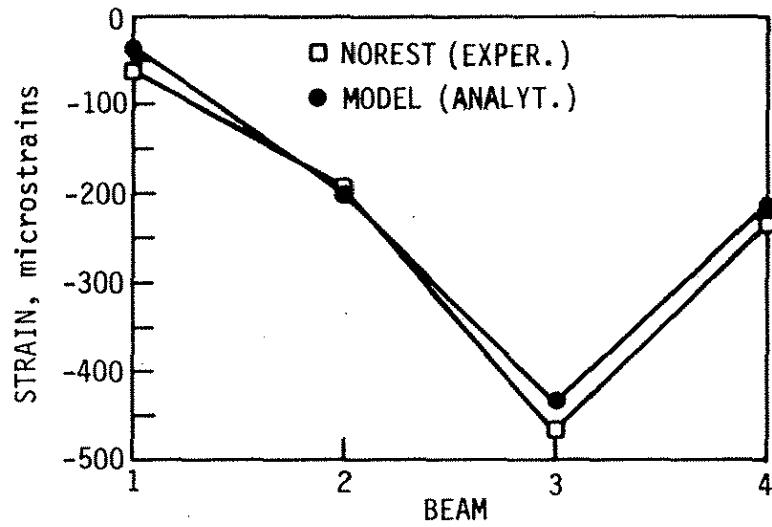


c. LP3

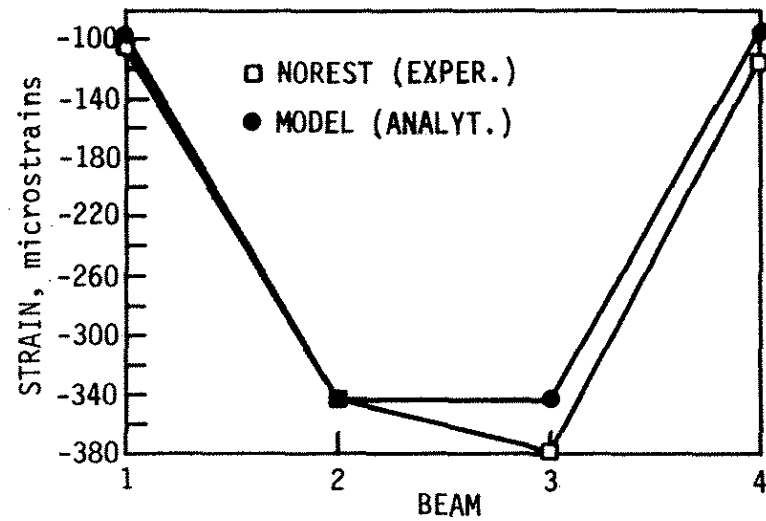


d. LP4

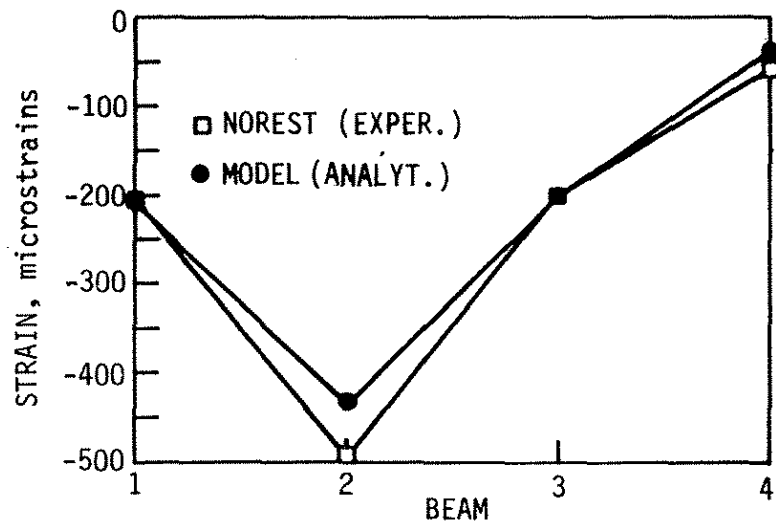
Fig. 1.30. Plot of transverse strain at Section 1 for one concentrated load at various load points for no end restraint--model vs. experimental(see Fig. 1.24).



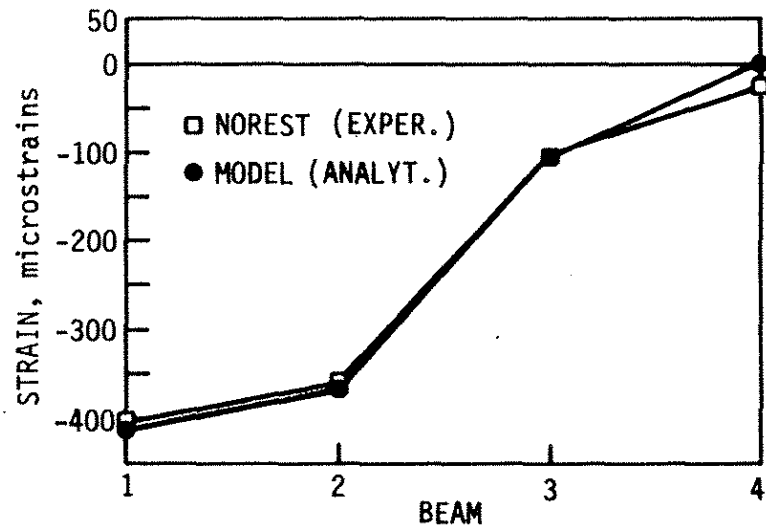
a. LPs 3 & 17



b. LPs 4 & 18



c. LPs 5 & 19



d. LPs 6 & 20

Fig. 1.31. Plot of transverse strain at Section 1 for two concentrated loads at various load points for no end restraint--model vs. experimental(see Fig. 1.24).

5. TEST RESULTS AND ANALYSIS

As in Chapters 2 and 3, this chapter is divided into two main sections. The first section focuses on the test beam and the second section discusses the model bridge. Analytical results will be compared with the experimental results from both the test beam and model bridge wherever possible. This comparison will aid in providing a complete picture of the behavior of the test beam and model bridge and will show the degree of correspondence between theoretical and experimental work. The correlation of the analytical and experimental work provides a basis for calibration of the analytical model so that the analytical models developed can be used to analyze other beams and bridges if desired. In addition to the above, the section pertaining to the test beam will include a comparison of theoretical results obtained by using classical methods of analysis to the actual experimental results. The significance and effectiveness of the various end-restraint mechanisms on the beam as well as on the bridge model both with respect to one another and to the overall behavior will be presented in the appropriate sections. As previously noted, for clarity each test program will be discussed separately.

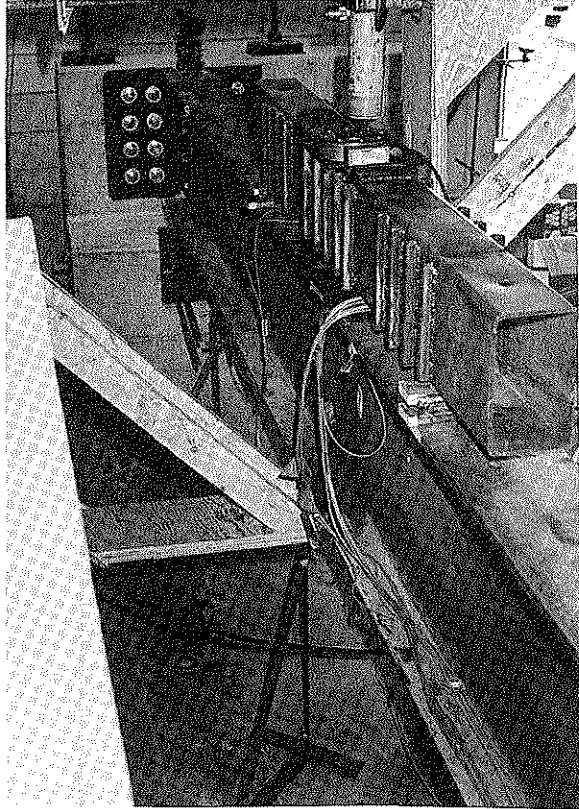
5.1. Test Beam Analysis and Test Results

Previously, test setups (Section 3.1.1) and bracket descriptions (Section 2.1.3) were presented. A total of seven tests were performed on the test beam, ranging from no restraint conditions to an approximation of complete fixity. A typical plot of midspan strains, midspan deflections, and end rotations for one test will be presented in this section; data from the remaining tests can be found in Appendix B. The experimental data obtained from all the tests will then be compared to one another. As previously mentioned, results from the finite-element model of the test beam will be presented for several of the cases.

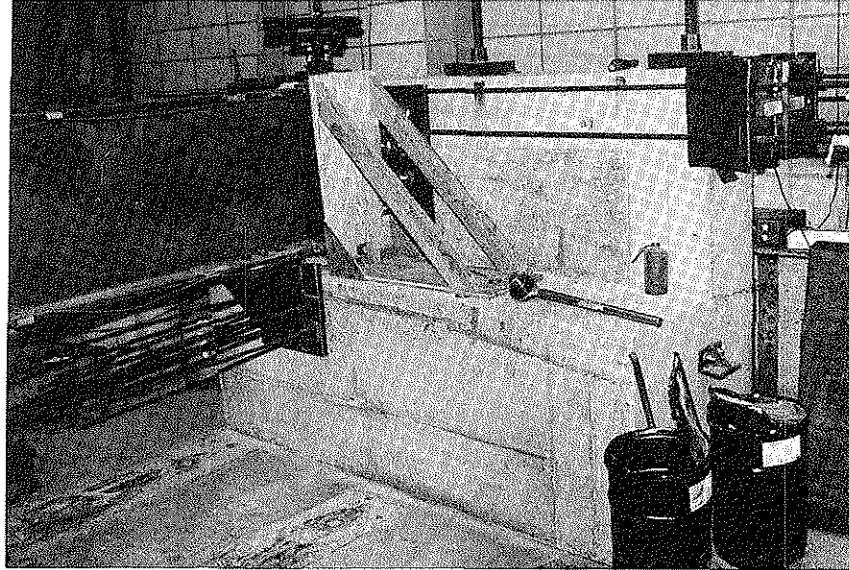
Although it was stated earlier that a comparison of theoretical values, based on classical methods of analysis, to actual experimental results would be presented, two major problems requiring attention developed when testing began on the test beam. First of all, in the analysis of the beam it is assumed that the moment of inertia of the beam is constant. The beam used in the beam test, a $W24 \times 84$, prior to being brought to the ISU Structures Laboratory, had been used as a temporary replacement beam for damaged bridge girder beams. Therefore, because of some physical damage and the effects of corrosion, it exhibited varying cross-sectional properties along its length. The dimensions (flange thickness, flange

width, etc.) at the five instrumented sections (see Fig. 1.17) were measured; based on these values it was determined that cross-sectional properties varied along the beam. These discrepancies were resolved by using average values of the various cross-sectional properties in theoretical calculations. Secondly, the four strain gages at each section are ideally supposed to record comparable strains, but this was not the case. The researchers attempted various loading schemes to overcome this. However, not until the bottom flange bracket (Bracket 1) was installed was a stabilizing effect noticed. This was an indication that the beam was not acting under the influence of pure bending alone, but that there was some lateral bending. To verify this hypothesis, mechanical dial gages were placed at various locations along the beam to detect lateral movement. The beam was then loaded and dial readings recorded. The most significant lateral movement occurred at midspan; when a load of approximately 35 kips was applied, the beam moved laterally 0.05 in. Lateral movement of the top flange was also noticeable at both supports. To counteract this lateral movement, a bracing system was designed. This system consisted of four wooden braces, which were placed at the locations where movement was noticed: two at midspan and one at each of the two supports (see Fig. 1.32). Two braces were required at midspan to restrain both the bottom and top flanges, whereas only the top flange needed to be restrained at the supports. This is because at the supports, the bottom flanges are already restrained due to the contact with the support, which increases as the load increases. To ensure that the braces restricted only lateral movement, "frictionless" rollers (attached to the top of each brace) were positioned between the beam and the braces. Figure 1.33 illustrates the configuration of a typical brace. The experimental data obtained after these braces were positioned were more realistic in that the four gage readings at a particular section were essentially equal and were very close to theoretical values.

In the following sections, results have been divided into two parts: The first part will be a presentation of the individual tests, and the second part will be a comprehensive review of all the tests combined.

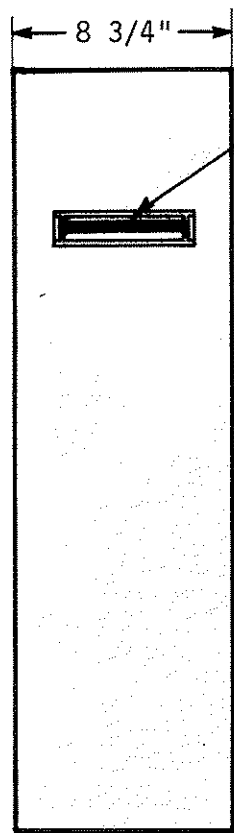


a. AT MIDSPAN

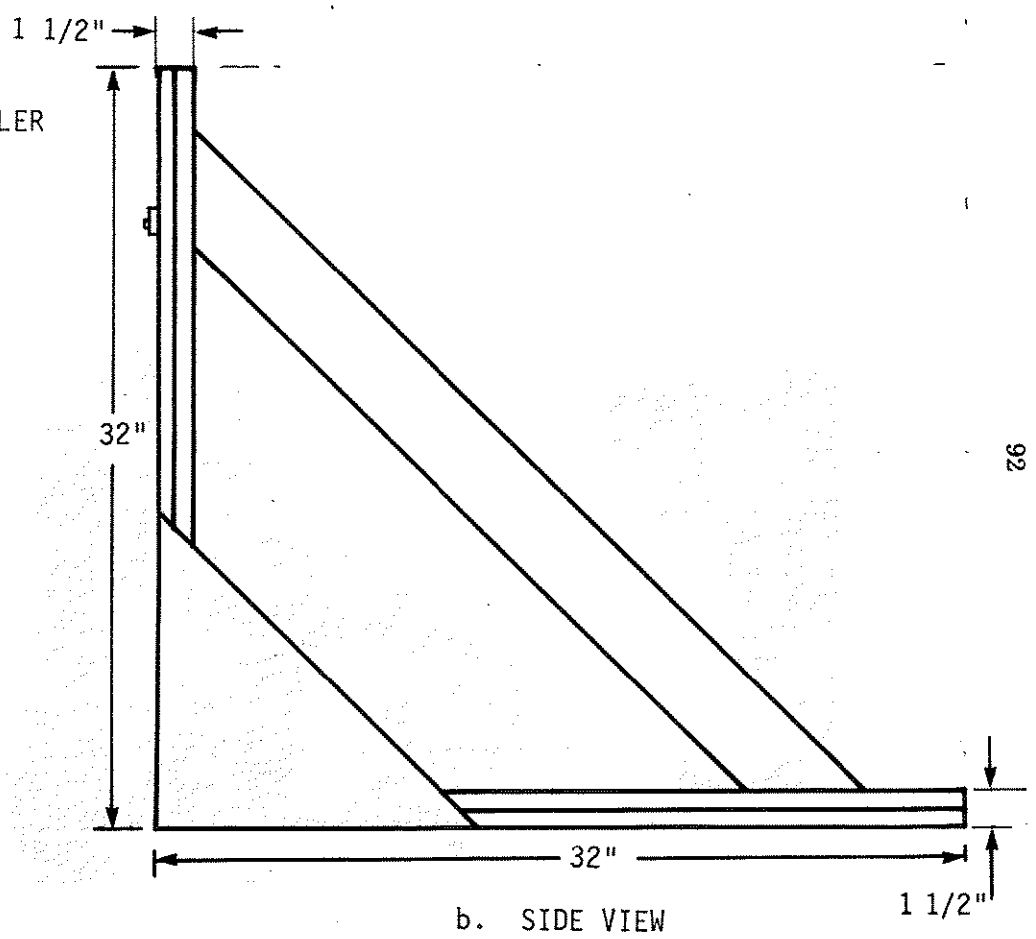


b. AT ABUTMENT 1

Fig. 1.32. Photographs of test-beam bracing system.



a. FRONT VIEW



b. SIDE VIEW

92

Fig. 1.33. Configuration of a typical test-beam brace.

5.1.1. Presentation of Test Data

5.1.1.1. Test 1

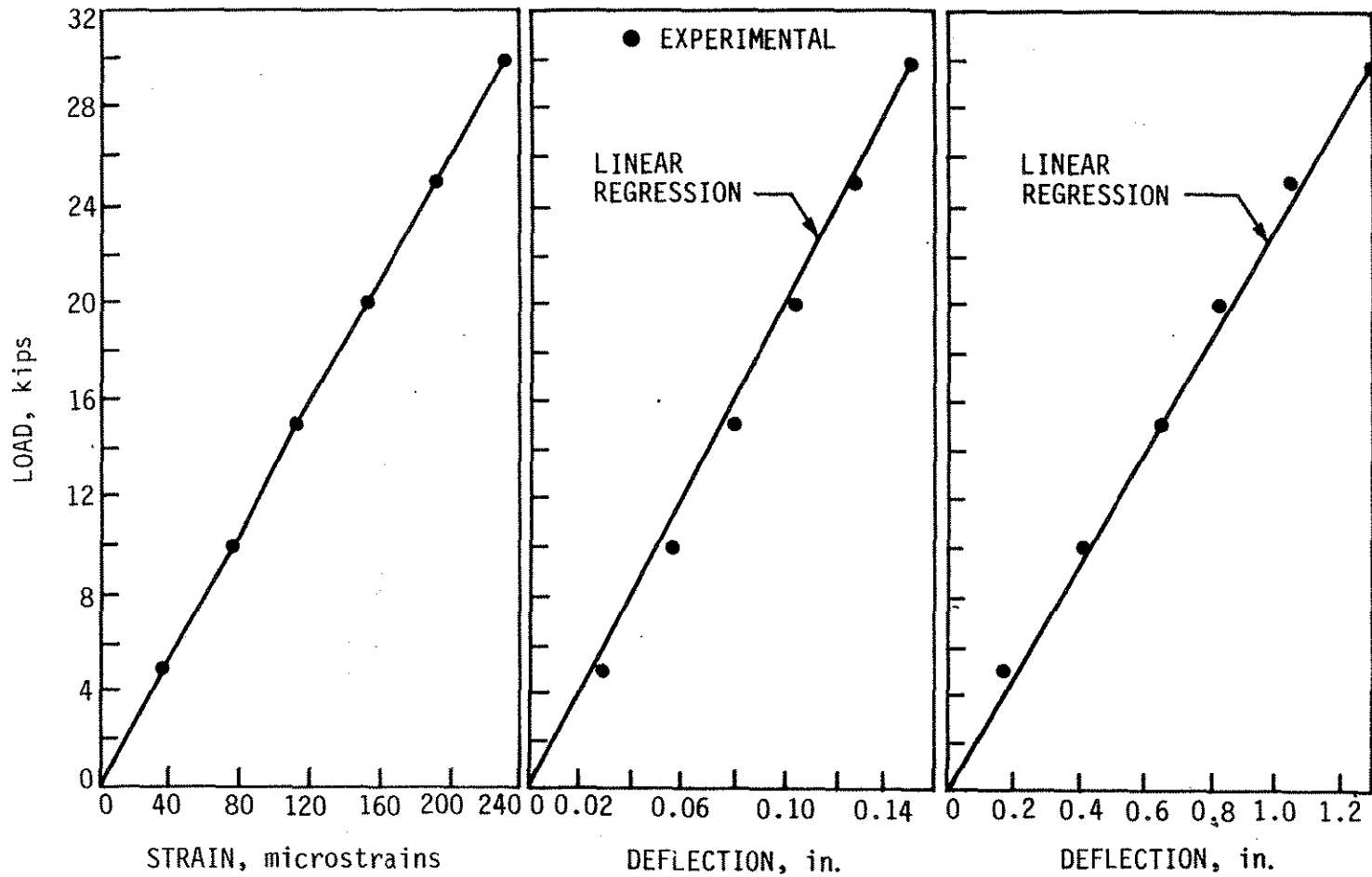
Test 1 involved the testing of the beam with no end restraint provided. Because of the simplicity of the test beam, analysis was performed using ordinary statics and classical methods of analysis; no finite-element methods of analyses were employed.

Results from Test 1 in the form of strains and deflections are presented in Fig. 1.34. The strain values plotted are the average of the four values measured at a section for a particular load. The strain distribution is linear, as expected, since loading was applied within the elastic range. Locations of the strain gages, DCDTs, and the transit were given in Fig. 1.17. As previously noted, the transit deflection (Fig. 1.34c) is a measure of how much the line of sight of the transit deflects as the beam is being loaded. This deflection can easily be converted to a rotation by dividing it by the distance to the far laboratory wall (see Fig. 1.18). Strain data obtained were then compared to data obtained from a theoretical analysis of a simply supported beam, shown in Fig. 1.35. Strain distribution plotted in Fig. 1.35 indicated that initial restraint of the test beam did exist, because the slopes are different, which indicates differences in the stiffnesses. This is expected because theoretical calculations are based on ideal support conditions, which are not possible under practical circumstances. The effectiveness of the end-restraint brackets will be based on the reduction of strains and deflections with respect to the experimental data from Test 1, which has some initial restraint.

A linear regression analysis using the method of least squares was performed on the midspan and transit deflection data in order to obtain the best curve fit for the experimental data. The results of the regression analysis and the actual experimental data can be seen in Fig. 1.34 for Test 1. The results of the linear regression analysis for all seven tests are presented in Table B.1 of Appendix B. In general, the correlation of the data is good.

5.1.1.2. Tests 2 through 7

The bottom flange bracket (Bracket 1) was fastened at Abutment 1 for Test 2. Bracket 1 was designed to resist a vertical load of 50 kip; however, it was only tested to approximately 50% of its capacity. Hence, the bracket displayed no apparent distress or deformation. Data from this test are presented in Fig. B.1 (see Appendix B). A finite-element analysis of this test



a. STRAIN DISTRIBUTION AT MIDSPAN

b. MIDSPAN DEFLECTION

c. TRANSIT DEFLECTION

Fig. 1.34. Test 1 data.

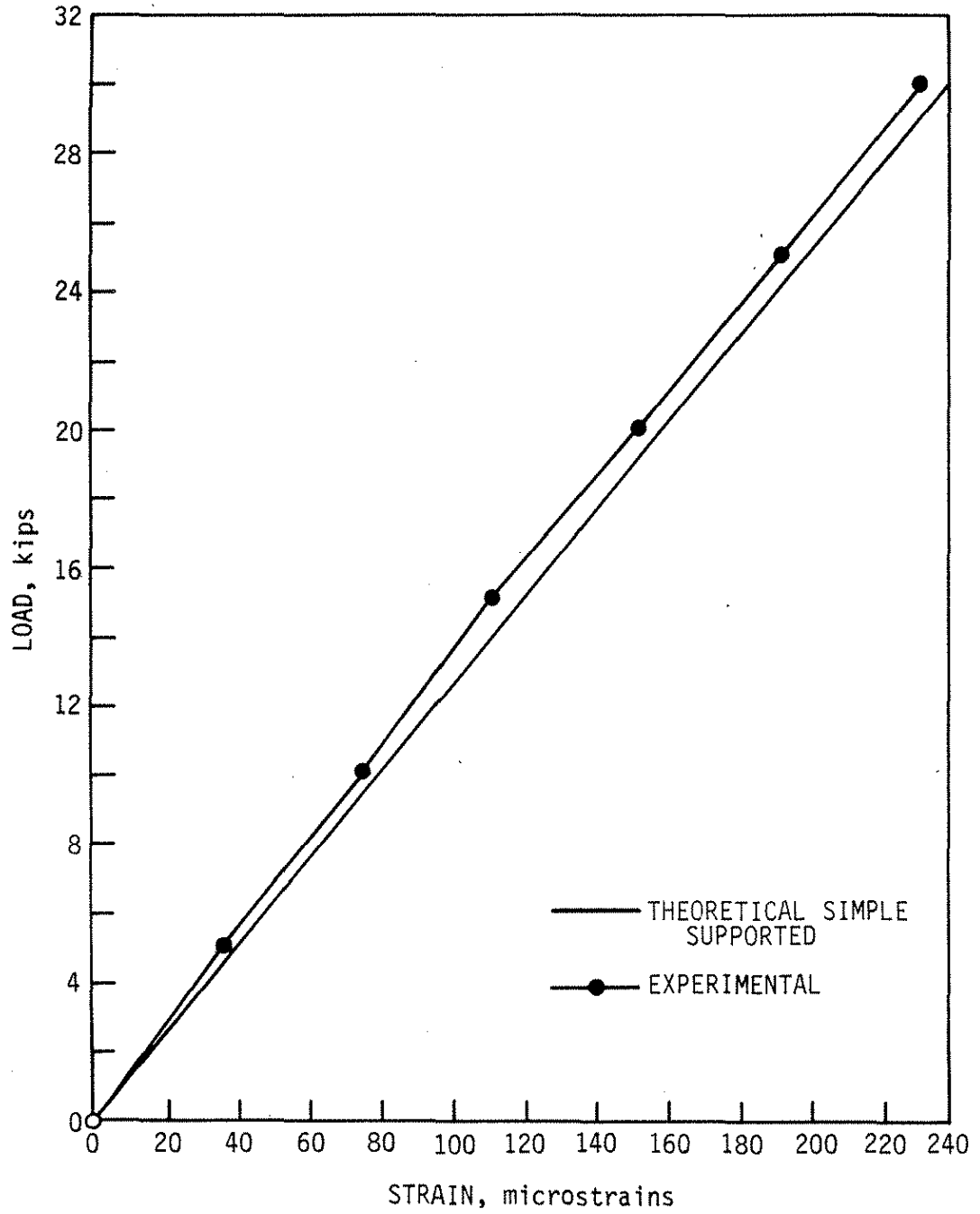


Fig. 1.35. Initial end restraint: Test 1.

beam and bracket was performed; results from this analysis will be presented in Section 5.1.2.4.

In Test 3, the bottom flange bracket (Bracket 1) and the web bracket (Bracket 2) were connected to restrain the beam. Figure B.2 (in Appendix B) illustrates the results from this test. As in the previous case, the design capacity was greater than that to which the connection was subjected, and both brackets revealed no signs of deformation. This test represents the greatest restraint possible with this type of test setup; it will be referred to as the full restraint condition. However, full restraint was not attained, as is illustrated in Fig. 1.36. The difference between the two conditions can be decreased by stiffening the restraint brackets.

The effects of bracket stiffness on strain distribution and deflections were investigated in Test 4. The configuration of Bracket 1 (see Fig. 1.4) was modified, resulting in Bracket 3 (see Fig. 1.9), by removing material from the stiffener plates as previously discussed in Section 4.1.1. The results of Test 4 are shown in Fig. B.3 of Appendix B. The finite-element model of the test beam and Bracket 1 was also modified to represent the setup of Test 4; the results of this analysis will be presented in Section 5.1.2.4. During the loading of the test beam, the behavior of the bracket was observed; no signs of distress were evident.

Test 5 was similar to Test 3, except that Bracket 1 was replaced by Bracket 3. The results are plotted in Fig. B.4 of Appendix B. The test data show, as expected, that the stiffness of the connection decreased with the removal of material.

The effectiveness of Bracket 4 was investigated in Test 6. Bracket 4 is a further modification of Bracket 3 (see Fig. 1.10) and as before the finite-element model was modified to represent this configuration. There was concern, based on high stresses determined in the finite-element analysis of Bracket 4 around the perimeter of the cut, that this bracket could not withstand the forces to which it was subjected. Therefore, after each load increment the bracket was examined. However, no sign of plate buckling or distress was apparent. The brackets were not instrumented because it was not within the scope of the project to investigate the local behavior of the bracket. Figure B.5 of Appendix B shows the test data.

Analogous to Tests 3 and 5, Test 7 was directed at determining the effect of material reduction on the full restraint condition. For this test Brackets 2 and 4 were acting together; test results are shown in Fig. B.6.

As was the case with Test 1, a linear regression analysis was performed on the midspan deflection and transit deflection data for Tests 2 through 7. The experimental and the

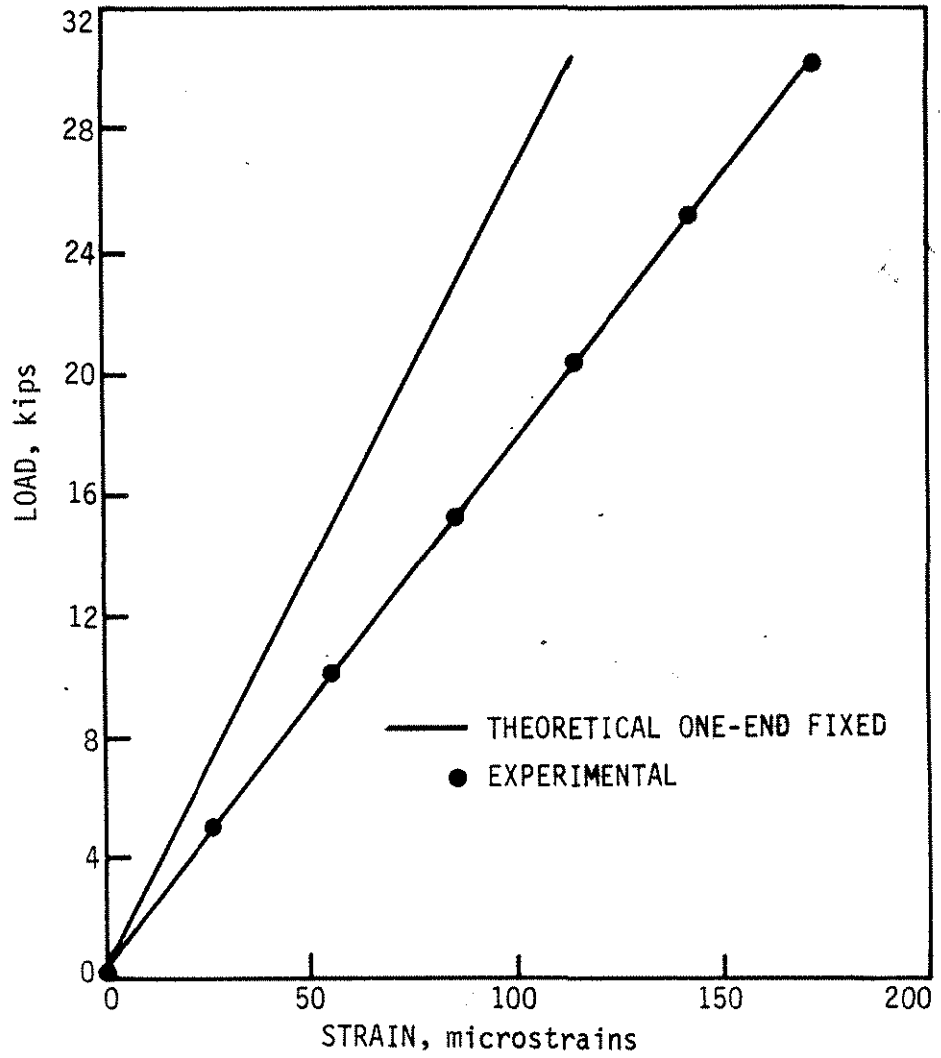


Fig. 1.36. Comparison of theoretical and experimental results at midspan for fixed simple support conditions.

regression results are plotted in Figs. B.1 to B.6. The correlation coefficients are presented in Table B.1 of Appendix B.

5.1.2. Analysis and Comparison of Test Beam Results

Previously, the results from the individual tests were presented separately to document the distinct effects of the various end restraints on the beam behavior. In this section, the various test results will be compared, thus establishing the effects and effectiveness of the various degrees of end restraint on the performance of the beam. The beam behavior will be quantified by comparing strains and deflections at critical sections. Comparisons of the experimental data on the test beam will be presented in three different parts. First, the results from Tests 1, 2, and 3 will be compared; Tests 2 and 3 basically represent the largest reductions in midspan deflections, midspan strains, and transit deflection data from Test 1, based on whether only the bottom flange or both the bottom flange and web are restrained, respectively. Second, the three different bottom flange brackets are compared; thus data from Tests 2, 4, and 6 are discussed. Also in the second part, a comparison of the finite-element results to the experimental data will be discussed. In the third part, data from Tests 3, 5, and 7 are presented. These tests involve having the various bottom flange brackets and the web bracket restraining the beam.

Note that all experimental data fell within the confines of the theoretical expectations, as is illustrated in Fig. 1.37. This, of course, was expected, but what provided greater insight was the fact that the data were closer in value to the simple support conditions. Thus, two major conclusions can be reached by examining Fig. 1.37: one, simple-simple support conditions were not attained, that is, some initial restraint did exist; two, in order to achieve "full fixity," at the restrained end, brackets considerably larger than those used in this investigation have to be provided. Providing significantly larger restraining brackets may not be practical because end restraint loses its cost effectiveness as compared to other available strengthening techniques because of the increase in bracket costs and attachment costs.

5.1.2.1. Tests 1, 2, and 3

Tests 2 and 3 represent the maximum attainable reductions in midspan strains, midspan deflections, and beam rotations induced by the two types of restraint mechanisms investigated in this research program. The results from the individual tests have previously been presented (see Section 5.1.1); however, comparisons between Tests 1, 2, and 3 are shown

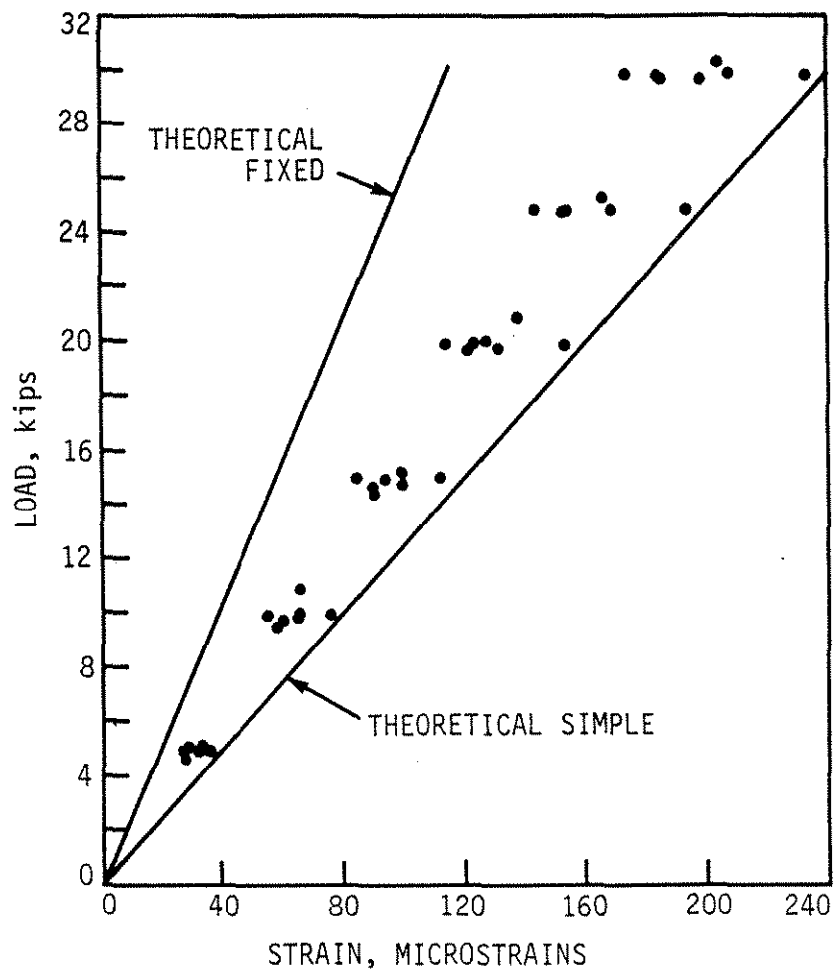


Fig. 1.37. Strain distribution vs. load for theoretical and experimental results.

in Fig. 1.38. As evident from Fig. 1.38, a significant reduction in midspan strains, midspan deflections, and beam rotations was achieved. The percentage of reduction in these variables is presented in Table 1.5. The values in the table are based on comparing the changes in slopes of the strain and deflection data.

Table 1.5. Effectiveness of restraint brackets.*

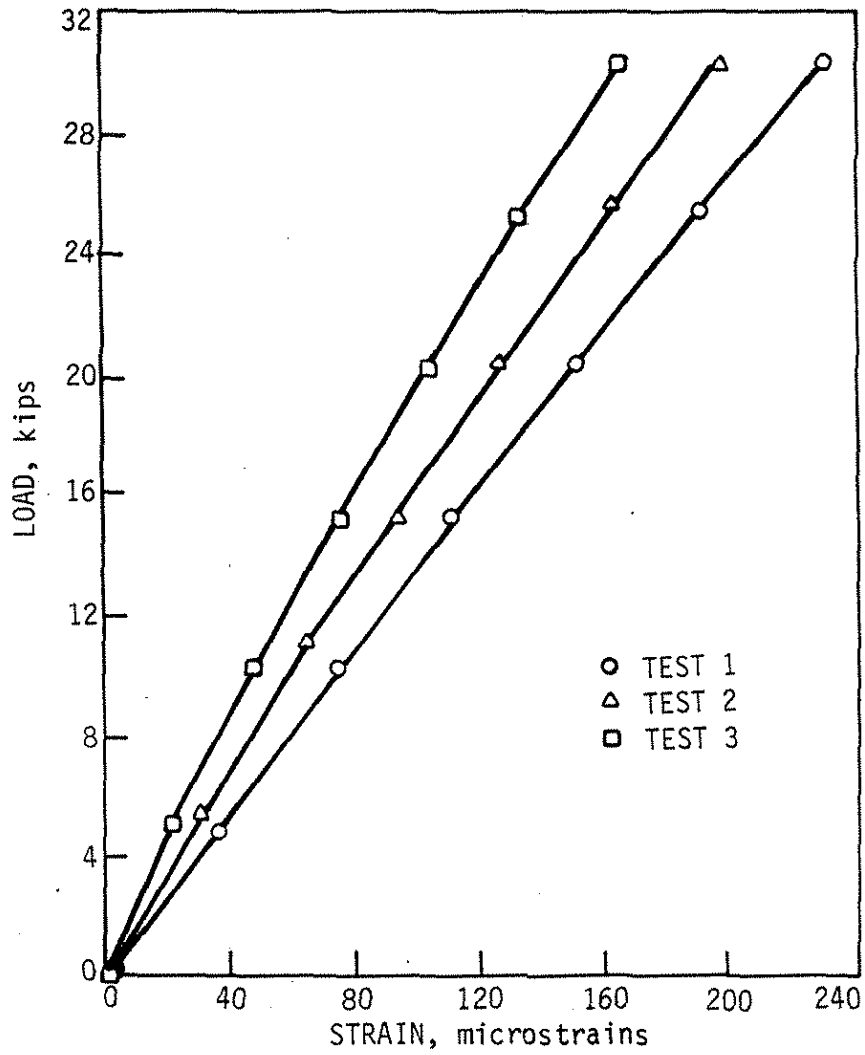
Percent Reduction In	Test 2	Test 3
Midspan strains	14.57	25.86
Midspan deflection	19.89	30.02
Transit deflection	13.01	31.80

*Based on reduction changes from Test 1 data.

As expected, the largest reduction was achieved by attaching both the bottom flange bracket and the web bracket. Table 1.5 reveals several interesting facts about the behavior of the beam and the effects of the brackets. Also as expected, the percent reduction in the various variables was not the same; this is better understood by examining the governing differential equation for the deflection of elastic beams. From this equation it can be seen that moment (or strain in this case) is proportional to the second derivative of the elastic curve, whereas rotation is proportional to the first derivative of the elastic curve. As a result of the variance in the derivatives, the strains, deflections, and rotation respond differently to end restraint. However, the researchers believe that another reason for this variance is the location of the end-restraint bracket, specifically whether it was restraining the bottom flange or restraining both the bottom flange and the web, and its effect on support conditions. This change in support conditions (i.e., a variable boundary condition) from one test to the next affected the beam deflection, beam rotation, and midspan strains in different ways. Essentially, the change in support conditions can be explained as follows:

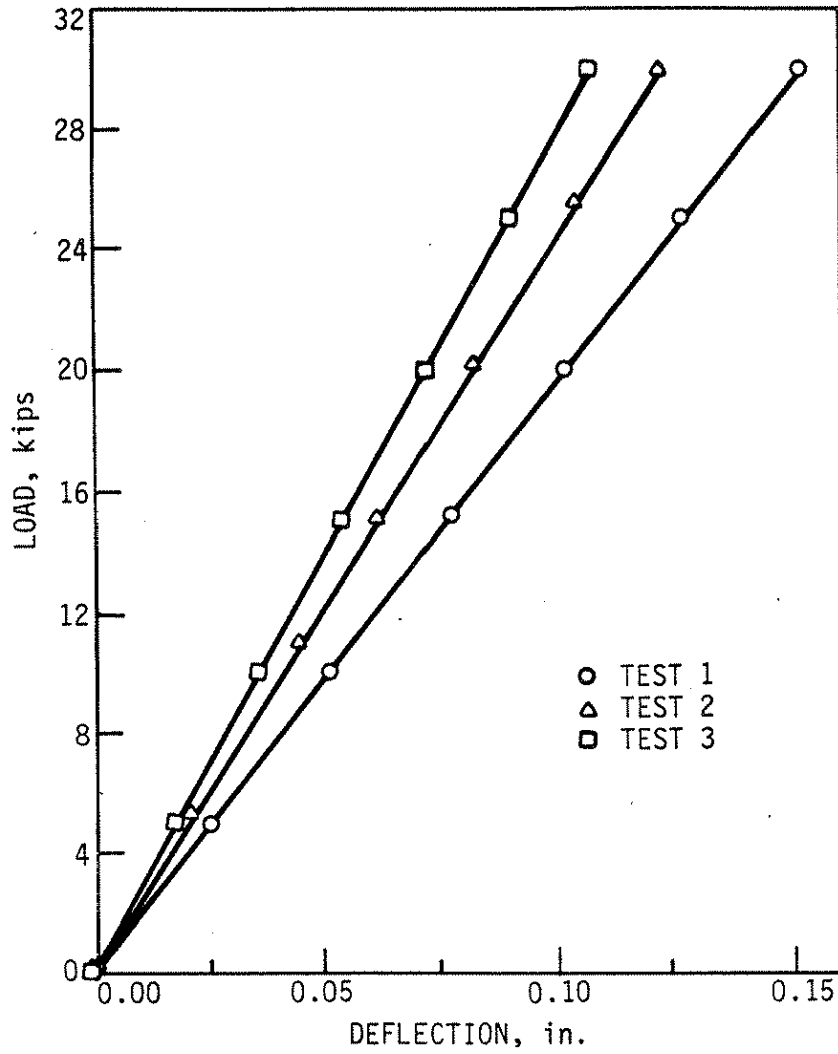
Case 1: Restraint of Bottom Flange Only

Prior to attaching the flange bracket, the support conditions were simple and the beam determinate. However, once the flange bracket was attached to the abutment and lower flange of the beam, a third support is imposed on the beam.



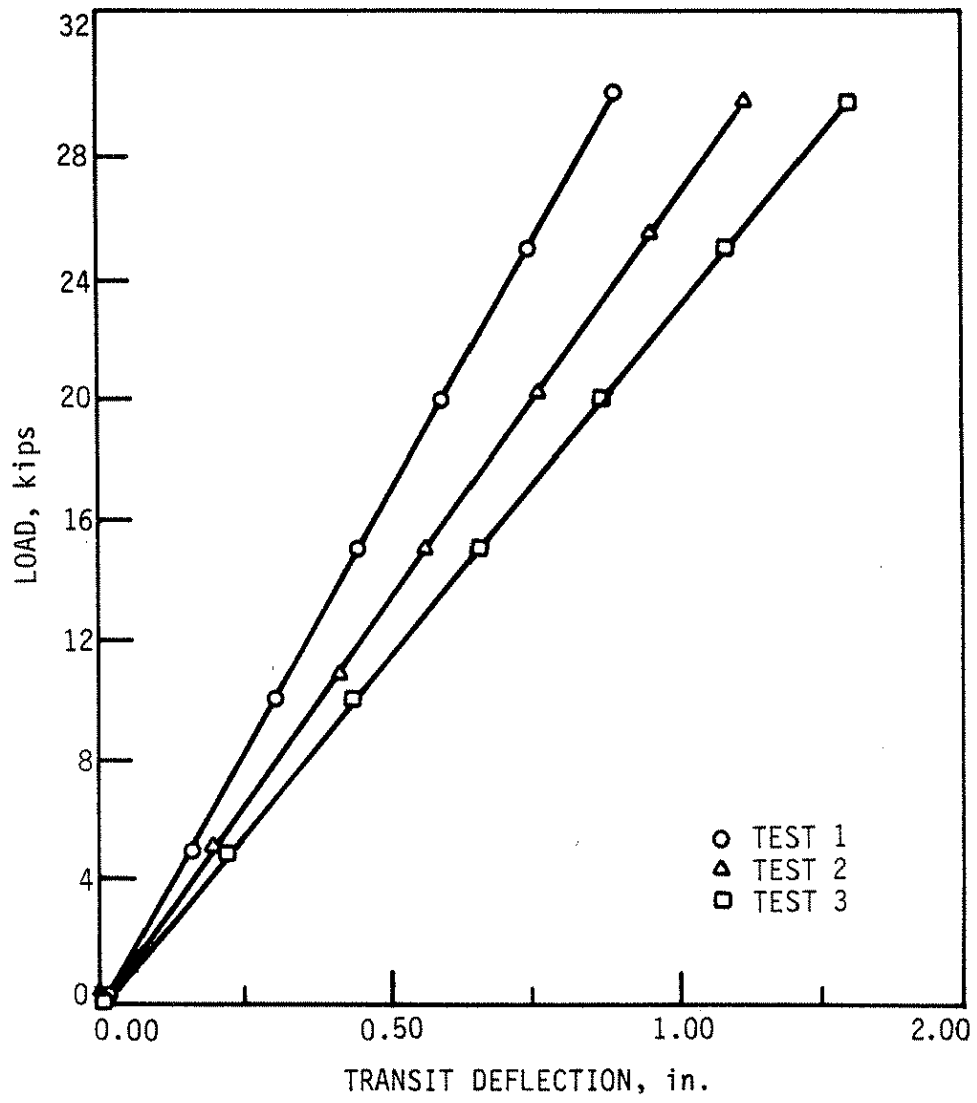
a. MIDSPAN STRAINS

Fig. 1.38. Effect of maximum restraint conditions.



b. MIDSPAN DEFLECTION

Fig. 1.38. Continued.



c. TRANSIT DEFLECTION

Fig. 1.38. Continued.

Depending on the type of loading applied and the location of the restraining bracket, two scenarios could develop to explain the effects of the third support. The first scenario is that the bottom flange bracket only shortens the span and that the initial hinge support uplifts and has no restraint capacity. In addition to this, the bottom flange bracket provides additional horizontal restraint and rotational restraint, which renders the beam indeterminate. The other possibility is that the initial hinge support does develop a resisting vertical tie-down reaction; therefore, the structure is divided into two spans and an additional degree of indeterminacy arises. This, in turn, may cause a restraining couple to develop between the vertical reaction transferred to the abutment from the bracket and the hinge support tie-down reaction. Thus, the beam is no longer determinate. The distance between the back plate of the bracket and hinge support is approximately nine inches and is significant enough to cause a couple to develop between the vertical reaction transferred to the abutment from the bracket and the hinge support reaction. Thus, the test setup was divided into two spans: one span length equal to 8.875 in. and the other span length equal to 228 in. This couple, in return, affected the beam behavior and resulted in the variance of reduction values observed in Table 1.5.

Case 2: Restraint of Bottom Flange and Web

This condition is an extension of the above situation; prior to providing the web restraint, the bottom flange was restrained. Once again, by imposing these external restraints, the beam becomes indeterminate. However, the degree of indeterminacy is not directly obtained because the web bracket extends between the hinge support and the bottom flange bracket. Hence, it not only restrains the beam web; it also stiffens the whole region because it extends over more material. This, in turn, affected both the top and bottom flange of the beam and reduced more significantly the degree of rotation, which is measured at the top flange only. Bracket 2 acting in conjunction with Bracket 1 was also designed to resist a 200 ft-kip moment, which resulted in a second couple developing between the resultant shear force in each bracket (see Section 2.1.3.2).

Test 2 showed that the percent reduction of midspan strains and transit deflection was essentially the same, while the reduction in midspan deflection was approximately 25% greater. In this test, the bottom flange of the beam was restrained by Bracket 1, and the

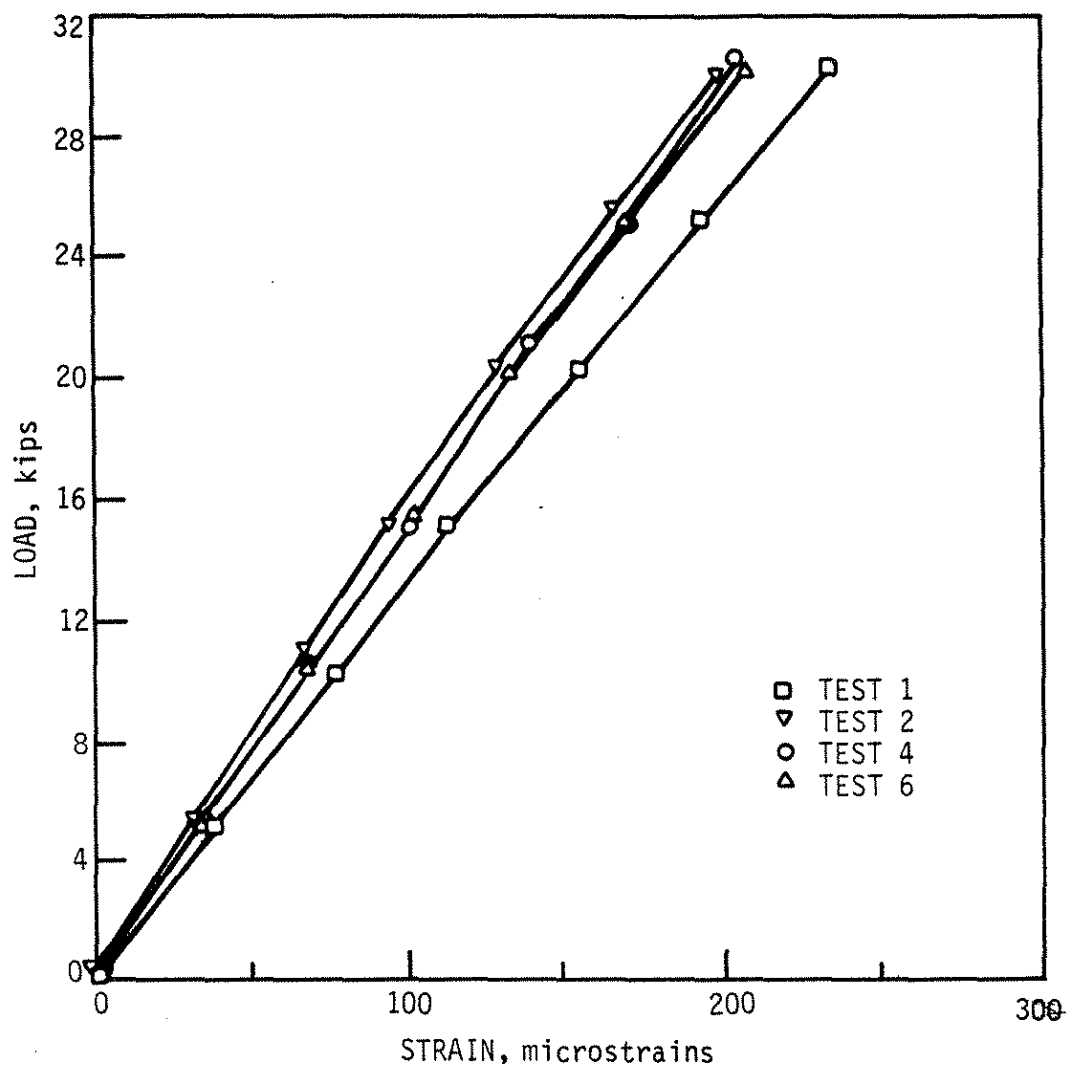
situation discussed in Case 1 developed. The fact that various support conditions existed and only the bottom flange was being restrained may have been the cause of a greater reduction in midspan deflections. A similar scenario occurred in Test 3 when the bottom beam flange and beam web were restrained. In this test, the reduction in transit deflection was greater than the reduction in midspan deflection and midspan strains. This is because Bracket 2, by restraining the beam web, was also restraining the flanges by preventing them from rotating. Hence, a greater reduction in rotation was recorded. This is similar to Case 2, previously discussed.

The implications of these results are significant, especially for determining the most effective restraint mechanism. The type of bracket configuration employed will depend on the degree of restraint desired. The results shown in Table 1.5 are an indication of the reductions that can be expected from providing end restraint.

5.1.2.2. Bottom Flange Bracket Tests—Tests 2, 4, and 6

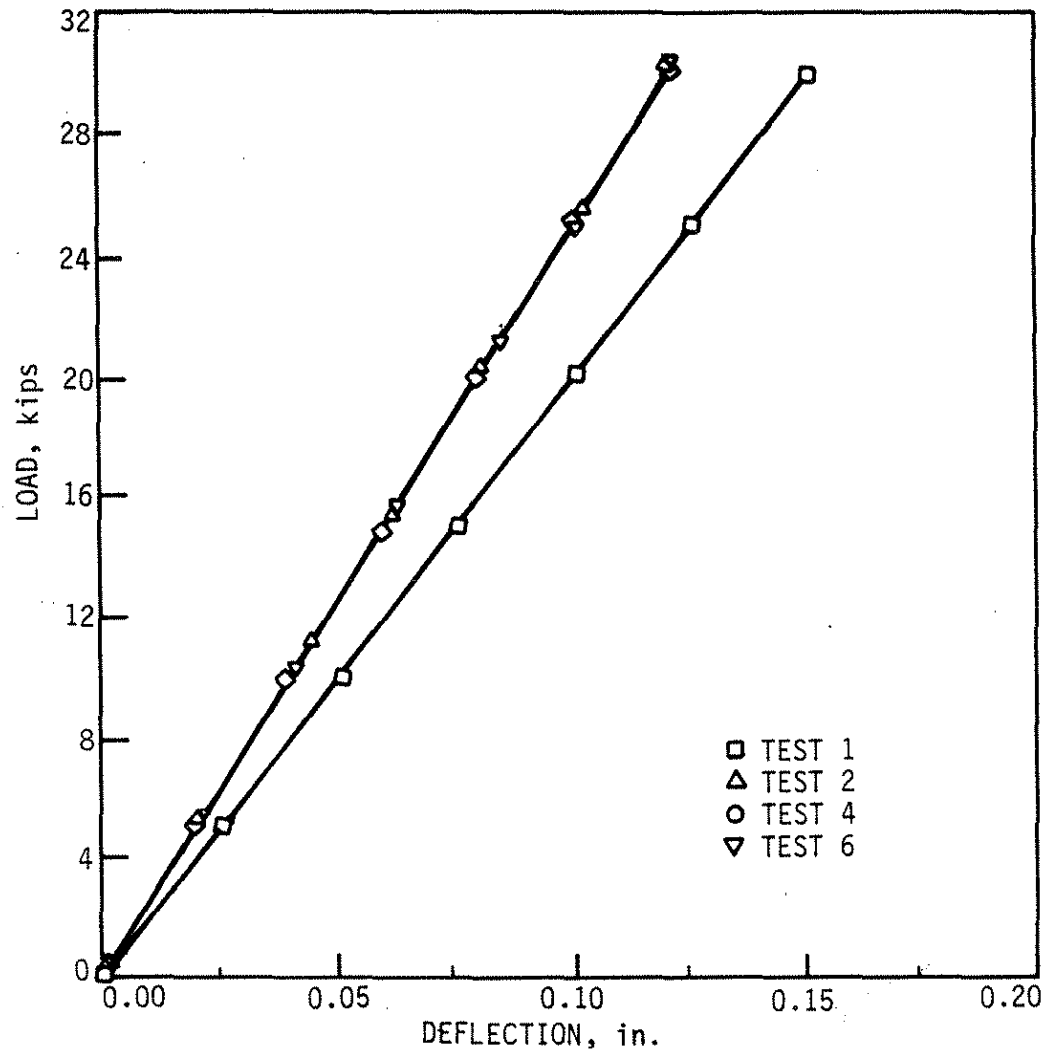
These tests represent the reductions in midspan strains, midspan deflections, and beam rotations due to the presence of the bottom flange bracket. Once again, Test 1 is for simple support conditions, Test 2 is with Bracket 1 attached, and Tests 4 and 6 illustrate beam behavior after material reductions have occurred. The stiffnesses of these brackets were determined from a finite-element model (see Section 5.1.2.4). These stiffnesses range from 571,639 k-in./rad for Bracket 1 (which is the largest value) to 419,994 k-in./rad for Bracket 4 (the smallest value). Hence, it is expected that Bracket 1 would provide the greatest restraint while Bracket 4 would provide the least restraint. Figure 1.39 illustrates the data obtained from these tests.

Examination of Fig. 1.39 indicates that the reductions in midspan strains, midspan deflections, and beam rotation occur because of the bottom flange bracket, as previously mentioned. Figure 1.39 also indicates that altering the bracket configuration (i.e., reducing the amount of material in the stiffener plates) did not significantly change the results. One of the reasons is that the stiffness of the horizontal "seat" plate versus the stiffness of the vertical plates is still large. Thus, the data obtained prior to any material reduction (Test 2) are similar to the data obtained after both modifications on Bracket 1 were made. This is especially evident in the case of midspan deflections (see Fig. 1.39b) where the data from Tests 2, 4, and 6 were essentially co-linear. The midspan strain distribution and transit deflection data from Tests 4 and 6, even though close in value to Test 2, provide a clearer



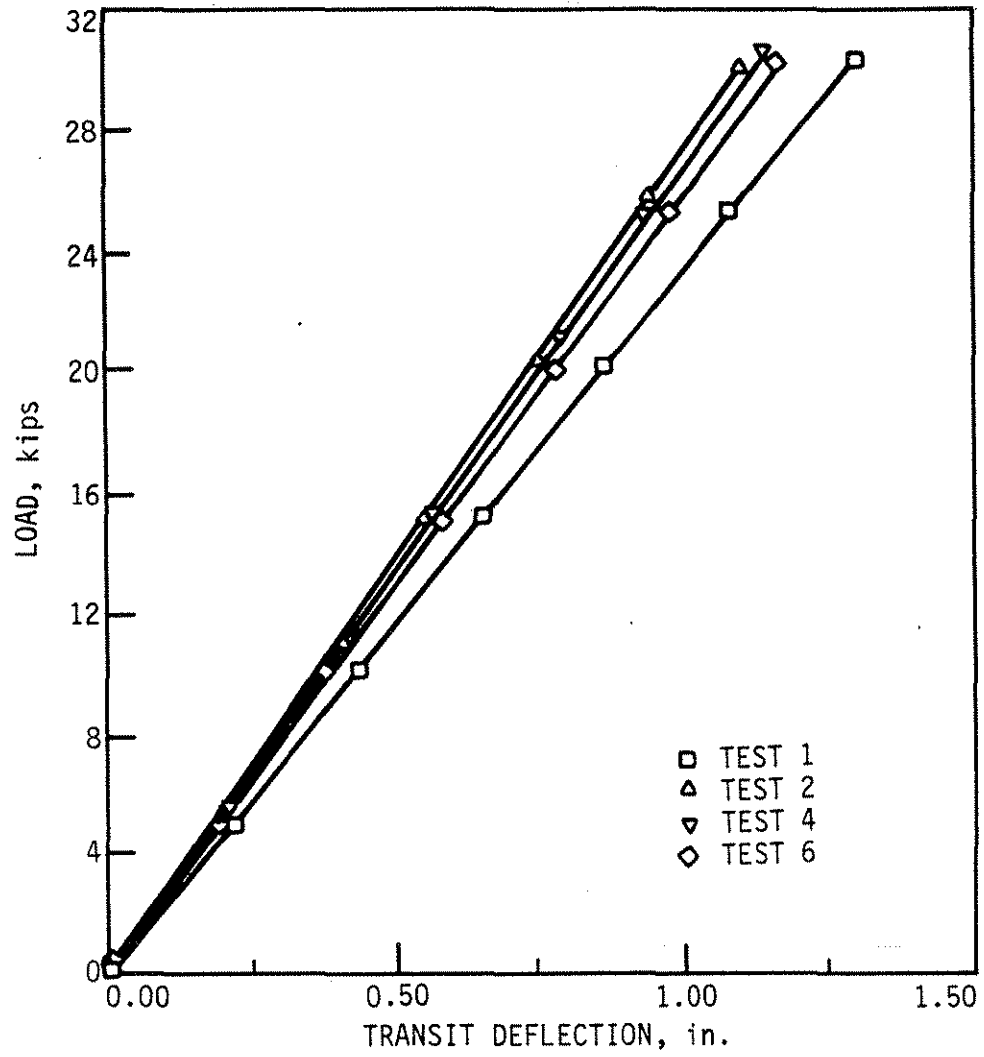
a. MIDSPAN STRAINS

Fig. 1.39. Comparison of results from tests 1, 2, 4, 6.



b. MIDSPAN DEFLECTION

Fig. 1.39. Continued.



c. TRANSIT DEFLECTION

Fig. 1.39. Continued.

understanding of beam behavior because the variance is better defined. As expected, the largest strains and transit deflections were obtained from Test 6, the test with the least stiff bracket.

The midspan strain distribution for these tests is presented in Fig. 1.39a. The figure illustrates that the reductions in strains because of Brackets 3 (Test 4) and 4 (Test 6) are very close in value. Also, it can be seen that Bracket 1 has the steepest slope and therefore is the stiffest of the three bottom flange brackets, thus providing the greatest restraint. These experimental values are better defined than those for midspan deflections because the strain gages were more sensitive than the DCDTs to small changes. Figure 1.39c depicts the transit deflection data. From the data, two major observations can be made: (1) Bracket 3 provided a rotational stiffness very close in magnitude to the rotational stiffness of Bracket 1, which is why the data from both tests are similar, (2) Bracket 4 was not as effective in restraining the beam from rotation as it was in reducing midspan deflections and midspan strains, as has previously been discussed in Section 5.1. The percent reduction in these variables because of the various restraint brackets is presented in Table 1.6. The values in the table are based on comparing the change in slopes of the strain and deflection data. Table 1.6 shows that for these tests, the largest reduction occurred in Test 2 with the bottom flange restrained by Bracket 2. This was anticipated because Bracket 2 was the stiffest of the three bottom flange brackets; thus, it provided the greatest restraint. As previously noted, the bottom flange brackets (Brackets 1, 3, and 4) reduced the midspan deflections by approximately the same percentage. The table also indicates that the bottom flange brackets reduced the transit deflections in various degrees, but once again the differences between the experimental results were small.

Table 1.6. Effects of reduction in bottom flange stiffness.*

Reduction In	Test 2	Test 4	Test 6
Midspan strains	14.57	14.00	11.64
Midspan deflections	19.89	19.99	20.03
Transit deflection	13.01	12.99	9.78

*Based on reduction changes from Test 1 data.

5.1.2.3. Bottom Flange and Web Restrained—Tests 3, 5, and 7

In these tests the web and bottom flange of the beam were restrained, thus idealizing full restraint conditions. As was discussed in Section 5.1.1, total restraint was not achieved; however, the conditions provided in Test 3 were the closest to fixed end conditions attained. For this series of tests, the greatest restraint was achieved in Test 3 and the smallest restraint was provided in Test 7. This was anticipated because the stiffness of the web bracket was the same throughout these tests and the only thing that changed was the stiffness of the bottom flange bracket. In Test 7, Bracket 4 was acting in conjunction with Bracket 2; in the previous section, it was established that Bracket 4 provided the least restraint.

The data from these tests are presented in Fig. 1.40. As with Tests 4 and 6, the reduction in the stiffness of the bottom flange bracket did not greatly affect midspan strains, midspan deflection, and beam rotation in Tests 5 and 7. A general examination of the test data (see Fig. 1.40) reveals that the beam behaved as would be expected with the greatest reduction attained with the largest end restraint. Hence, the brackets in Test 3 were more effective than the brackets in Test 5, and these were more efficient than the brackets in Test 6. However, it must be reiterated that the variance in the data, after some material was removed from the bracket stiffeners, was very small.

In Fig. 1.40a, the strain distribution at midspan is presented. These data along with the transit deflection data (see Fig. 1.40c) provided a clearer representation of beam behavior because the variations between the results were better defined. However, this was not the case for midspan deflections (Fig. 1.40b) where the data did not follow the same pattern as was seen in other tests. Figure 1.40b shows that the midspan deflection measured in Test 5 was greater than that measured in Test 7. This implied that the stiffer bracket was providing less restraint, which obviously is not the case. This perturbation probably occurred because the change in the experimental data was smaller than the DCDT could detect and therefore it was not properly measured by the DCDT. This was also observed in Fig. 1.40c and discussed in Section 5.1.2.2.

The overall reductions in midspan strains, midspan deflections, and transit deflection are presented in Table 1.7. These values are based on a comparison of the slopes. As can be concluded from the above table, the greatest reductions in midspan strains, midspan deflections, and transit deflection were achieved when both the bottom flange and web were restrained (i.e., Test 3). The reduction in midspan deflections and transit deflection from Tests 5 and 7 are similar; the reasons for this have been discussed in Section 5.1.2.1.

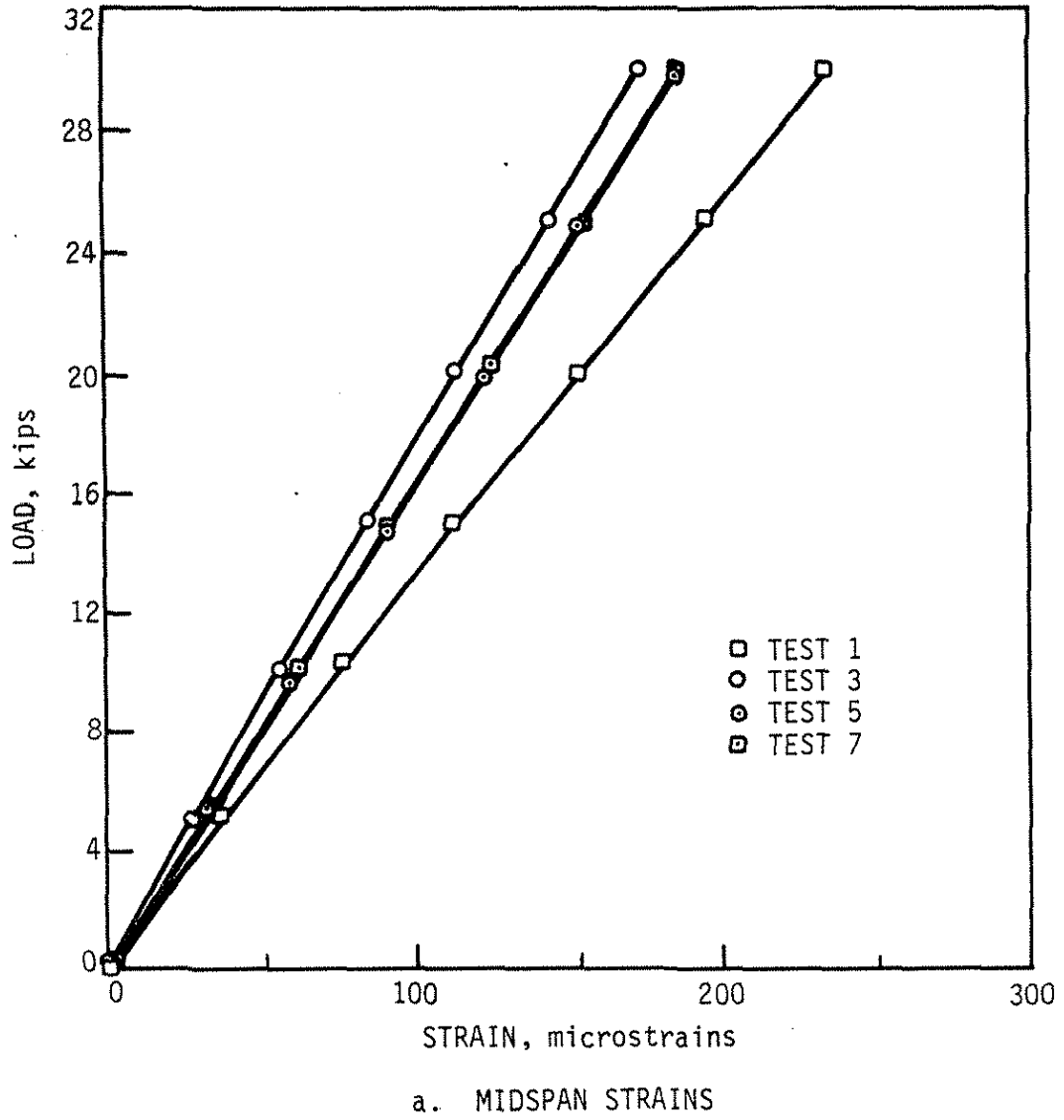
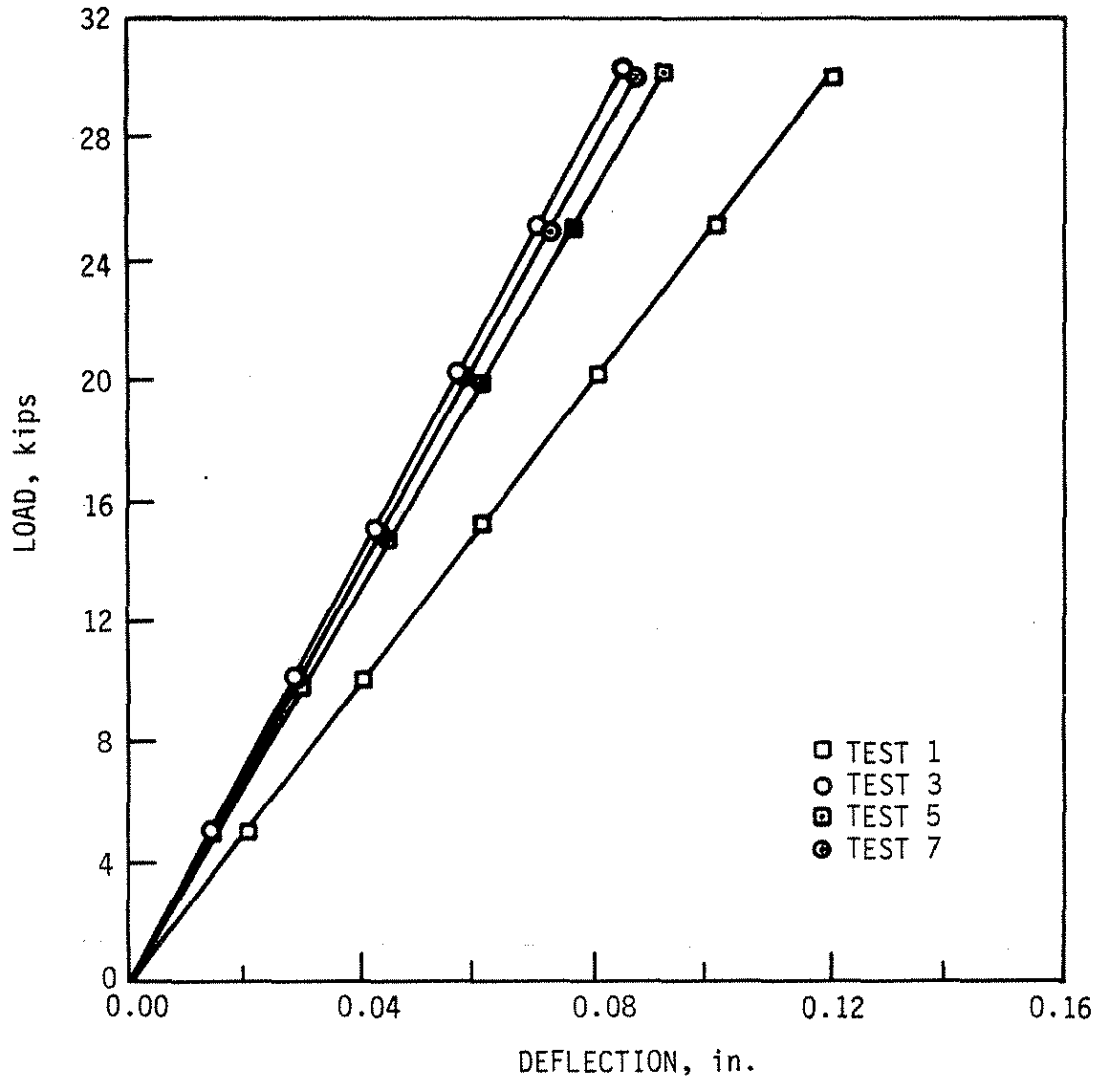
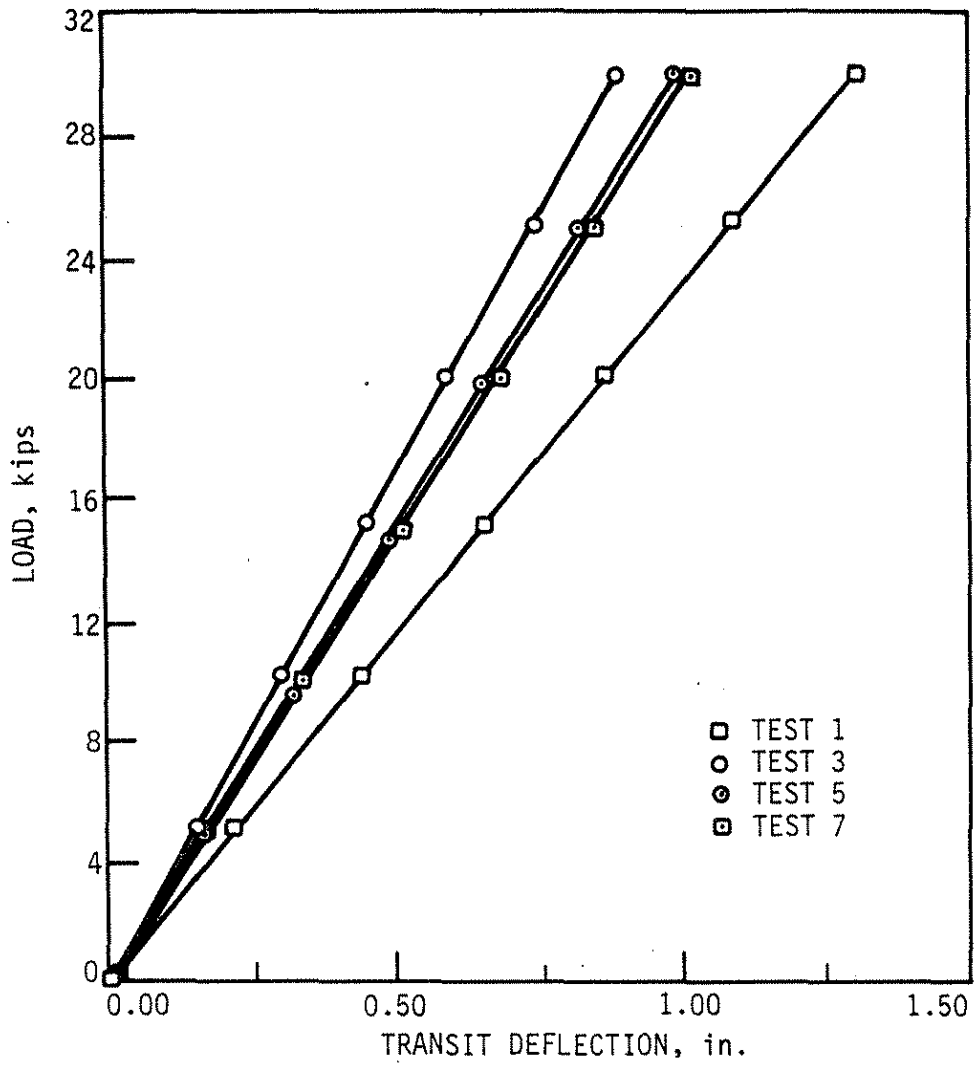


Fig. 1.40. Comparison of results from tests 1, 3, 5, 7.



b. MIDSPAN DEFLECTION

Fig. 1.40. Continued.



c. TRANSIT DEFLECTION

Fig. 1.40. Continued.

Table 1.7. Percent reductions due to full restraint conditions.*

Reduction In	Test 3	Test 5	Test 7
Midspan strains	25.86	20.86	20.37
Midspan deflections	30.02	23.99	28.00
Transit deflection	31.80	24.13	22.28

*Based on reduction changes from Test 1 data.

5.1.2.4. Determination of Bracket Stiffness

As a result of the complicated nature of the bottom flange bracket, the bracket stiffness could not be determined directly. To resolve this dilemma, the researchers resorted to developing a finite-element model of the test beam (see Section 4.1.2) with various degrees of rotational restraint. The model enabled the researchers to determine the restraining moment, M , and also obtain the angle of rotation, θ . From these values, the rotational stiffness, K , was determined such that $K = M/\theta$. In this section the approach used in determining the restraining moment and thus the rotational stiffness will be presented.

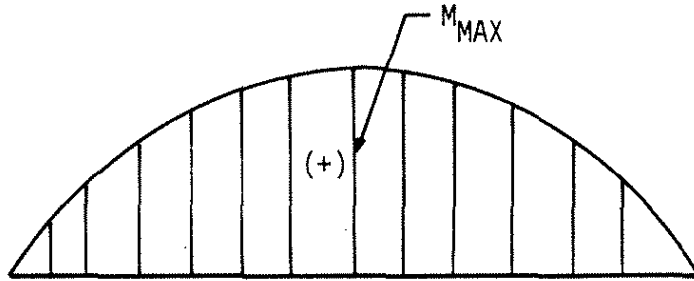
The manner in which the presence of end restraint affects the moment distribution along a beam is illustrated in Fig. 1.41. In general, end restraint shifts the moment diagram such that the moments along the beam are reduced. The amount of moment reduction is a function of the end restraint. Hence, by determining the amount by which the moment was reduced after providing end restraint (i.e., the restraining moment) the rotational stiffness could be determined.

The restraining moment can be determined by equating the moment at various locations, prior to providing any restraint, to the moments from the finite-element analysis at the same locations, plus some fraction of the restraining moment. This fraction can be determined from a linear interpolation if it is known that for the test beam model no restraint existed at Abutment 2 and an unknown amount of restraint existed at Abutment 1.

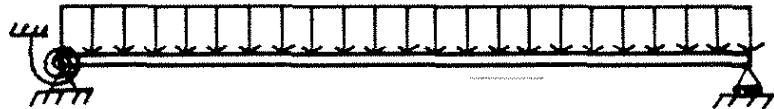
The method of determining the restraining moment, previously described, is presented in Fig. 1.42. This figure shows the loading on the beam and the accompanying moment diagram assuming simple support conditions Fig. 1.42a. The beam was symmetrically loaded;



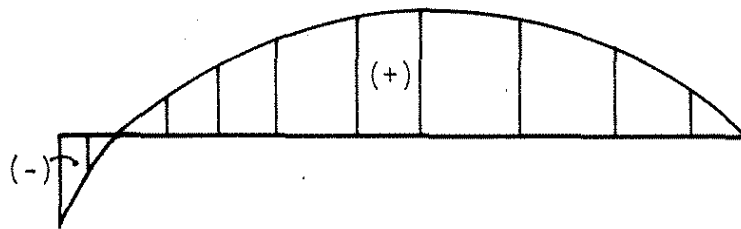
a. ASSUMED SIMPLY SUPPORTED BEAM



b. SIMPLE BEAM MOMENT DISTRIBUTION

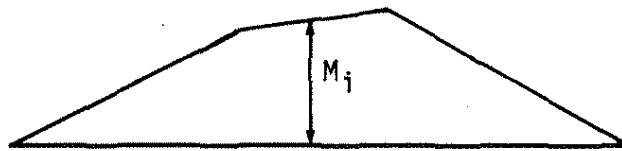
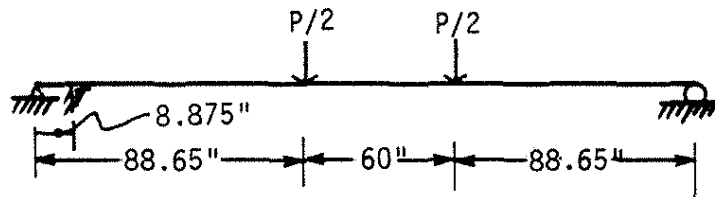


c. BEAM WITH RESTRAINING END CONNECTION

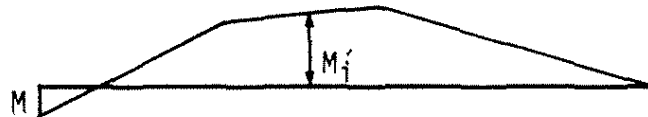
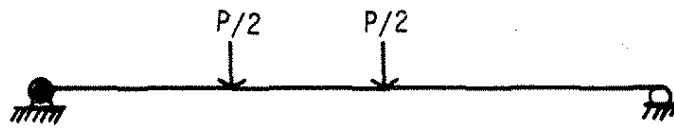


d. MOMENT DISTRIBUTION WITH END RESTRAINT INCLUDED

Fig. 1.41. Effects of end restraint in beams.



a. SIMPLE SUPPORT CONDITIONS



b. ROTATIONAL RESTRAINT PROVIDED



c. MOMENT FRACTION

Fig. 1.42. Determination of restraining moment.

however, after the bottom flange was attached, the span length decreased. Hence, for the analytical work the support conditions were assumed to exist at the back attachment of Bracket 1 and at Abutment 2 and that is why the lengths in Fig. 1.42 are not equal. Part b of Fig. 1.42 illustrated the location of the rotational restraint and the moment distribution obtained from the finite element model. Finally, part c of Fig. 1.42 shows the moment fractions at various locations. From this, the governing equation takes the following general form:

$$M_i = M'_i + C_i M$$

where

- M_i = moment from simple beam analysis at any point (i)
- M'_i = moment from finite-element analysis at any point (i)
- M = restraining moment
- C_i = moment distribution fraction at any point (i)

The only unknown is the restraining moment, which can be determined by using the above equation. In this study, reductions in midspan moments were of greatest interest. Therefore, all subsequent comparisons were made at midspan. The following table (Table 1.8) presents moment values at midspan obtained from the finite-element model and from the experimental results for the three bottom flange bracket configurations.

Table 1.8. Comparison of analytical and experimental midspan moments.

Bracket	Midspan Moments, k-in.		
	Analytical	Experimental	% Difference
1	1215	1339	9
3	1236	1355	8.8
4	1246	1372	9.2

From the results it can be seen that the analytical model was stiffer than the actual test beam. Two probable reasons account for that: the beam might be corroded at various locations (i.e., reduced section properties) and the bottom flange bracket was not providing as much restraint as assumed in the model.

The three bottom flange brackets—Brackets 1, 3, and 4—were analyzed with the finite-element model. By using the method previously discussed the restraining moment for each case was determined. The angle of rotation was determined by taking the average rotation of the top plate of the bracket. There were a total of 15 nodes on the top plate and the average of the rotation at all the nodes gave the rotation of the bracket. Hence, with these two values defined, the rotational stiffness can be determined. The results are presented in Table 1.9. As can be seen from the table, the first reduction in bracket material reduced the bracket stiffness by 18%, and the second reduction reduced the stiffness by an additional 8%. Thus, this indicated that the second material reduction would not affect the data greatly. This was also cited in the experimental data, which will be discussed in subsequent sections. These stiffness values were then used to model the restraint conditions on the model bridge (see Section 4.2.1).

Table 1.9. Bracket stiffnesses.

Bracket	Restraining Moment (M, k-in.)	Angle of Rotation (θ , rad.)	Rotational Stiffness, (K, k-in./rad.)	Reduction Stiffness
1	510.76	0.8935×10^{-3}	571639	—
3	469.06	0.1001×10^{-2}	468730	18
4	447.96	0.1066×10^{-2}	419994	26

The finite-element analysis of the test beam and brace also provided the researchers with information on the magnitude of forces that could be expected to be transmitted to the abutment. This information is presented in Table B.2 of Appendix B for the three brackets investigated. Assuming six connectors, the largest tensile and shear forces found were 9 kips and 10 kips, respectively. Based on this it was determined that a 1 1/8-in. diameter, 12-in.-long anchor bolt would provide the required capacity. These anchor bolts are readily available on the market.

5.2. Model Bridge Analysis and Test Results

Descriptions of the testing program and restraining mechanisms used have previously been presented in Sections 3.2.2 and 2.2.3, respectively. A total of 14 tests were performed on the model bridge; half of these tests used one concentrated load at various locations and the other half used two concentrated loads. These tests ranged from providing no restraint to restraining the flanges and webs of all stringers. Graphical and tabular results of these tests will be discussed in this section. The graphs will focus on the transverse strain distribution at various load points, while the tables will present the strain reductions induced by the different restraining brackets for all load points.

This section will be divided into two parts: The first will discuss only the experimental results and the second will focus on the analytical results and their correlation to the experimental work. In addition to this, the first part will be subdivided into two sections. This first section presents the results for one concentrated load and the second section discusses the result for two concentrated loads. The analytical work will also be subdivided into two sections. The first one presents a comparison of the analytical and experimental results for both types of loading and the second one discusses the sensitivity of the bridge to various rotational stiffnesses. As was previously mentioned, a finite-element analysis of the model bridge, including end-restraint effects, was performed.

5.2.1. Experimental Results

5.2.1.1. One Concentrated Load

In the testing program for the vertical load tests with one concentrated load (Section 3.2.2.1), the effects of restraint were minimal in the span farthest from the restrained end (far span). Therefore, this span was not loaded during the first phase of testing. Figure 1.43 shows a plot of the longitudinal strain distribution along Beam 2 for the load at load point 5 (i.e., midspan of Beam 2 in the span closest to the restraint, near span). The abscissa represents sections at various locations along the beam; Sections 1, 3, and 5 refer to the center of each of the three spans with Section 1 closest to the restrained end. Sections 2 and 4 represent locations at the two interior supports. (See Fig. 1.21 for additional information on the location of these sections.) As the graph shows, the effects of the various restraint brackets are relatively insignificant in the far span (i.e., at Sections 4 and 5). This behavior

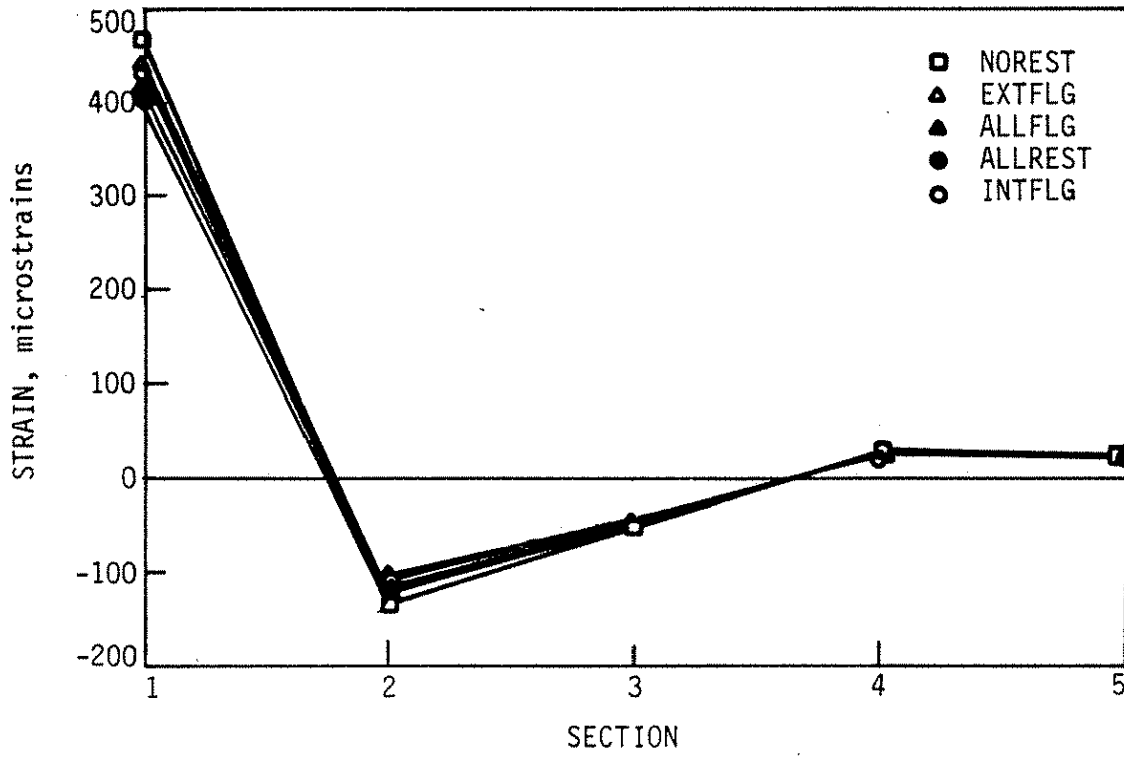


Fig. 1.43. Plot of longitudinal strain distribution for Beam 2; load at LP 5.

was typical for all stringers and load points. The strain varied from approximately 450 microstrains in the first span to approximately 20 microstrains in the far span. Thus, it was concluded that loading the farthest span from the restrained end would not be beneficial.

Symmetrical restraint conditions were imposed on the bridge for the first five tests. These tests simulated no restraint provided (NOREST), the bottom flange only of the two exterior beams restrained (EXTFLG), bottom flanges of all stringers restrained (ALLFLG), bottom flanges of the two interior stringers restrained (INTFLG) and full restraint (web and bottom flange brackets) of all four stringers (ALLREST). As previously stated, the objective of these various tests was to determine the most effective combinations of restraining brackets.

All the data from these five tests are presented in Table C.1 of Appendix C. This table shows what is happening to the four beams as the load is applied. The table shows several cases where the strain readings are very small (under 100 microstrains). This is an indication that the stringer was essentially not affected by the position of the load. For instance, a strain of 28 microstrains was measured at Beam 1 when the load was applied at load point 1 (see Fig. 1.24). The table basically gives the percent reduction in strains. However, there were instances where the strains increased when restraint was provided; these cases are identified with a negative sign. It can also be concluded from the table that providing full restraint will not necessarily always give the best results. For instance, restraining all the flanges when the load was at load point 2 for Beam 1 was more effective than if all the flanges and webs were restrained. In addition to this, it was noticed that restraining the interior beams reduced the strains on the exterior unrestrained beams by very little, whereas restraining the exterior flanges reduced the strains on the interior beams by a greater percentage.

The effects of asymmetrical restraint conditions were also investigated in Tests AS4 and AS3 in which only Beam 4 and Beam 3 were fully restrained, respectively. The data from these tests are presented in Table C.2 of Appendix C. However, the major portion of the investigation focused on the first five tests since it is perceived that symmetrical restraint conditions will prove to be more effective. In all the tests, the transverse strains, as opposed to the longitudinal strains, were plotted so as to portray the behavior of the four beams together.

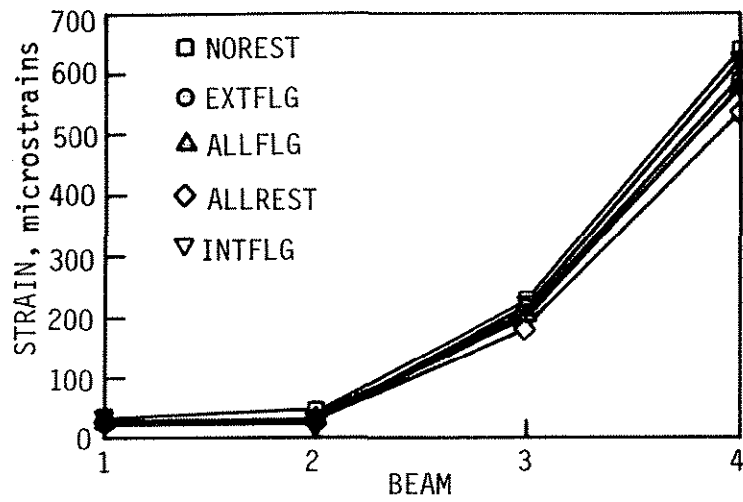
The concentrated load was placed at a total of ten different locations for this series of tests. Graphs of strains were plotted for all these load points at a transverse section near midspan of the near span. The graphs illustrate the bridge's responses to the restraint and showed that reductions in strains were achieved, especially in the near span. These graphs also validated the assumption that symmetry existed and could be taken advantage of in the

data reduction. In addition, the graphs showed that the greatest reduction in strains and deflection occurred in the span nearest the restraint. These two observations determined that only the stringer behavior caused by loading in the first span needed to be further examined and presented in this section. In addition, because of symmetry, only half of the load points in the first span needed examining. Hence, the response of the four stringers to the application of the load at four representative locations will be presented. These four locations are at LP 1, 2, 3, and 4 (see Fig. 1.24). The plots in Fig. 1.44 indicate that for these load points, the greatest reductions were achieved when all the flanges and webs of the four stringers were restrained. However, the effectiveness of the other restraint schemes varies, depending on the location of the load and the type of restraint provided. For instance, at LP 1, restraining the interior stringer flanges did not reduce the strains significantly and the difference was not too great between restraining only the exterior flanges as compared to all the flanges. At LP 2 there was not a significant reduction in strains because of restraining the interior, exterior, or all flanges of the stringers. In Fig. 1.44c, it can be seen that at LP 3 restraining the exterior flanges greatly reduced the strains on the exterior Beam 4, whereas it did not affect the strain reduction on the interior beams. However, only restraining the interior flanges significantly reduced the strains on both the interior and exterior beams. In Fig. 1.44d, the load is positioned at the center of the first span and therefore should produce a symmetrical strain distribution; however, the load was slightly off-center and therefore the readings are not identical.

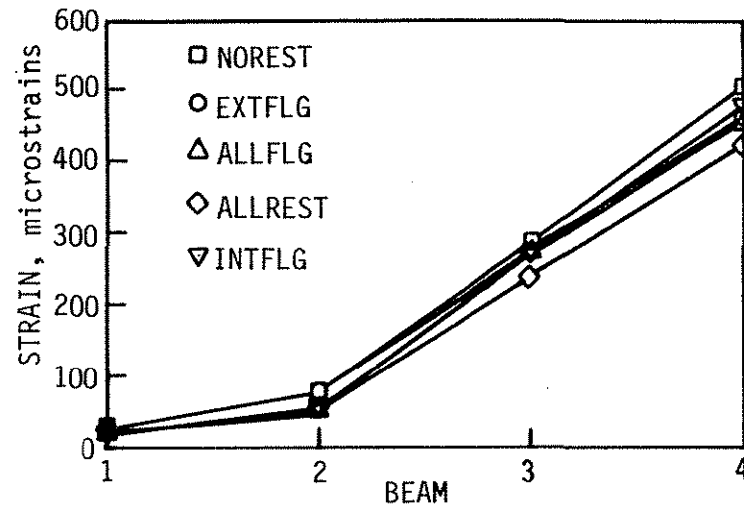
The plots of the asymmetrical restraint conditions are shown in Fig. 1.45. As can be seen in Fig. 1.45a, fully restraining the exterior Beam 4 did not affect Beams 1 and 2 and only slightly affected Beam 3. However, fully restraining the interior Beam 3 significantly affected the other beams. The amount by which the strains were reduced is presented in Table C.2 of Appendix C.

5.2.1.2. Two Concentrated Loads

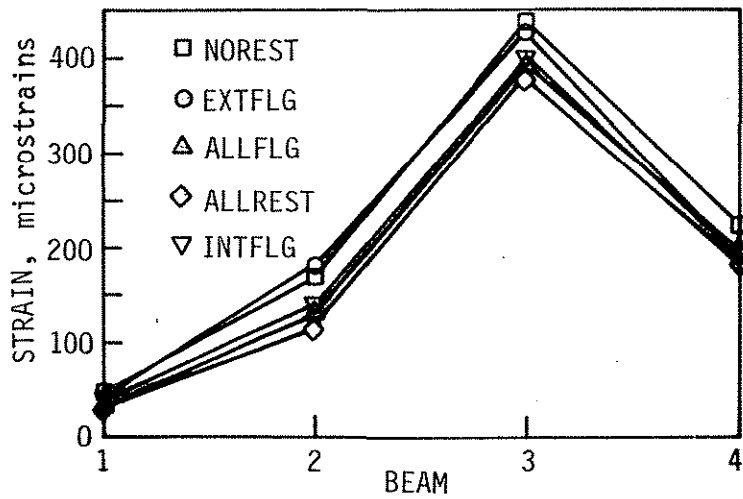
It would have been desirable to investigate the effects of end restraint on a single span bridge; however, since the three-span continuous model bridge already existed in the laboratory, it was tested. For these tests, pattern loading using two concentrated loads was used to attain the maximum positive and negative moments in the bridge. There were a total of eight loading combinations examined for each test. In addition, the effects of symmetric and asymmetrical restraint conditions were examined and will be presented in this section.



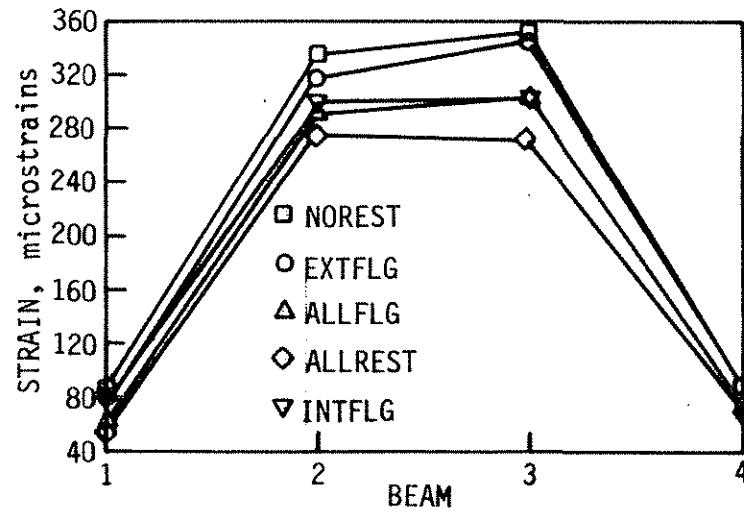
a. LP1



b. LP2



c. LP3



d. LP4

Fig. 1.44. Plot of transverse strain at Section 1 for one concentrated load (symmetrical restraint) at various load points.

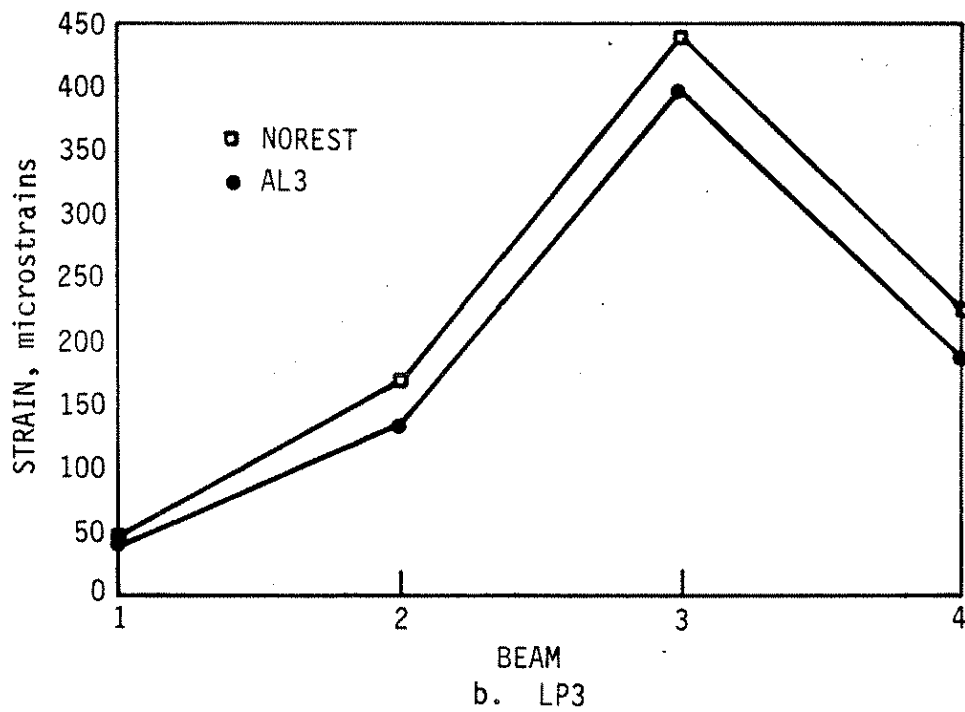
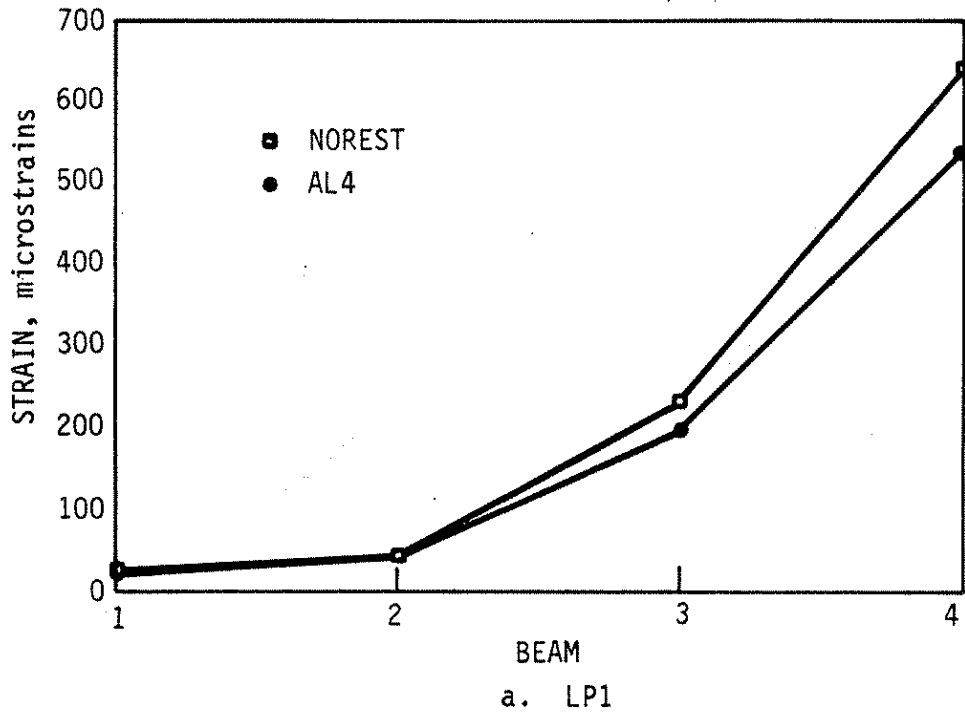


Fig. 1.45. Plot of transverse strain at Section 1 for one concentrated load (asymmetrical restraint) at various load points.

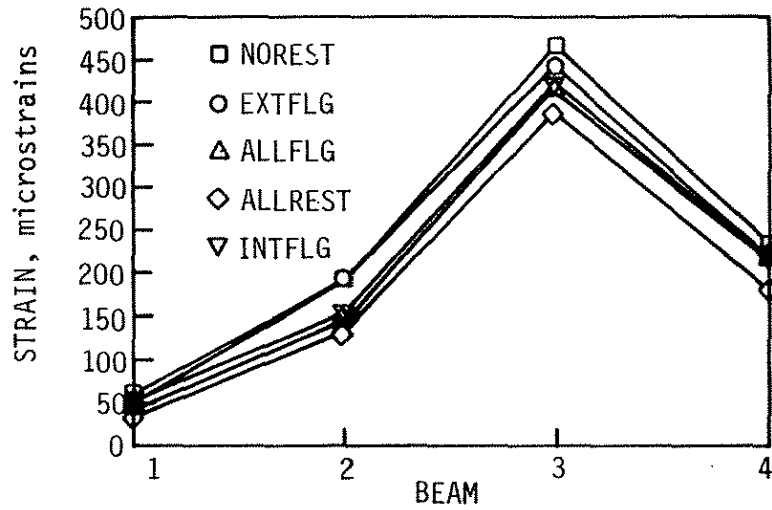
Symmetrical restraint conditions were imposed on the bridge for the first five tests (see Section 5.1.1.1). The objective was to determine the most effective combination of restraining brackets. All the data from these five tests are presented in Table C.3 of Appendix C.

As shown in Table C.3, the strains on the interior beams were larger than those on the exterior beams, because the pattern of two concentrated loads could not be directly placed on the exterior beams due to space limitations within the laboratory. Data also indicated that providing full restraint to all the beams was the most effective in substantially reducing the strains on the exterior beams. This was also the case for the interior beams; however, the percentage difference in reduction between full restraint and the other restraint conditions was greater for the exterior beams. This is expected because the exterior stringers in the model bridge were not as stiff as the interior stringers. The exterior beams were not greatly affected when the interior stringer flanges were restrained, and the beams responded in a similar way when either all the flanges or only the exterior flanges were restrained. The interior beams, on the other hand, were not affected greatly when the exterior flanges were restrained and responded better to restraining the interior or restraining all flanges. However, unlike the behavior of the exterior beams, the interior beams did not respond similarly to having only the interior flanges restrained as opposed to having all flanges restrained.

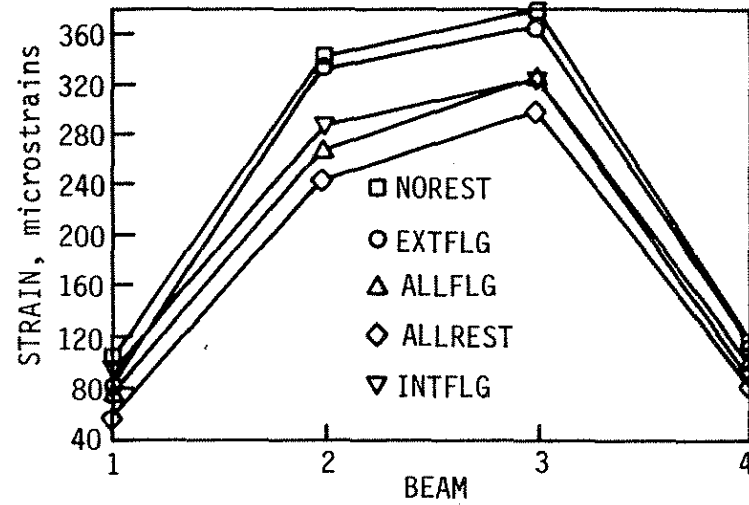
Asymmetrical restraint conditions were also examined while two concentrated loads were being applied. In AS4 the exterior beam, Beam 4, was fully restrained; in AS3 the interior beam, Beam 3, was fully restrained; the results are presented in Table C.4 of Appendix C.

As previously mentioned, the two loads were applied in eight different arrangements producing maximum positive moment and maximum negative moment regions. Load points 2, 4, 6, and 8 produced the maximum positive moments in the near and far span, and load points 1, 3, 5, and 7 produced the maximum negative moments over the first interior pier (nearest to restrained abutment). However, since the investigation focused on the reduction of positive moment, only the effects of load points 2, 4, 6, and 8 on the bridge will be further examined. Graphs of the transverse strain distribution were plotted and are shown in Fig. 1.46. In a subsequent section, comparisons will be made between the analytical data and experimental data at which time some deflection data will be presented.

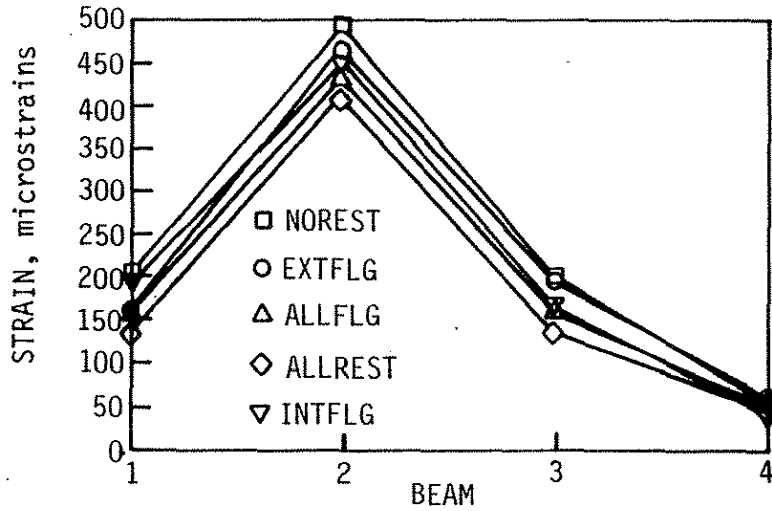
The graphs in Fig. 1.46 are useful in determining the restraint mechanism most useful within a region and in comparing the magnitude of strains on various beams. In general, providing full restraint to all the stringers produced the best results. In Fig. 1.46a,



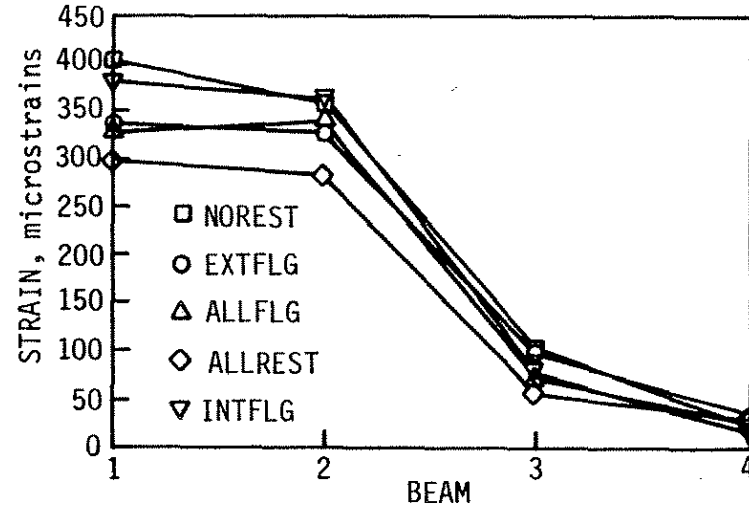
a. LPs 3 & 17



b. LPs 4 & 18



c. LPs 5 & 19



d. LPs 6 & 20

Fig. 1.46. Plot of transverse strain at Section 1 for two concentrated loads (symmetrical restraint) at various load points.

restraining only the exterior flanges did not reduce the strains by very much, whereas restraining only the interior flanges or all flanges had essentially the same effect. These same conclusions can be reached by examining Fig. 1.46c, which is a mirror image of Fig. 1.46a. Figure 1.46b shows the loads positioned at midspan, which should produce a symmetrical strain distribution. Examination of Fig. 1.46b reveals that the results were slightly asymmetrical. Once again, full restraint of the bottom flanges and webs for all four stringers was the most effective in reducing the strains. Restraining the exterior flanges was not as effective as restraining either the interior flanges or all the flanges. The strain distribution in Fig. 1.46d reveals that for this type of loading, the behavior of the bridge cannot be simply characterized because the effectiveness of the various restraint configurations varies continuously.

In Fig. 1.47, the case of providing asymmetrical restraint conditions is illustrated. This graph is plotted for LP2 when the interior beam, Beam 3, is fully restrained. As noted in the previous section, fully restraining the interior beam had a significant impact on the strain reduction at all the stringers.

5.2.2. Analytical Results

5.2.2.1. Comparison of Analytical and Experimental Results

The analytical bridge model discussed earlier (Section 4.2.1) was modified for simulating end bracket attachments, and analyses were performed to further study the bracket effects on overall bridge behavior. The model, with end restraint capabilities, was validated by comparing strain and deflection data with laboratory experimental tests. As the bottom flange bracket was modeled with the test beam (see Section 4.1.2), providing full restraint to the bottom beam flange, a similar configuration was modeled for the bridge. This was achieved by restraining the bottom flanges of the four bridge stringers. For validation, a bracket stiffness of $K = 3000\text{k-in./deg.}$ was used to simulate the lower flange bracket. This stiffness value represents an appropriate scaled value from the prototype flange bracket stiffness of $K = 580,000\text{k-in./rad.}$ Analytical and experimental data are compared for one and two concentrated load cases in Figs. 1.48 through 1.50, respectively. As shown in Figs. 1.48 and 1.49, representing strain comparisons, the model provided an accurate simulation of the experimental results. The largest discrepancy (for one stringer) was approximately 20%; however, most other data points compared within 5% of each other. The primary reason for the 20% discrepancy was the initial "stiffer" bridge model discussed in

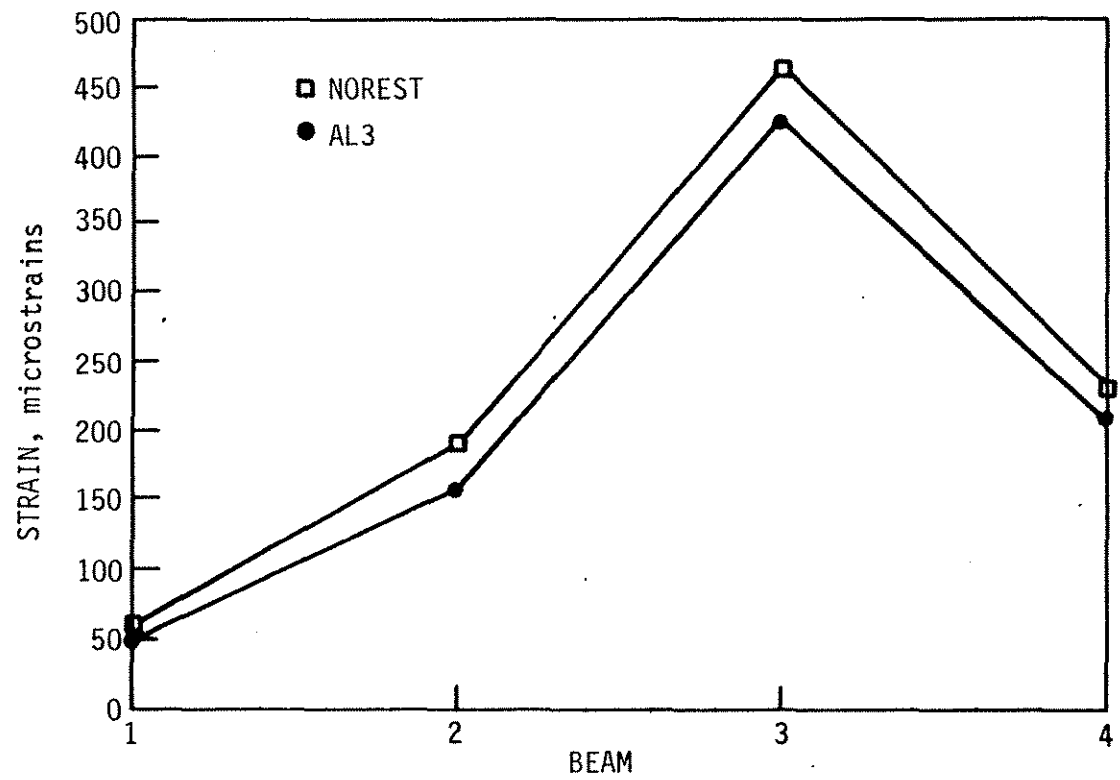
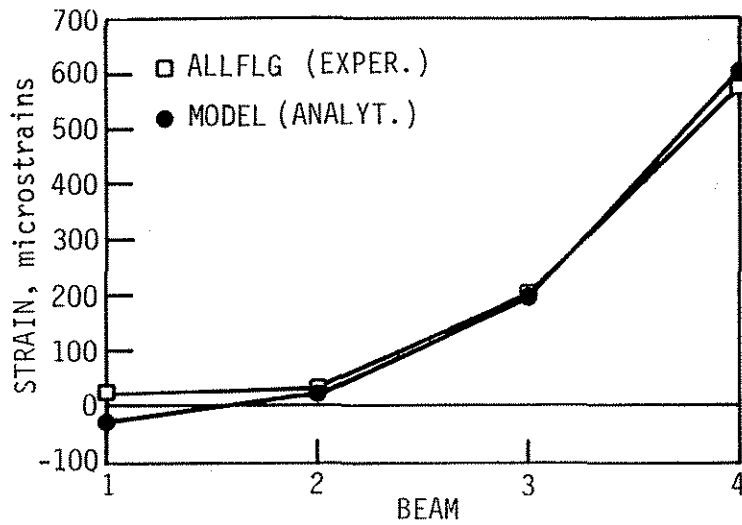
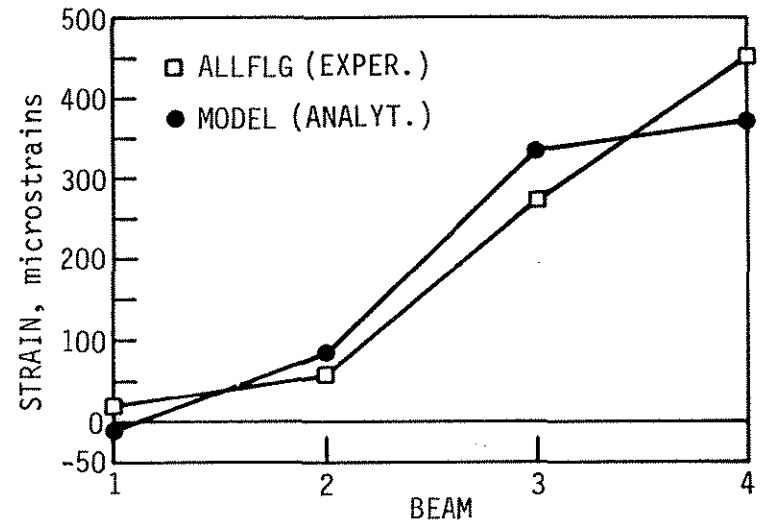


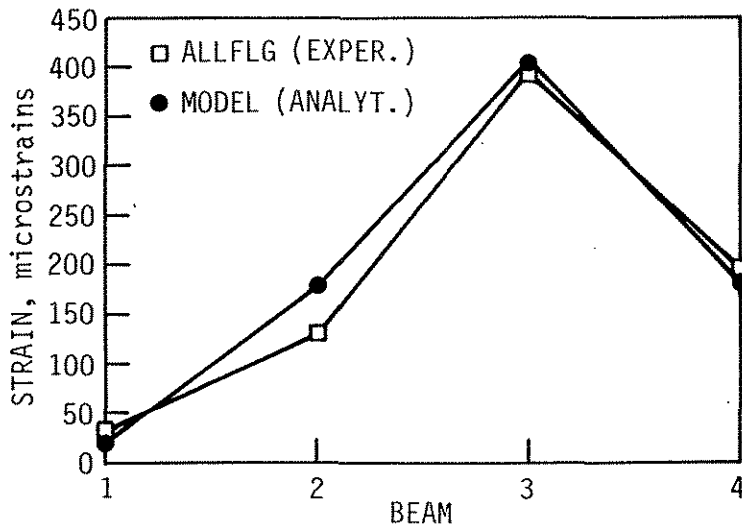
Fig. 1.47. Plot of transverse strain at Section 1 for two concentrated loads (asymmetrical restraint); loads at LPs 3 & 17.



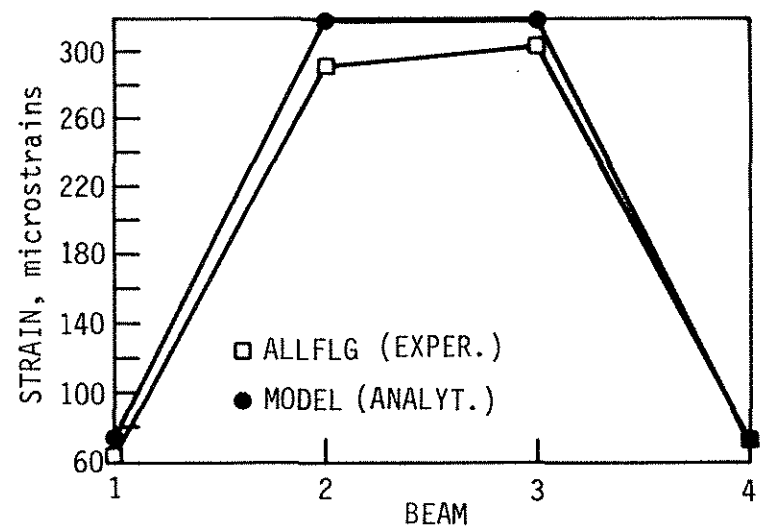
a. LP1



b. LP2

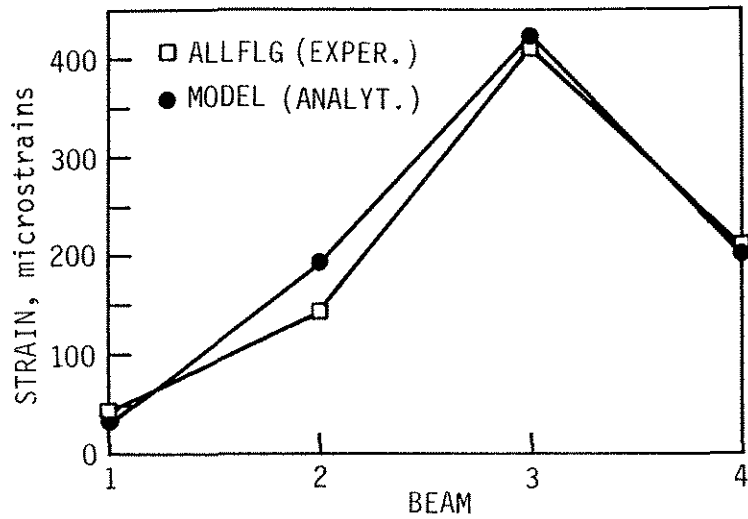


c. LP3

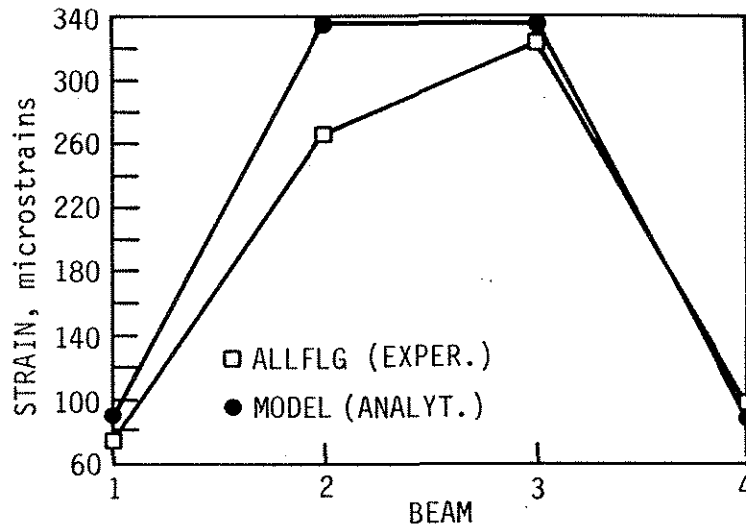


d. LP4

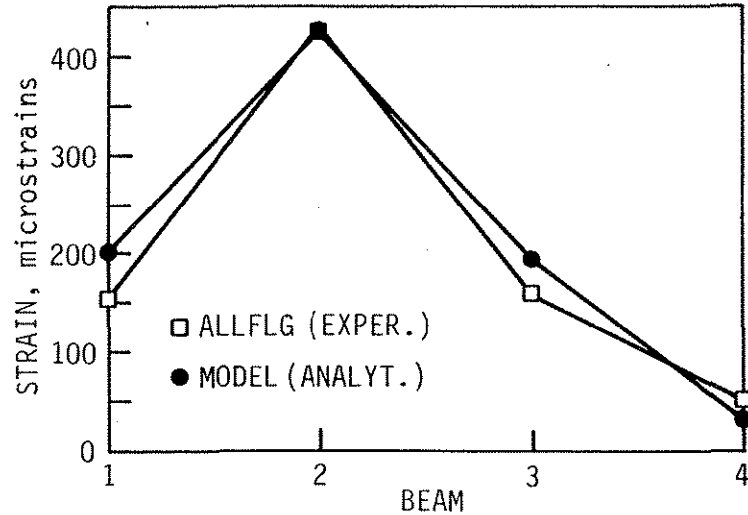
Fig. 1.48. Plot of transverse strain at Section 1 for one concentrated load at various load points for all flanges restrained--model vs. experimental.



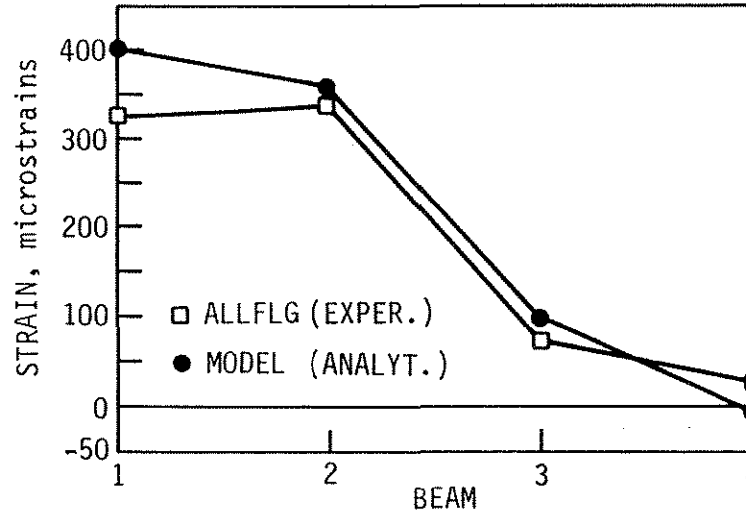
a. LPs 3 & 17



b. LPs 4 & 18



c. LPs 5 & 19



d. LPs 6 & 20

Fig. 1.49. Plot of transverse strain at Section 1 for two concentrated loads at various load points for all flanges restrained--model vs. experimental.

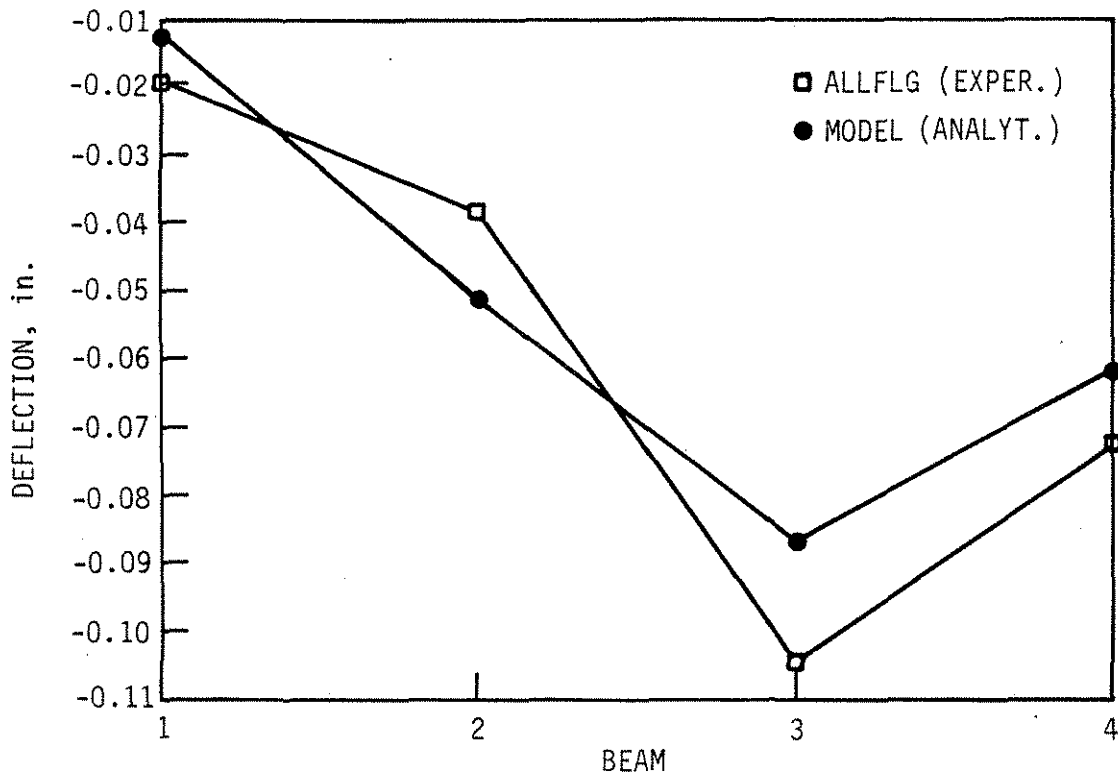


Fig. 1.50. Plot of transverse deflection at Section 1 for two concentrated loads at LPs 3 & 17 for all flanges restrained--model vs. experimental.

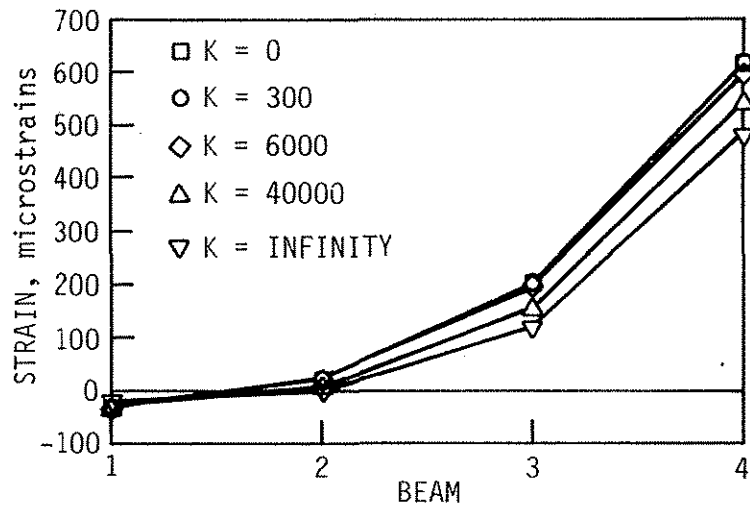
Chapter 4. This is shown for the load point 2 in Fig. 1.48. (Load point is referred to as LP in all figures.) The deflection comparisons were fairly similar to strain results. Figure 1.50 shows a typical plot for load point 2 for the two concentrated load cases. Based upon these results, it was concluded that the analytical model accurately simulated the prototype.

5.2.2.2. Sensitivity Study

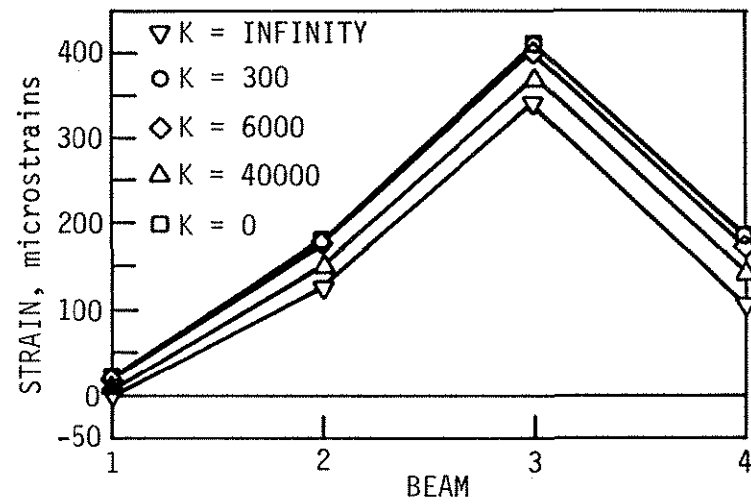
Once the model was validated, a sensitivity study was performed that included varying the end bracket stiffness to study corresponding effects on strain and deflection. The range of stiffness values included the values in the range of the lower flange bracket, as well as the upper and lower limit values of $K = 0$ and $K = \infty$. Two other values were selected: $K = 300$ k-in./deg and $K = 40,000$ k-in./deg. The smaller value was selected arbitrarily to determine the effect of an extremely lower limit value. The larger stiffnesses referred to reasonable values that may be obtained by adding additional thickness to the plate material in the bracket or by using web brackets with the flange bracket.

Plots are shown for three load cases associated with one concentrated load (load points 1, 3, and 4) and for three load cases for two concentrated loads (load points 2, 4, and 6). Figures 1.51 through 1.54 show strain and deflection effects for five and four different end bracket stiffnesses, respectively. As the plots illustrate, the sensitivity of the results for the change of stiffness from $K = 6000$ to $40,000$ k-in./deg. was relatively significant, with strains decreasing by approximately 5%. The change in strain from $K = 6000$ to $10,000$ k-in./deg was obviously not as significant, but it is of interest to note that the change in strain for this range of stiffness in the bridge was similar to that noted for the prototype laboratory test beam for similar changes in stiffness. In other words, after the first material reduction (Bracket 1 to Bracket 3), a significant reduction in stiffness occurred and this had a definite impact on the data obtained. However, the second material reduction did not further decrease the stiffness by a significant amount. Hence, a significant increase or decrease in stiffness was required in order to affect the data one way or another.

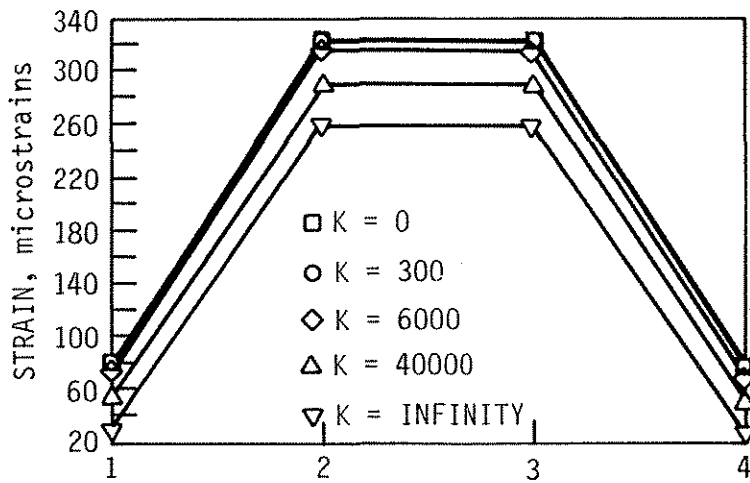
In addition to what was previously presented, the researchers thought it advantageous to determine the magnitude of stiffness required to produce a certain predetermined reduction in strains. Hence, an analytical study was performed with the validated bridge model to determine the magnitude of end restraint required to cause an approximate 10% reduction in midspan strain in the near span region. The 10% value was selected arbitrarily, but the authors believe this is a realistic design value should consideration be given to strengthening an existing stringer bridge by providing end restraint. The 10% reduction was relative to the



a. LP1

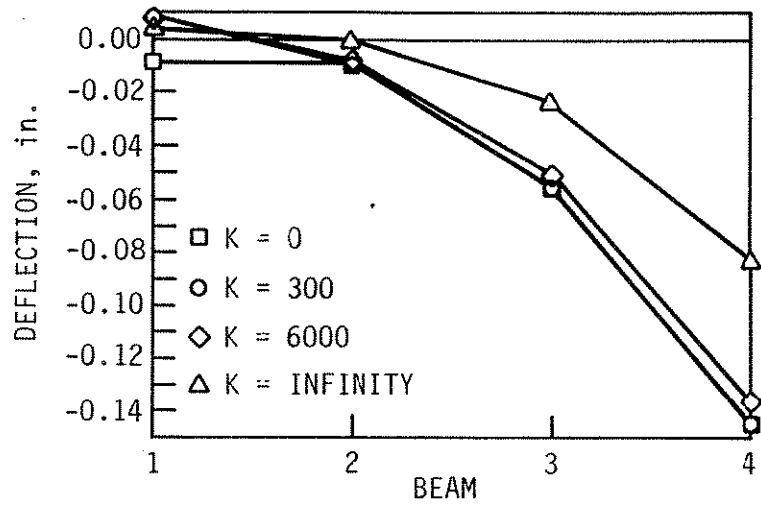


b. LP3

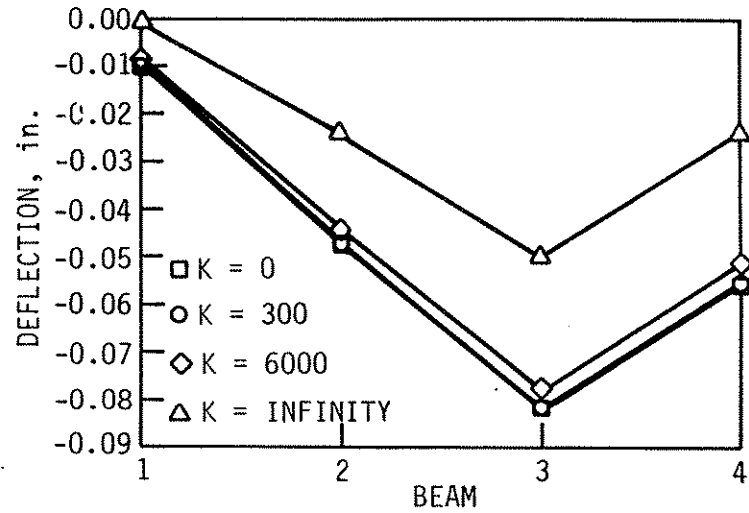


c. LP4

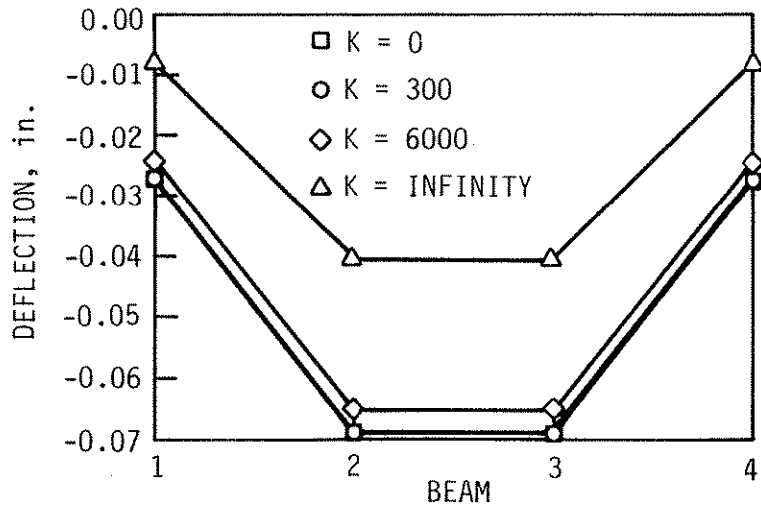
Fig. 1.51. Plot of analytical transverse strains at Section 1 for one concentrated load at various load points for various conditions of end restraint.



a. LP1

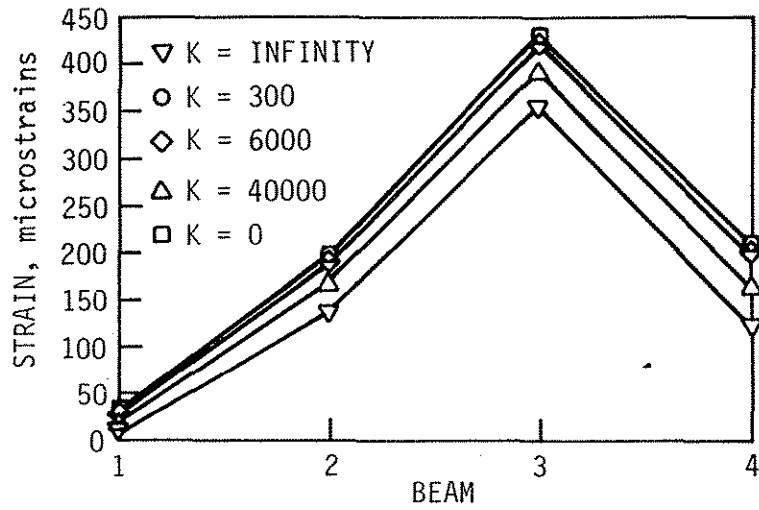


b. LP3

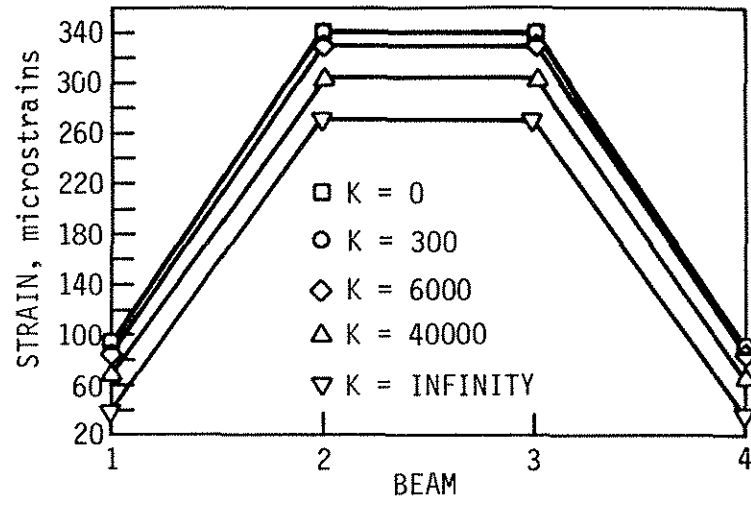


c. LP4

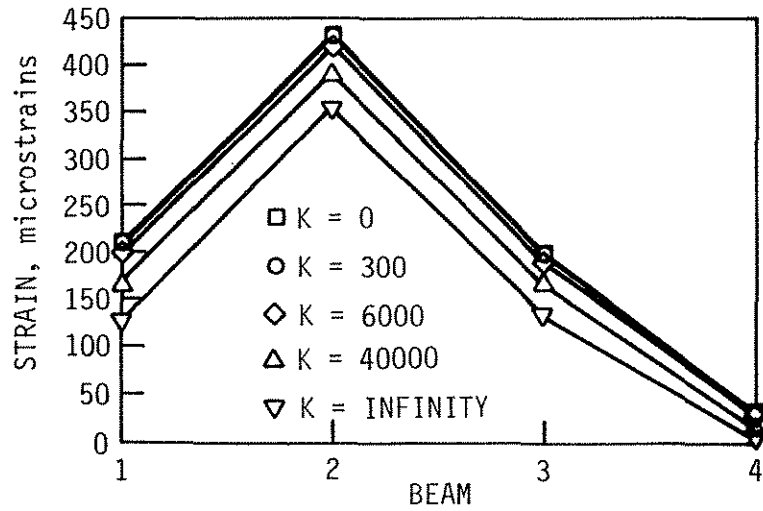
Fig. 1.52. Plot of analytical transverse deflections at Section 1 for one concentrated load at various load points for various conditions of end restraint.



a. LPs 3 & 17



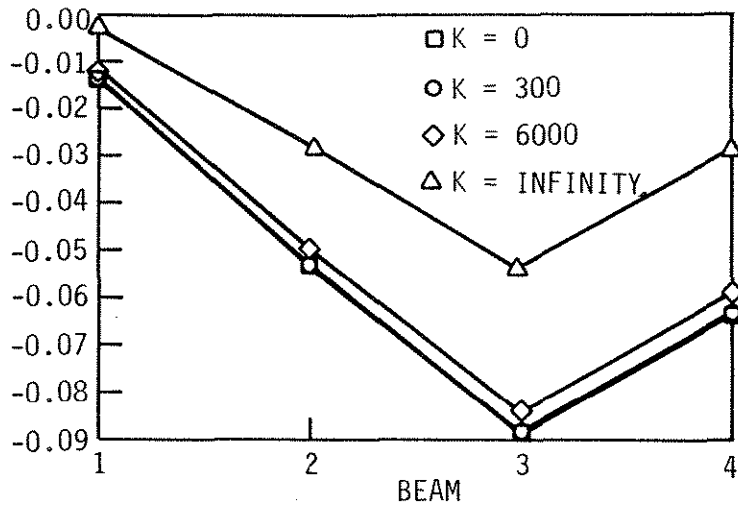
c. LPs 5 & 19



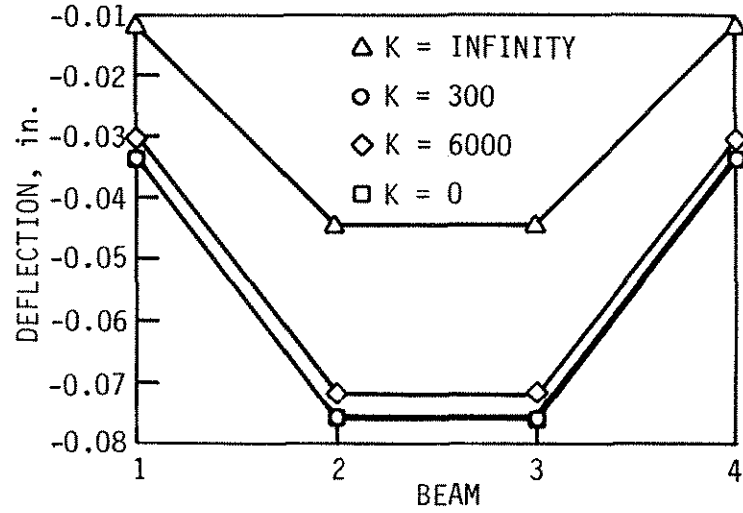
b. LPs 4 & 18

Fig. 1.53. Plot of analytical transverse strains at Section 1 for two concentrated loads at various load points for various conditions of end restraint.

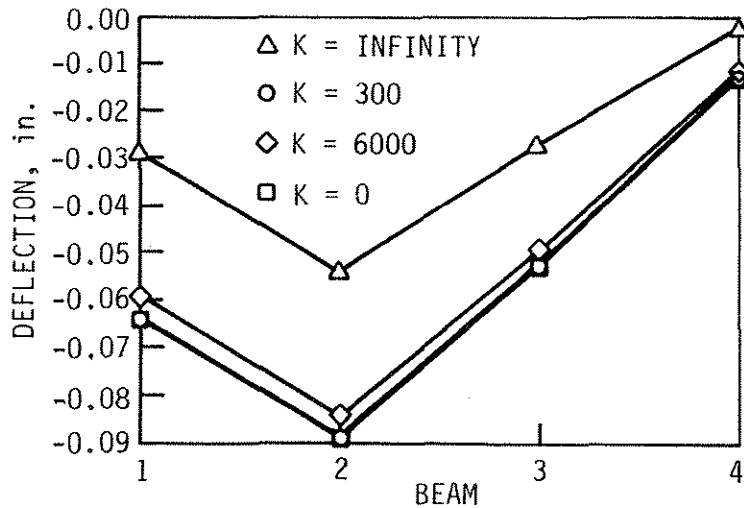
DEFLECTION, in.



a. LPs 3 & 17



b. LPs 4 & 18



c. LPs 5 & 19

Fig. 1.54. Plot of analytical deflections at Section 1 for two concentrated loads at various load points for various conditions of end restraint.

case with no end-restraint bracket (i.e., the *in situ* condition). The 10% reduction criterion was considered with respect to the most heavily loaded (or most stressed) stringer, and thus is the basis on which the data are presented. Data for two cases (load points 1 and 3) for the one concentrated load case and three cases (load points 2, 4, and 6) for the two concentrated load cases are presented. A summary of the results are shown in Table 1.10. To satisfy the above-mentioned criteria, the required end-restraint stiffness needs to approach approximately 10 times that provided by the flange bracket designed in this study (i.e., $K = 3000$ k-in./deg.). The implications of this analytical study are that either the flange bracket needs to be stiffened, or the web bracket must be used in combination with the flange bracket to achieve strain reductions of this magnitude. It should be noted that although the deflection data are not presented for these tests, the decrease in deflection was more significant than for strain. In some of the cases in Table 1.10, the deflection reductions were approximately 20%.

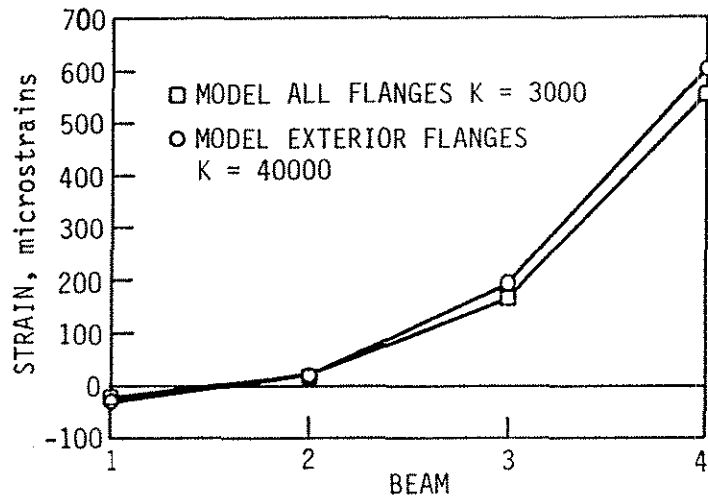
Table 1.10. Results of study to obtain 10% strain reduction.

Load Point (No. of Concentrated Loads)*	% Reduction in Strain for Heaviest Loaded Stringer (%)		
	K = 30,000 k-in./deg	K = 40,000 k-in./deg	K = 50,000 k-in./deg
LP 1 (1)	9.8	11.4	12.6
LP 3 (1)	7.7	8.9	9.9
LPs 3 and 17 (2)	8	9.3	10.3
LPs 4 and 18 (2)	9.1	10.7	11.9
LPs 5 and 19 (2)	8.1	9.5	10.5

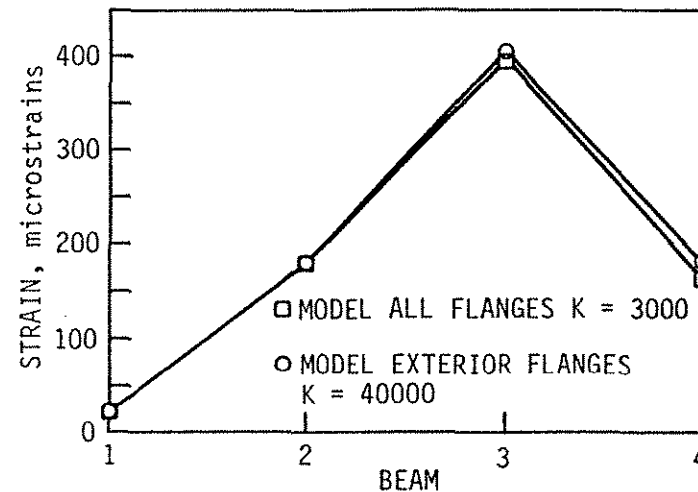
*See Fig. 1.24 for location of load points.

Based on the experimental and analytical data presented thus far, it was noted that a more effective restraint bracket system (i.e., greater positive strain reduction) occurred when exterior only, rather than interior only, stringers were restrained. This suggested that it may be possible to restrain only exterior stringers to reduce strains in the exterior and interior stringers and therefore reduce the amount of field work needed to employ the system. However, to gain the same benefits obtained by restraining all stringers would require increases

in the stiffness of the brackets on the exterior stringers. Therefore, a brief analytical study was performed to determine the effectiveness of this idea. The exterior stringers were assigned stiffnesses of $K = 40,000$ k-in./deg. and the interior stringers left unrestrained. This exterior stiffness is approximately ten times greater than that provided by the flange brackets used in the model bridge tests. Figures 1.55 and 1.56 show the results of this investigation, with strains plotted for two cases (load at LPs 1 and 3) for one concentrated load and two cases (loads at LPs 3 and 17 and LPs 6 and 20) for two concentrated loads. In each of the plots shown, the most effective condition for reducing midspan strain occurs for the case of exterior stringers restrained with the large stiffness. The strain reductions relative to the flange restrained condition ranged from 2% to 9% for the highest stressed stringers. Depending on the adequacy of the abutment of a given bridge for handling the applied moment as well as the adequacy of the bracket connection, this idea of restraining only exterior stringers has merit.

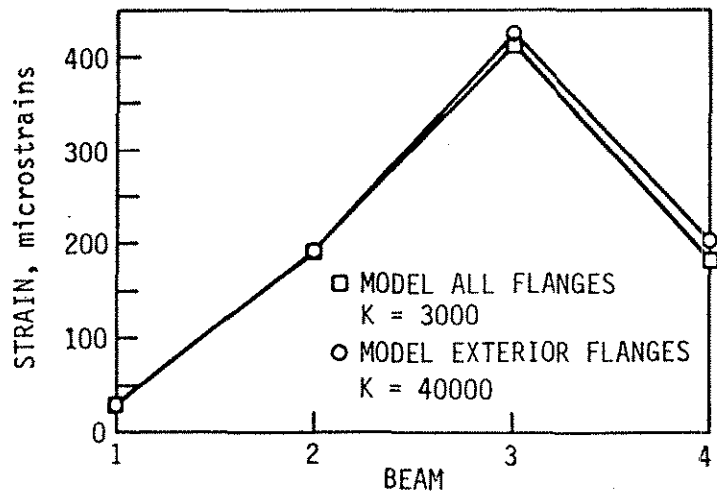


a. LPs 3 & 10

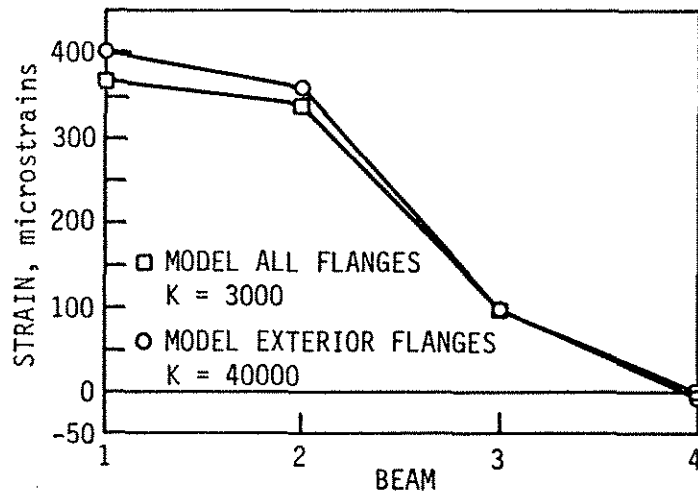


b. LPs 4 & 11

Fig. 1.55. Plot of transverse strain at Section 1 for one concentrated load at various load points--exterior flanges only restrained.



a. LPs 3 & 17



b. LPs 6 & 20

Fig. 1.56. Plot of transverse strain at Section 1 for two concentrated loads at various load points-- exterior flanges only restrained.

6. SUMMARY AND CONCLUSIONS

6.1. Summary

This section summarizes the initial research in determining the feasibility of strengthening existing bridges by restraining the end of bridge stringers against rotation. The research program included a review of existing literature, testing of a full-scale bridge beam, testing of a 1/3-scale bridge model, and a finite-element analysis of the restraint brackets, the test beam, and the model bridge.

The literature search involved a review of existing publications on end-restraint connections for bridge stringers. Although several cases were found that cited the effects of end restraint on the behavior of a bridge, none of the literature attempted to quantify the degree of the restraint present. A considerable amount of literature reviewed was related to general building connection behavior; it served only as background information.

The primary purpose of this investigation was to determine the feasibility of utilizing partial end restraint to strengthen simple-span bridges as well as continuous bridges. Although this method would reduce the existing positive moment along the length of the stringers, only the reduction at the midspan of the stringers was investigated. Assuming no cover plates, this would be the overstressed location in a simple-span bridge. As end restraint is increased, larger stress reductions at midspan can be achieved. In stringers with cover plates, the location of the overstress may be at the cover plate cutoff points rather than near midspan. If this is the case, sufficient end restraint would have to be provided to reduce stresses at the overstressed section(s) (i.e., midspan and/or cutoff points). End restraint may be achieved with a variety of end-restraint brackets, including bottom flange and web connections. The effectiveness of these end-restraint brackets in reducing midspan moments and deflections is a function of the bracket stiffness. In general, larger stress reductions can be obtained with a larger bracket stiffness. However, the correlation between stress reduction and bracket stiffness is nonlinear. This implies that after a certain stiffness, the reductions obtained may not offset the additional expenses required to attain that stiffness. Also, greater stiffnesses will result in larger forces to be resisted by the abutment. This may not be desirable because the abutment may not be able to withstand these additional forces. In addition to this, the bridge bearings already provide a certain amount of restraint and the restraining bracket will be adding to the inherent restraint. This inherent restraint

obviously varies from one bridge to another depending on the type of bearings used, the maintenance program, and so forth.

A secondary purpose of providing partial end restraint was to determine the effects of various end-restraint mechanisms on stress reductions and to determine the most effective location for the restraint. The effects of the restraining brackets were measured in the testing of both the beam and the model bridge. However, determination of the most effective location to place the restraint brackets was a part of the testing scheme on the model bridge. This was achieved by restraining the four stringers in a variety of ways ranging from completely restraining all four stringers to restraining only one of the exterior stringers.

The test beam setup was fabricated to represent one beam of a single-span bridge. The beam has section properties similar to those of a V12 series bridge; the abutment was specifically designed to accommodate the attachment of the various restraint brackets and to approximate the interaction between beam and abutment found in the field. The model bridge was designed for a previous, unrelated research project; therefore certain modifications had to be made so that it could be used in this project. The most significant change was the addition of the abutment back wall. The back wall attachment was designed to closely resemble the back wall portion of Abutment 1 of the test beam in both capacity and capabilities for attaching brackets. Both the test beam and model bridge were instrumented to measure strains and deflections at critical locations.

In addition to the experimental work, finite-element analyses were performed on the bottom flange brackets, test beam, and model bridge. Two finite-element software packages, ANSYS and SAP IV, were used in conducting this analytical work. ANSYS was used in modeling the end restraint brackets and also in modeling the test beam. Several of the preprocessing and postprocessing computer programs from earlier research programs were adapted for use with continuous bridges and were used with SAP IV to analyze the laboratory model bridge. The three finite-element models were all interrelated. For instance, the results from the bracket analysis were needed in order to model the test beam, and the results of test beam analysis were needed to model the laboratory bridge.

6.2. Conclusions

The following conclusions were developed as a result of this study:

- (1) Composite concrete-deck steel-beam bridges, especially single span, can be strengthened by providing partial end restraint. The restraint may be provided by various bracket configurations; however, bottom flange and web brackets were investigated in this research program and found to be effective.
- (2) Attachment of the restraint brackets to existing bridges in the field is feasible. Anchorage systems are on the market that would facilitate the attachment of these brackets and allow for the transmittal of forces from the superstructure to the substructure. However, the ability of the substructure (abutment, piles, etc.) to resist these additional forces must first be investigated further. In addition, the effect of abutment response to the restraint must be quantified to determine the effect on the restraint mechanism effectiveness.
- (3) The effectiveness of the restraint brackets is a function of their stiffnesses. In general, the larger the stiffness, the greater the anticipated reductions. This is valid to a certain point after which the increase in stiffness is perhaps no longer physically or economically practical.
- (4) For the brackets investigated, restraining the test beam (simulated bridge stringer), restraining both the bottom flange and web was most effective in reducing midspan strains and beam rotation, and not as effective in reducing midspan deflections, whereas restraining only the bottom flange was most effective in reducing midspan deflections and less effective in reducing midspan strains and beam rotation.
- (5) Providing end restraint to one end of a continuous bridge is only effective in reducing strain in that span and in the adjacent interior span.
- (6) The effectiveness of the end restraint brackets in reducing midspan strains and deflections is a function of the location of the restraining brackets. In general, it was found that restraining the flanges and webs of all stringers was the most effective.

7. RECOMMENDED FURTHER RESEARCH

The present study has shown that composite concrete-deck steel-beam bridges, especially single span, can be strengthened by providing partial end restraint. On the basis of the literature review, test results, and finite-element analyses, the following research should be undertaken to take the concept to the implementation stage.

- (1) An investigation of bridge standards and existing bridges in the state of Iowa needs to be undertaken in order to categorize these bridges based on support conditions, type of abutments, presence and length of the various types of cover plates, and so forth. On the basis of this categorization of bridges, end restraint brackets could then be designed.
- (2) One or more actual bridges should be strengthened by using the end-restraint technique. The strengthening of the bridge should be tested initially and then monitored for a period of several years to ensure that no unforeseen problems develop.
- (3) An in-depth analysis of the bridge abutments and soil conditions needs to be conducted. This is to determine whether or not some of the weaker abutments can withstand the additional forces that would be imposed because of the end restraint. This is of great importance to ensure against localized failure, stability problems, or both.
- (4) A review of existing anchorage systems available on the market will be needed for design of brackets.
- (5) Development of a design methodology, standard series of end-restraint mechanism, and so forth for use by the practicing engineer.

8. BIBLIOGRAPHY

1. Bahkt, Baidar, and L. G. Jaeger, "Bearing Restraint in Slab-on-Girder Bridges," *Journal of Structural Engineering*, 114(12):2724-2740, December 1988.
2. Bathe, K. J., E. L. Wilson, and F. E. Peterson, *SAP IV, A Structural Analysis Program for Static and Dynamic Response of Linear Systems*, Berkeley: College of Engineering, University of California, 1974.
3. Beal, David B., "Failure Test of a Jack-Arch Bridge," Interim Report on Research Project 156-2, Engineering Research and Development Bureau, New York State Department of Transportation, Albany, New York, February 1984.
4. Bjorhovde, Reidar, "Effect of End Restraint on Column Strength--Practical Applications," *Engineering Journal*, 21(1):1-13, 1984.
5. Chen, W. F., "End Restraint and Column Stability," *Journal of the Structural Division*, 106(ST11):2279-2295, November 1985.
6. Dunker, K. F., F. W. Klaiber, B. L. Beck, and W. W. Sanders, Jr., "Strengthening of Existing Single-Span Steel Beam and Concrete Deck Bridges, Final Report--Part II," ERI Project 1536, ISU-ERI-Ames-85231, Ames: Engineering Research Institute, Iowa State University.
7. Dunker, K. F., F. W. Klaiber, F. W. Daoud, W. E. Wiley, and W. W. Sanders, Jr., "Strengthening of Existing Continuous Composite Bridges, Final Report," ERI Project 1846, ISU-ERI-Ames-88007, Ames: Engineering Research Institute, Iowa State University, 1987.
8. Dunker, K. F., F. W. Klaiber, and W. W. Sanders, Jr., "Design Manual for Strengthening Single-Span Composite Bridges by Post-Tensioning, Final Report--Part III," ERI Project 1536, ISU-ERI-Ames-85229, Ames: Engineering Research Institute, Iowa State University, 1985.
9. Dunker, K. F., "Strengthening of Simple Span Composite Bridges by Post-Tensioning," Ph.D. Dissertation, Iowa State University, Ames, Iowa, 1985.
10. El-Metwally, S. E., and W. F. Chen, "Moment-Rotation Modeling of Reinforced Concrete Beam-Column Connections," *American Concrete Institute Structural Journal*, No. 85-S36, 1988.
11. Ferjencik, P., and M. Tochacek, *Die Vorspannung im Stahlbau* (Prestressing in Steel Structures) (in German). Berlin: Wilhelm Ernest & Sohn, 1975.
12. Griffiths, T. M., and A. R. Kukreti, "Simplified Design of 8-Bolt Stiffened Moment End Plates," *American Institute of Steel Construction Engineering Journal*, 25(2):52-53, 1988.
13. Hambly, E. C., and Pennells, E., "Grillage Analysis Applied to Cellular Bridge Decks," *The Structural Engineer*, 267-275, 1975.

14. Jaeger, L. G., and Bahkt, Baidar, "The Grillage Analogy in Bridge Analysis," *Canadian Journal of Civil Engineering*, 9:224-235, 1982.
15. Jones, S. W., P. A. Kirby, and D. A. Nethercot, "Influence of Connection Stiffness on Column Strength," *The Structural Engineer*, 65A(11):399-405, November 1987.
16. Kandall, C., "Increasing the Load-Carrying Capacity of Existing Steel Structures," *Civil Engineering*, 38(10):48-51, October 1968.
19. Kim, J. B., R. J. Brungraber, and J. M. Yadlosky, "Truss Bridge Rehabilitation Using Steel Arches," *Journal of Structural Engineering*, 110(7):1588-1597, July 1984.
20. Klaiber, F. W., D. J. Dedic, K. F. Dunker, and W. W. Sanders, Jr., "Strengthening of Existing Single Span Steel Beam and Concrete Deck Bridges (Phase I)," ERI Project 1536, ISU-ERI-Ames-83185, Ames: Engineering Research Institute, Iowa State University, 1983.
21. Klaiber, F. W., K. F. Dunker, T. J. Wipf, and W. W. Sanders, Jr., "Methods of Strengthening Existing Highway Bridges," National Cooperative Highway Research Program Report 293, Transportation Research Board, 1987.
22. Klaiber, F. W., K. F. Dunker, and W. W. Sanders, Jr., "Feasibility Study of Strengthening Existing Single Span Steel Beam Concrete Deck Bridges, Final Report," ERI Project 1460, ISU-Ames-81251, Ames: Engineering Research Institute, Iowa State University, 1981.
23. Krishnamurthy, Natarajau, Jorng-Te Huang, Paul K. Jeffery, and Louie K. Avery, "Analytical M-Theta Curves for End-Plate Connections," *Journal of the Structural Division*, 105(ST1):133-145, January 1979.
24. Lee, K. K., Duen Ho, and Huang-Wan Chung, "Static and Dynamic Tests of Concrete Bridge," *Journal of Structural Engineering*, 113(1):61-73, January 1987.
25. Lindsey, Stanley D., Socrates A. Ionnides, and Arvind Goverdahn, "LRFD Analysis and Design of Beams with Partially Restricted Connections," *Engineering Journal*, 22(4):157-162, 1985.
26. Lui, E. M., and W. F. Chen, "End Restraint and Column Design Using LRFD," *Engineering Journal*, 20(1):29-39, 1983.
27. Mazroi, Ali, Leon Ru-Liang Wang, and Thomas M. Murray, "Effective Coefficient of Friction of Steel Bridge Bearings," *Transportation Research Record 903*, 1983.
28. Moulton, Lyle K., "Observations of Highway Bridge Movements and Their Effects on Joints and Bearings," *Transportation Record 903*, 1983.
29. Mueller, T., "Umbau der Strassenbruecke ueber die Aare in Aarwangen," (Alteration of the Highway Bridge over the Aare River in Aarwangen) (in German), *Schweizerische Bauzeitung*, 87(11):199-203, March 13, 1969.

30. Murray, Thomas M., and Anant R. Kukreti, "Design of 8-Bolt Stiffened Moment End Plates," *American Institute of Steel Construction Engineering Journal*, 25(2):45-52, 1988.
31. Reiffenstuhl, H., "Eine Bruecke mit Druckspannbewehrung-Konstruktion, Berechnung, Baudurchfuehrung, Messungen," (A Bridge with Compression-Stressed Reinforcing-System, Computation, Construction, Field Measurements) (in German), *Beton-und Stahlbetonbau*, 77(11):273-278, November 1982.
32. Reiffenstuhl, H., "Das Vorspannen von Bewehrung auf Druck: Grundsatzliches and Anwendungsmoeglichkeiten," (Prestressing of Reinforcing in Compression: Fundamentals and Application Possibilities) (in German) *Beton-und Stahlbetonbau*, 77(3):69-73, March 1982.
33. Reiffenstuhl, H., "Verstaerkung eines Sporthallendaches mit Druckspannbewehrung" (Strengthening of an Athletic Building Roof with Compression Stressed Reinforcement), *Beton-und Stahlbetonbau*, 78(6):149-154, June 1983 (German).
34. Sawko, F., "Recent Developments in the Analysis of Steel Bridges Using Electronic Computers," London: British Constructional Steelwork Association Conference on Steel Bridges, 1-10, 1968.
35. Schilling, Charles G., "Moment-Rotation Tests of Steel Bridge Girders," *Journal of Structural Engineering*, 114(1):134-149, January 1988.
36. Vinnakota, Srirmulu, "Planar Strength of Restrained Beam Columns," *Journal of the Structural Division*, 108(ST11):2496-2516, November 1982.
37. Yettram, A. L., and M. H. Husain, "A Grid Framework Method for Plates in Flexure," *Journal of the Engineering Mechanics Division*, 91(Em3): 53-64, 1965.

**9. APPENDIX A: DETAILS OF REINFORCEMENT
FOR ABUTMENT 1**

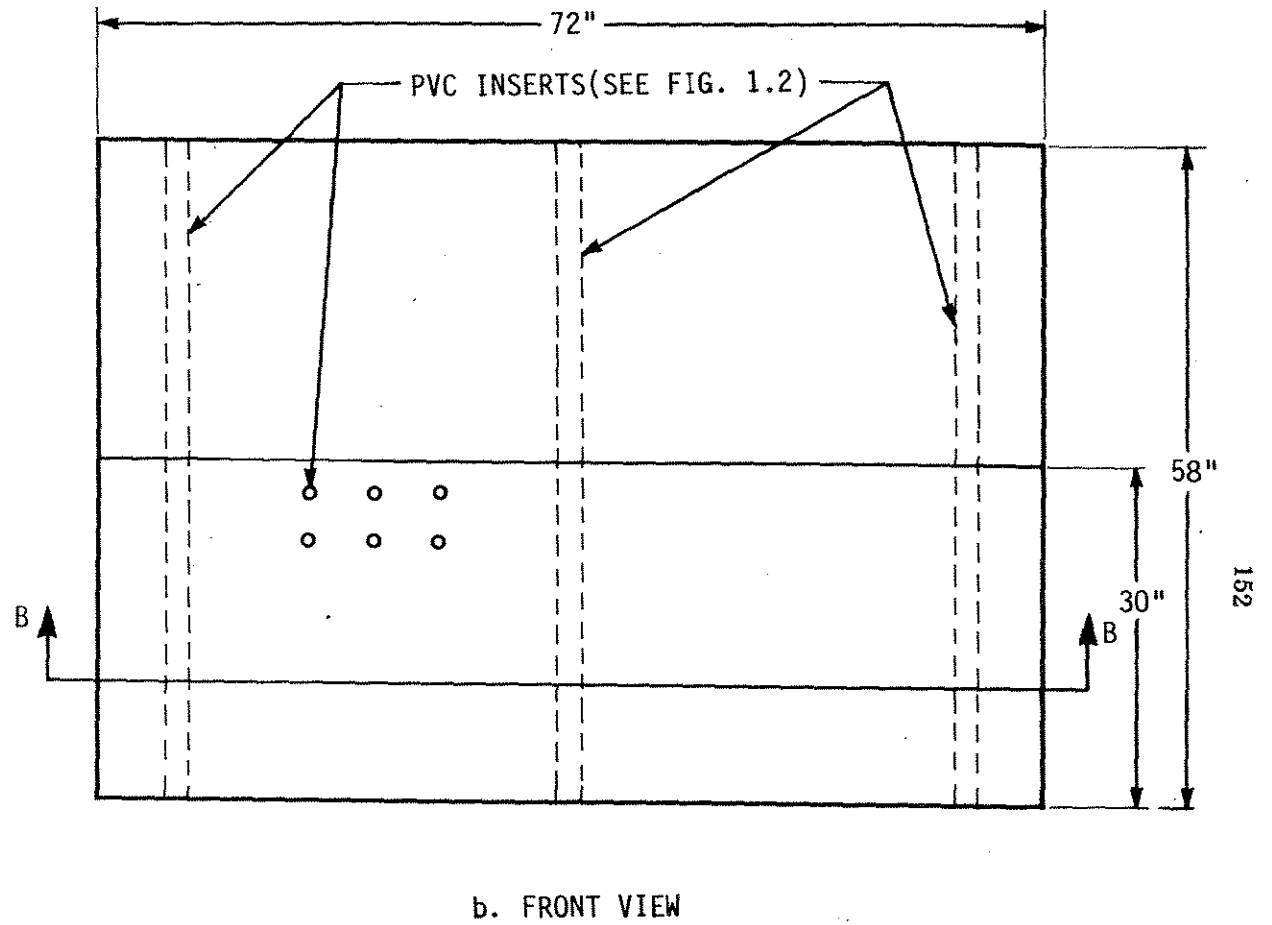
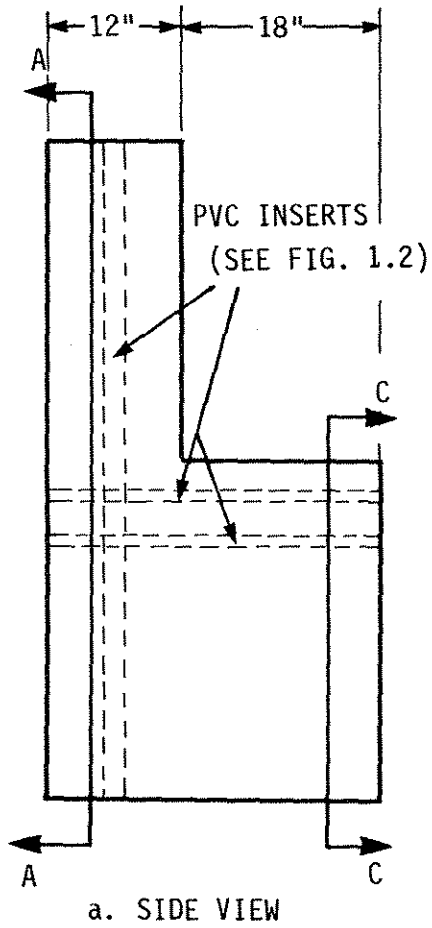
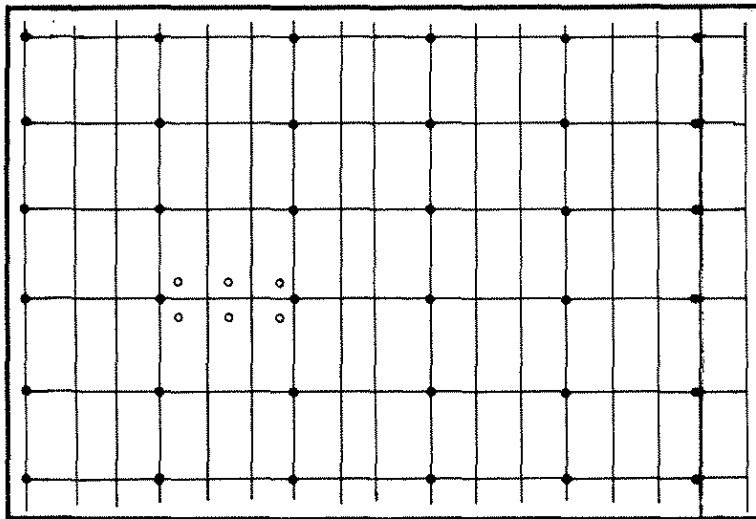
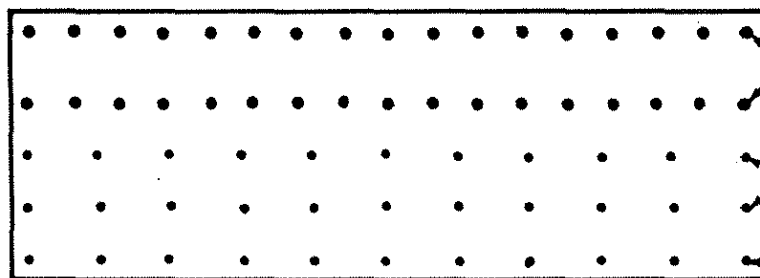


Fig. A.1. Reinforcement details for Abutment 1.

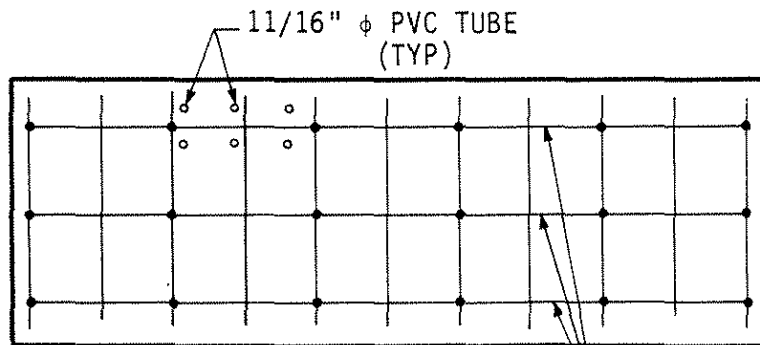


c. SECTION A-A



d. SECTION B-B

17#11@
5 in. o.c.
L = 50 in.
11#6@
8 in. o.c.
L = 27 in.
11#4@
8 in. o.c.
L = 27 in.



e. SECTION C-C

6-#3@
8 in. o.c.

Fig. A.1. Continued.

10. APPENDIX B: TEST BEAM DATA

Table B.1. Linear-regression analysis results of beam tests 1-7.*

Test	Midspan Deflection			Transit Deflection		
	Slope, k k/in.	See Fig.	r	Slope, k k/in.	See Fig.	r
1	200.00	1.34b	0.9981	23.20	1.34c	0.9996
2	249.67	B.1b	0.9999	26.67	B.1c	0.9998
3	285.81	B.2b	0.9997	34.02	B.2c	0.9998
4	249.98	B.3b	0.9987	27.25	B.3c	0.9980
5	263.11	B.4b	0.9979	30.58	B.4c	0.9994
6	250.08	B.5b	0.9996	27.32	B.5c	0.9996
7	277.79	B.6b	0.9989	29.85	B.6c	0.9966

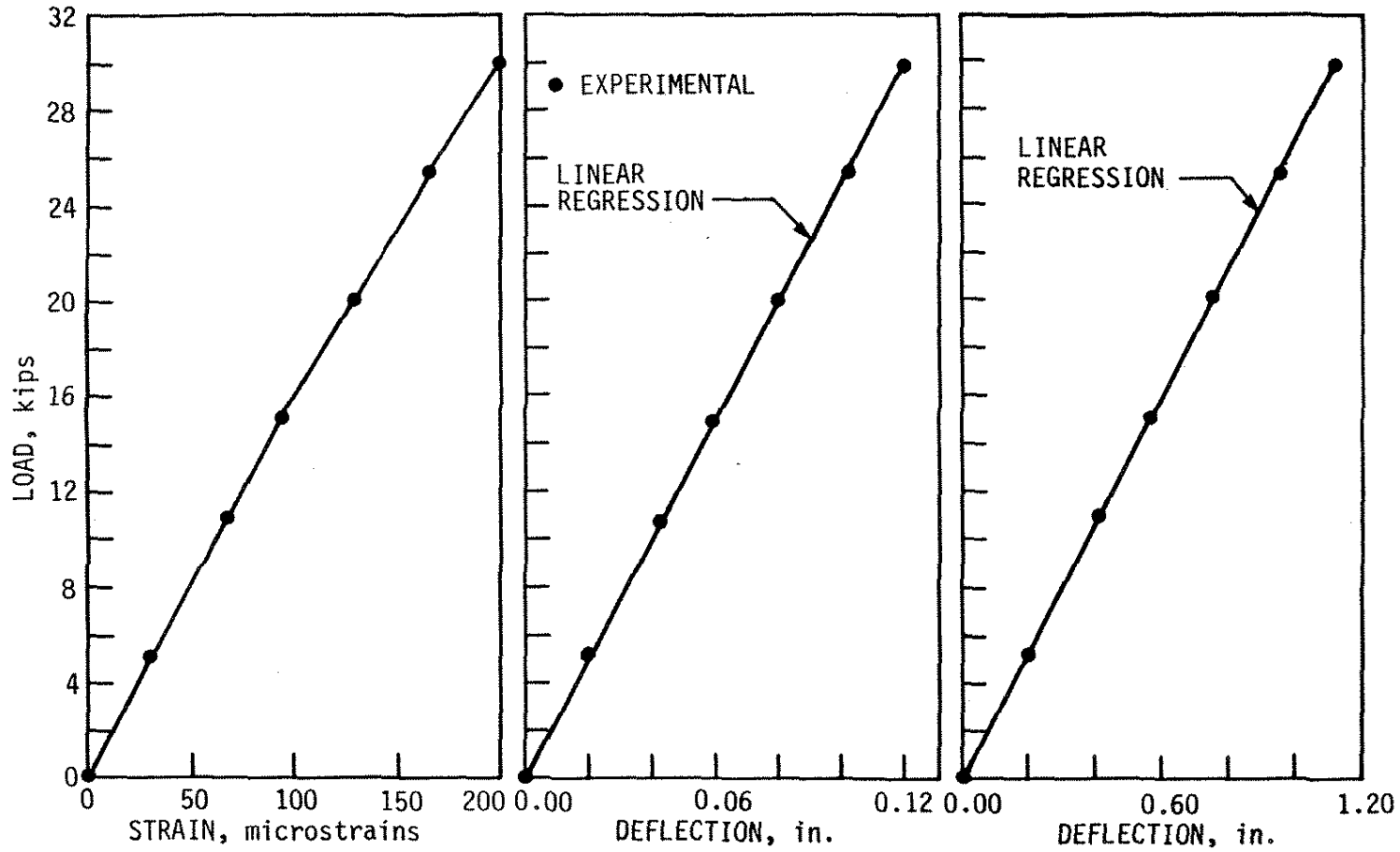
*See Table 1.1 for a description of beam tests.

Table B.2. Forces transferred to abutment from finite-element analysis.

Model*	Nodes†	Reaction Forces		
		Fx, lb	Fy, lb	Mz, lb-in.
1	1	926	5024	49
	2	3698	10328	912
	3	2605	3664	1046
	4	8880	7756	1930
2	1	1011	5471	-263
	2	2742	10248	449
	3	2301	3579	1004
	4	8141	6968	1797
3	1	655	5458	-811
	2	701	10119	-1679
	3	2529	3620	1825
	4	8509	6878	4125

*The model refers to the type of bracket used. Model 1 is the actual initial flange bracket (Bracket 1), Model 2 is after the first reduction (Bracket 3), and Model 3 is after the second reduction (Bracket 4).

† Refers to the nodes that were fully restrained on the finite-element models of the bottom flange bracket (see Fig. 1.25 for location of nodes).

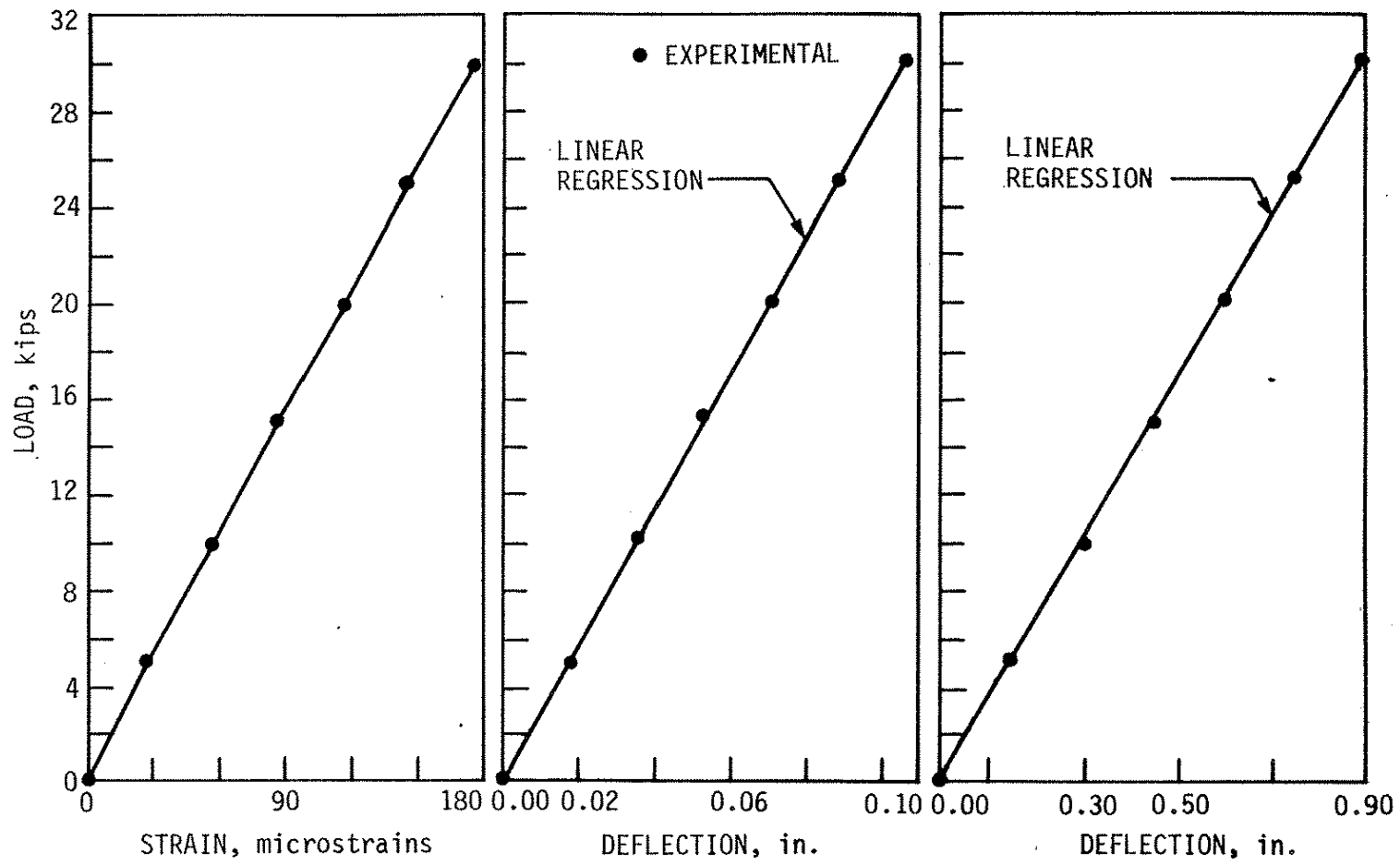


a. STRAIN DISTRIBUTION AT MIDSPAN

b. MIDSPAN DEFLECTION

c. TRANSIT DEFLECTION

Fig. B.1. Test 2 data.



a. STRAIN DISTRIBUTION AT MIDSPAN

b. MIDSPAN DEFLECTION

c. TRANSIT DEFLECTION

Fig. B.2. Test 3 data.

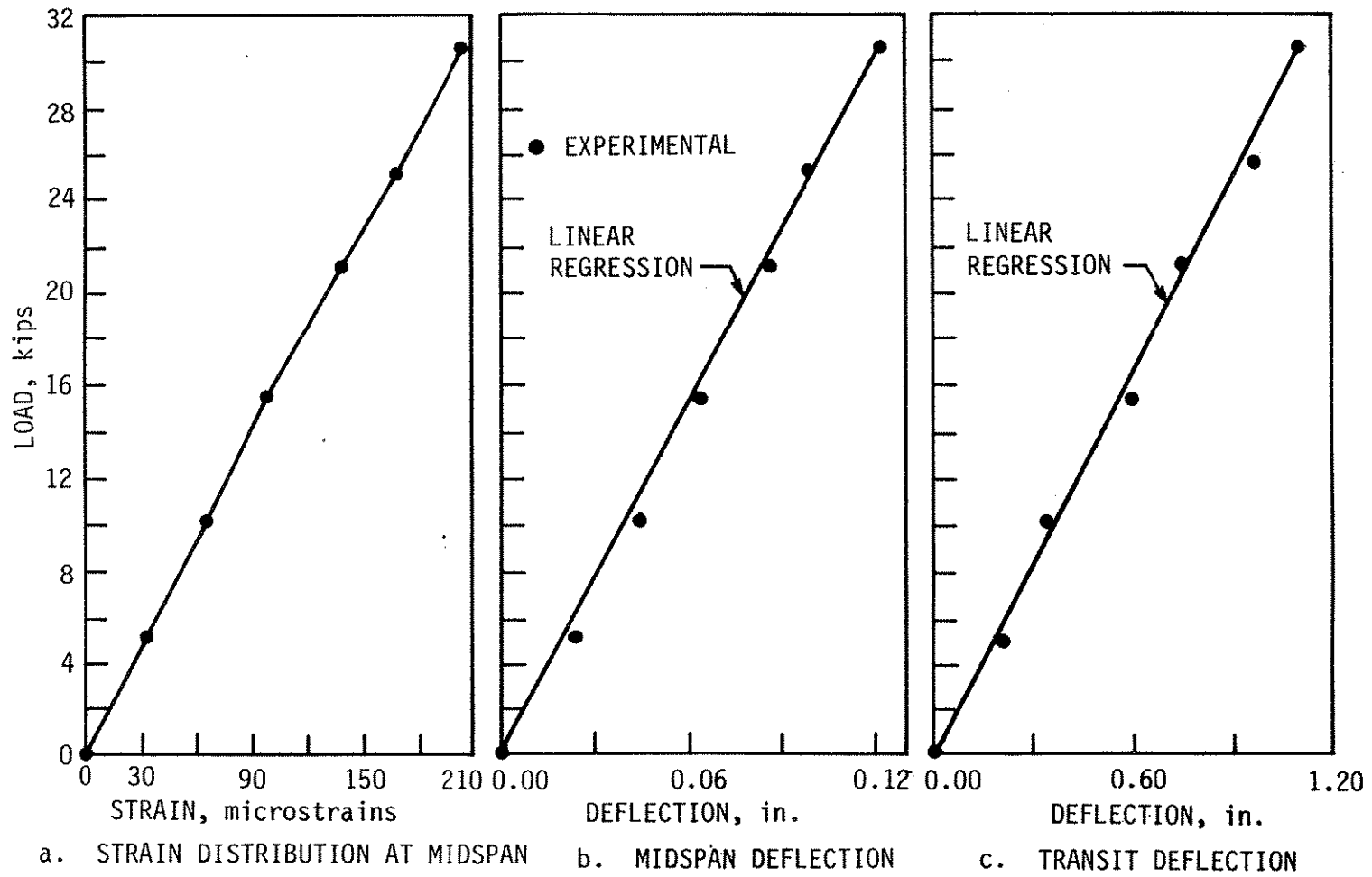


Fig. B.3. Test 4 data.

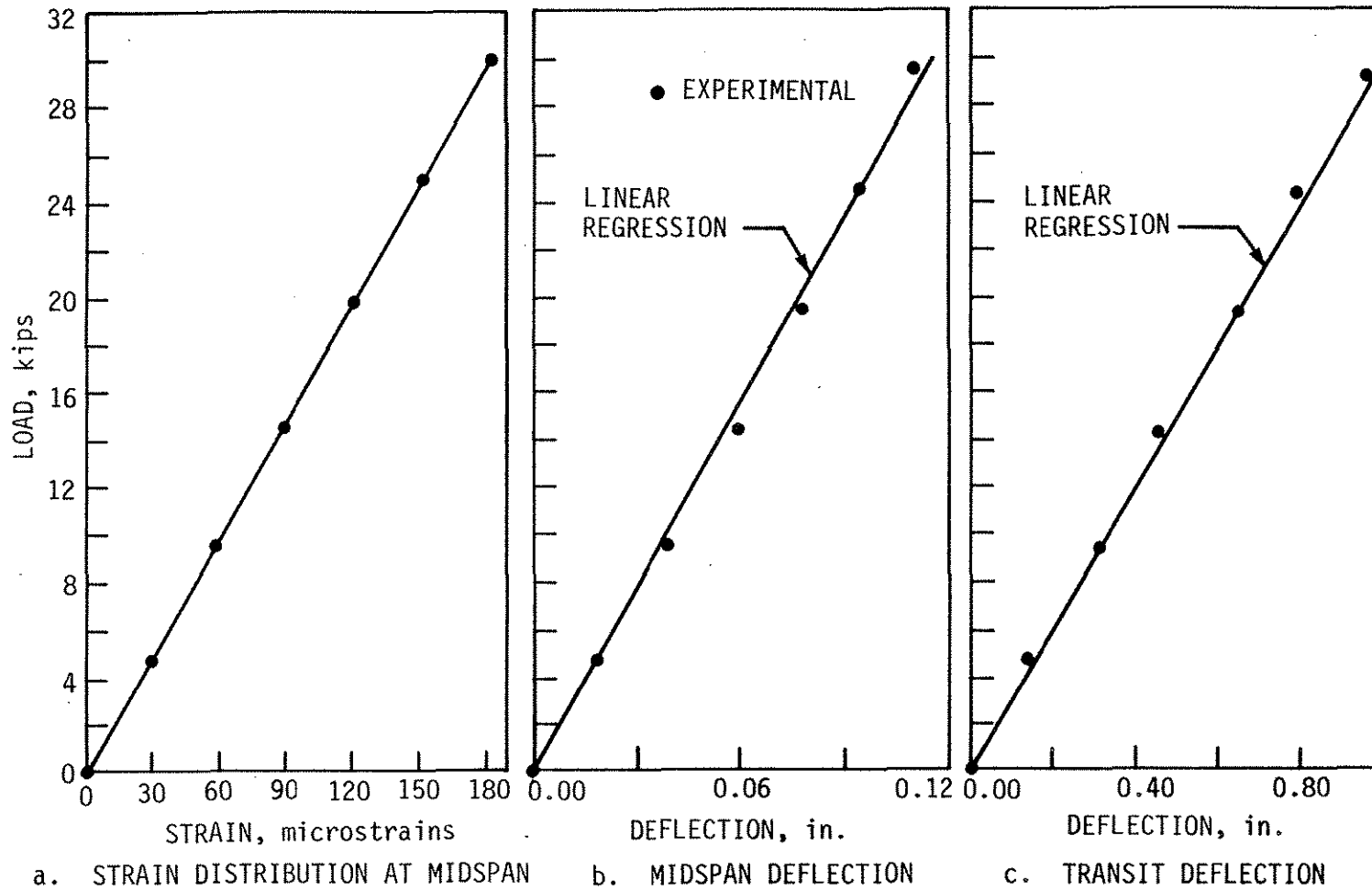
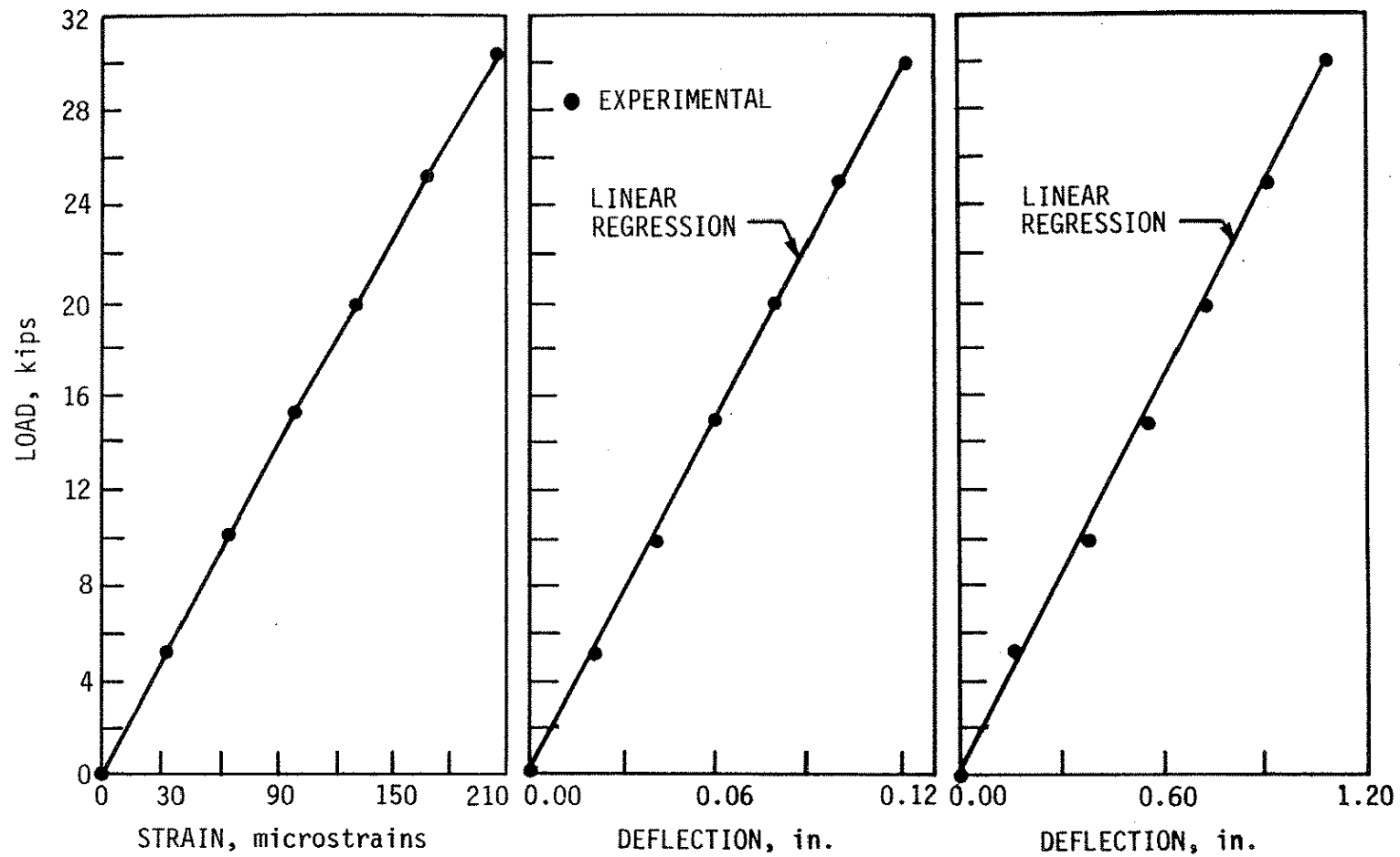


Fig. B.4. Test 5 data.



a. STRAIN DISTRIBUTION AT MIDSPAN

b. MIDSPAN DEFLECTION

c. TRANSIT DEFLECTION

Fig. B.5. Test 6 data.

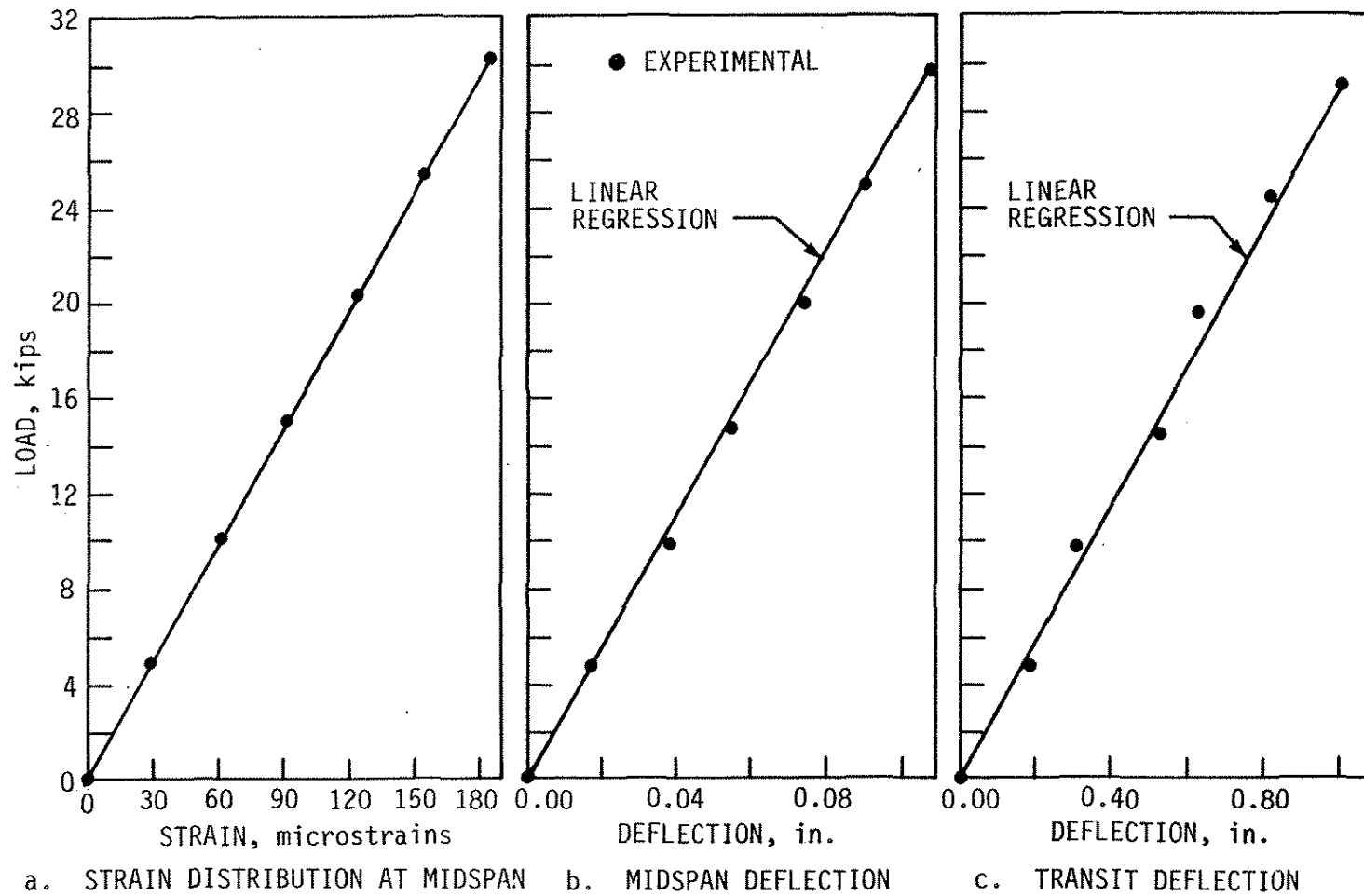


Fig. B.6. Test 7 data.

**11. APPENDIX C: STRAIN REDUCTION TABLES
FOR MODEL BRIDGE**

Strain Reduction for Model Bridge

The experimental data from all the tests on the model bridge are presented in this appendix. In general, the tables follow the following format:

- First column identifies the beam (see Fig. 1.24)
- Second column identifies the load points (See Fig. 1.24)
- Third column presents the actual magnitude of strain when no restraint is provided
- Remaining columns present the percent reduction in strains produced by the various restraint conditions; negative sign indicates an increase in strain
 - EXTFLG the bottom flanges of the exterior beams restrained
 - ALLFLG the bottom flanges of all beams restrained
 - INTFLG the bottom flanges of the interior beams restrained
 - ALLREST the bottom flanges and webs of all beams restrained
 - AS4 Beam 4 fully restrained
 - AS3 Beam 3 fully restrained

Table C.1. Strain reductions at Section 1 with symmetric restraint conditions (one concentrated load).

Beam	Load Points	Initial Strains (10^{-6} in./in.)	% Reduction in Strains			
			EXTFLG	ALLFLG	INTFLG	ALLREST
Beam 1	LP 1	28	-3.45	17.86	3.57	7.14
	LP 2	27	-3.70	29.63	14.81	25.92
	LP 3	46	10.87	30.43	10.87	36.97
	LP 4	87	20.69	27.59	11.49	40.23
	LP 5	180	17.78	22.78	6.11	30.56
	LP 6	363	11.02	12.40	1.38	17.63
	LP 7	-48	22.92	25.00	16.67	50.00
	LP 8	-58	20.69	18.97	12.07	43.10
	LP 9	-88	26.14	27.27	7.95	40.90
	LP 10	-109	22.94	24.77	4.59	4.59
Beam 2	LP 1	44	4.54	21.59	36.36	37.50
	LP 2	79	1.26	26.58	29.75	37.34
	LP 3	169	-5.06	23.08	16.86	32.84
	LP 4	336	5.50	13.09	10.42	18.89
	LP 5	471	6.37	11.89	7.01	14.97
	LP 6	344.5	7.84	14.80	4.93	14.80
	LP 7	-65.5	11.45	28.24	19.85	45.80
	LP 8	-73	12.32	26.03	15.75	42.47
	LP 9	-86.5	15.03	29.48	16.18	41.04
	LP 10	-86.5	15.61	27.17	12.14	12.14
Beam 3	LP 1	230	11.52	11.74	5.00	21.30
	LP 2	290	4.83	4.83	5.52	17.59
	LP 3	440	2.95	10.45	9.09	13.86
	LP 4	353	2.27	13.88	13.88	23.09
	LP 5	187	1.07	20.86	23.53	31.02
	LP 6	90	0	27.78	32.22	21.11
	LP 7	-78	8.97	21.79	5.13	41.03
	LP 8	-73	10.96	24.66	16.67	42.47
	LP 9	-66	9.09	30.30	18.18	48.48
	LP 10	-49	8.16	30.61	16.33	53.06
Beam 4	LP 1	640.5	7.89	9.37	2.10	16.55
	LP 2	508	-8.96	10.14	5.12	16.73
	LP 3	224.5	14.48	12.25	14.03	18.49
	LP 4	89	-2.20	16.29	19.66	19.10
	LP 5	*	-	-	-	-
	LP 6	17.5	2.78	31.43	48.57	-20.00
	LP 7	-87.5	2.29	12.57	7.43	37.71
	LP 8	-62.5	5.30	10.62	6.40	36.00
	LP 9	-42.5	12.37	21.90	7.06	43.53
	LP 10	-23	23.33	-4.15	41.77	15.22

*Strain gage not working.

Table C.2. Strain reductions at Section 1 with asymmetric restraint conditions (one concentrated load).

Beam	Load Points	Initial Strains (10 ⁻⁶ in./in.)	% Reduction in Strains	
			AS4	AS3
Beam 1	LP 1	28	28.57	35.71
	LP 2	27	29.63	33.33
	LP 3	46	17.39	21.74
	LP 4	87	6.90	11.49
	LP 5	180	88.89	6.11
	LP 6	363	122.04	-1.65
	LP 7	-48	4.17	6.25
	LP 8	-58	-1.72	0
	LP 9	-88	2.27	4.55
	LP 10	-109	1.83	1.83
Beam 2	LP 1	44	12.50	48.86
	LP 2	79	3.80	36.71
	LP 3	169	-0.30	21.60
	LP 4	336	2.38	10.12
	LP 5	471	91.83	6.16
	LP 6	344.5	2.03	4.50
	LP 7	-65.5	6.11	21.37
	LP 8	-73	3.42	16.44
	LP 9	-86.5	4.62	13.87
	LP 10	-86.5	1.16	10.40
Beam 3	LP 1	230	16.74	8.26
	LP 2	290	8.97	7.93
	LP 3	440	4.09	9.77
	LP 4	353	3.40	13.31
	LP 5	187	-1.60	15.51
	LP 6	90	-4.44	16.67
	LP 7	-78	17.95	16.67
	LP 8	-73	16.44	19.18
	LP 9	-66	16.67	24.24
	LP 10	-49	12.24	26.53
Beam 4	LP 1	640.5	16.63	2.97
	LP 2	508	16.93	7.09
	LP 3	224.5	20.27	16.70
	LP 4	89	10.67	33.15
	LP 5	*	-	-
	LP 6	17.5	-14.29	88.57
	LP 7	87.5	177.71	196.00
	LP 8	-62.5	16.80	0.80
	LP 9	-42.5	15.29	2.35
	LP 10	-23	8.70	4.35

*Strain gage not working.

Table C.3. Strain reductions at Section 1 with symmetric restraint conditions (two concentrated loads).

Beam	Load Points	Initial Strains (10 ⁻⁶ in./in.)	% Reduction in Strains			
			EXTFLG	ALLFLG	INTFLG	ALLREST
Beam 1	LP 3,10	-3	33.33	62.5	-25.00	-80.00
	LP 3,17	61	21.31	29.51	9.84	40.18
	LP 4,11	25	52.00	64.00	28.00	92.00
	LP 4,18	104	24.04	28.85	9.62	46.15
	LP 5,12	89	26.97	26.97	4.49	48.31
	LP 5,19	204	22.06	23.53	5.39	36.27
	LP 6,13	280	17.50	21.79	7.50	29.29
	LP 6,20	404	17.08	19.31	5.19	26.73
Beam 2	LP 3,10	109.5	0	27.85	24.20	33.79
	LP 3,17	102	3.13	24.48	18.75	32.29
	LP 4,11	256.5	1.17	23.98	18.52	30.21
	LP 4,18	343	3.35	22.16	16.04	29.45
	LP 5,12	387.5	3.87	10.45	7.61	14.45
	LP 5,19	492.5	5.69	12.49	8.43	17.36
	LP 6,13	256	5.47	-1.95	-7.81	17.58
	LP 6,20	358	8.79	5.31	-1.68	21.37
Beam 3	LP 3,10	369	2.98	8.94	7.86	13.82
	LP 3,17	465	4.95	10.97	9.25	16.99
	LP 4,11	293	2.73	13.99	14.33	19.45
	LP 4,18	379	3.43	14.25	14.25	21.37
	LP 5,12	122	3.28	17.21	16.39	32.79
	LP 5,19	200	3.00	20.50	17.50	32.50
	LP 6,13	40	0	35.00	22.50	57.50
	LP 6,20	102	5.88	29.42	23.53	46.08
Beam 4	LP 3,10	119	2.94	3.78	8.40	13.87
	LP 3,17	232	6.03	8.84	7.97	22.63
	LP 4,11	30.5	-12.86	13.11	60.66	34.43
	LP 4,18	115.5	0.87	13.86	23.38	29.44
	LP 5,12	*	-	-	-	-
	LP 5,19	55	-11.29	6.36	24.54	18.18
	LP 6,13	-8.5	0.00	64.70	-19.05	76.47
	LP 6,20	23.5	31.88	-9.62	27.66	-11.32

*Strain gage not working.

Table C.4. Strain reductions at Section 1 with asymmetric restraint conditions (two concentrated loads).

Beam	Load Points	Initial Strains (10 ⁻⁶ in./in.)	% Reduction in Strains	
			AL4	AL3
Beam 1	LP 3,10	-3	-166.67	-66.67
	LP 3,17	61	9.84	19.67
	LP 4,11	25	16.00	52.00
	LP 4,18	104	4.81	14.42
	LP 5,12	89	3.37	19.10
	LP 5,19	204	196.57	7.84
	LP 6,13	280	6.07	8.57
	LP 6,20	404	4.21	4.95
Beam 2	LP 3,10	109.5	2.74	15.07
	LP 3,17	192	0.26	17.97
	LP 4,11	256.5	-2.34	6.04
	LP 4,18	343	-0.44	7.87
	LP 5,12	387.5	0.13	2.71
	LP 5,19	492.5	1.62	4.97
	LP 6,13	256	-3.32	0
	LP 6,20	358	-1.26	3.07
Beam 3	LP 3,10	369	1.63	6.78
	LP 3,17	465	5.16	8.39
	LP 4,11	293	5.46	11.26
	LP 4,18	379	6.33	11.35
	LP 5,12	122	2.46	11.48
	LP 5,19	200	2.00	14.00
	LP 6,13	40	2.50	20.00
	LP 6,20	102	6.86	21.57
Beam 4	LP 3,10	119	17.23	10.92
	LP 3,17	232	19.83	10.34
	LP 4,11	30.5	14.75	49.18
	LP 4,18	115.5	20.35	18.61
	LP 5,12	*	-	-
	LP 5,19	55	12.73	17.27
	LP 6,13	-8.5	82.35	23.53
	LP 6,20	23.5	-2.13	14.89

*Strain gage not working.

Part 2: Post-Compression of Stringers

F. W. Klaiber, K. F. Dunker, and S. M. Planck

PART 2: POST-COMPRESSION OF STRINGERS

	<u>Page</u>
LIST OF TABLES	175
LIST OF FIGURES	177
ABSTRACT	183
1. INTRODUCTION	185
1.1. General Background	185
1.2. Objectives	186
1.3. Research Program	189
1.4. Literature Review	190
1.4.1. Applied Strengthening Mechanisms	190
1.4.2. Post-Compression	192
2. DESCRIPTION OF TEST SPECIMENS	195
2.1. Full-Scale Mockup of the Negative Moment Region	195
2.2. Post-Compression Strengthening Technique (ST2.1)	200
2.2.1. Live Bracket	204
2.2.2. Dead Brackets	204
2.2.3. Compression Tubes	206
2.3. Superimposed Truss-Strengthening Techniques (ST2.2, ST2.3)	208
2.3.1. Pin Bracket	208
2.3.2. Compression Struts	213
2.3.3. End Conditions	213
2.3.3.1. ST2.2	213
2.3.3.2. ST2.3	215
3. TESTS AND TEST PROCEDURES	217
3.1. Vertical Load Mechanism	217
3.2. Instrumentation	217
3.2.1. Mockup Instrumentation	219
3.2.2. ST2.1 Instrumentation	219
3.2.3. ST2.2 and ST2.3 Instrumentation	219
3.3. Preliminary Vertical-Load Tests	224
3.4. ST2.1 Tests	226
3.5. ST2.2 and ST2.3 Tests	227

	<u>Page</u>
4. ANALYSIS AND TEST RESULTS	229
4.1. Preliminary Vertical-Load Tests	229
4.2. Finite-Element Analysis	231
4.3. Effects of ST2.1 on Mockup	234
4.4. Effects of ST2.2 and ST2.3 on Mockup	240
5. SUMMARY AND CONCLUSIONS	255
5.1. Summary	255
5.2. Conclusions	257
6. RECOMMENDED FURTHER RESEARCH	259
7. BIBLIOGRAPHY	261

LIST OF TABLES

	<u>Page</u>
Table 2.1. Tests on the full-scale mockup.	225

LIST OF FIGURES

	<u>Page</u>	
Fig. 2.1.	Negative moment strengthening schemes and force diagrams.	187
	a. Post-tensioning and applied moment	
	b. Increase number of supports	
	c. Post-compression with jacking brackets	
	d. Applied moment	
	e. Superimposed truss	
	f. Pretensioned post-compression tube	
	g. Post-compression scissor tube	
Fig. 2.2.	Correlation between full-scale mockup and prototype.	190
	a. Spans for V12 (1957) bridge series	
	b. Moment diagram for V12 (1957) bridges with uniform load	
	c. Mockup spans	
	d. Moment diagram for mockup	
Fig. 2.3.	Full-scale mockup.	197
	a. Elevation	
	b. Cross-section A-A	
Fig. 2.4.	Photographs of mockup.	199
	a. Installation of hold-down	
	b. Deck blockouts and cable grooves	
Fig. 2.5.	Forces and moments applied to three-span beam by post-compression and truss-strengthening schemes.	201
	a. ST2.1 tension forces and moments	
	b. ST2.1 moment diagram	
	c. ST2.2 and ST2.3 shear forces	
	d. ST2.2 and ST2.3 moment diagram	
Fig. 2.6.	Post-compression strengthening technique (ST2.1)	202
	a. Post-compression tubes on full-scale mockup	
	b. Dead bracket	
	c. Live bracket	

	<u>Page</u>
Fig. 2.7. ST2.1 brackets.	203
a. Live bracket	
b. Dead bracket	
Fig. 2.8. Photographs of ST2.1 on full-scale mockup.	205
a. Live bracket and compression tube with 60-ton hydraulic cylinder in place	
b. Dead bracket with compression tube	
c. Compression tube lateral restraint	
Fig. 2.9. ST2.1 compression-tube lateral restraints.	207
a. Internal lateral restraints	
b. Independent lateral restraint	
Fig. 2.10. Superimposed truss-strengthening technique (ST2.2)	209
a. ST2.2 on full-scale mockup	
b. Pin bracket	
Fig. 2.11. ST2.2 bearing plate assembly..	210
a. Transverse bearing plate section (Section A-A)	
b. Longitudinal bearing plate section (detail A)	
Fig. 2.12. Superimposed truss-strengthening technique (ST2.3).	211
a. ST2.3 on full-scale mockup	
b. Section A-A	
c. Detail A	
Fig. 2.13. Photographs of ST2.2 and ST2.3 on full-scale mockup.	212
a. Pin brackets	
b. ST2.2 end condition	
c. ST2.3 end condition	
Fig. 2.14. Photographs of ST2.2 and ST2.3 compression struts.	214
a. Compression strut pin bracket end	
b. Compression strut bearing plate end	
Fig. 2.15. Vertical loading mechanism for full-scale mockup.	218
Fig. 2.16. Strain gage locations for full-scale mockup	220
a. Layout	
b. Section A-A	
c. Section B-B	

	<u>Page</u>
Fig. 2.17. Vertical displacement measurement (DCDT) locations on full-scale mockup.	221
Fig. 2.18. ST2.1 strain gage locations.	222
a. Layout	
b. Section A-A	
c. Compression-tube strain gage locations	
Fig. 2.19. ST2.2 and ST2.3 strain gage locations.	223
a. Layout	
b. Compression-strut strain gage locations	
Fig. 2.20. Experimental and theoretical strains at Section 4 for nominal loads.	230
a. 43 kips vertical.	
b. ST2.1	
c. ST2.2	
d. ST2.3	
Fig. 2.21. Half-symmetry SAP IV finite-element model.	232
a. Model schematic near pier support	
b. Complete model with ST2.3	
Fig. 2.22. Test schematic and compression-tube load vs. deflection curve for ST2.1 on mockup.	235
a. Test schematic	
b. ST2.1 Compression-tube load vs. deflection curve	
Fig. 2.23. Response of ST2.1 to vertical load.	236
a. Vertical load vs. deflection curves for three tube loads	
b. Vertical load vs. average tube load for three tube loads	
Fig. 2.24. Strains at Sections 4 and 5 for full-scale mockup with ST2.1 in place.	238
a. 40 kips/tube	
b. 60 kips/tube	
c. 75 kips/tube	
d. 40 kips/tube	
e. 60 kips/tube	
f. 75 kips/tube	
Fig. 2.25. Tendon load vs. deflection for ST2.2 and ST2.3.	241

	<u>Page</u>
Fig. 2.26. Response of ST2.2 and ST2.3 to vertical load.	243
a. Vertical load vs. deflection curves for ST2.2 subjected to various tendon forces	
b. Vertical load vs. deflection curves for ST2.3 subjected to various tendon forces	
Fig. 2.27. Strains at Sections 4 and 5 for full-scale mockup with ST2.2 in place.	245
a. 50 kips/tendon	
b. 100 kips/tendon	
c. 130 kips/tendon	
d. 50 kips/tendon	
e. 100 kips/tendon	
f. 130 kips/tendon	
Fig. 2.28. Strains at Sections 4 and 5 for full-scale mockup with ST2.3 in place.	247
a. 50 kips/tendon	
b. 100 kips/tendon	
c. 130 kips/tendon	
d. 50 kips/tendon	
e. 100 kips/tendon	
f. 130 kips/tendon	
Fig. 2.29. Vertical load vs. average strut load for ST2.2 and ST2.3.	249
a. Mockup with ST2.2 in place	
b. Mockup with ST2.3 in place	
Fig. 2.30. Response of tendons (ST2.2 and ST2.3) and ties (ST2.3) to vertical loading.	250
a. Changes in tendon load due to vertical load (ST2.2 or ST2.3 in place on mockup)	
b. Changes in tie bar load due to vertical load (ST2.3 in place on mockup)	
Fig. 2.31. Photographs of mockup with ST2.3 tested to failure.	252
a. Restrained end of mockup at failure	
b. Location of failure with respect to ST2.3	
c. Lower beam flange at failure	

	<u>Page</u>
Fig. 2.32. Vertical-load deflection curve for mockup with ST2.3 in place tested to failure.	253

ABSTRACT

Part 2 summarizes the research that has been completed in an investigation of strengthening continuous, composite bridges by two new methods: (1) post-compression of stringers and (2) superimposed trusses within stringers. Both strengthening schemes were designed to reverse the moments and resulting stresses from service loads. The research program included reviewing the literature, testing each strengthening scheme on a full-scale mockup of the negative moment region of a bridge stringer and conducting a finite-element analysis of the laboratory bridge mockup for each strengthening scheme. The literature review involved a search of publications from both the United States and foreign countries. A series of tests was conducted on the full-scale mockup, first with the post-compression strengthening scheme in place, and then with the superimposed truss strengthening scheme in place. A test was also conducted on the full-scale mockup with the superimposed truss in place, in which the mockup was tested to failure. In addition to the experimental work, finite-element analyses were also performed on the full-scale bridge mockup for each of the three strengthening schemes in place. The post-compression strengthening scheme was effective in reducing the bottom flange stresses. The top flange stresses, however, were actually slightly increased, due to the tension applied to the section. The superimposed truss strengthening scheme was very effective in reducing both the top and bottom flange stresses since it applied only positive bending to the full-scale mockup.

1. INTRODUCTION

1.1. General Background

Nearly half of the approximately 600,000 highway bridges in the United States were built before 1940. The majority of those bridges were designed for lower traffic volumes, smaller vehicles, slower speeds, and lighter loads than they experience today. In addition, maintenance has not been adequate on many of these older bridges. According to the Federal Highway Administration (FHWA), almost 40% of the nation's highway bridges are classified as deficient and thus in need of rehabilitation or replacement.

The deficiency in some of these bridges is their inability to carry current, legal live loads. Rather than posting these bridges for reduced loads or replacing them, strengthening has been found to be a cost-effective alternative in many cases.

Many different methods exist for increasing the live load-carrying capacity of various types of bridges. One series of research projects, sponsored by the Iowa Department of Transportation (Iowa DOT), examined the concept of strengthening steel-beam simple-span bridges by external post-tensioning; the research covered the feasibility phase through the implementation and design methodology phases. Results of these projects verified that strengthening of the simple-span bridges by post-tensioning is a viable, economical strengthening technique.

As a result of the success in strengthening simple-span bridges by post-tensioning, a laboratory investigation, Iowa DOT project HR-287 [7], was undertaken to examine the feasibility of strengthening continuous composite steel-beam and concrete-deck bridges by post-tensioning. This research program indicated that the strengthening of continuous composite bridges by post-tensioning is also feasible. Longitudinal as well as transverse distribution of post-tensioning must be considered if only exterior or only interior stringers are post-tensioned. Laboratory testing of a 1/3-scale model bridge constructed for this project and finite-element analysis showed that post-tensioning of positive moment regions with straight tendons was more effective than post-tensioning negative moment regions with straight tendons. It was also determined that changes in the tension in tendons may either be beneficial or detrimental when live loads are applied to strengthened bridges and thus must be carefully considered in design.

Results of Iowa DOT project HR-287 have shown that by post-tensioning the positive moment regions of continuous bridges, stress reduction can also be obtained in the negative

moment regions. However, in certain instances, additional stress reduction is required in the negative moment region. Because post-tensioning tendons in negative moment regions would need to be placed above the neutral axis located near the top flange, post-tensioning would require removal of a portion of the bridge deck. Since this action is usually undesirable (extra cost, closure of bridge, etc.), an alternate method of reducing stress in the negative moment regions of continuous, composite bridges is needed.

As a result of work on the National Cooperative Highway Research Program NCHRP-12-28(4) [21] project, several concepts for strengthening bridges were conceived; some concepts are applicable to strengthening the negative moment regions of continuous spans. This part of the project (Part 2) describes the investigation of two strengthening schemes for use in the negative moment regions of continuous spans.

1.2. Objectives

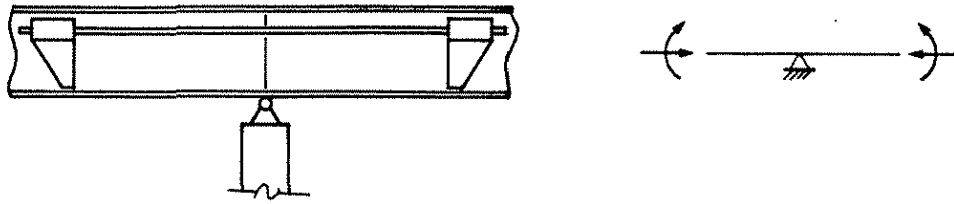
From the seven strengthening schemes (shown in Fig. 2.1) conceived for use in negative moment regions of continuous beams, two were selected for additional investigation in this study. Therefore, the primary objective of this study was to determine the feasibility of strengthening the negative moment region of composite bridges by two new methods:

1. Post-compression of stringers
2. Superimposed truss within stringers.

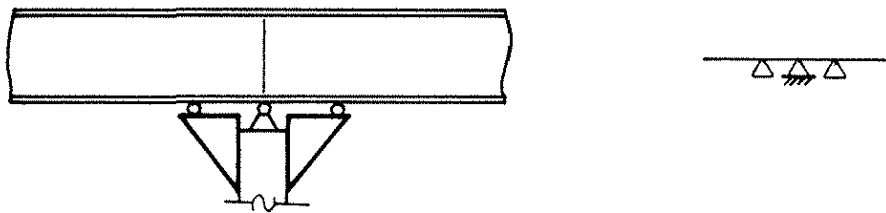
To evaluate the feasibility of these strengthening techniques, the more detailed objectives of this study were as follows:

- Determine the best design for applying and maintaining post-compression in negative moment regions of composite bridges.
- Determine the effectiveness of post-compression in reducing flexural stress in the negative moment region.
- Determine the best configuration and design for a superimposed truss.
- Determine the effectiveness of the superimposed truss in reducing flexural stress in the negative moment regions.

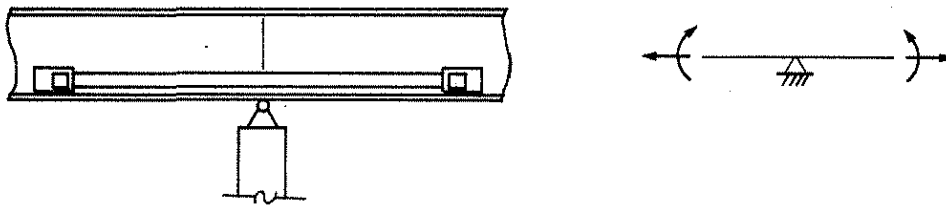
These objectives were pursued by the research team through reviewing available engineering literature, testing a full-scale mockup of a composite bridge beam in the Iowa State University (ISU) Structural Engineering Research Laboratory, and conducting a finite-



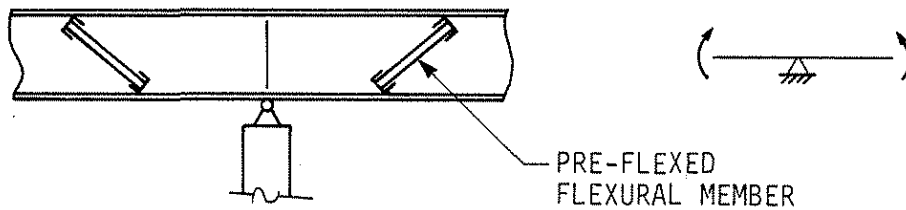
a. POST-TENSIONING AND APPLIED MOMENT



b. INCREASE NUMBER OF SUPPORTS

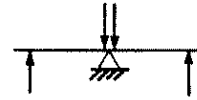
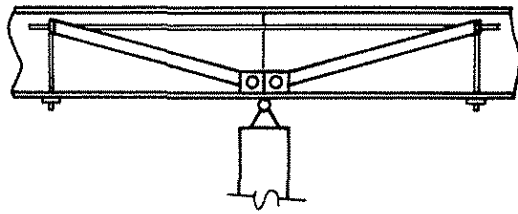


c. POST-COMPRESSION WITH JACKING BRACKETS

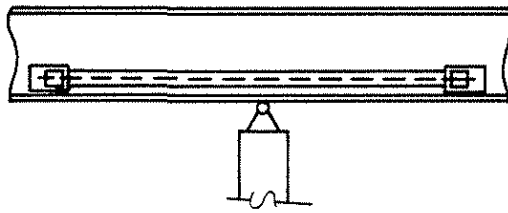


d. APPLIED MOMENT

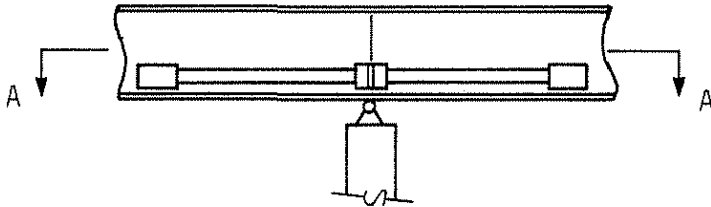
Fig. 2.1. Negative moment strengthening schemes and force diagrams.



e. SUPERIMPOSED TRUSS



f. PRETENSIONED POST-COMPRESSION TUBE



SECTION A-A

g. POST-COMPRESSION SCISSOR TUBE

Fig. 2.1 . Continued.

element analysis of the laboratory bridge mockup with each of the previously described strengthening schemes in place.

1.3. Research Program

The research program consisted of the distinct parts as outlined above; however, a strong emphasis was placed on laboratory testing. As part of a previous research project (Iowa DOT project HR-287) [7], plans for standard continuous, composite bridges were obtained from the Iowa DOT Office of Bridge Design. From the various sets of plans provided, the V12 (1957) series of composite, three-span bridges was selected for additional review. This series of bridges was wide enough for two standard 12-ft traffic lanes; also a considerable number of these bridges were constructed in Iowa. Based upon these plans, a full-size mockup was constructed representing the negative moment region of a typical bridge stringer above an interior support. The mockup consisted of a $W24 \times 76$ beam on which a composite concrete deck was cast (see Ref. [7]).

Post-compression (ST2.1) and the superimposed trusses (ST2.2 and ST2.3) were tested on this mockup as part of this investigation. Post-compression tests consisted of a series of vertical load cycles applied to the mockup with varying magnitudes of post-compression force initially applied to the compression members. Two variations of the superimposed trusses were developed and also tested on the full-scale mockup previously described.

Tests similar to those conducted for post-compression were performed with the superimposed trusses in place so a comparison of the three strengthening schemes could be made. During all tests, deflection of the full-scale mockup as well as strains in both the mockup and the strengthening system were monitored.

The full-scale mockup was also analyzed with SAP IV [2], a finite-element program. Each of the three strengthening techniques was analyzed with the finite-element program for the operating level of loads tested in the laboratory.

The results from the various parts of the research program are summarized in this report. The literature review for the project is given in Section 1.4. Chapter 2 describes the full-scale mockup and the strengthening schemes developed. Chapter 3 covers the tests and test procedures used to evaluate the effectiveness of the strengthening systems. The results from the laboratory testing program and the finite-element analysis schemes are summarized

in Chapter 4. Following the results are the summary and conclusions, which are presented in Chapter 5. In Chapter 6 recommendations for further research are presented.

1.4. Literature Review

The research completed in this project can be viewed as extensions of work in two separate areas: applied strengthening mechanisms and post-compression. Applied strengthening mechanisms are independent structures that, when added to an existing structure, "double" the structure at some or all locations. Strengthening mechanisms give redundancy to the original structure because the mechanisms are independent, except for lateral stability, of the original structure. Failure of either the original structure or the applied strengthening mechanism does not necessarily cause collapse of the entire structure.

Post-compressing of a structure is analogous to post-tensioning of a structure. Although strengthening of structures by post-tensioning is much more common, the engineering literature contains one example of strengthening an existing structure by attaching elements that were subsequently compressed.

1.4.1. Applied Strengthening Mechanisms

A railway bridge in Ostrava, Czechoslovakia, required strengthening for increased load. The bridge, which consisted of a deck structure supported on two steel-plate girders, had a 67-ft single span. The strengthening occurred prior to 1964 [11].

For each of the two plate girders, a strengthening mechanism was constructed. The mechanism was a closed loop, similar in shape to a bar joist, built with a steel tee, top and bottom, spaced by steel plate stiffeners. The steel tees provided additional compression and tension flange material for the existing girders.

The entire bridge was jacked upward from cribbing placed underneath at approximately the outer quarter points. After the bridge was thus stress-relieved, each of the strengthening mechanisms was attached to the outside of a plate girder. The new plate stiffeners for each mechanism were anchored to the existing girder stiffeners. After the mechanisms were attached, the jacks were removed. Each of the plate girders then had the additional strength provided by the attached mechanism. There also was redundancy of top and bottom flanges because either an existing flange or an attached flange could fail without causing collapse of a girder.

In 1968 Kandall proposed strengthening existing structures by means of prestressing with additional, independent compression members [16]. Kandall discussed the advantages and disadvantages of adding cover plates, of adding prestressing tendons, and of adding prestressing tendons with associated compression members. He concluded that prestressing with the compression members was the best of the three options.

Kandall noted that adding prestressing tendons provided desirable moments that are the reverse of applied dead- and live-load moments. Prestressing alone, however, also caused axial compression forces in the existing structure, which could be undesirable. To avoid adding the compression forces, Kandall proposed linking compression members with the prestressing tendons. If the compression members are attached with bolts in longitudinally slotted holes, the compression-member tendon mechanism exerts only upward forces on the existing structure. Thus, the mechanism reverses applied load effects without generating unwanted axial forces.

Kandall's concept was applied in strengthening of a wrought-iron truss bridge in Switzerland [29]. Each of the two 157-ft truss spans in the bridge was strengthened by adding mechanisms of the type proposed by Kandall. A longitudinal sliding compression member was attached to the top of each truss (which also served as the bridge rail). Tendon saddles were attached to the truss posts at the quarter points. Tendons attached to the ends of the compression members and bent under the saddles, when tensioned, provided upward forces to each truss at the quarter points. The independent compression members allowed the tendons to provide lift forces to each truss without overloading the existing compression chords.

In the United States, Kim, Brungraber, and Yadlosky have proposed and used applied strengthening mechanisms in through-truss bridges [19]. Steel through-truss bridges generally lack redundancy and have many members and connection parts that are subject to corrosion and fracture. Failure of a single member or joint could cause collapse of the entire bridge and as adequate inspection of all elements is not feasible, a degree of uncertainty in the soundness of truss bridges always exists.

In order to provide redundancy, Kim, Brungraber, and Yadlosky have developed a separate arch mechanism that can be constructed within a truss. Once in place and stressed against the truss, the arch mechanism is independent of the truss except for lateral stability. The arch mechanism provides additional load-carrying capacity with the safety of redundancy.

1.4.2. Post-Compression

The use of slender compressed elements in concrete structures was suggested by Kurt Billig in the early 1950s [32]. About one year later, in 1953, a West German patent was filed and, in 1956, a separate patent was filed in Austria. As is often the case, neither patent resulted in immediate use of the system in construction.

In the early 1970s, Dr. Hans Reiffenstuhl, an Austrian university professor, successfully developed the design methodology and construction details for the use of post-compressed steel bars in concrete structures. Dr. Reiffenstuhl noted that eccentric post-tensioning of a concrete beam creates both a bending moment and an axial compression force. Eccentric post-compressing of a concrete beam creates a bending moment in the same direction as the post-tensioning moment and an axial tension force. If a beam is both post-tensioned and post-compressed to the same extent, the axial forces cancel and the moments add. Thus, it is possible to induce twice the usual prestressing moment without the axial force [32].

Post-compressing a beam using slender bars does have associated problems. Achieving compression in a slender bar throughout the member, without significant friction losses or buckling of the bar in the duct, requires careful design and experiments. Providing the tension anchorages also requires careful design and testing to ensure that the beam will carry design loads during the life of the structure. These problems apparently have been solved by Dr. Reiffenstuhl.

Dr. Reiffenstuhl designed a concrete, single box and girder bridge that made use of both post-tensioning and post-compressing [31]. The Almbruecke in Austria spans 249 ft with a constant depth of 8.2 ft. The span/depth ratio for the bridge is 30.4, an unusually slender proportion. The bridge was constructed in 1977 and thus had been used for five years when reported in the literature in 1982.

In addition to using post-compression for new structures, Dr. Reiffenstuhl used the method for strengthening of an existing structure [33]. In 1979, it was necessary to strengthen the roof of an athletic building that had been constructed in 1972. The prestressed-concrete folded-plate roof spanned 121 ft.

Analysis of the existing V-members indicated that almost all of the compression capacity of the concrete had been utilized in the original design. Although the existing steel tendons could have provided adequate force, retensioning them would have overstressed the anchorages. For structural reasons, the preservation of the architectural character of the

roof, and the necessity of using the athletic building during strengthening, it was decided to add a 1 3/8 in.-diameter post-compressed bar to the exterior of each plate of all V-members.

The duct for each bar was sheathed in a concrete appendage to the roof plate. The cross section for the appendage was about 4 in. by 10 in. After dowels were attached to the roof plate, the compression duct was placed, transverse and longitudinal reinforcing were placed, formwork and concrete were placed, and each bar was compressed and anchored. The strengthening allowed addition of roof insulation and replacement of the deteriorated roofing.

2. DESCRIPTION OF TEST SPECIMENS

This chapter outlines the physical details of the full-scale mockup, the post-compression strengthening system (ST2.1), and the superimposed truss strengthening system (ST2.2 and ST2.3).

2.1. Full-Scale Mockup of the Negative Moment Region

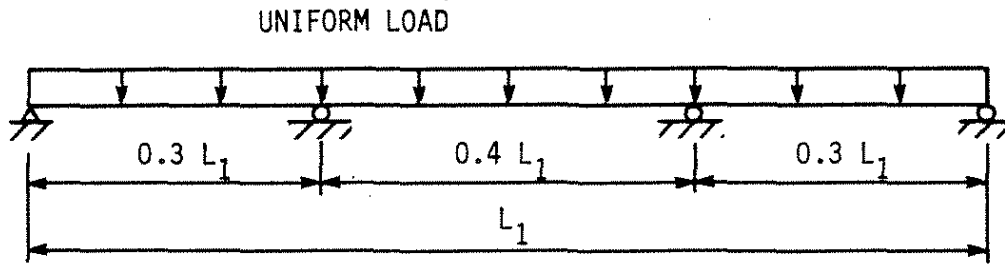
The full-scale mockup of the negative moment region was initially fabricated to test negative moment region post-tensioning schemes. The theoretical development and fabrication of the mockup are reported in detail in the final report for Iowa DOT Project HR-287 [7] and thus will only be briefly discussed in this report. This full-scale model of the negative moment region in a stringer of a continuous bridge will henceforth simply be referred to as the mockup.

The mockup was designed to simulate the negative moment region of the V12 (1957) series of bridges as shown in Fig. 2.2. General dimensions of the mockup are given in Fig. 2.3, whereas photographs of the mockup are given in Fig. 2.4.

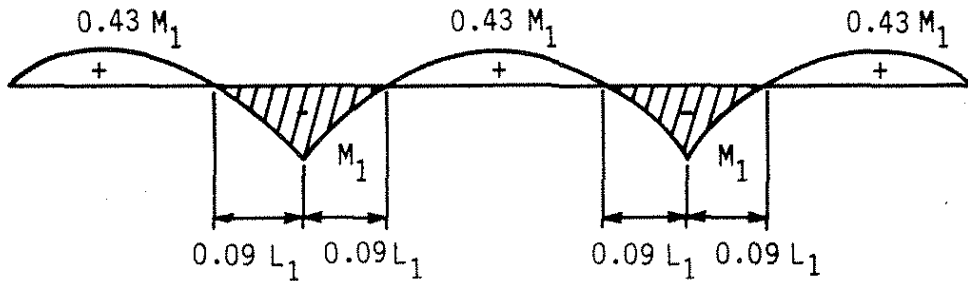
A W24 \times 76 beam 30 ft long, which is the size on an interior stringer in a 150 ft V12 (1957) series bridge, was provided by the Iowa DOT for use in the mockup. AASHTO effective-width requirements for an interior stringer in this type of bridge required a concrete slab 6 ft 3 in. wide (see Fig. 2.3). Also shown in these figures is the slab thickness of 6.5 in., which is the specified thickness of V12 (1957) bridge decks.

Figure 2.4b shows the 2 ft \times 2 ft blockouts that were left in the deck from the original post-tension testing. Since the blockouts were not required in the strengthening procedures investigated in this study, appropriate reinforcing and concrete were placed in the blockouts, thus essentially eliminating them when the mockup was subjected to loads causing deck compression.

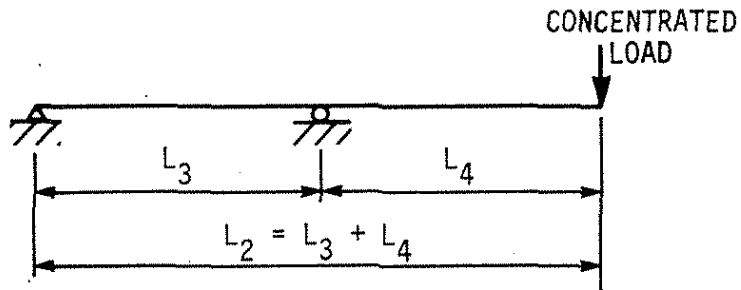
While preparing the mockup for the installation of the post-compression strengthening scheme, researchers noted a considerable number of cracks in the concrete deck. In Fig. 4.28 of Ref. [7] the final crack patterns due to initial vertical load tests are documented. The additional cracks found in the deck at the initiation of this investigation (which was approximately eight months after the cracks shown in Fig. 4.28 of Ref. [7] were noted) were attributed to negative moment bending during loading of the mockup and to the age of



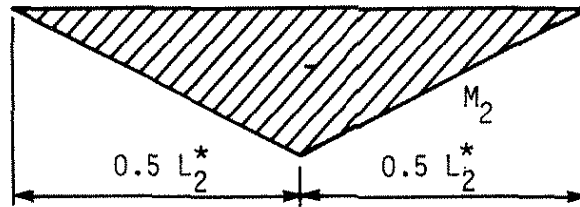
a. SPANS FOR V12 (1957) BRIDGE SERIES



b. MOMENT DIAGRAM FOR V12 (1957) BRIDGES WITH UNIFORM LOAD



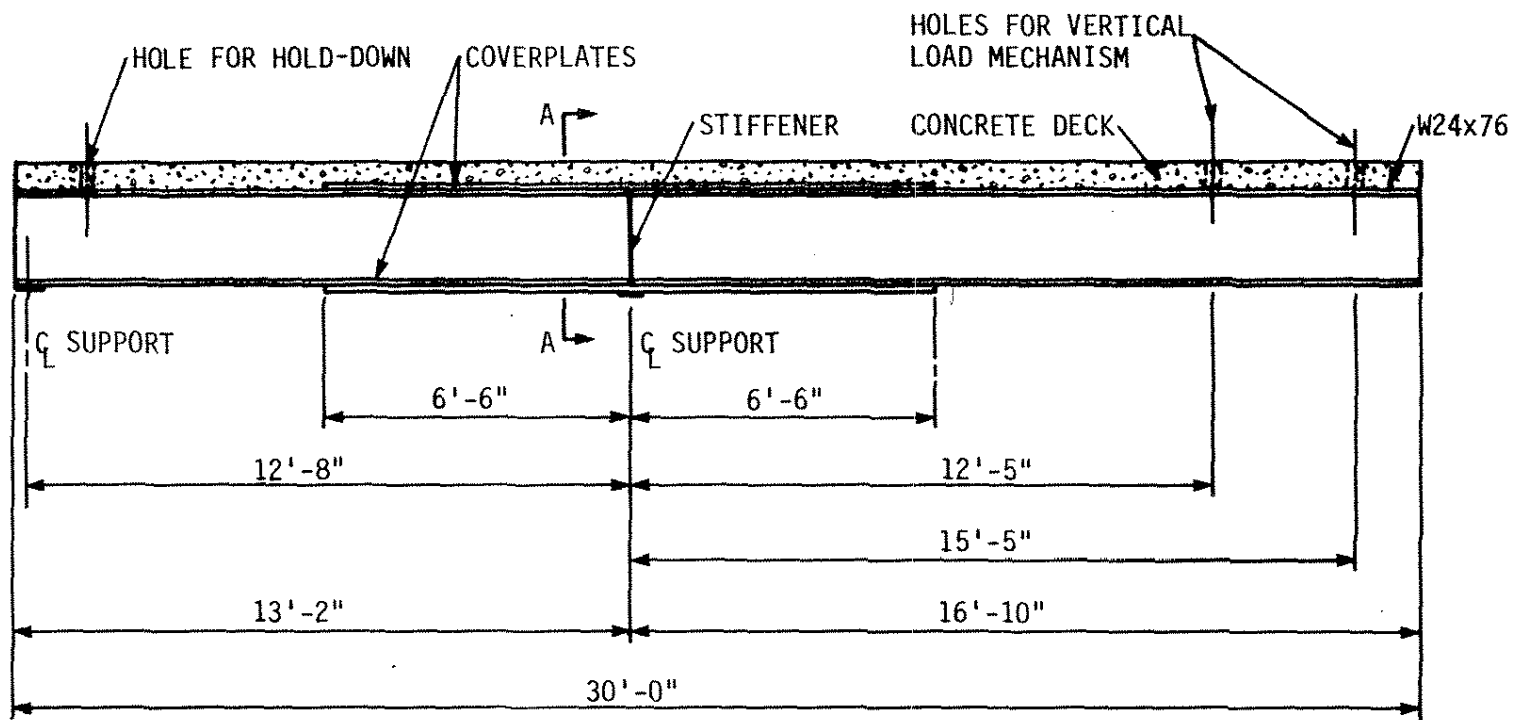
c. MOCKUP SPANS



*ASSUMING $L_3 = L_4$

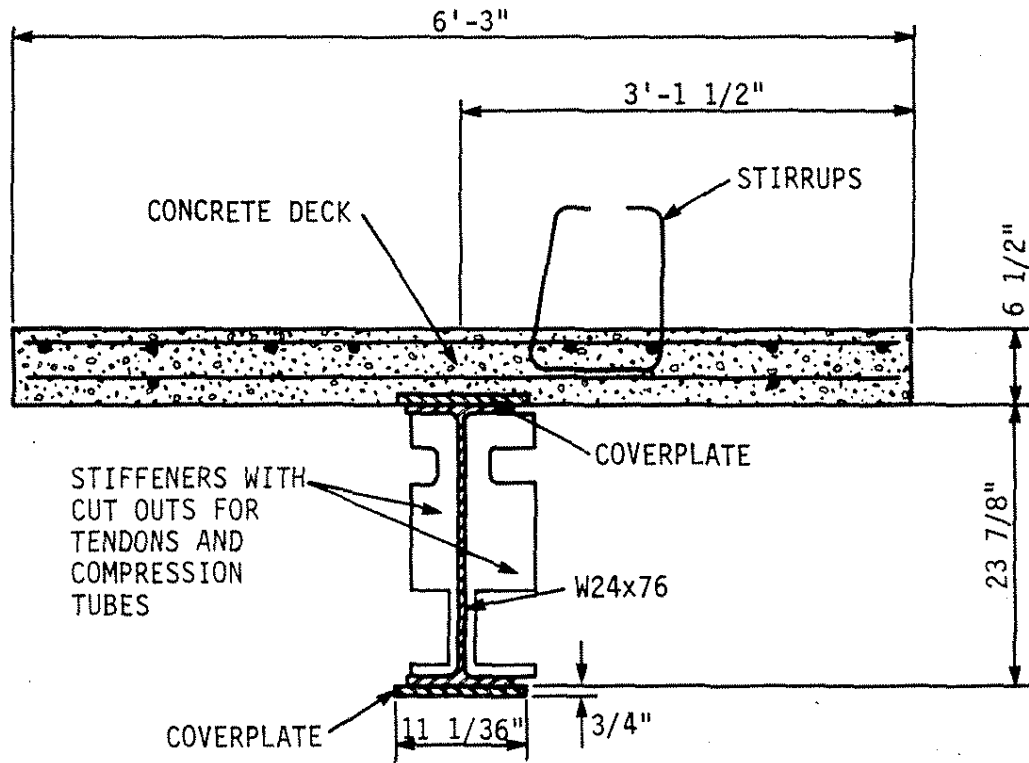
d. MOMENT DIAGRAM FOR MOCKUP

Fig. 2.2. Correlation between full-scale mockup and prototype.



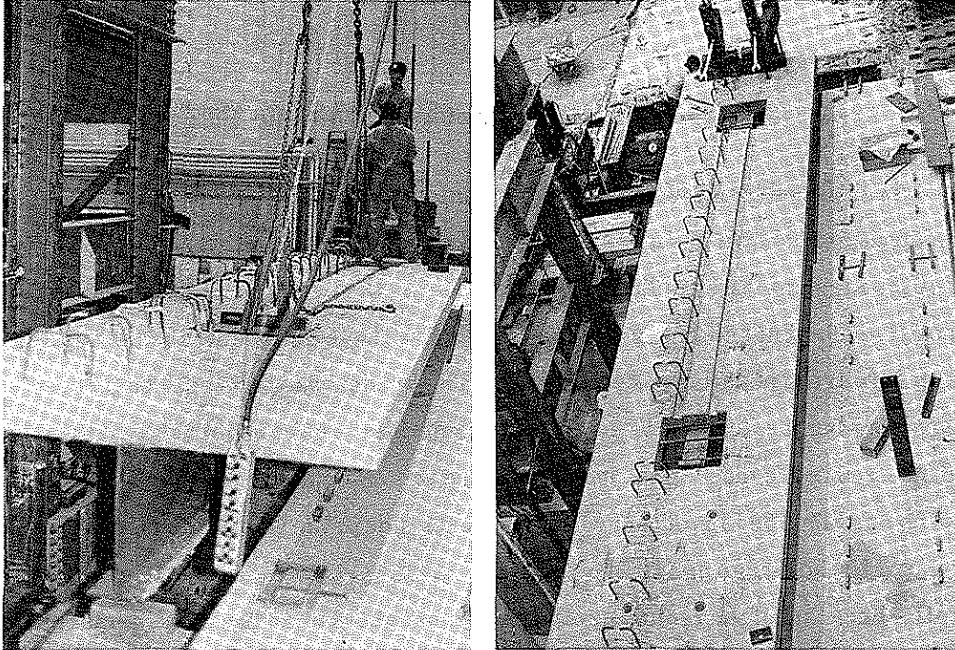
a. ELEVATION

Fig. 2.3. Full-scale mockup.



b. CROSS-SECTION A-A

Fig. 2.3. Continued.



a. INSTALLATION OF HOLD-DOWN b. DECK BLOCKOUTS AND CABLE GROOVES

Fig. 2.4. Photographs of mockup.

the mockup. As a result of this cracking, additional loss of composite action and increased flexibility in the mockup were expected.

2.2. Post-Compression Strengthening Technique (ST2.1)

ST2.1 was designed to produce positive moment bending in the negative moment region of the mockup as shown in Figs. 2.5a,b. The moment diagram in Fig. 2.5b is exactly the same as if the moment were applied by post-tensioning the negative moment regions. To create the positive moment bending, a tension force below the beam's neutral axis was applied to the mockup within the negative moment region. The tension was to be applied by post-compressing a member located in this region. The compressive force required to reduce the service load stresses in the mockup the desired degree was calculated to be approximately 200 kips. Thus, the need for 100 kips of compression on each side of the web of the mockup was the controlling factor in the design of ST2.1.

Potential buckling of the required compression members introduced problems that obviously are not encountered with post-tensioned systems. (In post-tensioned systems, tendons will not buckle; however, post-tensioned portions of the structure when compressed are subject to buckling.) A method for locking the compression into the compression members also had to be designed. The locking mechanism required great precision since the 100 kip forces would create only small deformations in the compressive members. Thus, small seating losses would cause large decreases in the compressive force in the compression members.

The final design for ST2.1 is shown in Figs. 2.6 and 2.7. The system consists of two brackets and one compression tube mounted on each side of the web of the mockup. One bracket was designed to transfer the required load to the compression member. Since this bracket was involved in loading, it was designated the live bracket (see Fig. 2.6c). The bracket at the opposite end of the compressive member was not used for loading and thus was designated the dead bracket (see Fig. 2.6b).

Matching brackets were bolted together through the web of the mockup; twelve 7/8-in.-diameter A325 bolts were used in double shear for each connection. Each bracket was designed to resist a load of 216 kips, which was approximately twice the design load.

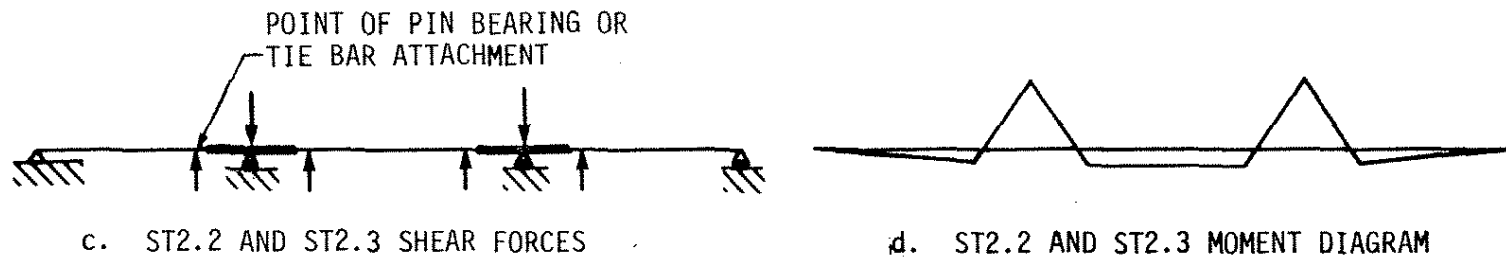
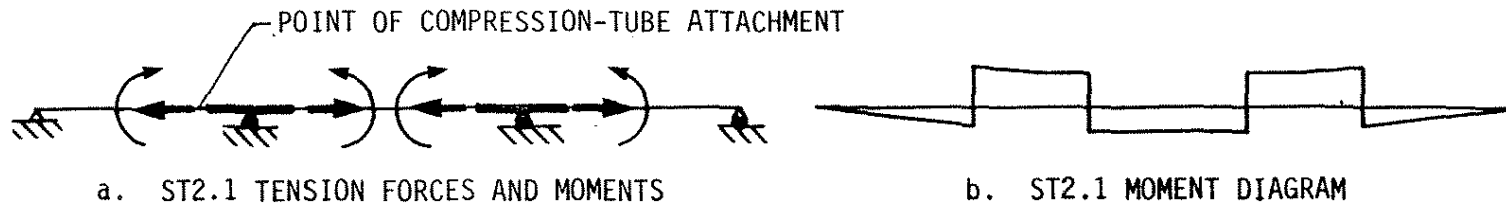
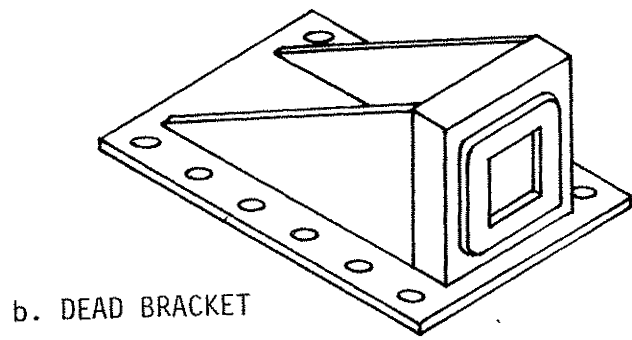
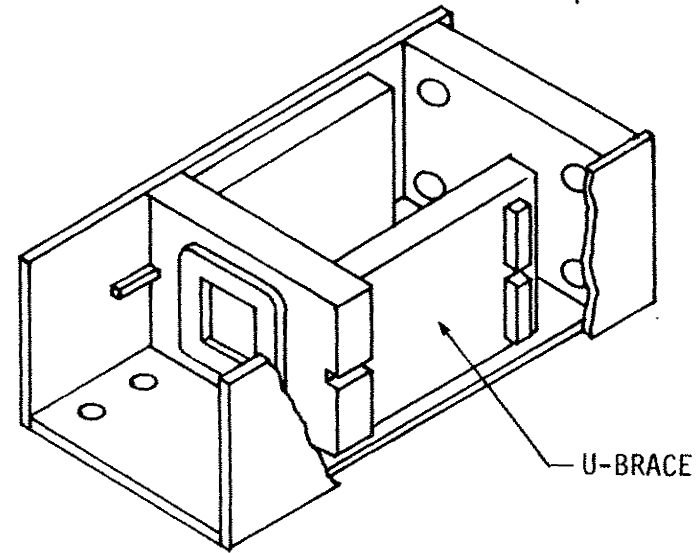


Fig. 2.5. Forces and moments applied to three-span beam by post-compression and truss-strengthening schemes.

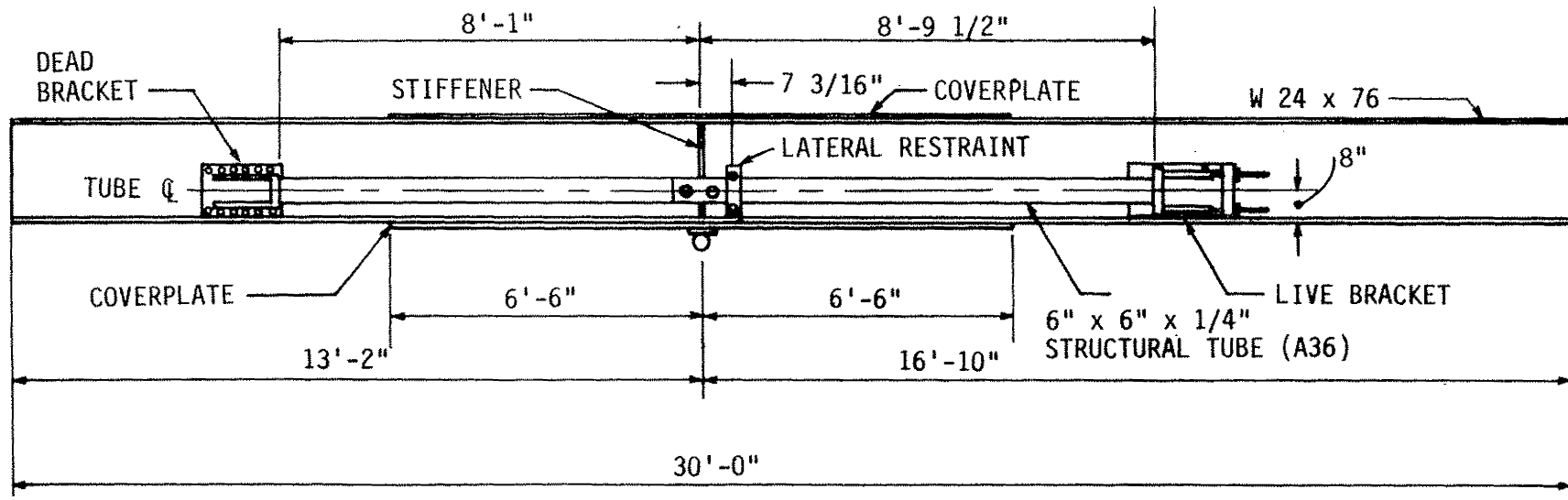


b. DEAD BRACKET



U-BRACE

c. LIVE BRACKET



a. POST-COMPRESSION TUBES ON FULL-SCALE MOCKUP

Fig. 2.6. Post-compression strengthening technique (ST2.1).

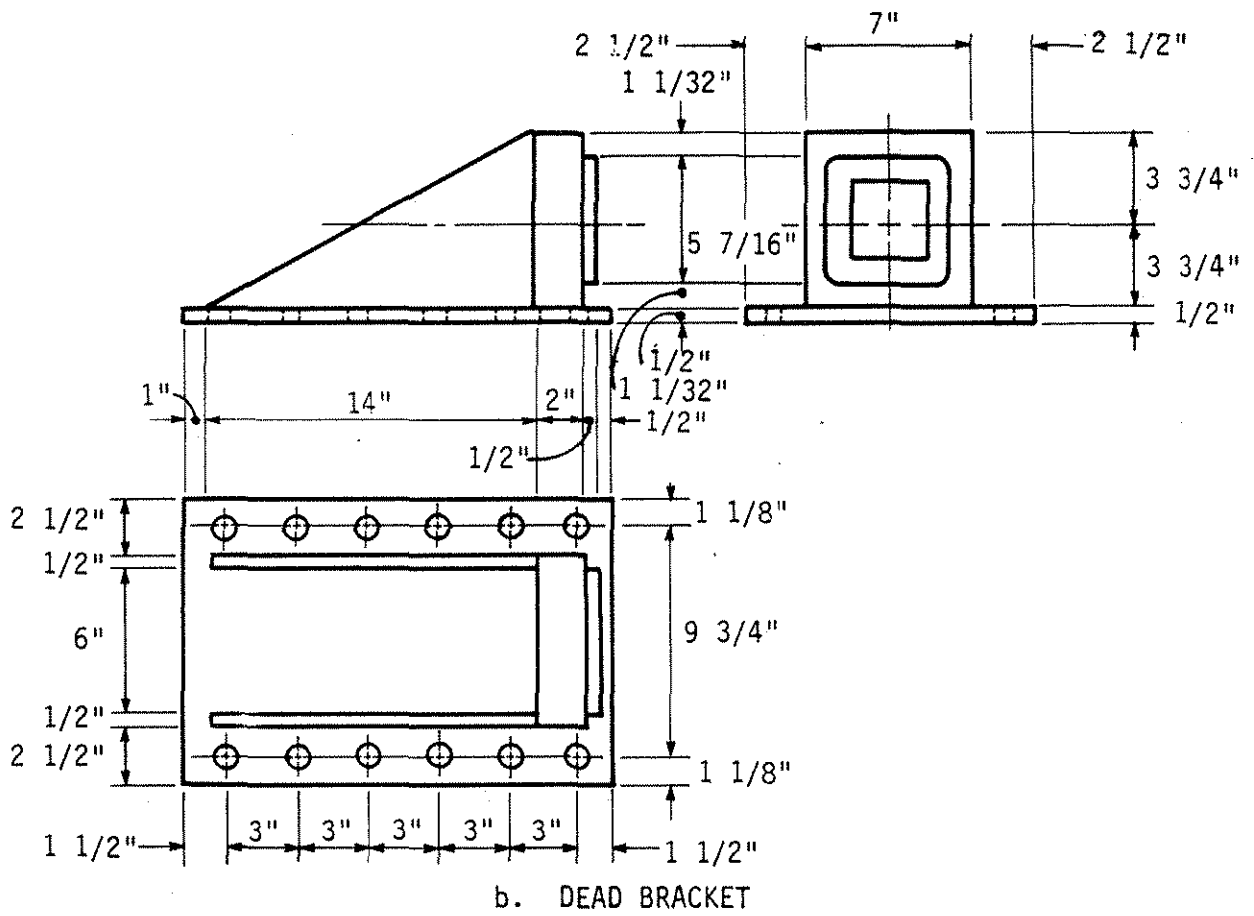
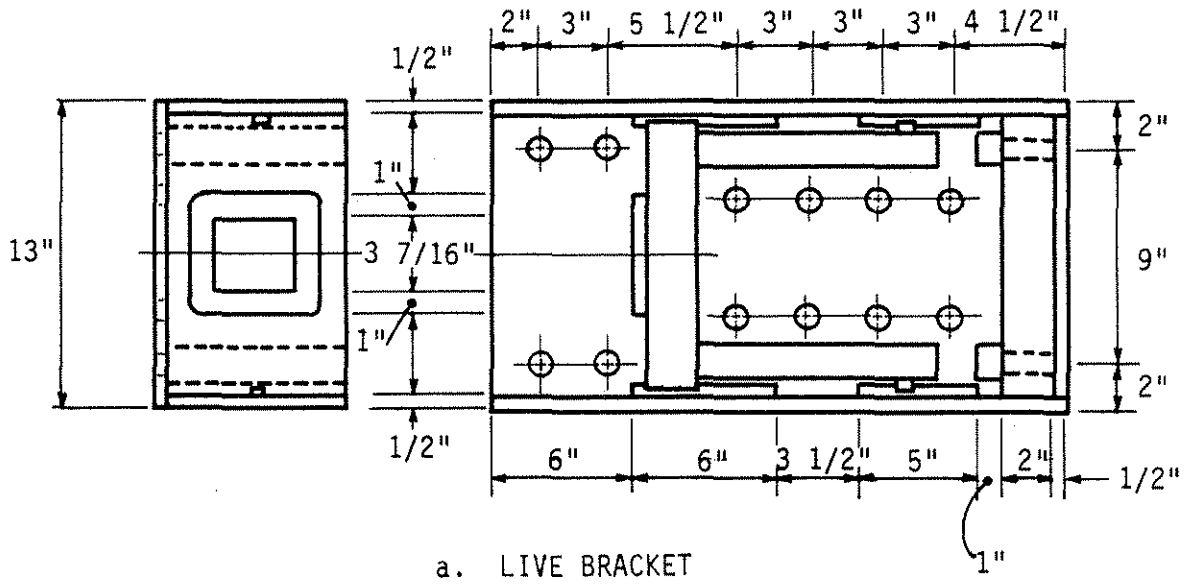


Fig. 2.7. ST2.1 brackets.

2.2.1. Live Bracket

The live bracket (shown in Figs. 2.6c, 2.7a, and 2.8a) was designed to accommodate a 60-ton hydraulic cylinder and to transfer the compressive force in the structural tubes to the beam web. The centerline of the live brackets was 9 ft-1 in. from the stiffener on the mockup and 8 in. above the bottom surface of the lower flange. General dimensions for the live bracket are given in Fig. 2.7a.

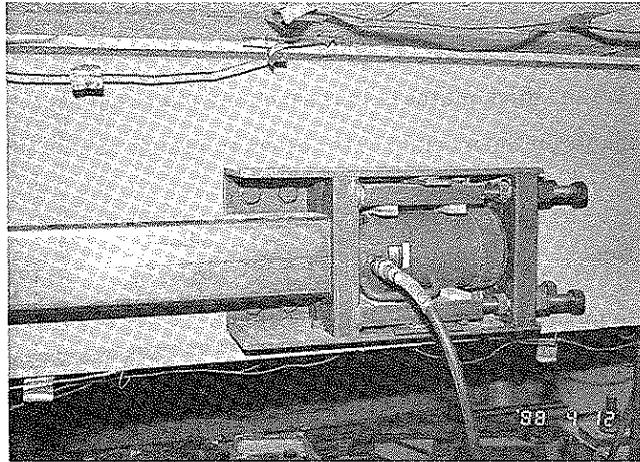
The transfer of the compressive force to the structural tubes was accomplished with a sliding cartridge called a U-brace (shown in Figs. 2.7a and 2.8a). The U-brace, which housed the hydraulic cylinder, was capable of sliding within the live bracket as compression was applied. The U-brace with the 60-ton hydraulic cylinder in place is shown in Fig. 2.8a. To lock a compression force in the compression tube, four 1-in.-diameter high strength threaded rods were tightened against the back of the U-brace. Each threaded rod transferred the compressive force through a nut to a 2-in.-thick bearing plate at the rear of the live bracket. Once the threaded rods were tightened against the U-brace, the hydraulic pressure was released and the hydraulic cylinder removed.

To lock the force into the compression tubes permanently, steel plates would be fit into the space previously occupied by the hydraulic cylinder. The threaded rods would then be loosened until the compressive force was carried by the steel plates. To prevent lateral movement of the U-brace within the live bracket, a series of restraints were designed to control any movement other than along the line of force. These restraints, which appear as slots in the U-brace, can be seen in Fig. 2.6c.

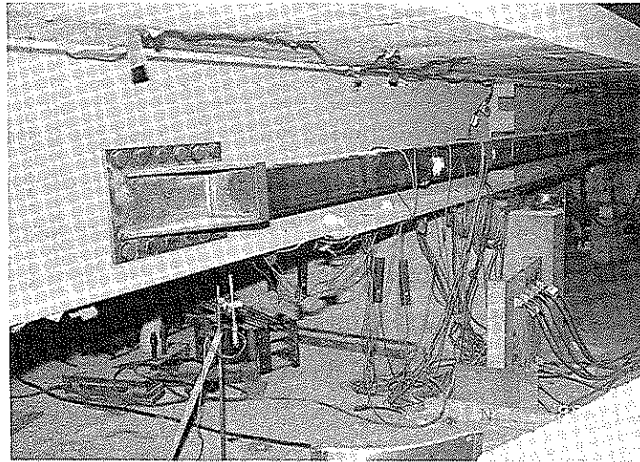
The front surface of the U-brace was the bearing plate for the compression tubes. To approximate a pinned connection, the compression tubes fit over 1/2-in.-thick plates, which were welded to the bearing surfaces. The plates that held the compression tubes in place are shown on the front surface of each bracket, in Figs. 2.6c and 2.7a.

2.2.2. Dead Brackets

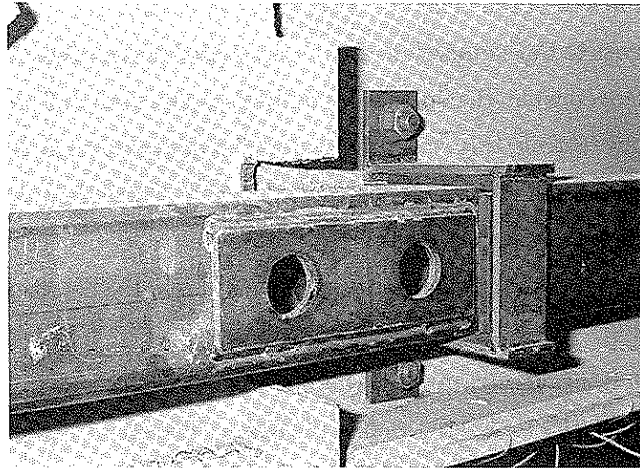
The dead brackets (shown in Figs. 2.6b, 2.7b, and 2.8b) were designed to resist the loads applied by the compression tubes and to transfer the force to the mockup. General dimensions for the dead brackets are given in Fig. 2.7b. The centerline of the dead brackets was located 8 ft 9 in. from the mockup stiffener and 8 in. above the bottom surface of the lower flange. As with the live bracket, the compression tube was not rigidly attached to the dead bracket. A



a. LIVE BRACKET AND COMPRESSION TUBE WITH 60-TON HYDRAULIC CYLINDER IN PLACE



b. DEAD BRACKET WITH COMPRESSION TUBE



c. COMPRESSION-TUBE LATERAL RESTRAINT

Fig. 2.8. Photographs of ST2.1 on full-scale mockup.

1/2-in.-thick plate was welded to the dead-bracket bearing plate. The compression tube fit snugly around the restraint, thus simulating a pinned connection similar to that on the live bracket. Two triangular 1/2-in.-thick plates held the bearing plate in place. Figure 2.8b shows one of the dead brackets on the mockup with the compression tube in place.

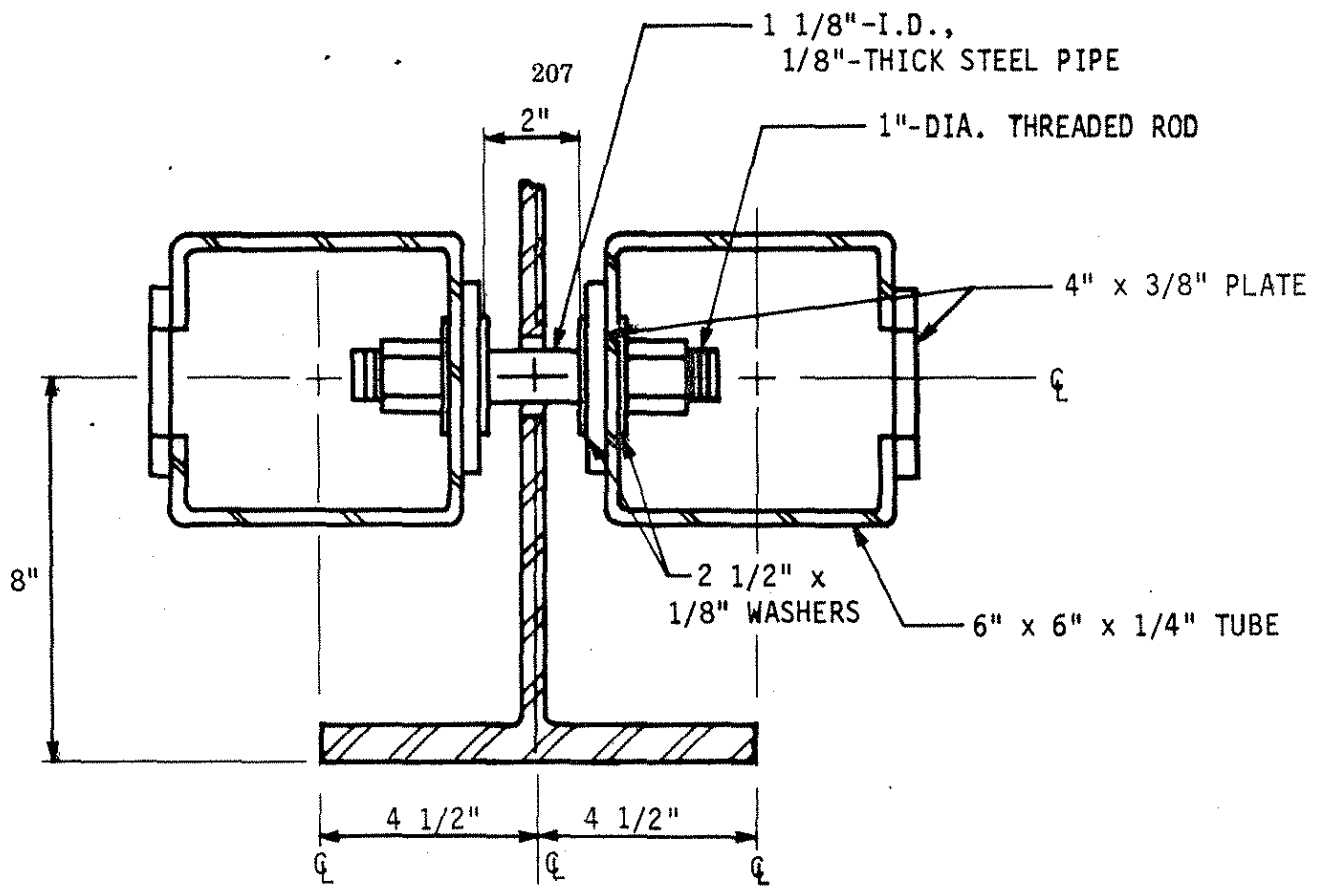
2.2.3. Compression Tubes

The compression members were designed to resist approximately 120 kips each. This design value was based on a 100-kip design load plus an expected increase in load due to vertical loading of the mockup. The total length of the members between the brackets was 16 ft-5 1/2 in. To increase the buckling strength of the compressive tubes, lateral restraint was located near the center of the members, resulting in a maximum unbraced length of 8 ft-9 1/2 in. Only symmetric sections were considered because of the potential for bending about either axis. Based on the design requirements, 6 in. \times 6 in. \times 1/4 in. A500 (46 ksi) structural tubes were selected for the compression members.

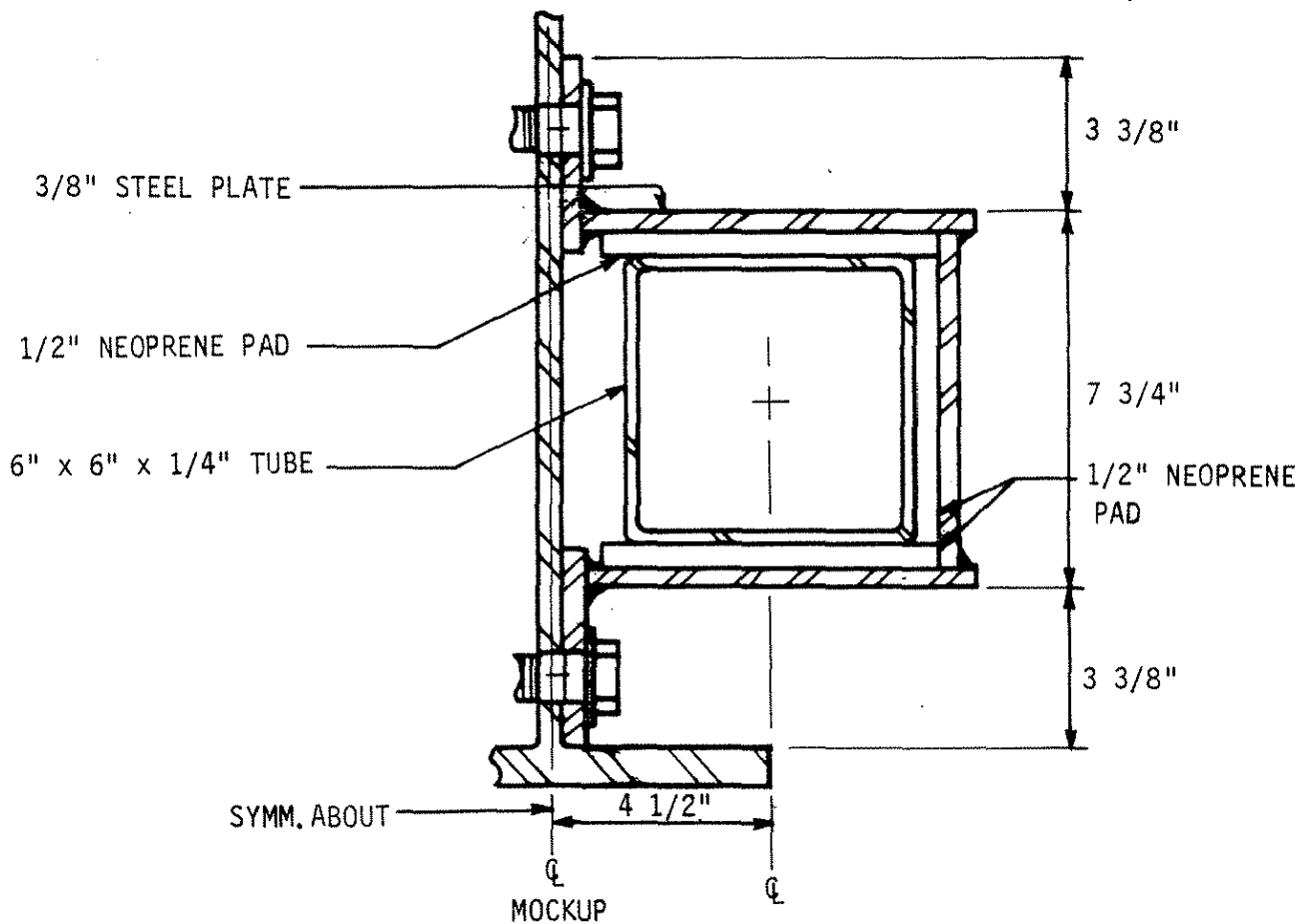
Two lateral restraint schemes were evaluated during preliminary tests of ST2.1. The first scheme is shown in Fig. 2.9a. This scheme consisted of two bolts connecting the tubes together through the web of the mockup. Steel pipes 1 1/4 in. in diameter enclosed the bolts. The pipes enabled the connection to be tightened without pulling the compression tubes together toward the mockup web. The pipes maintained the correct distance between the compression tube on each side of the web. Two slots were cut in the web of the mockup beam so that the mockup did not prevent movement of the tubes when they were compressed. Nuts were tightened against the inside of each tube as shown in Fig. 2.9a to restrain the tubes from movements away from the web of the mockup. Two holes were cut in the outside face of each compression tube for access to the connection. Stiffeners added to the tubes at this section, to replace the material removed when the holes were drilled, can be seen in Figs. 2.8c and 2.9a.

During preliminary testing, this restraint system did not perform as desired. The compression tubes did not respond in proportion to the loading. Since the tubes were connected, bending in one tube resulted in bending in the other tube. The restraining system that connected the compression tubes together actually increased the bending stresses in the tubes.

The second type of lateral restraining system investigated was a strap that confined the compression tube and was bolted to the web of the beam. The strap, shown in Figs. 2.8c



a. INTERNAL LATERAL RESTRAINTS



b. INDEPENDENT LATERAL RESTRAINT

Fig. 2.9. ST2.1 compression-tube lateral restraints.

and 2.9b was offset from the beam stiffener by $7 \frac{3}{16}$ in. By providing independent restraint to each tube, researchers reduced flexural stresses in the tubes to acceptable levels.

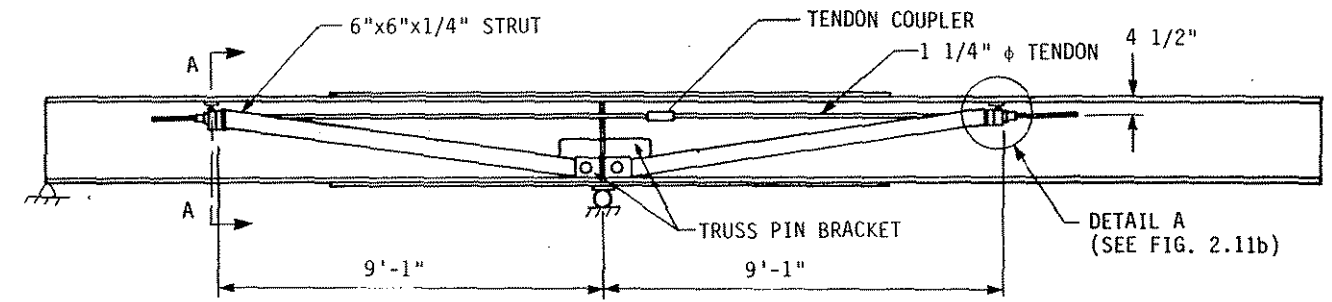
2.3. Superimposed Truss Strengthening Techniques (ST2.2, ST2.3)

The superimposed truss was designed with two configurations for applying the required upward strengthening load to the mockup. Although each design had unique end conditions, identical tendons and compression struts were used by both ST2.2 and ST2.3.

ST2.2 and ST2.3 were also designed to produce positive moment bending in the negative moment region of the mockup. Tensioning the truss created upward forces on the mockup at 9 ft 1 in. on either side of the stiffener. Loading the truss was accomplished by tensioning the 1 1/4-in.-diameter Dywidag thread bar shown in Figs. 2.10a and 2.12a. The trusses on each side of the beam web were tensioned simultaneously from the same end of each truss. The force schematic and moment diagram for ST2.2 and ST2.3 are shown in Figs. 2.5c,d. The upward force required to reduce the service load stresses in the mockup to the desired degree was calculated to be approximately 25 kips. Since one truss was located on each side of the web of the mockup, approximately 12.5 kips of upward force were required at each end of the truss. As shown in Figs. 2.10a and 2.12a, the compression members were inclined at an angle of 7° to longitudinal axis of the mockup. To obtain the desired upward force, the researchers used basic truss analysis to determine that each compression tube and tension member would have to support forces of 102 kips and 100 kips, respectively.

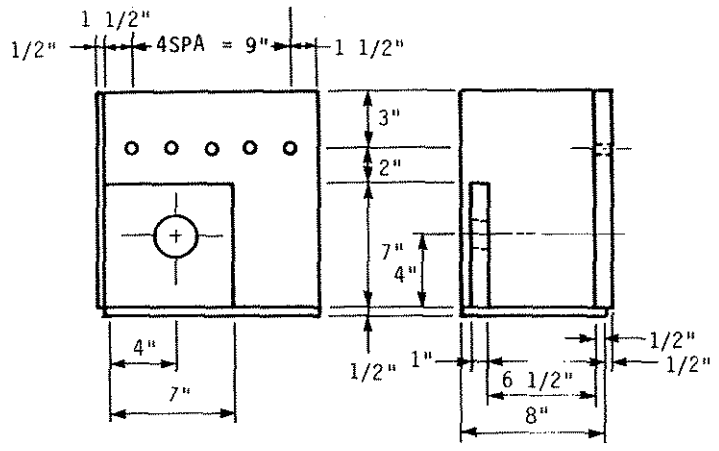
2.3.1. Pin Bracket

The pin bracket (see Fig. 2.10b) for the truss acted as a true pin-ended condition for the compression struts as a 2 1/2-in.-diameter pin passed through the webs of the compression struts and into the bracket on each side of the beam. Figure 2.13a shows two pin brackets with compression struts bolted to the mockup. Since the brackets reacted against each other (horizontal) and into the bottom flange (vertical), the connection to the mockup had to resist lateral forces only. Five 7/8-in.-diameter A325 bolts, also shown in Fig. 2.13a, connected the two brackets through the web and thus prevented lateral movement.



SECTION A-A
(SEE FIG. 2.11a)

a. ST2.2 ON FULL-SCALE MOCKUP



b. PIN BRACKET

Fig. 2.10. Superimposed truss-strengthening technique (ST2.2).

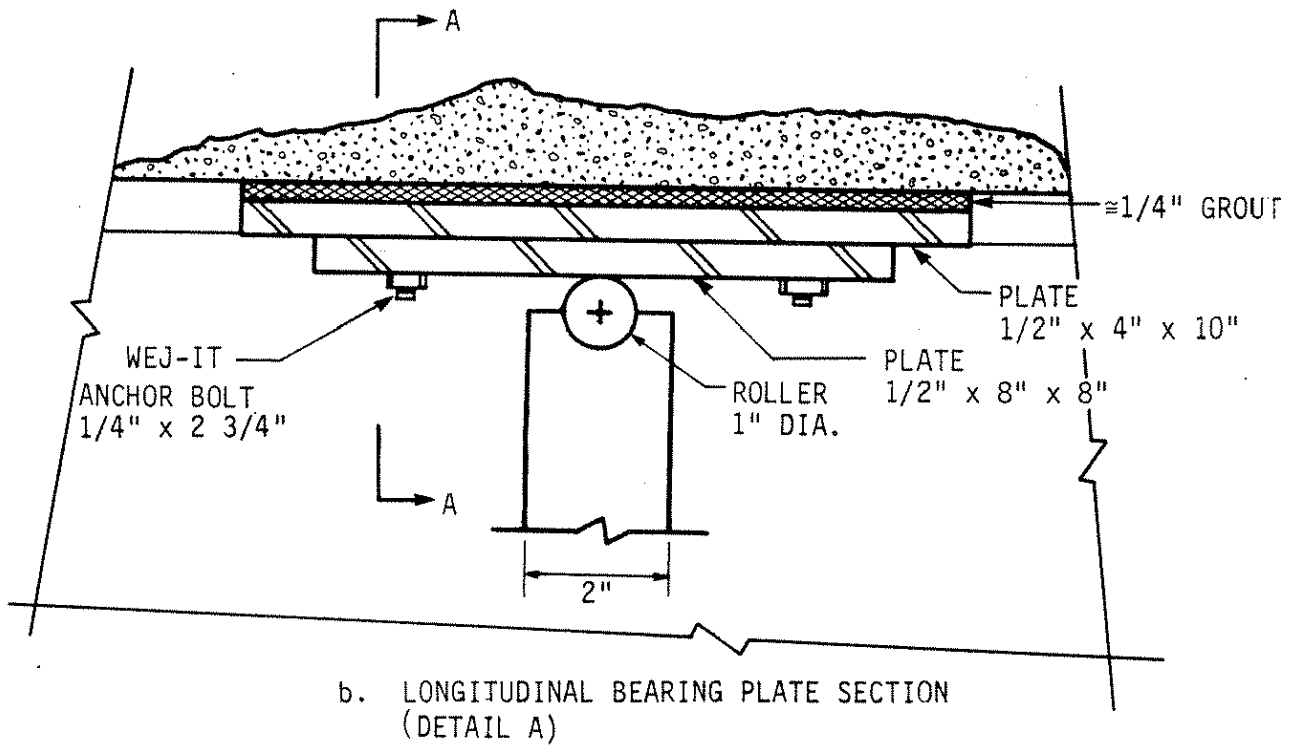
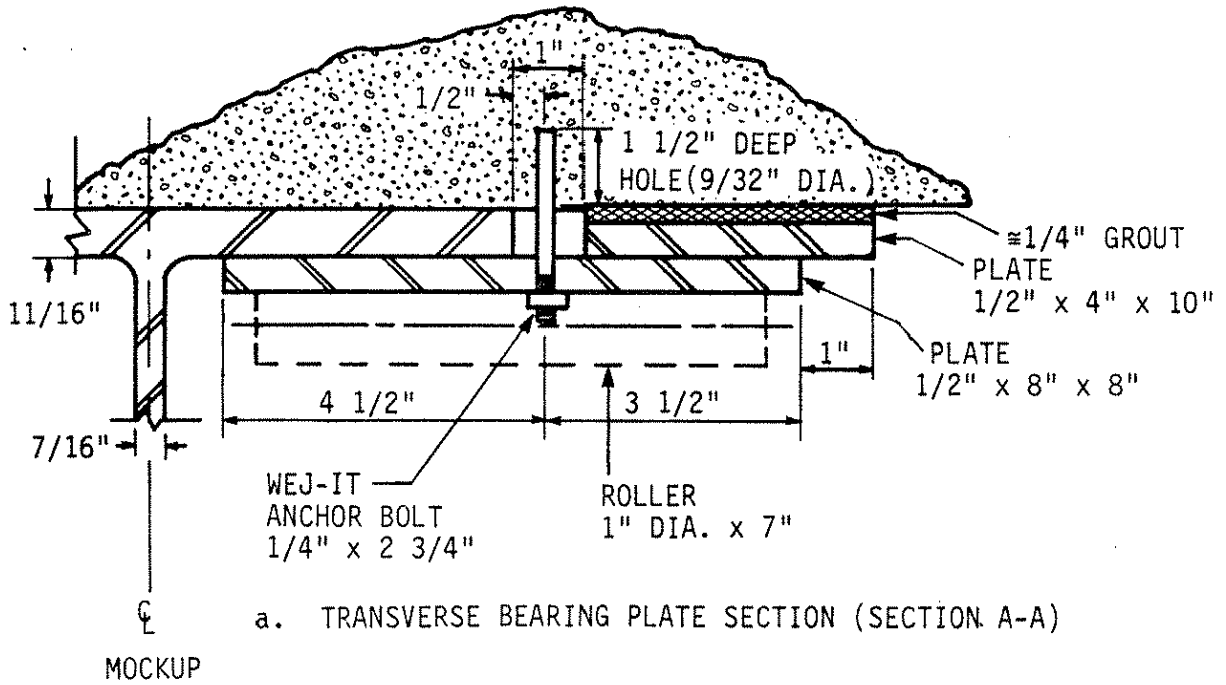
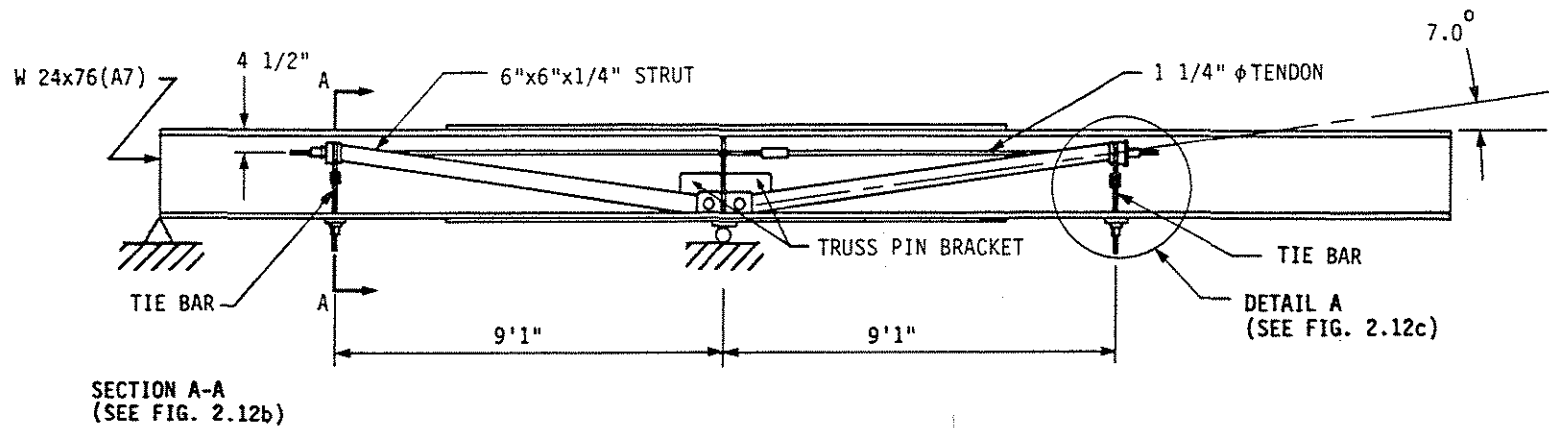
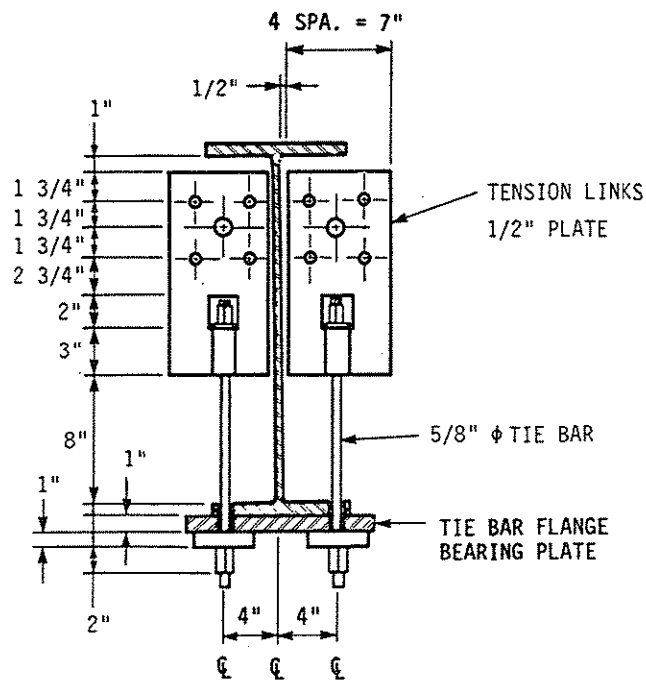


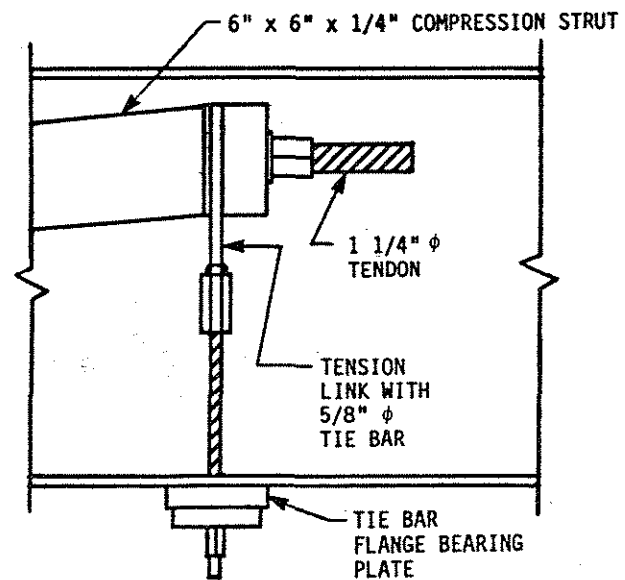
Fig. 2.11. ST2.2 bearing plate assembly.



a. ST2.3 ON FULL-SCALE MOCKUP

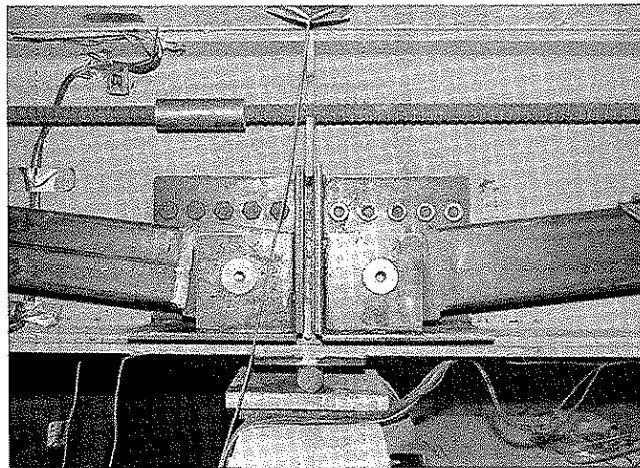


b. SECTION A-A

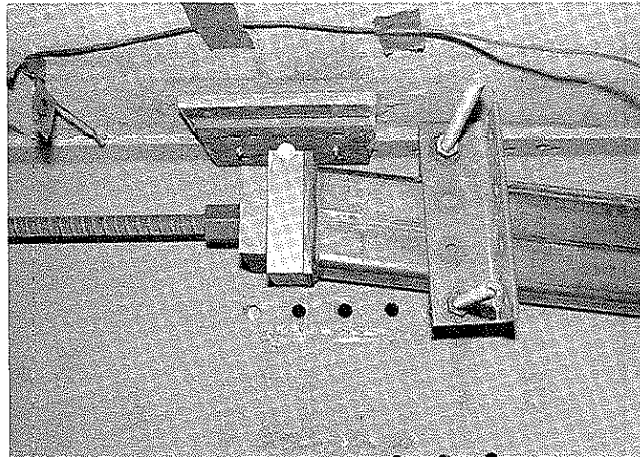


c. DETAIL A

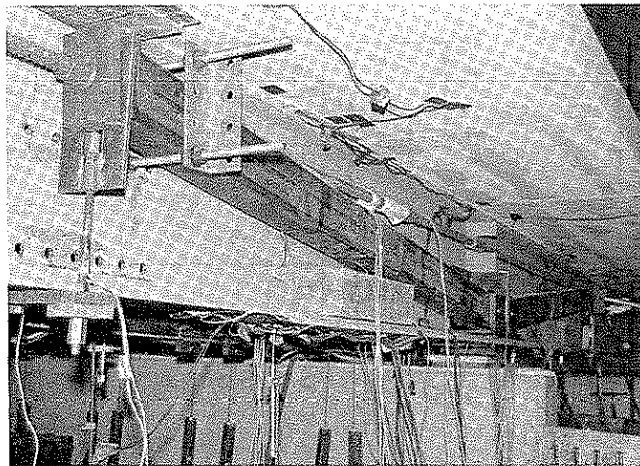
Fig. 2.12. Superimposed truss-strengthening technique (ST2.3).



a. PIN BRACKETS



b. ST2.2 END CONDITION.



c. ST2.3 END CONDITION

Fig. 2.13. Photographs of ST2.2 and ST2.3 on full-scale mockup.

2.3.2. Compression Struts

Based on the required load, researchers selected 6 in. \times 6 in. \times 1/4 in. A500 (46 ksi) structural tubes as compression struts for ST2.2 and ST2.3. The tubes had to be significantly modified for use in the trusses. At the pin bracket end, stiffeners were added to two sides of each tube. The stiffeners shown in Fig. 2.14a were necessary for distributing the compressive load to the bearing pin. Bearing plates, shown in Fig. 2.14b, were welded on the jacking end of each strut. The plates were at a 7° angle to create a vertical surface when the truss was in place. The bearing plate also had four pins that allowed attachment of the two types of end conditions. A 1 3/4-in.-diameter hole at the center of the bearing plate allowed the 1 1/4-in.-diameter tendon to pass through the end of the truss (see Figs. 2.10a and 2.12a). The tubes were also modified in order for the 1 1/4-in.-diameter tendons to pass through the top surface of each tube, as shown in Figs. 2.10a and 2.12a. An 18-in.-long, 2-in.-wide slot was cut in the tubes and stiffened with two 30-in. \times 1 1/4-in. \times 1/2-in. steel plates welded along each side of the slot. The stiffeners were necessary to replace the steel removed from the tube for the slot.

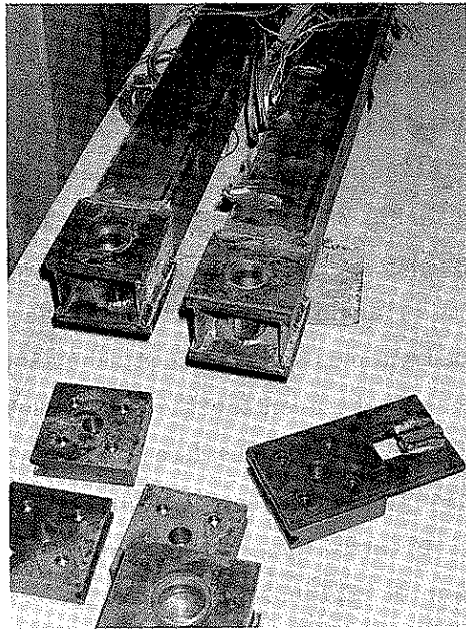
Lateral restraints, which are shown in Figs. 2.13b and c, were bolted to the beam web near the end of each compression strut. Although no out-of-plane forces would normally be expected in the truss system, the restraints were added as a safety precaution. They were essential when the mockup with ST2.3 in place was tested to failure.

2.3.3. End Conditions

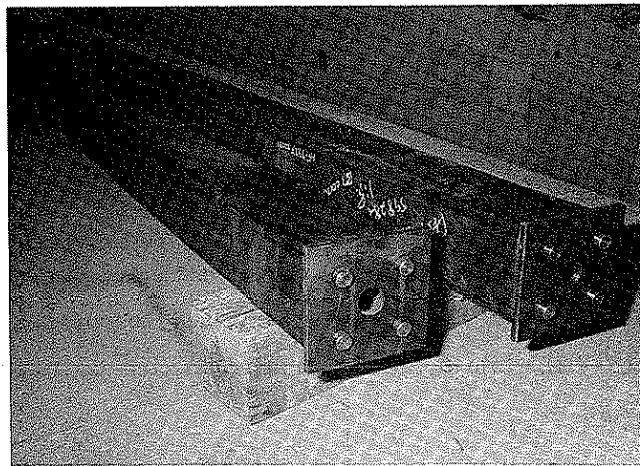
As previously noted, two different schemes were investigated for applying the vertical strengthening force to the mockup. The first scheme involved the truss bearing up against the bottom of the deck (ST2.2), while the second scheme connected the truss to the bottom flange of the beam (ST2.3).

2.3.3.1. ST2.2

For applying the upward force to the lower surface of the top flange of the mockup, a 7-in. \times 7-in. \times 2-in. plate with a bearing roller was attached to the compression struts (see Figs. 2.10a, 2.11, and 2.13b). A bearing plate was anchor-bolted to the bottom of the deck of the mockup as shown in Fig. 2.11. Approximately half the area of the bearing plate was on the bottom of the concrete deck, and half was on the bottom of the upper beam flange. As the



a. COMPRESSION STRUT PIN BRACKET END



b. COMPRESSION STRUT BEARING PLATE END.

Fig. 2.14. Photographs of ST2.2 and ST2.3 compression struts.

1 1/4-in.-diameter tendon was tensioned, the ends of the compression struts deflected upward into contact with the bearing plate on the lower surface of the mockup.

2.3.3.2. ST2.3

In ST2.3 the vertical component of force in the truss, which produced the positive moment, was resisted by the lower flange of the beam. Tension links consisting of four 5/8-in. 150-grade, Dywidag threadbars (see Figs. 2.12 and 2.13c) connected the end of each compression strut to the bottom flange of the mockup. The strap shown in Figs. 2.12b,c distributed the vertical force across the bottom flange of the mockup. When the 1 1/4-in.-diameter tendon was tensioned, the tension links reacted against the bottom flange of the mockup truss producing positive moment.

3. TESTS AND TEST PROCEDURES

This chapter outlines the details of the instrumentation and testing of the full-scale mockup and the strengthening systems. Locations of instrumentation for measuring strain and displacement will be given for the mockup and each of the strengthening schemes. A detailed description of the tests performed on the unstrengthened mockup, as well as on the mockup with each strengthening scheme in place will also be given. Discussion and analysis of results obtained will be presented in Chapter 4.

3.1. Vertical Load Mechanism

The vertical loading mechanism used to create the negative moment is shown in Fig. 2.15. This figure indicates that the left and right "inflection points" were located 12 ft. 8 in. and 12 ft. 5 in., respectively, from the "interior support". The left inflection point hold down was preloaded with a 75-kip clamping force to hold the beam on the support when loading was applied to the free end of the beam. As previously noted, Fig. 2.2 illustrates how this loading mechanism simulated negative moment regions of a prototype bridge.

The load cell shown in Fig. 2.15 measured the force of one of the two hollow-core hydraulic cylinders used. Since the cylinders were in parallel, the load cell read one-half the total vertical load. This loading mechanism produced the desired negative moment between the two inflection points of approximately 534 ft-kips when a 43-k vertical load was applied at the load point (i.e., the right inflection point).

3.2. Instrumentation

The instrumentation for all tests consisted of electrical-resistance strain gages (strain gages), direct current displacement transducers (DCDTs), and a load cell. Strain gages were temperature compensated and were attached to the specimens with recommended surface preparation and adhesive. Three-wire leads were used to minimize the effect of long lead wires and temperature changes. All strain gages were waterproofed with a minimum of two layers of protective coatings. Strain gages and DCDTs on the mockup and strengthening systems were read and recorded with a computerized data acquisition system (DAS). Each strain gage was bonded with its axis parallel to the axis of the beam, tube, or tendon.

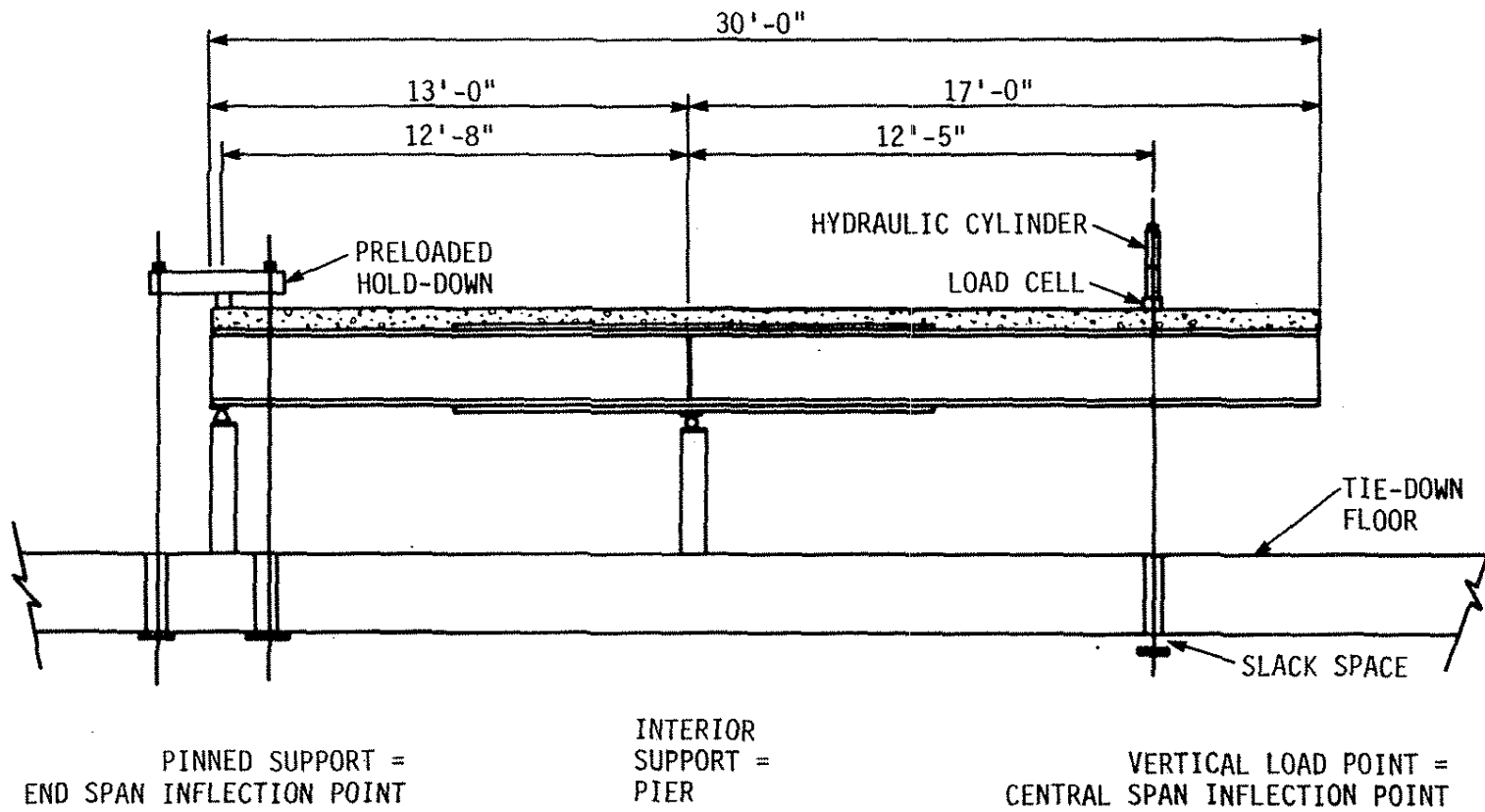


Fig. 2.15. Vertical loading mechanism for full-scale mockup.

3.2.1. Mockup Instrumentation

The locations of strain gages used on the beam and cover plates are shown in Fig. 2.16. Strain gages were offset from the support centerline because of the sole plate. They were also offset from the cover plate cutoff points to avoid the high stress gradients at these locations. A total of 28 strain gages were placed on the beam and cover plates. At each of the numbered sections in Fig. 2.16, there were four strain gages on the beam: two on the top surface of the top beam flange and two on the bottom surface of the bottom beam flange. Figure 2.17 shows the position of the DCDTs used for measuring the vertical displacements. Although not shown in Fig. 2.17, a dial gage was located at the loaded end of the mockup to detect any lateral movement.

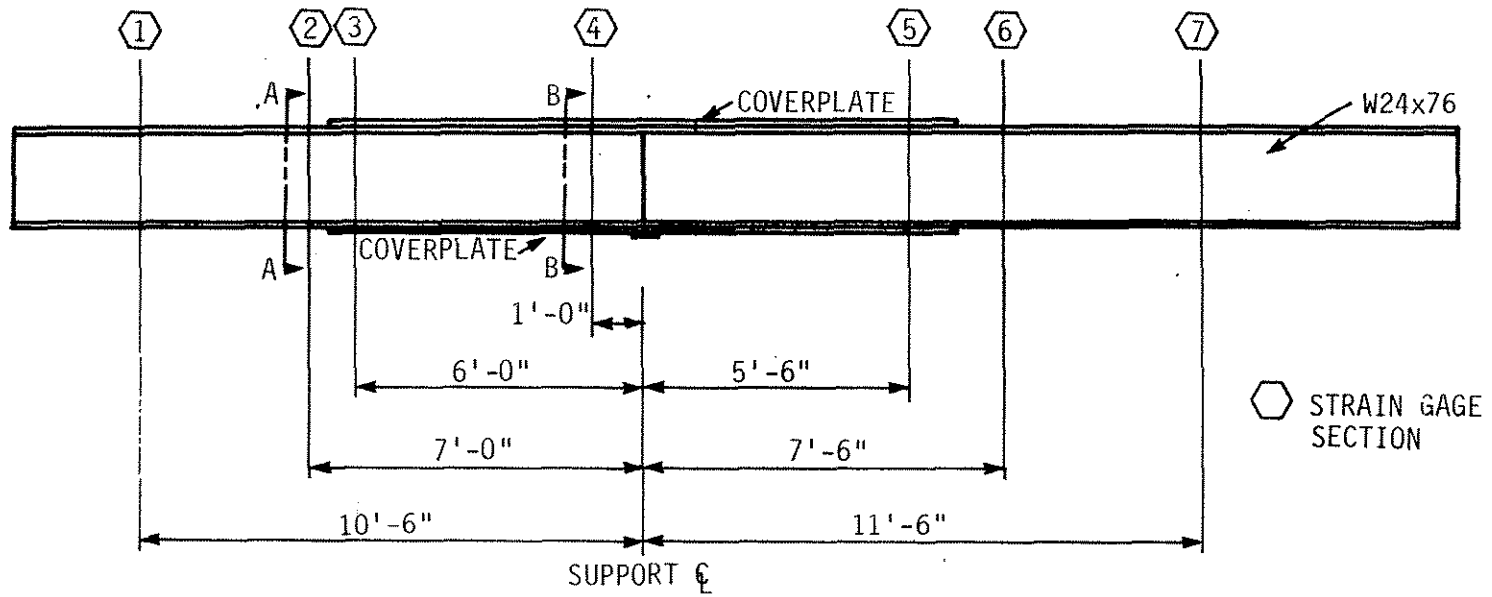
3.2.2. ST2.1 Instrumentation

Strain gage locations on the post-compression tubes are shown in Fig. 2.18. A total of 30 strain gages were placed on the post-compression tubes. Strain gages were located at a section approximately midway between the lateral restraint and each end of the tubes. If any bending took place in the tubes, it would be a maximum at these locations and thus easy to detect. An additional section located 1 ft from the lateral restraint on one tube was instrumented with strain gages to determine the effectiveness of the lateral restraint in reducing bending.

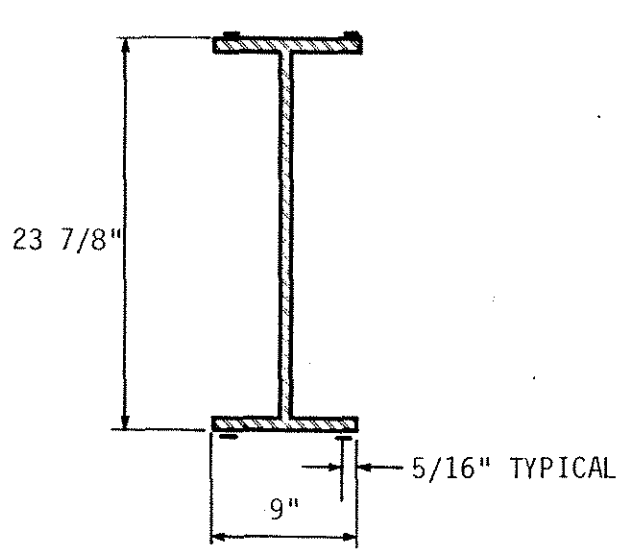
At each section, six strain gages were arranged around the tube as shown in Fig. 2.18b,c. Two strain gages were located on the top surface of the tubes to straddle the weld seam, which ran along the centerline. Locating the strain gages as shown in Fig. 2.18c avoided stress concentrations at the seam and the corners of the tubes. Strain gages on the bottom surface of the tubes were placed similarly, for consistent data. The arrangement of six strain gages at each instrumented section made it possible to determine accurately the bending and axial force at each section.

3.2.3. ST2.2 and ST2.3 Instrumentation

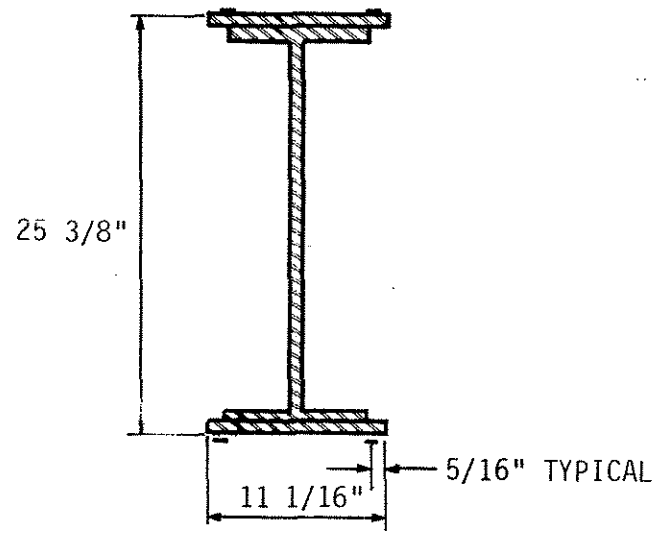
Instrumentation used on the superimposed truss is illustrated in Fig. 2.19. A total of 38 strain gages were used on ST2.2. Strain gages on the compression struts were similar to those on the post-compression tubes described in Section 3.2.2. Sections of six strain gages



a. LAYOUT



b. SECTION A-A



c. SECTION B-B

Fig. 2.16. Strain gage locations for full-scale mockup.

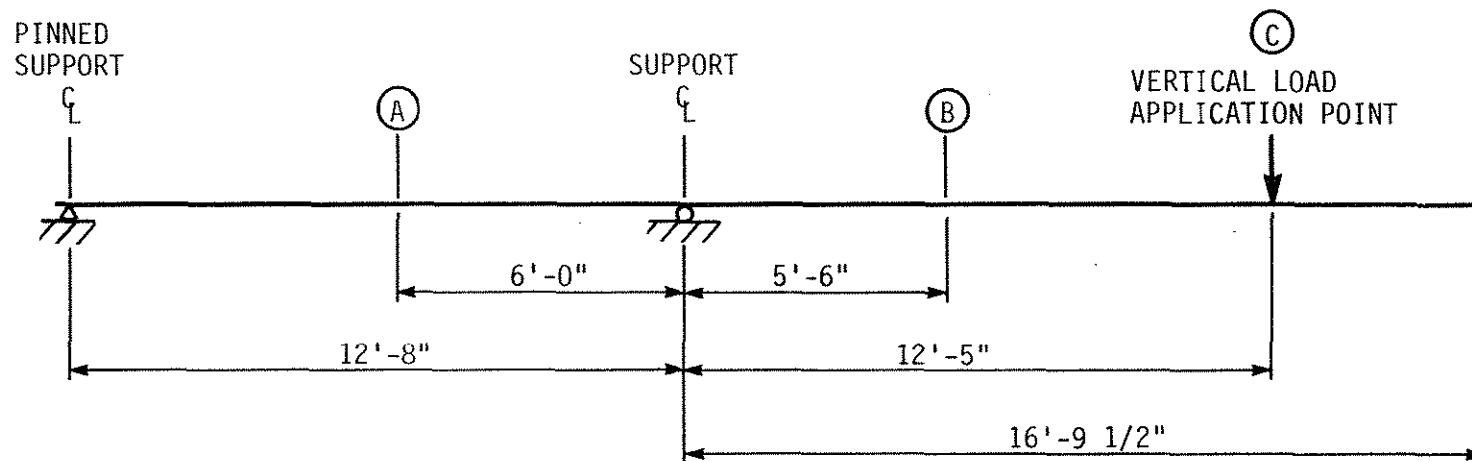


Fig. 2.17. Vertical displacement measurement (DCDT) locations on full-scale mockup.

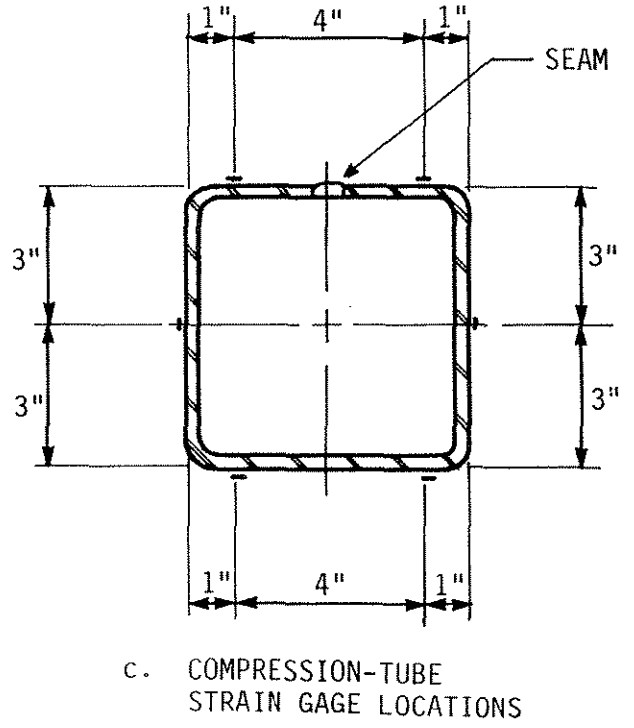
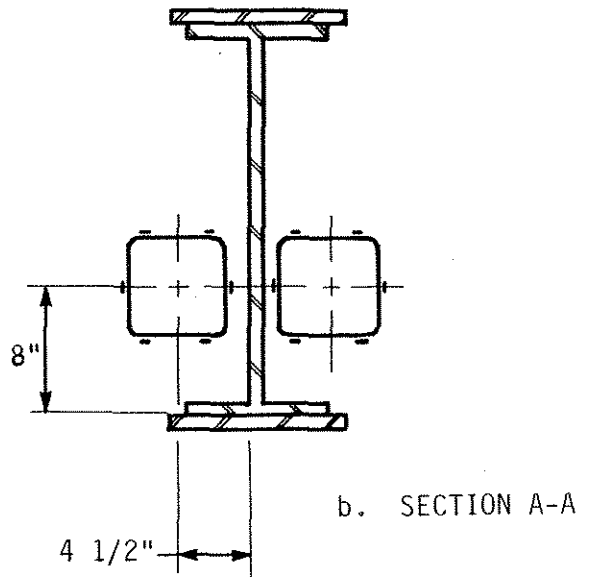
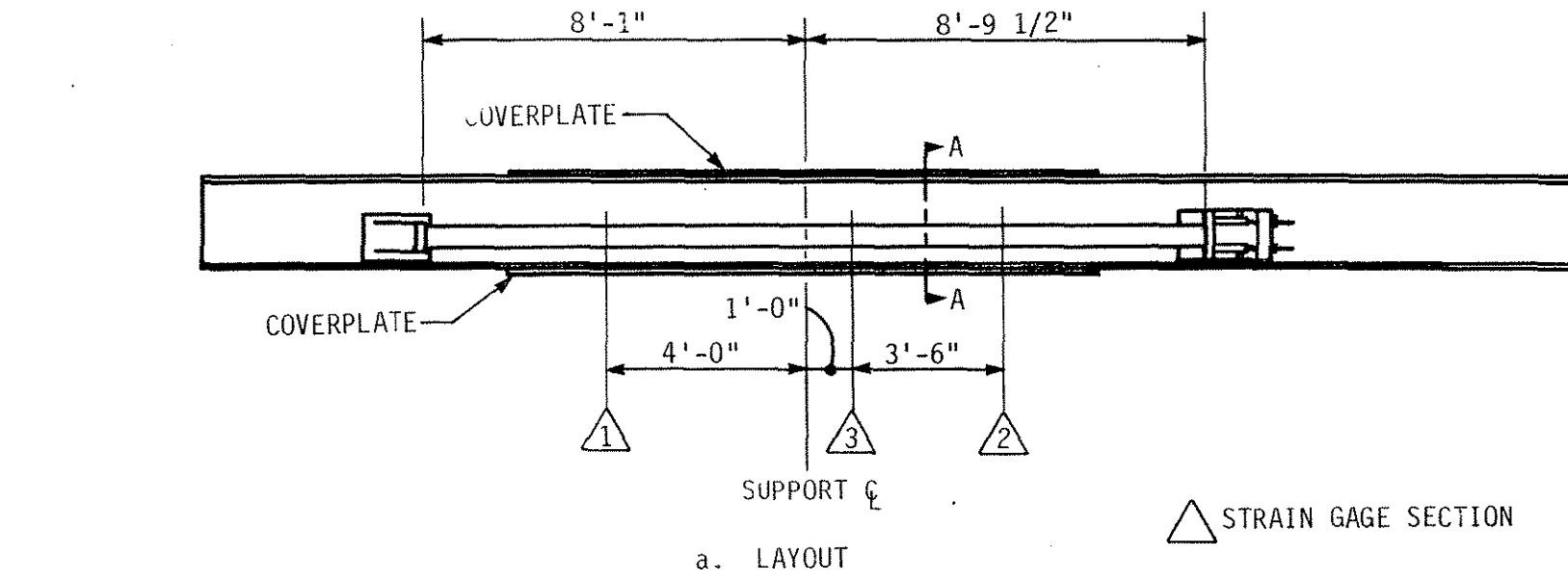
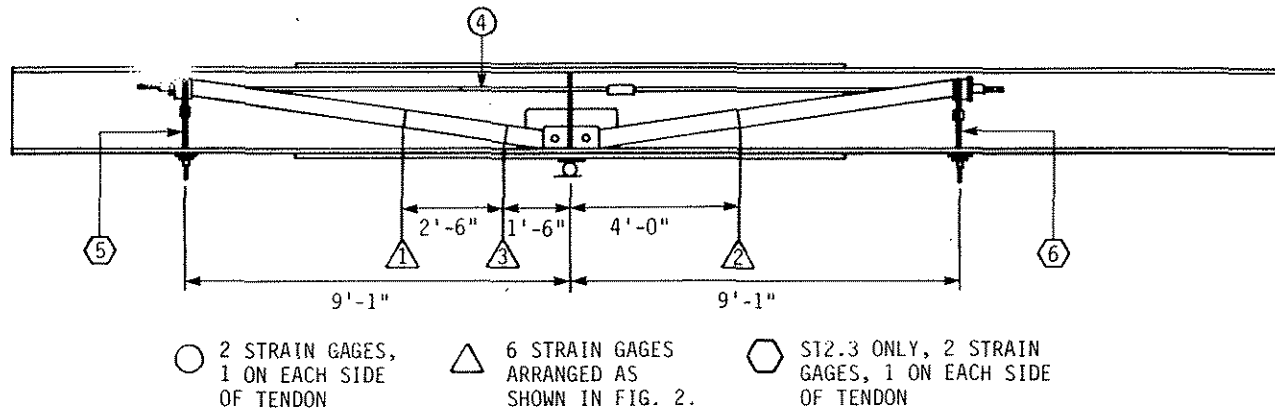
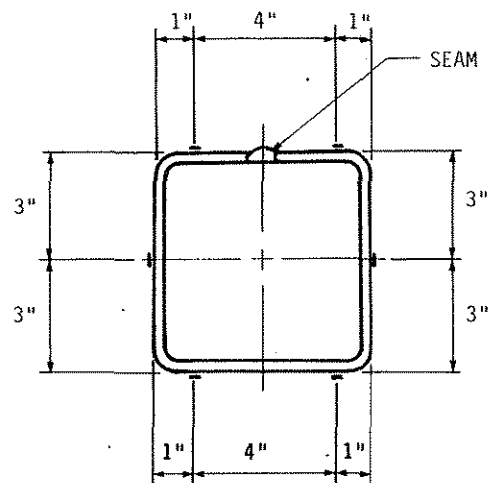


Fig. 2.18. ST2.1 strain gage locations.



a. LAYOUT



b. COMPRESSION-STRUT STRAIN GAGE LOCATIONS.

Fig. 2.19. ST2.2 and ST2.3 strain gage locations.

were located at the midpoint of each strut. An additional section of strain gages was located 1 ft 6 in. from the pin bracket on one tube to determine the amount of bending near the bracket. Two strain gages were located on each of the 1 1/4-in.-diameter tendons to determine the tension being applied to the truss. These strain gages were located symmetrically on each side of a tendon to compensate for the effects of bending. For ST2.3, an additional eight strain gages were used. Two strain gages were placed on each tiebar (see Fig. 2.19) to measure the vertical force applied to the lower flange of the beam. As with the 1 1/4-in.-diameter tendons, strain gages were located on opposite sides of the tie bars to compensate for the effects of bending.

3.3. Preliminary Vertical-Load Tests

As noted in Ref. [7], initial tests on the mockup were performed prior to the post-tensioned strengthening tests. These tests included an initial cracking test, a post-cracking test, and a strengthened beam test. Descriptions and results of these tests can be found in Section 4.2 of the final report for HR-287 [7].

Unstrengthened mockup tests were also run prior to ST2.1, ST2.2, or ST2.3. Although one of the strengthening systems was in place at the time of the tests, it was not structurally attached to the mockup. These tests established a reference for the unstrengthened mockup. A summary of all the tests performed on the mockup is presented in Table 2.1.

For the given tests, Table 2.1 lists the strengthening technique in place, the maximum design strengthening load in the compression tubes (ST2.1) or tendons (ST2.2, ST2.3), the maximum nominal vertical load applied to the mockup, and the amount of partial vertical load (if any) applied to the mockup before the strengthening systems were stressed.

For each of the strengthening schemes, a nominal strengthening force was established. This force was the amount of compression in the tubes (ST2.1) or tension in the tendons (ST2.2, ST2.3) determined to produce the desired change in stress in the mockup. For ST2.1 this was 60-kips compression per tube. For ST2.2 and ST2.3, the nominal strengthening force was 100-kips tension per tendon. For the majority of tests performed on the mockup, the strengthening schemes were loaded to these levels. However, in order to determine the behavior of the mockup with each strengthening scheme in place, tests were also performed with strengthening loads both above and below the nominal design values. For ST2.1,

Table 2.1. Tests on the full-scale mockup.

Test	Strengthening Technique	Maximum Strengthening Load (kips)	Maximum Vertical Load (kips)	Partial Vertical Load (kips)
1	---	0	43	0
2	ST2.1	60/tube	0	0
3	ST2.1	40/tube	43	0
4	ST2.1	60/tube	43	0
5	ST2.1	75/tube	43	0
6	ST2.1	60/tube	43	20
7	ST2.2	100/tendon	0	0
8	ST2.2	50/tendon	85	0
9	ST2.2	100/tendon	85	0
10	ST2.2	130/tendon	85	0
11	ST2.2	100/tendon	85	40
12	ST2.3	100/tendon	0	0
13	ST2.3	50/tendon	85	0
14	ST2.3	100/tendon	85	0
15	ST2.3	130/tendon	85	0
16	ST2.3	100/tendon	85	40
17	ST2.3	130/tendon	120	0

compression loads of 40 and 75 kips per tube were also investigated. For ST2.2 and ST2.3, tension forces of 50 and 130 kips per tendon were examined.

A maximum applied vertical load of 43 kips was initially chosen for the mockup to limit stress in the steel beam and cover plates to 18 ksi compression or tension under various test conditions. For the test of the mockup with ST2.2 and ST2.3, this value was increased to approximately 85 kips of vertical load applied in order to investigate the behavior of the mockup and strengthening scheme at higher stress levels.

3.4. ST2.1 Tests

Tests 2 through 6 in Table 2.1 were performed to evaluate the strengthening effects of ST2.1 in place. These tests examined how the mockup responded to various levels of post-compression force in the tubes throughout a vertical load cycle. Strengthening was also done while a partial vertical load was present (Test 6) to simulate the replacement of a portion of the bridge deck. In an actual bridge, there would be stresses in the stringers even when the deck was removed due to a significant portion of the dead load still being present.

Test 2 examined the behavior of the mockup with post-compression alone. The test was also conducted to determine the amount of lockoff (seating) loss in the post-compression arrangement. Initially, the tubes were compressed to 60 kips each. Data were recorded by the DAS at 5-kip increments during compression. At 60 kips, the sliding U-braces were locked in place and the jacking pressure was released. At this point a reading was taken to determine the loss in compression force due to lockoff.

Tests 3, 4, and 5 evaluated the combination of vertical loading plus compressive strengthening loads. Three compressive forces were investigated: 40 kips, 60 kips, and 75 kips per tube. To begin these tests, the tubes were compressed to the desired load with data taken every 10 kips. The U-braces were locked in place and the hydraulic pressure was released. A reading at this point determined the actual compressive force in each tube. A vertical load cycle was then applied to a maximum of 43 kips with data recorded using the DAS at 5-kip intervals. The vertical load was then decreased to zero with data taken every 10 kips.

As previously noted, Test 6 simulated the replacement of a portion of a bridge deck. During Test 6, the tubes were compressed while a partial vertical load was present. After the initial readings were taken, a vertical load of 20 kips, approximately half the peak load, was applied with data recorded every 5 kips. The U-braces were then compressed to 60 kips each with data recorded every 5 kips. The tubes were then locked in place and the hydraulic pressure released. Readings were again taken at this point to determine the actual compressive force in each tube. The vertical load was next increased to 43 kips and data were recorded every 5 kips. The vertical load was then removed and reapplied (simulating the replacement of the bridge deck) with data recorded at the same 5-kip increments.

3.5. ST2.2 and ST2.3 Tests

Tests 7 through 11 for ST2.2 and Tests 12 through 16 for ST2.3 were similar to Tests 2 through 6 for ST2.1. Vertical loads on the mockup with ST2.2 or ST2.3 in place, however, were increased to twice that used when ST2.1 was mounted on the mockup (i.e., approximately 85 kips). By using a vertical load of 85 kips, researchers could examine higher stress levels in preparation for the ultimate load test. Test 17, the ultimate load test, was performed with ST2.3 in place on the mockup.

Tests 7 and 12 (similar to Test 2) determined the behavior of the mockup with ST2.2 or ST2.3 alone. During these tests, the truss tendons were tensioned to 100 kips each with data recorded by the DAS every 5 kips.

Tests 8, 9, and 10 (similar to Tests 3, 4, and 5) evaluated the effects of a vertical load on the mockup with ST2.2 and ST2.3. Tensions of 50 kips, 100 kips, and 130 kips per tendon were investigated. To begin these tests, the tendons were tensioned to the desired load with data taken at 10-kip increments. The truss tendons were then locked in place and the hydraulic pressure was released. Data were then taken to determine the actual tension in each of the truss tendons. The vertical load was then applied to a maximum of approximately 85 kips with data being recorded at 10-kip intervals. The vertical load was removed and data taken every 10 kips.

Tests 11 and 16 were similar to Test 6 with ST2.1 in place in that a partial vertical load and vertical load cycle were used to simulate the replacement of a portion of a bridge deck. In Tests 11 and 16, however, the partial vertical load on the mockup was 40 kips and the maximum vertical load was 85 kips. In Test 17, the mockup with ST2.3 in place was tested to failure. After an initial reading, the tendons in each truss were tensioned to 130 kips each. The tendons were locked off and data were taken after the hydraulic pressure was released. Vertical load was then applied to the mockup until failure occurred. Data were recorded at 20-kip intervals of vertical load throughout the test.

4. ANALYSIS AND TEST RESULTS

This section presents both the data obtained from tests of the mockup and the analysis of the finite-element model. To illustrate the effectiveness of the strengthening systems on the mockup, two types of data were recorded and are presented: deflections of the vertical load point and strain distributions at the critical sections, 4 and 5. Section 4 is at the support; Section 5 is within the cover-plated region 5 ft 6 in. from the support (see Fig. 2.16).

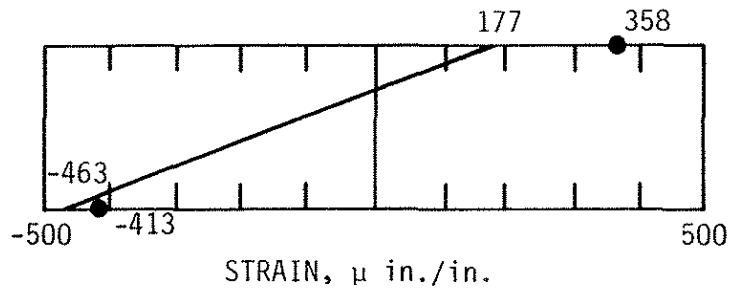
Data unique to the behavior of each strengthening scheme will also be presented in the appropriate section. For ST2.1, data relating to the change in force and bending of the compression tubes due to vertical load will be presented. For ST2.2 and ST2.3 the effects of vertical load on the force in the tendons and compression struts will be presented. Also for ST2.3 the change in force in the tie bars resulting from vertical loading will be presented.

4.1. Preliminary Vertical-Load Tests

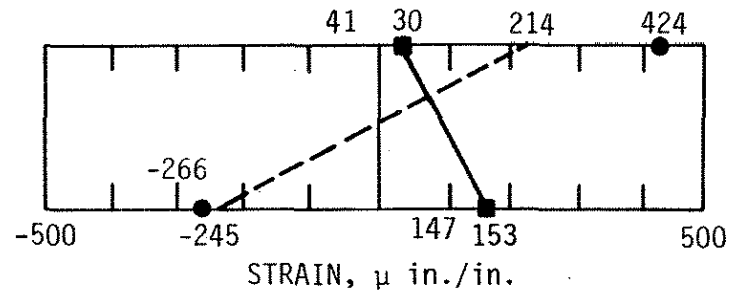
Initial cracking and performance tests of the mockup were performed prior to the post-tensioned tests of HR-287. The results of these tests are presented in Section 4.2 of Ref. [7]. Test 1 of the present investigation (listed in Table 2.1) established the deflection and strain characteristics of the unstrengthened mockup. At a vertical load of 43 kips, the deflection at the load point was 0.735 in. downward. This value is approximately 20% larger than the unstrengthened beam deflection of 0.603 in. reported in HR-287 (Ref. [7]). This suggests that the testing program of HR-287 caused additional cracking in the deck of the mockup, thus making the mockup more flexible. (Tests were performed on the mockup after the initial unstrengthened tests (see Table 43 of Ref. [7]).) Another reason for this increase in deflection could be that more of the friction bond between deck and beam was broken as a result of the testing program of HR-287.

The finite-element analysis of the mockup predicted a downward deflection of 0.531 in. for a 43-kip load. This indicated that the finite-element model was stiffer than the mockup under negative moment bending. However, it should be noted that although the finite-element model accounted for connector stiffness, it did not account for cracks in the concrete deck.

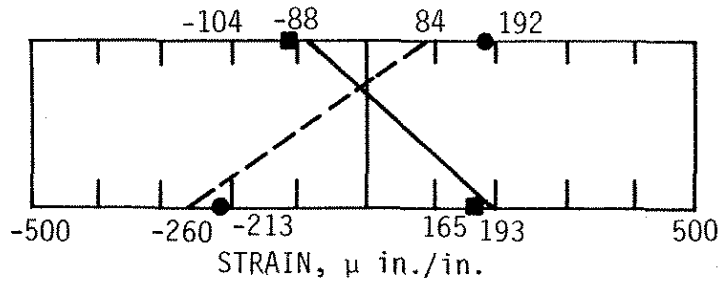
In Fig. 2.20a the theoretical and experimental average top and bottom strains at Section 4 of the mockup with 43-kips vertical load are illustrated. The solid line on the diagram represents strains predicted by the finite-element analysis for a vertical load of 43



— THEORETICAL
 ● EXPERIMENTAL
 a. 43k, VERT.

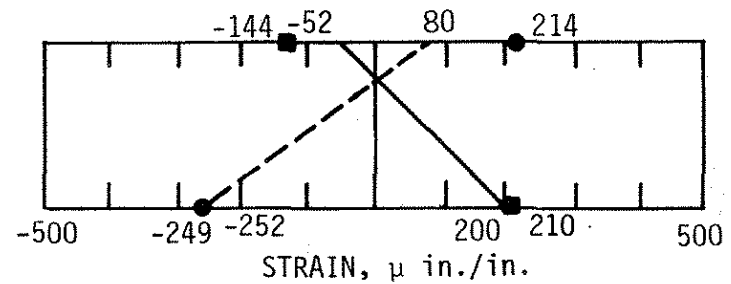


— 60k/TUBE-- THEORETICAL
 ■ 60k/TUBE-- EXPERIMENTAL
 - - - 60k/TUBE, 43k VERT.--THEORETICAL
 ● 60k/TUBE, 43k VERT.--EXPERIMENTAL
 b. ST2.1



— 100k/TENDON-- THEORETICAL
 ■ 100k/TENDON-- EXPERIMENTAL
 - - - 100k/TENDON, 43k VERT.-- THEORETICAL
 ● 100k/TENDON, 43k VERT.-- EXPERIMENTAL

c. ST2.2



— 100k/TENDON-- THEORETICAL
 ■ 100k/TENDON-- EXPERIMENTAL
 - - - 100k/TENDON, 43k VERT.-- THEORETICAL
 ● 100k/TENDON, 43k VERT.-- EXPERIMENTAL

d. ST2.3

Fig. 2.20. Experimental and theoretical strains at Section 4 for nominal loads.

kips, while the two data points are experimental strains recorded when the mockup was subjected to the same vertical loading. As may be noted, the bottom flange theoretical and experimental compression strains are in good agreement. However, the experimental tension strain on the top flange is approximately twice the theoretical strain. One explanation for this variation is that the deck of the mockup was much less effective in tension than the finite-element analysis predicted.

4.2. Finite-Element Analysis

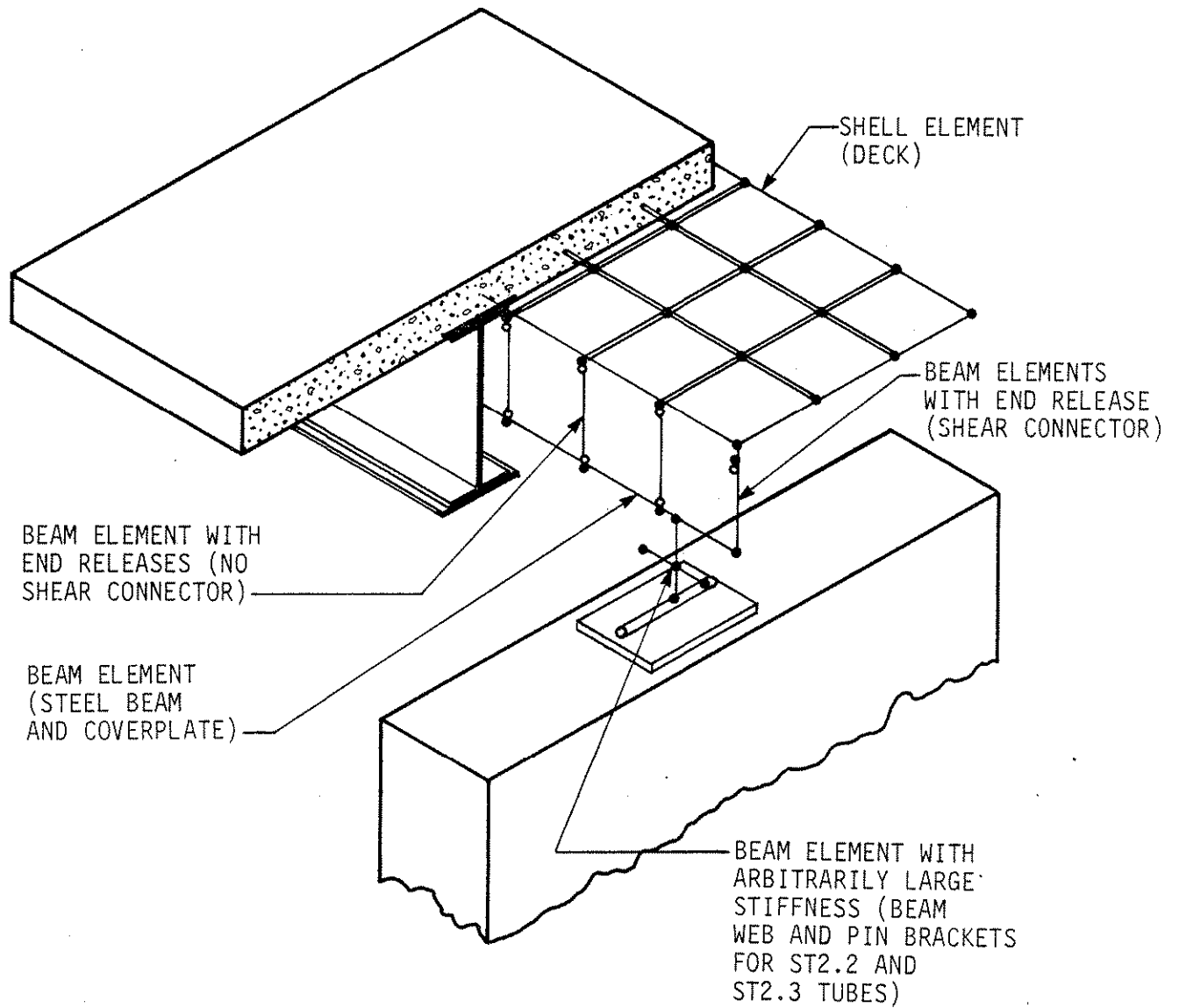
The mockup tested in the ISU Structural Engineering Laboratory is structurally complex. The composite beam has a variable stiffness because of blockouts in the concrete deck (filled in for compression but not for tension), intermittent shear connectors, and application of cover plates to the portion of the beam nearest the pier. Strengthening schemes ST2.1, ST2.2, and ST2.3 applied various forces to the mockup.

In order to consider as many structural irregularities of the mockup as possible, the composite beam was analyzed using SAP IV [2] finite-element analysis. The basic finite-element model was adapted from model studies conducted in 1985 [9]. Because the mockup is symmetrical with respect to the plane of the beam web but not with respect to the pier support, the finite-element model was developed with half symmetry, as illustrated in Fig. 2.21.

Based on the study in Ref. [9], the concrete deck was modeled with rectangular plate elements 12 in. by 12 1/2 in., as shown in Fig. 2.21a. The 12-in. plate-element side is parallel with the beam. Load points and blockouts interrupted the basic element pattern, and some triangular plate elements were used at those locations. The shallow grooves in the deck (see Fig. 2.4b) were neglected.

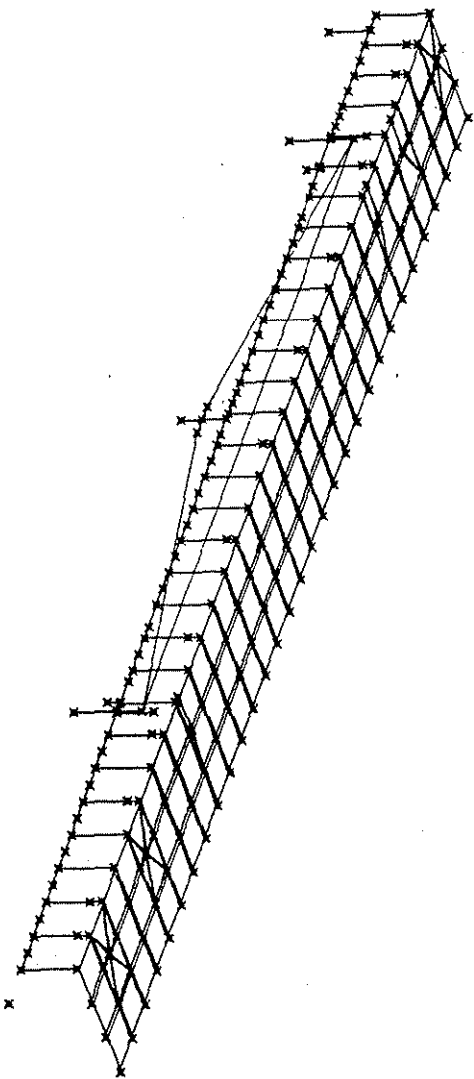
Element properties were based on the 6 1/2-in.-thick concrete deck without reinforcing. From the previous study, it is apparent that the deck elements model the compression behavior better than the tension behavior of the deck. The deck elements in tension will be stiffer than the cracked deck in the mockup.

The steel beam and beam with cover plates were modeled with beam elements capable of bending and shear deflections. Beam and deck elements were linked with shear connector assemblies at nodes nearest shear connectors. Thus, the beam and deck elements were linked



a. MODEL SCHEMATIC NEAR PIER SUPPORT

Fig. 2.21. Half-symmetry SAP IV finite-element model.



b. COMPLETE MODEL WITH ST2.3.

Fig. 2.21. Continued.

with longitudinal force resisting elements only at eight points. Other links, shown in Fig. 2.21a, provided only a vertical tie between the beam and deck elements.

In the earlier study in Ref. [9], comparison of the results from the finite-element model and simple-span composite beam tests conducted by Dedic [20] gave differences of up to 16%. The finite-element model always gave strains and deflections less than those measured experimentally. The model gave better results for positive moment with the deck in compression than for negative moment.

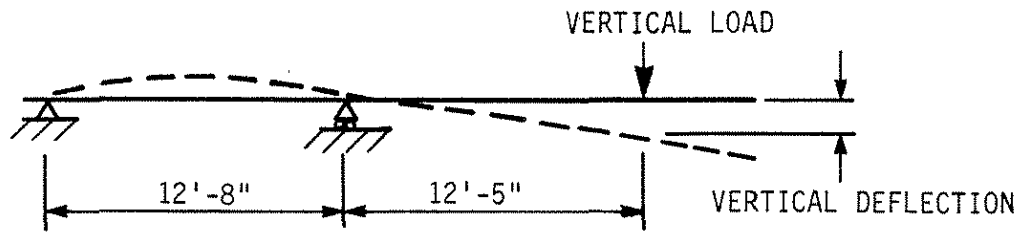
The strengthening schemes applied to the mockup were modeled by providing arbitrarily stiff beam elements from steel beam elements to points of connection. Steel tubes and tendons in the strengthening schemes then were modeled with beam elements of appropriate properties. Figure 2.21b shows the complete half-symmetry finite-element model with strengthening truss ST2.3 in place.

4.3. Effects of ST2.1 on Mockup

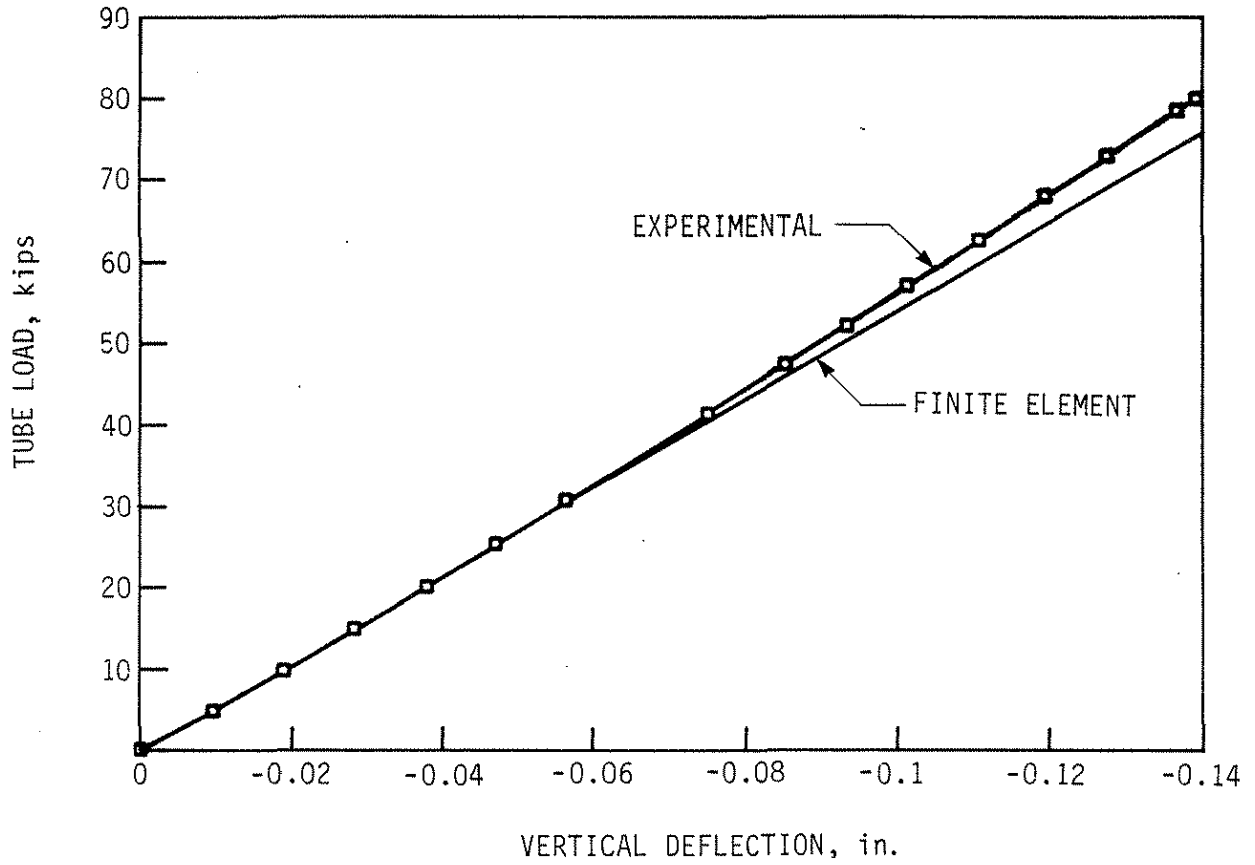
In this section, the performance of ST2.1 when applied to the mockup will be presented. Shown in Fig. 2.22b is the effect of increasing the compression force in the compression tubes of ST2.1 on the deflection at the load point; note that no vertical load has been applied to the system at this time. An approximately linear relationship between the compressive forces in the compression tubes and the upward vertical deflection of the mockup is clearly shown. A maximum deflection of approximately 0.14 in. occurs at a load of 80-kips compression per tube. The solid line on the graph is the vertical deflection obtained from the finite-element analysis of ST2.1 applied to the mockup. For a given tube load, the finite-element model shows a larger deflection than was recorded experimentally for the mockup. Although the data are in good agreement, this indicates that while the section was undergoing positive bending, the mockup was slightly stiffer than the theoretical finite-element model with blockouts predicted.

Figure 2.23a illustrates the effects of vertical loading on the strengthened mockup. The graph plots vertical load versus deflection at the vertical load point for three different magnitudes of post-compression forces. Compressive forces of 40, 60, or 75 kips per tube were in place when the vertical load was applied.

The initial deflections due to post-compression are shown as negative (upward). The solid line is the deflection of the unstrengthened mockup with the same vertical loading. A

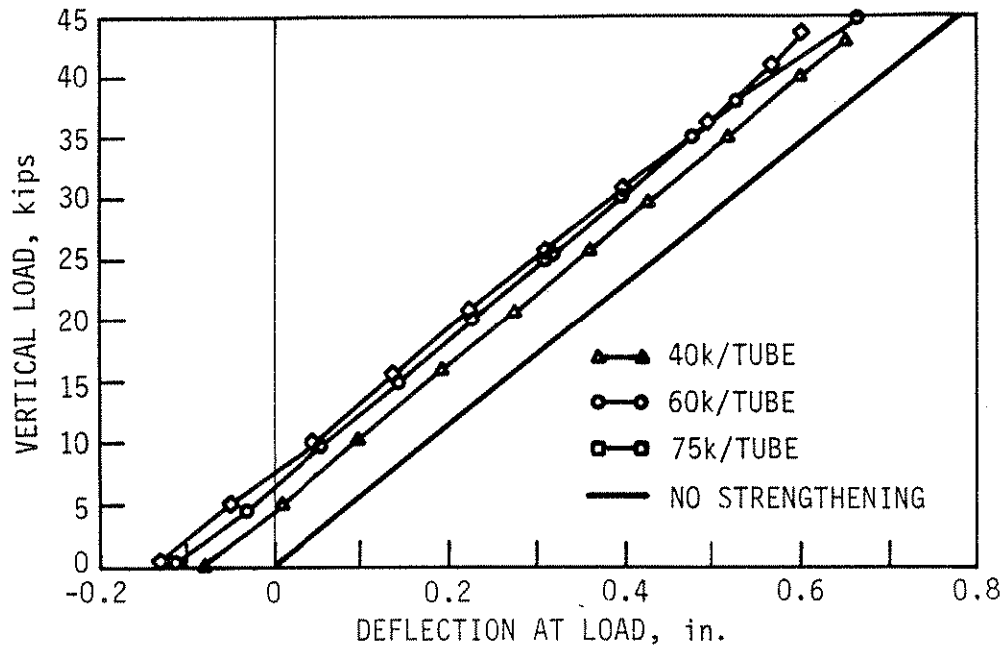


a. TEST SCHEMATIC

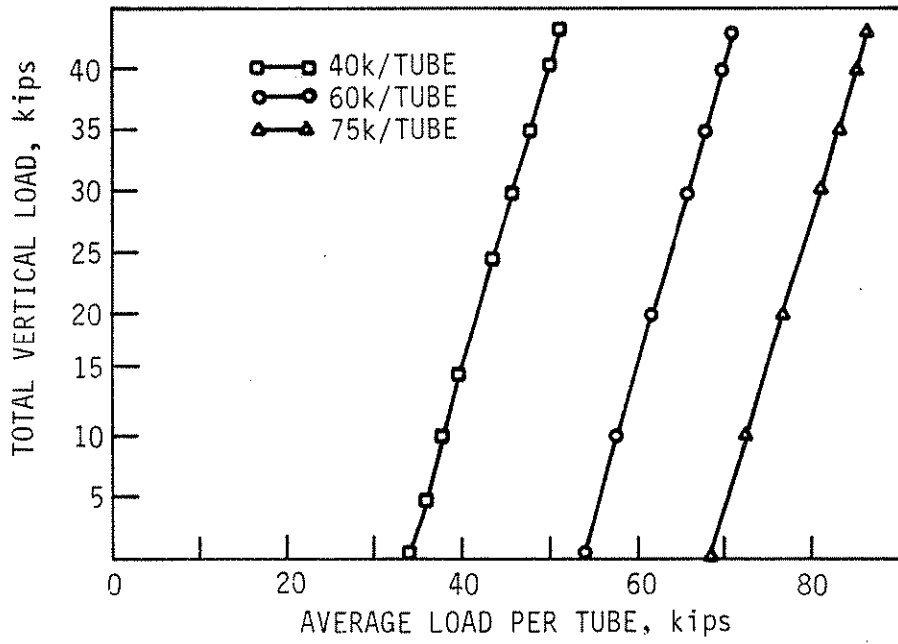


b. ST2.1 COMPRESSION-TUBE LOAD VS. DEFLECTION CURVE

Fig. 2.22. Test schematic and compression-tube load vs. deflection curve for ST2.1 on mockup.



a. VERTICAL LOAD VS. DEFLECTION CURVES FOR THREE TUBE LOADS



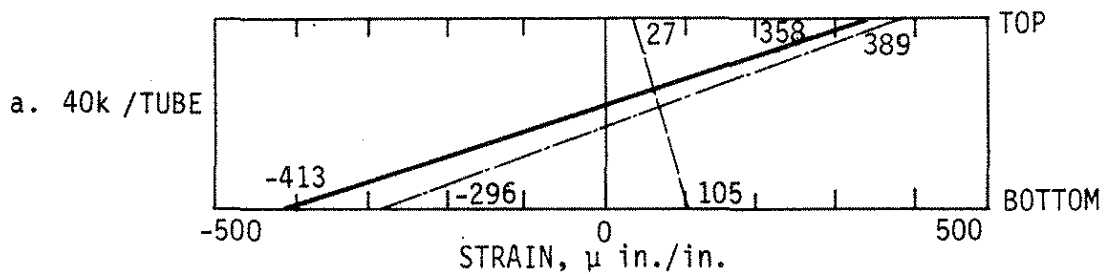
b. VERTICAL LOAD VS. AVERAGE TUBE LOAD FOR THREE TUBE LOADS

Fig. 2.23. Response of ST2.1 to vertical load.

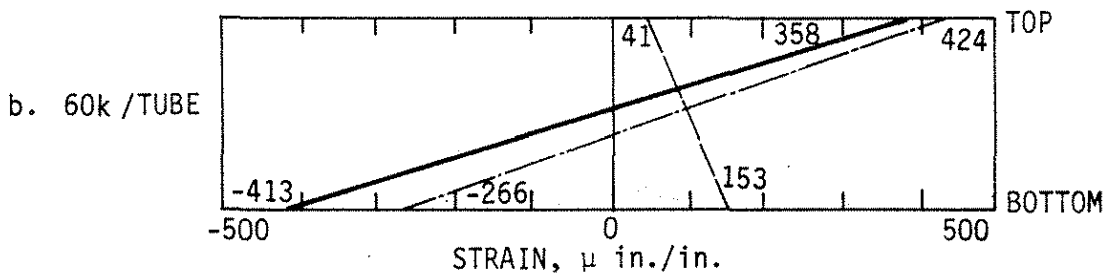
review of the various curves in Fig. 2.23a indicated that the deflection at the load point decreased (i.e., deflected upward) with increasing post-compression force. The data in this figure also indicated that the deflection of the unstrengthened mockup was reduced by the amount of upward deflection due to post-compression. It was also apparent that the reduction in deflection due to ST2.1 remained essentially constant throughout the application of vertical loading. When researchers examined the data for the mockup with 60 kips per tube post-compression and 43 kips vertical load, the graph indicated that the deflection was reduced from 0.735 in. to 0.621 in., a 15.5% reduction. Because the slope of the various lines did not change noticeably, the compression tubes added no significant stiffness to the beam cross-section. The tubes thus behaved similarly to post-tensioning tendons, which also do not add significant stiffness.

Figure 2.20b illustrates a comparison of the experimental and theoretical strains for ST2.1 at Section 4 of the mockup. The solid line represents the theoretical strains predicted by the finite-element analysis of the mockup with 60 kips per tube post-compression applied by ST2.1. The experimental strains for the same post-compression force are represented by squares. These values indicated that positive moment bending of the section was occurring due to the post-compression being applied. The theoretical and experimental values are in very good agreement. The second set of data in Fig. 2.20b corresponds to 60 kips per tube post-compression and 43 kips of vertical load being applied to the mockup. For this condition, the theoretical strains are represented with a dashed line and the experimental strains are represented by dots. Experimental and theoretical bottom flange compressive strains for this loading were in good agreement, within 10%. The experimental tension strain on the top flange was again approximately twice the theoretical value. This supported the results of the earlier comparison between experimental and theoretical results when the 43-kip load was acting alone. It indicated that during negative moment bending, the deck of the mockup was less effective in tension than the finite-element model predicted. This was most likely due to cracking in the deck, resulting in a reduction in the composite action of the mockup.

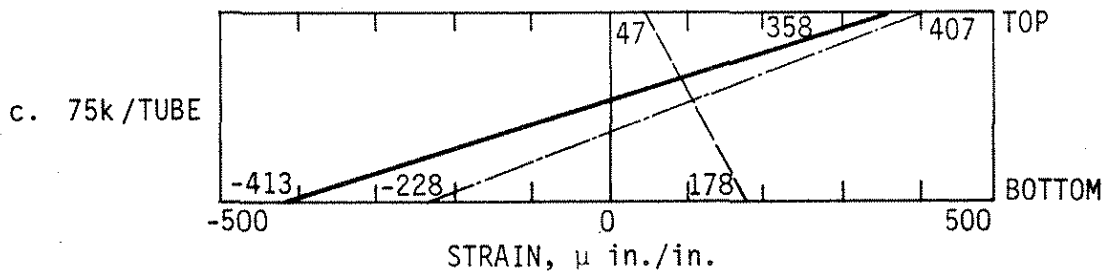
Figure 2.24 gives the strain distributions for the mockup at Sections 4 and 5. Parts a, b, and c of the figure represent strains at Section 4 for post-compression loads of 40, 60, and 75 kips per tube, respectively. Parts d, e, and f correspond to strains at Section 5 for the same loads. The heavy line in each graph represents the strains for an unstrengthened beam with a vertical load of 43 kips. For a given section, this would be constant. At Section 4, the top (tension) strain is $358 \mu \text{ in./in.}$ (10.38 ksi) and the bottom (compression) strain is $413 \mu \text{ in./in.}$ (12.0 ksi). At Section 5 the top and bottom strains are $206 (6.0 \text{ ksi}) \mu \text{ in./in.}$ and $278 \mu \text{ in./in.}$



- - - - NO VERT. LOAD--AVG. 43.7k/TUBE
 - . - . VERT. LOAD = 43.0k--AVG. 60.3k/TUBE
 ——— NO STRENGTHENING--43k VERT. LOAD



- - - - NO VERT. LOAD--AVG. 63.5k/TUBE
 - . - . VERT. LOAD = 44.0k--AVG. 78.8k/TUBE
 ——— NO STRENGTHENING



- - - - NO VERT. LOAD--AVG. 74.8k/TUBE
 - . - . VERT. LOAD = 43.6k--AVG. 89.8k/TUBE
 ——— NO STRENGTHENING

Fig. 2.24. Strains at Sections 4 and 5 for full-scale mockup with ST 2.1 in place.

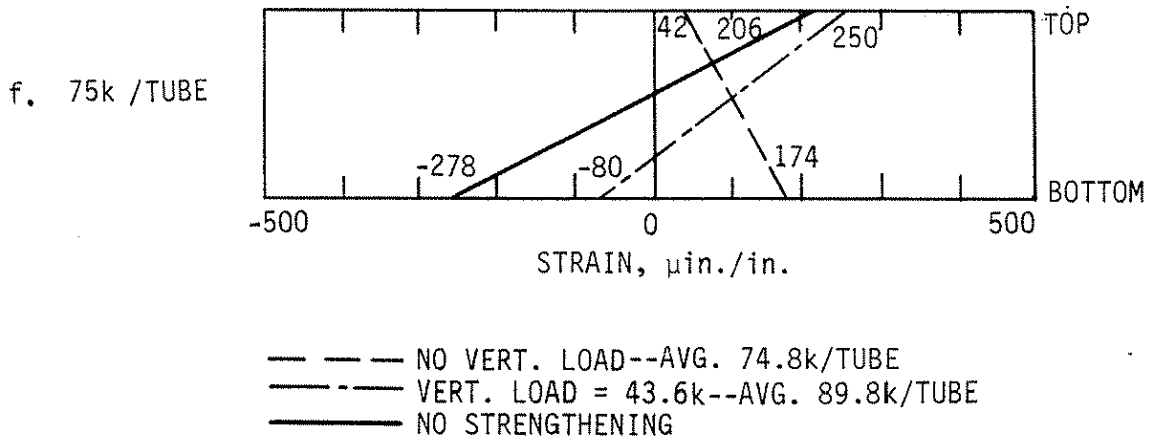
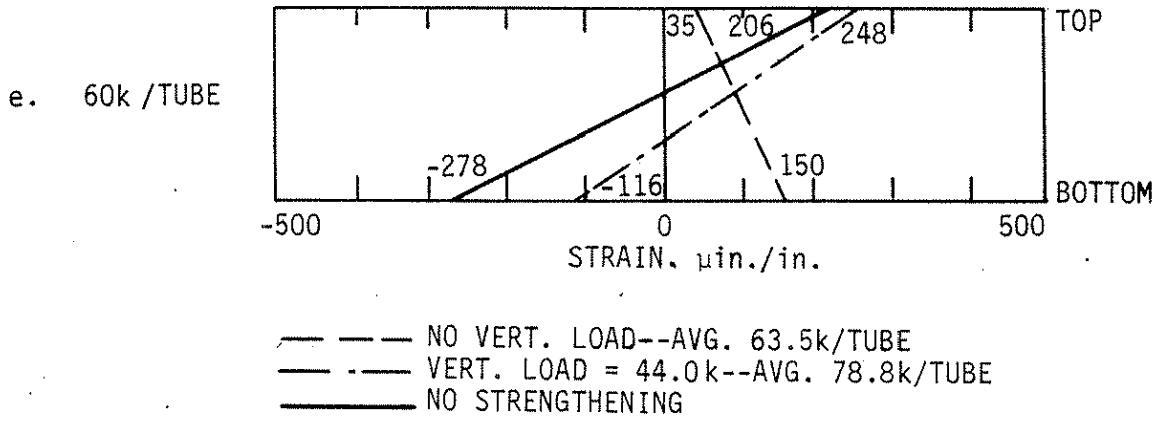
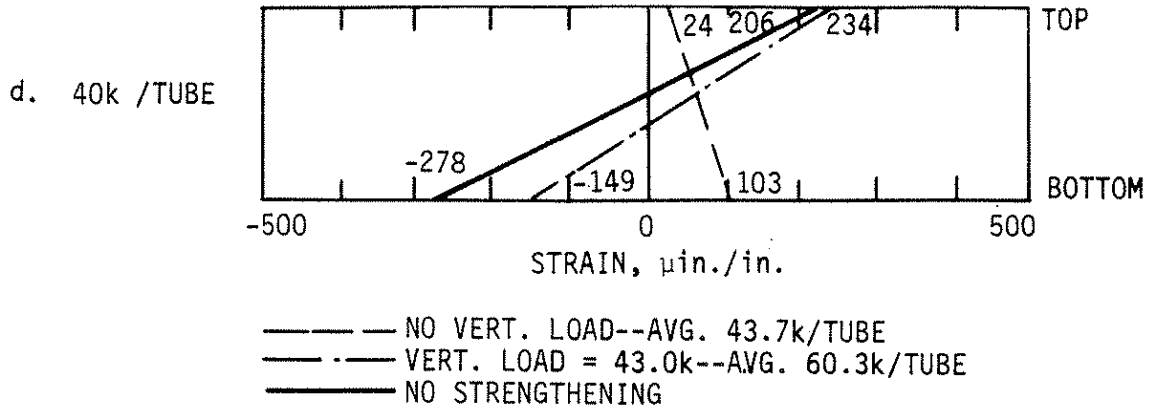


Fig. 2.24. Continued.

(8.1 ksi), respectively. The dashed line labeled no vertical is for the mockup with the amount of post-compression indicated, and no vertical load. This corresponds to an upward deflection of the mockup. In each figure, this line indicates a tensile force and positive moment are acting on the section. As expected, the tension strains increased with the amount of post-compression applied. Also on each figure is a line representing strains due to ST2.1 and a vertical load of 43 kips. These lines are the strengthened beam strains. By comparing the strengthened and unstrengthened beam results, one can determine the change in strain due to ST2.1. The strain diagrams for each magnitude of compressive load at Section 5 are similar to those at Section 4.

Each diagram indicates that the effect of ST2.1 on the mockup was to decrease the bottom flange compression strains and increase the top flange tension strains. At Section 4 with 60 kips per tube post-compression (Fig. 2.24b), the compressive strains were reduced from 413 μ to 266 μ (4.3 ksi reduction); however, the tensile strains increased from 358 μ to 424 μ (1.9 ksi increase). These changes were approximately equal to the strains created by post-compression alone. They correspond to an 18% increase in tension top (flange) and a 36% decrease in compression bottom (flange).

Figure 2.23b illustrates the increase in post-compression force due to vertical load. The tube compression increased approximately 0.4 kips per kip of vertical load. Bending of the compression tubes was also examined. Prior to installation of the independent lateral restraints (see Section 2.3.3), considerable bending occurred in the compression tubes. The change in lateral restraints significantly reduced the bending in the tubes. To further reduce the bending, small shims were fit between the ends of the tubes and the brackets. The shims evenly distributed the loading on the tubes and reduced bending due to small misalignments in the ends of the tubes and the bearing surface on the brackets.

4.4. Effects of ST2.2 and ST2.3 on Mockup

In this section the effects of ST2.2 and ST2.3 when applied to the mockup will be presented. As previously noted, essentially the only difference between ST2.2 and ST2.3 (see Figs. 2.10 and 2.11) is that ST2.2 applies upward force to the lower surface of the upper flange, while ST2.3 applies upward force to the lower surface of the lower flange. Figure 2.25 shows the effect of ST2.2 and ST2.3 acting on the mockup without a vertical load. The figure illustrates that ST2.3 created a larger upward deflection than ST2.2. At 100-kips tension per

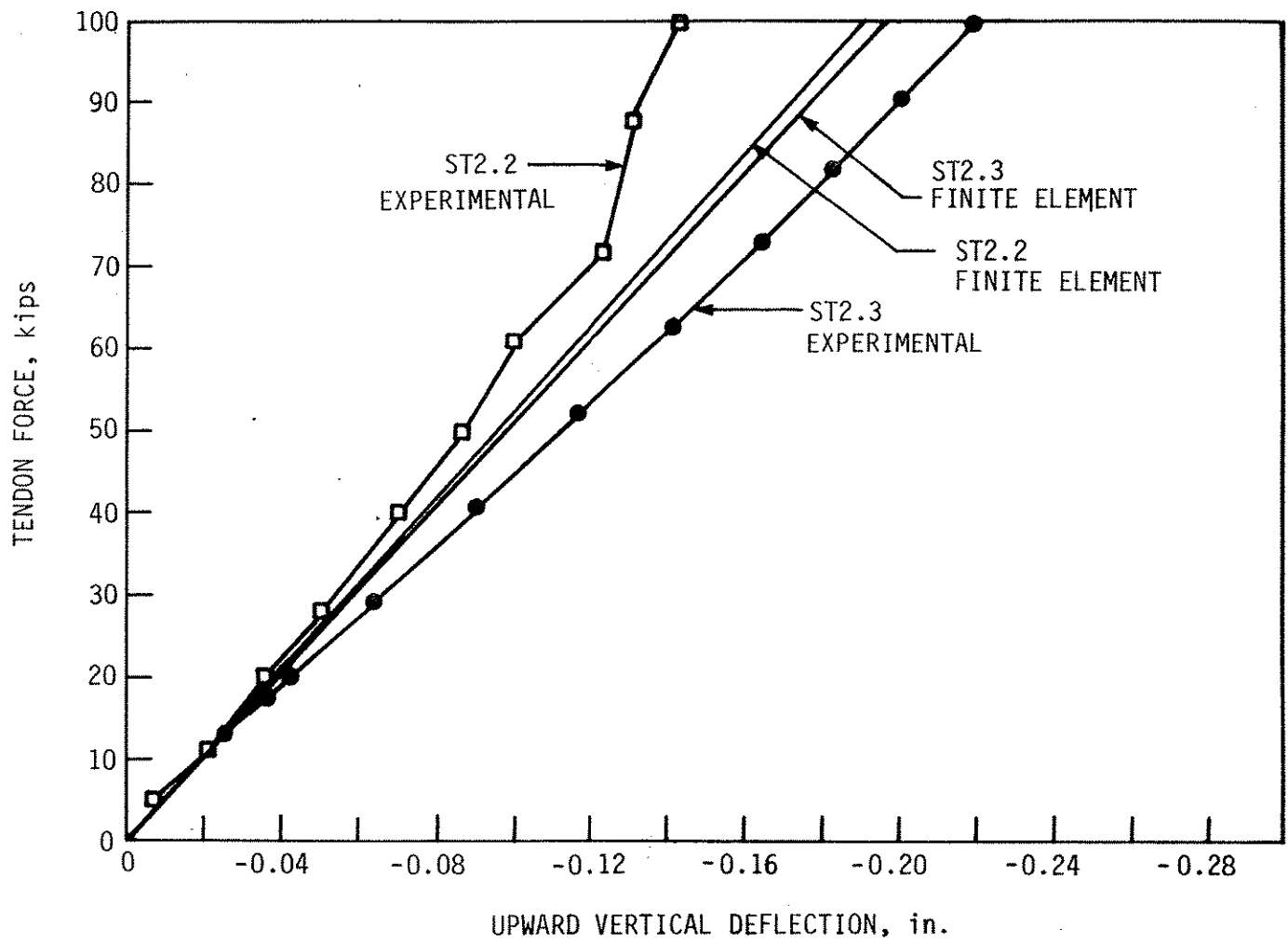


Fig. 2.25. Tendon load vs. deflection for ST2.2 and ST2.3.

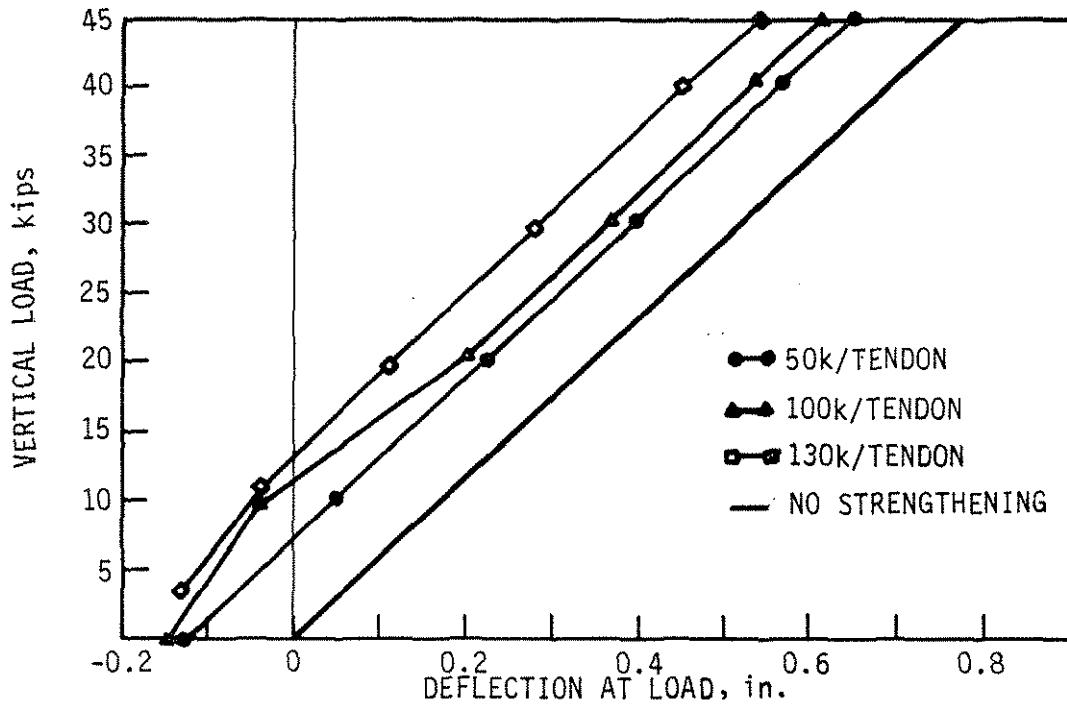
tendon the deflections for ST2.2 and ST2.3 were 0.147 in. and 0.219 in., respectively. Because the experimental results were not linear and somewhat irregular near the origin of the graph, there apparently were some minor seating effects at low loads. The large irregularities in the deflections for ST2.2 at loads above 50 kips are most likely due to movement of the pin bearing as the truss was loaded.

The solid lines on the graph are the deflection obtained from the finite-element model with either ST2.2 or ST2.3. The lines fell between the experimental deflections for the two strengthening techniques.

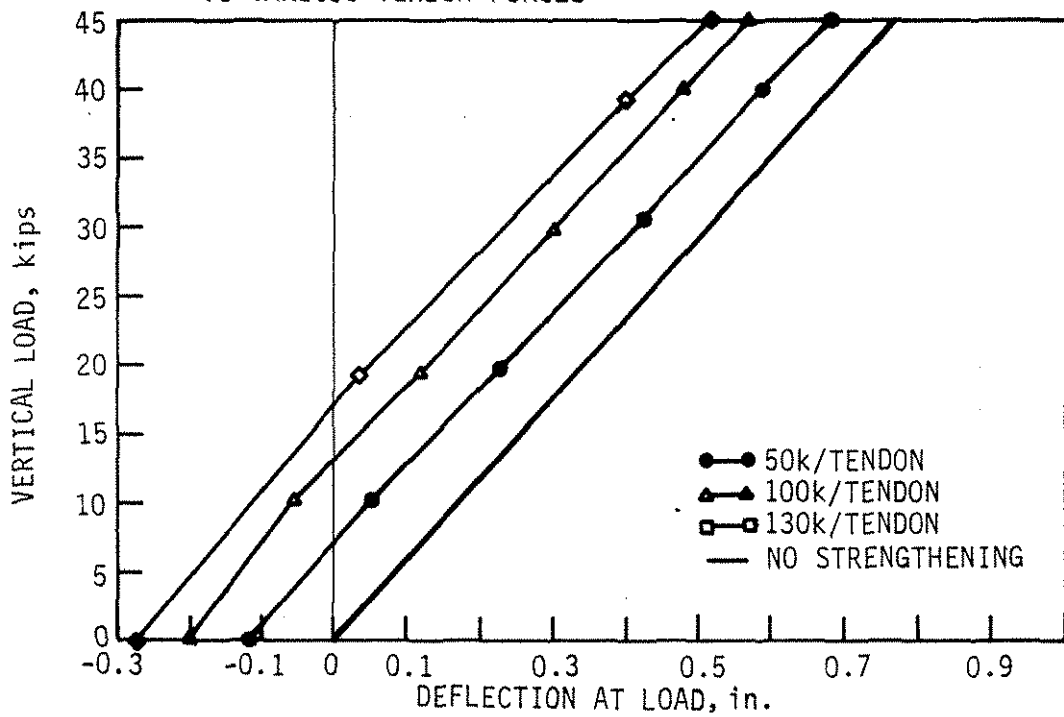
ST2.2 and ST2.3 should have caused near identical deflections on the mockup. The finite-element model, however, does not consider local bearing effects at the point of contact between the lower surface of the deck and beam flange and the strengthening truss (ST2.2). Apparently, these effects are a major source of the difference between theoretical and experimental values.

Figures 2.26a and b illustrate the effects of vertical loading on the mockup when ST2.2 and ST2.3, respectively, were attached to the mockup. The graphs plot vertical load versus deflection for three truss loads. Deflections for an unstrengthened mockup are also shown. The graphs display information similar to that found for ST2.1 in Fig. 2.23a. The deflection of the mockup remained linear after strengthening was applied. Again this indicated that the deflection was being reduced by the amount of initial deflection caused by strengthening. Since the initial deflections for the mockup with ST2.2 were less than those for the mockup with ST2.3, the final reduction in deflection was also less for ST2.2 than for ST2.3. For a load of 100 kips per tendon, the deflection of the mockup with ST2.2 was reduced from 0.735 in. to 0.359 in. (36%), while the deflection of the mockup with ST2.3 was reduced from 0.735 in. to 0.533 in. (27%). Thus, it can be concluded that ST2.2 was more effective than ST2.3 in reducing the deflection of the mockup. For both ST2.2 and ST2.3 the strengthened beam curves paralleled the unstrengthened curves; thus, the truss strengthening did not add stiffness to the beam cross-section.

Figures 2.20c and d display the experimental and theoretical strains at Section 4 due to ST2.2 and ST2.3, respectively. For each diagram, one line and pair of data points corresponds to an initial 100 kips per tendon acting alone. A second set of data corresponds to 100 kips per tendon and a vertical load of 43 kips. The comparisons are similar to those for ST2.1. While the deck was in compression (positive moment bending), the theoretical model and the experimental mockup strains were in good agreement.



a. VERTICAL LOAD VS. DEFLECTION CURVES FOR ST2.2 SUBJECTED TO VARIOUS TENDON FORCES



b. VERTICAL LOAD VS. DEFLECTION CURVES FOR ST2.3 SUBJECTED TO VARIOUS TENDON FORCES

Fig. 2.26. Response of ST2.2 and ST2.3 to vertical load.

When the 43-kip load was applied, the deck went into tension (negative moment bending), and the finite-element model predicted a stiffer section than occurred experimentally. The experimental compression strains on the bottom flange during negative moment bending, however, were again close to the theoretical strains.

Shown in Figs. 2.27 and 2.28 are the strain distributions for the mockup with ST2.2 and ST2.3, respectively. For each of the strengthening techniques, parts a, b, and c of the figures represent strains at Section 4 for tendon loads of 50, 100, and 130 kips per tendon. Parts d, e, and f of these figures correspond to strains at Section 5 for tendon loads of 50, 100, and 130 kips per tendon. The strain data within each diagram are illustrated as was done with ST2.1 (see Fig. 2.24). Data in these figures indicated that ST2.2 and ST2.3 were essentially causing only positive moment bending on the mockup. As one would expect, ST2.2 and ST2.3 acting alone resulted in compression strains in the top flange and tension strains in the bottom flange.

The positive moment bending increased as the force in the tendons increased. Comparing the strengthened and unstrengthened beam strains indicated that both techniques were very effective in reducing the strains in the loaded mockup. Since ST2.2 and ST2.3 caused pure positive moment bending in the mockup, both the top and bottom flange strains were reduced. At Section 4 with ST2.2, 100 kips per tendon and 43 kips vertical load, (Fig. 2.27b), the top flange tension strain was reduced from 358 μ in./in. to 192 μ in./in. (4.8 ksi reduction). The bottom flange compression strain was reduced from -413 μ in./in. to -213 μ in./in. (5.8 ksi reduction). This represents a 46% stress reduction in the top flange and a 48% stress reduction in the bottom flange.

The strains for ST2.3 at the same section and loading (Fig. 2.28b) were reduced slightly less. The top flange tension strain was reduced from 358 μ in./in. to 214 μ in./in. (4.3 ksi reduction). The bottom flange strain was reduced from -413 μ in./in. to -249 μ in./in. (4.8 ksi reduction). This represents a 40% stress reduction in both the top and bottom flange.

Figures 2.29 and 2.30 illustrate the behavior of ST2.2 and ST2.3 on the mockup. Figures 2.29a and b display the change in strut load due to an increasing vertical load for ST2.2 and ST2.3, respectively. On each graph, three lines appear, corresponding to the three magnitudes of tensile forces (50 k, 100k, and 130k) that were applied before the vertical loading was applied.

The lines on Figs. 2.29a and b are parallel, indicating that the increase in force in the struts due to vertical loading, remained essentially linear regardless of the initial force in the tendon. These results supported the deflection data, which indicated that the strengthening

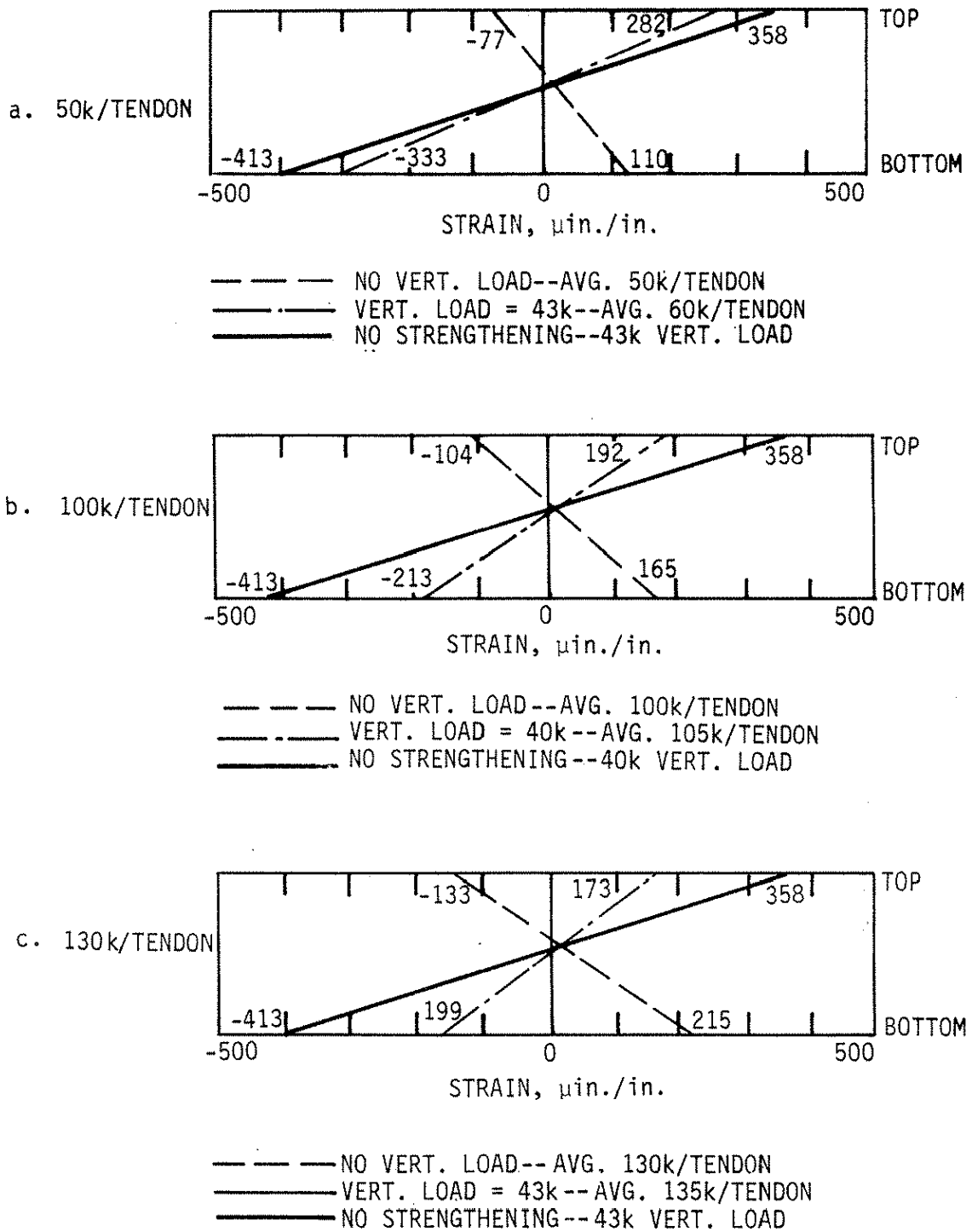


Fig. 2.27. Strains at Sections 4 and 5 for full-scale mockup with ST2.2 in place.

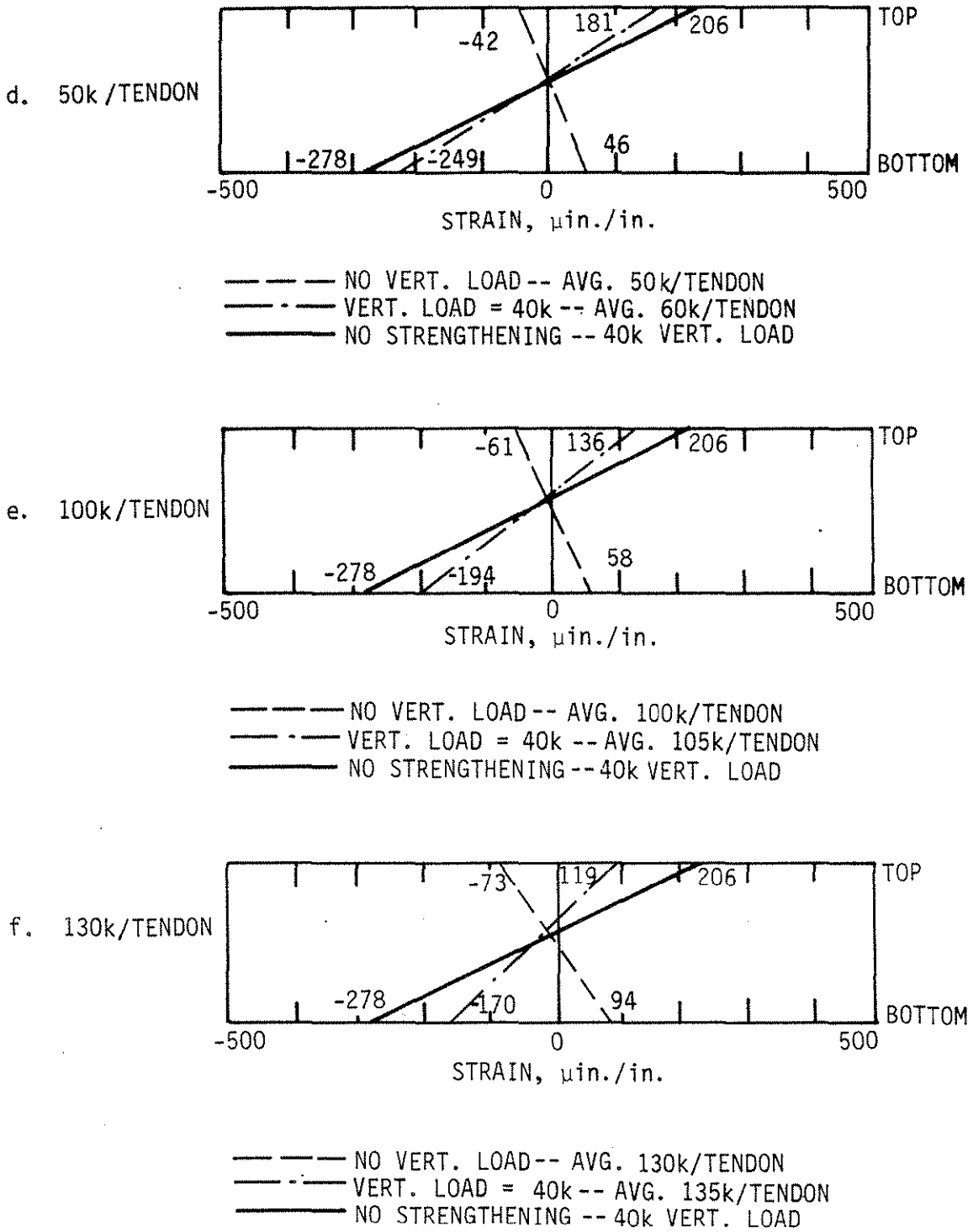


Fig. 2.27. Continued.

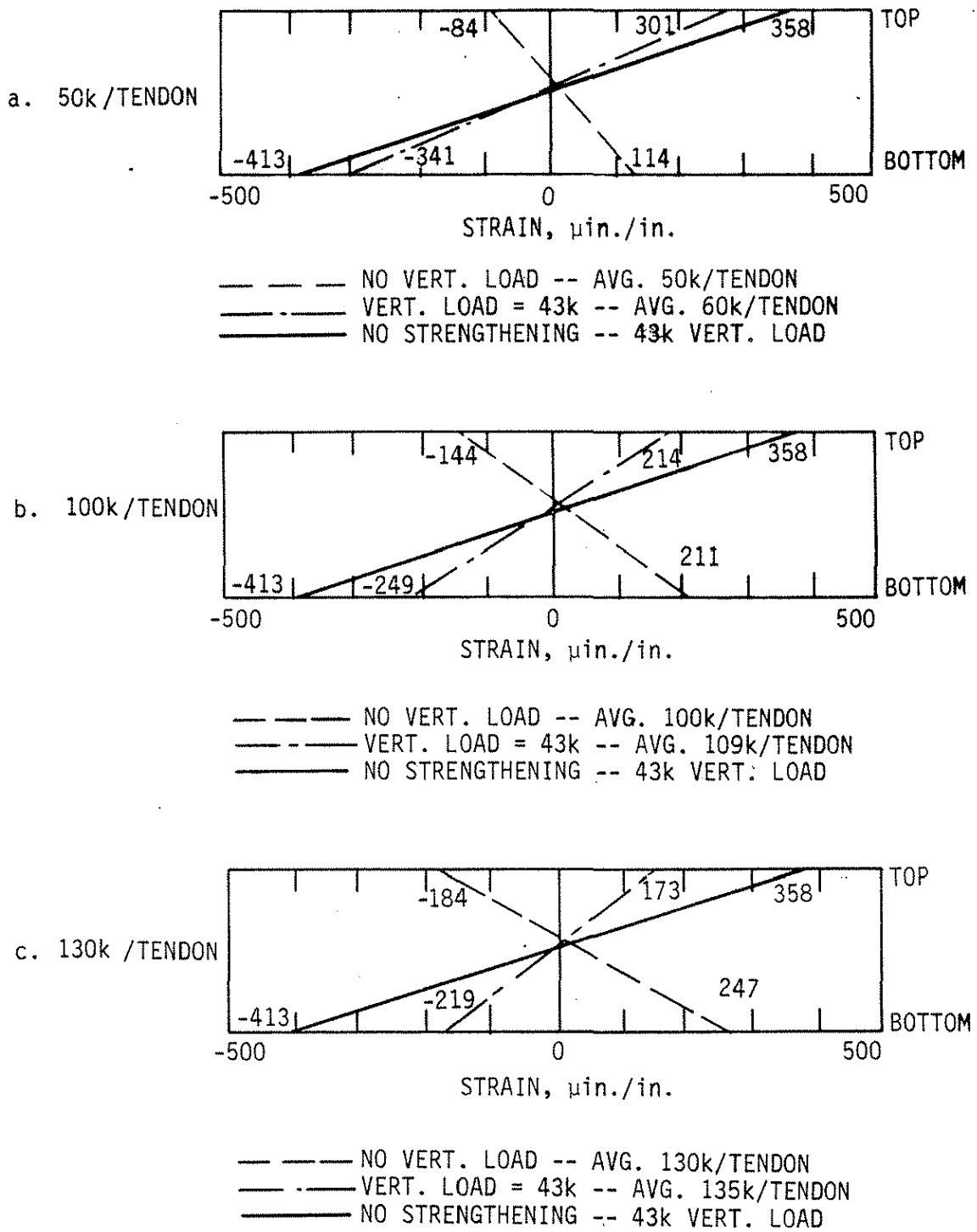


Fig. 2.28. Strains at Sections 4 and 5 for full-scale mockup with ST2.3 in place.

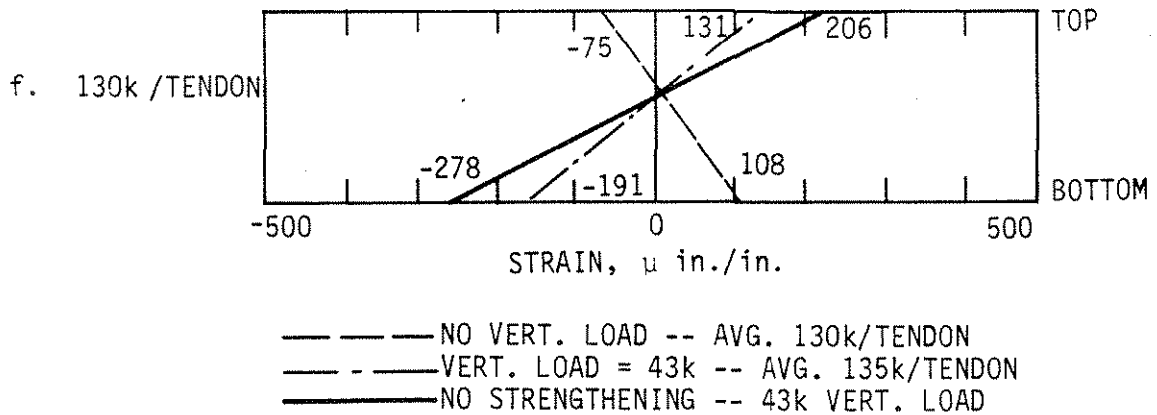
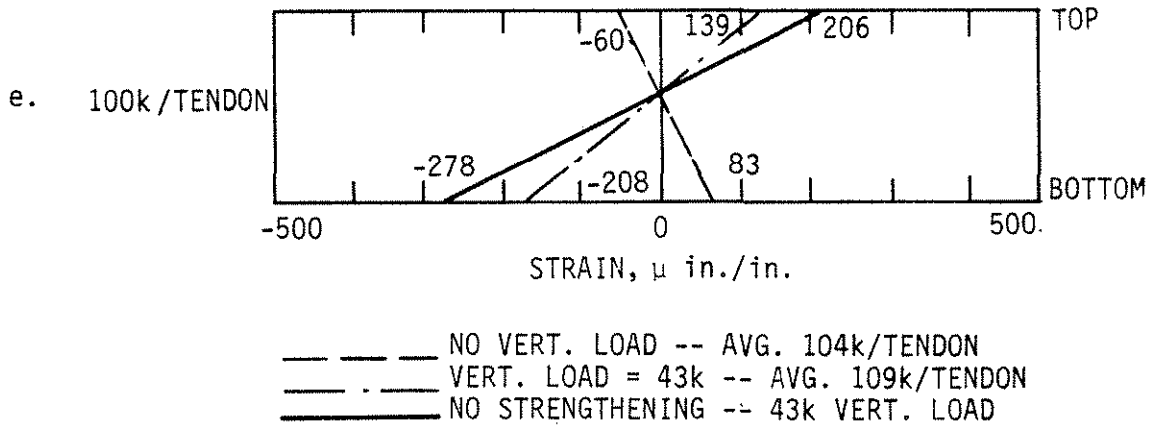
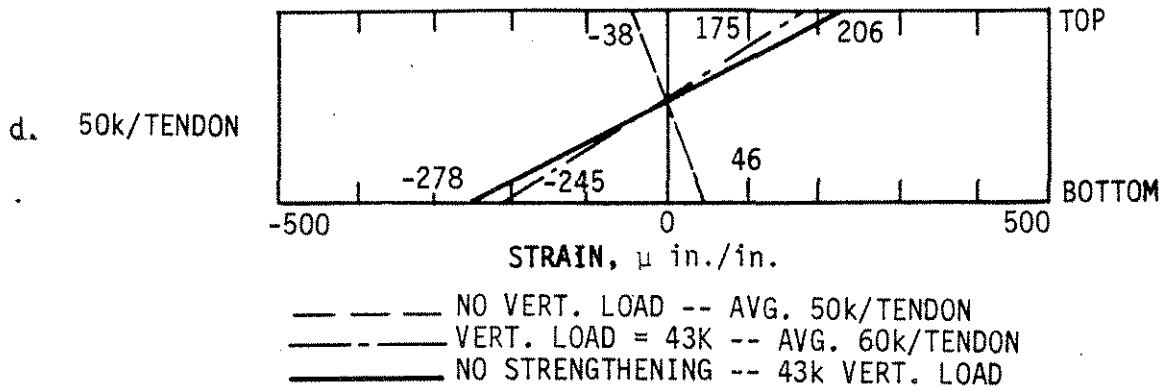


Fig. 2.28. Continued.

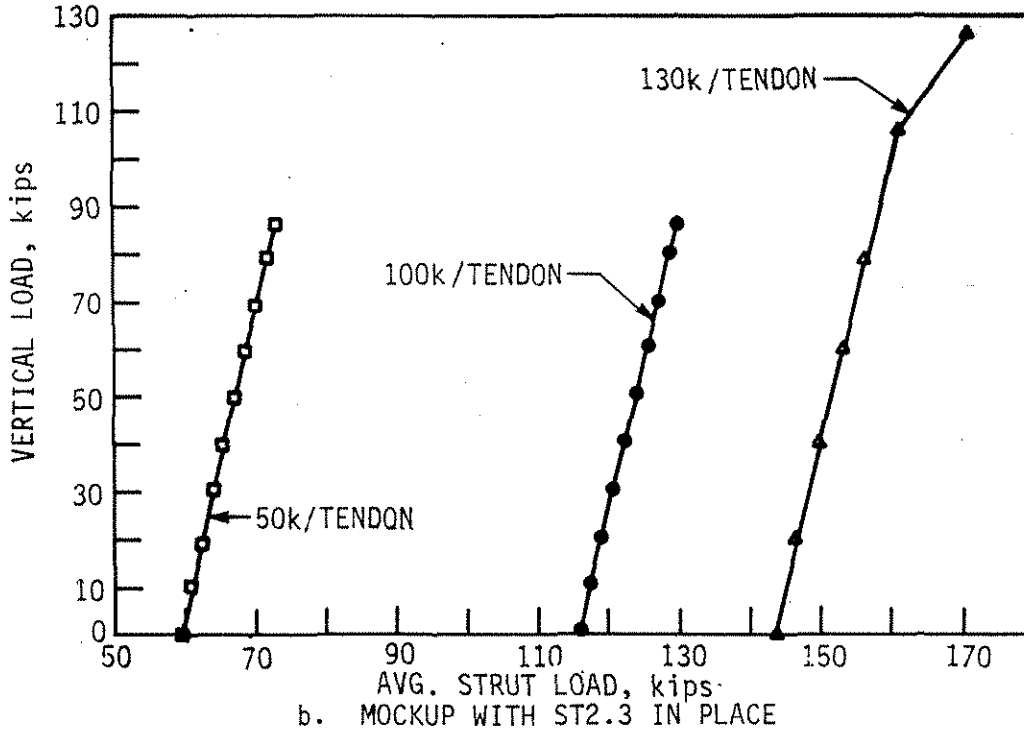
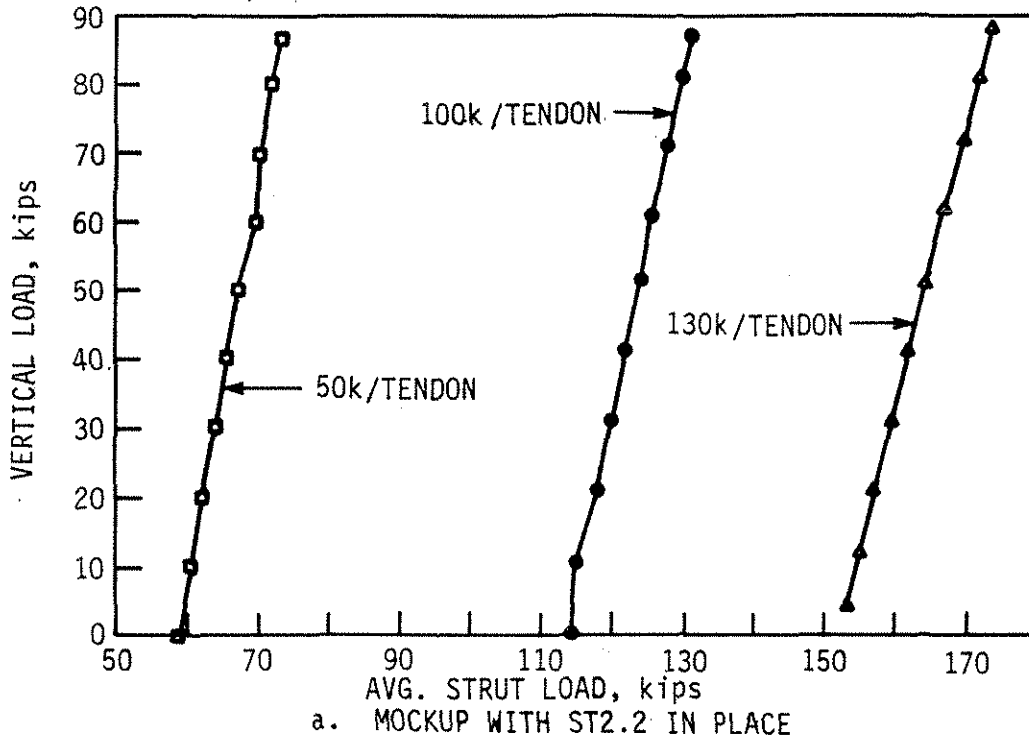
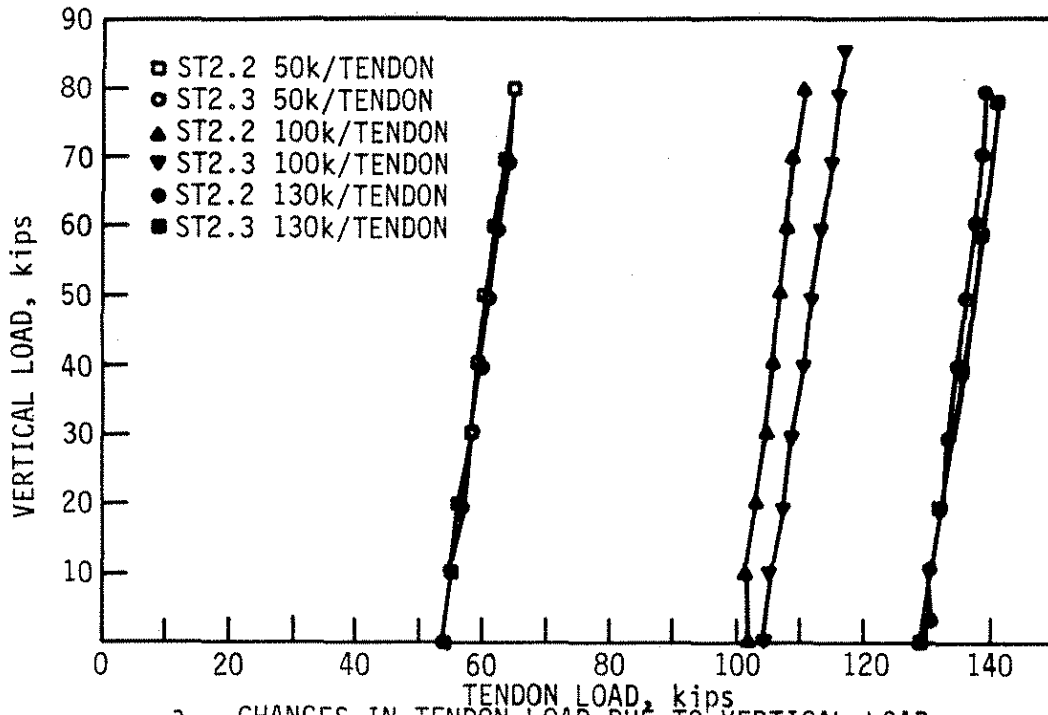
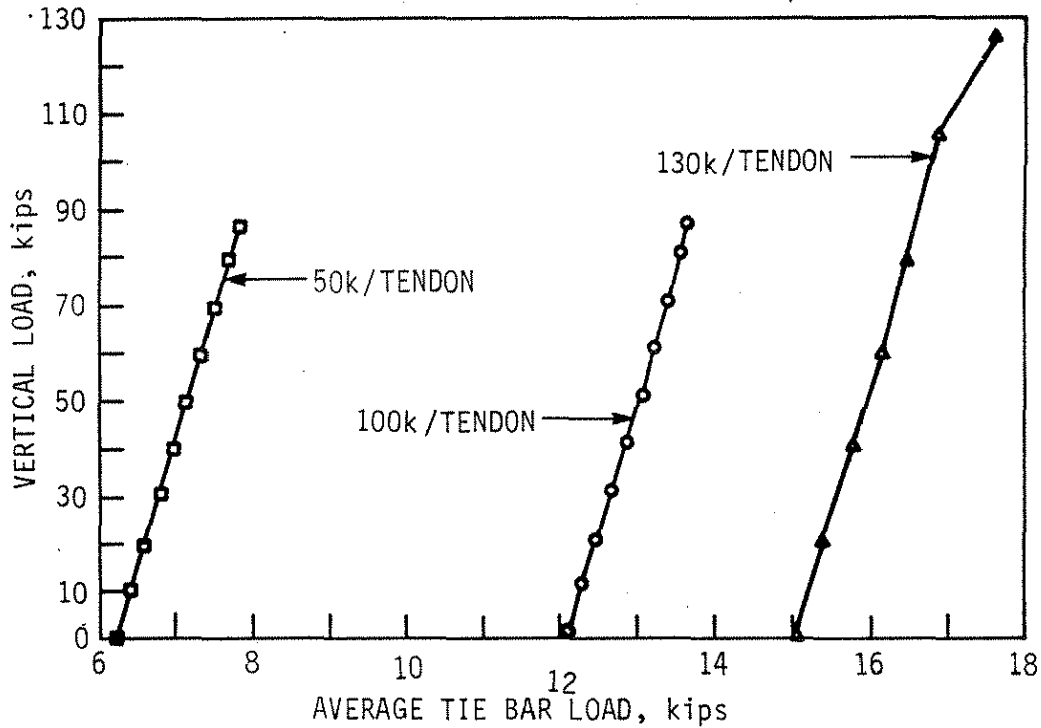


Fig. 2.29. Vertical load vs. average strut load for ST2.2 and ST2.3.



a. CHANGES IN TENDON LOAD DUE TO VERTICAL LOAD (ST2.2 OR ST2.3 IN PLACE ON MOCKUP).



b. CHANGES IN TIE BAR LOAD DUE TO VERTICAL LOAD (ST2.3 IN PLACE ON MOCKUP).

Fig. 2.30. Response of tendons (ST2.2 and ST2.3) and ties (ST2.3) to vertical loading.

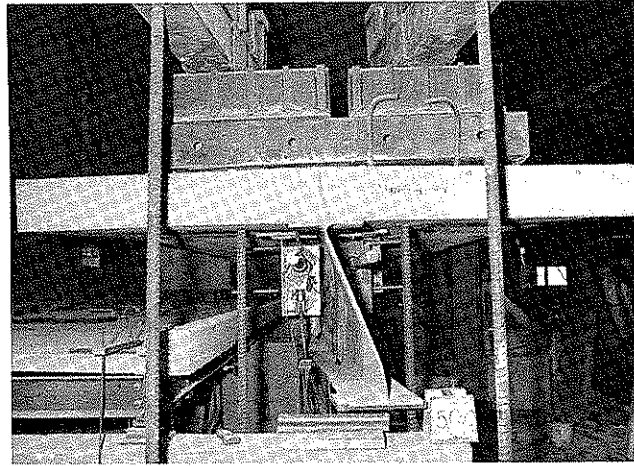
schemes did not add stiffness to the section. For ST2.2, the increase in strut load was approximately 0.25 kips per kip of vertical load. For ST2.3 the increase in strut load was approximately 0.20 kips per kip of vertical load. The results of tests on the mockup with ST2.2 and ST2.3 also showed that the loads in the four compression struts were within 4% of one another at all times. This indicated that the tendon was correctly distributing the force to the compression struts and that loading on the mockup was symmetric. Bending of the compression struts in ST2.2 and ST2.3 was not significant. The short length of the strut and the pin bracket were apparently effective in reducing bending.

Figure 2.30a illustrates the change in tendon force due to increasing vertical load. As previously noted, the initial tendon forces used in the testing of ST2.2 and ST2.3 were 50, 100, and 130 kips. As may be seen in Fig. 2.30a, the increase in tendon force for ST2.2 and ST2.3 as vertical loading was applied (or as the region was subjected to positive moment) was essentially the same, 0.15 kips per kip of applied vertical loading.

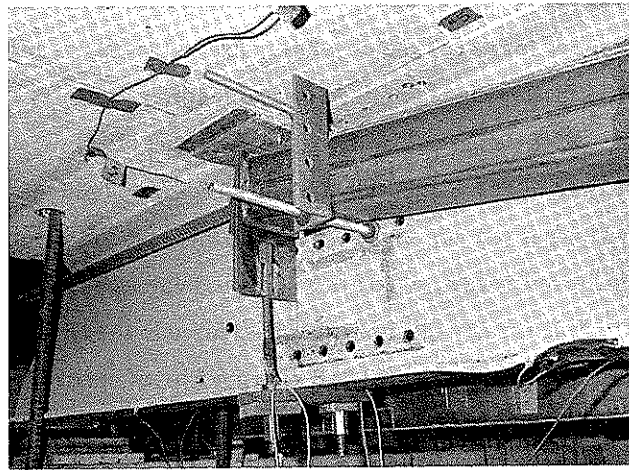
For ST2.3 the force in the tie bars also increased as vertical loading was applied. This increase in force is illustrated in Fig. 2.30b. The tie bar forces are given for the initial tendon loads of 50, 100, and 130 kips per tendon. As noted for the increase in tendon forces, the lines for the increase in the bar forces were also parallel. This indicates that the increase in tie bar force remained essentially linear regardless of the initial force in the tie bar. For each initial tendon force, the increase in tie bar load was 0.018 kips per kips of vertical load.

The final test of the investigation involved the load testing to failure of the mockup with ST2.3 applied. Photographs of the failed mockup are shown in Fig. 2.31. The load deflection curve for this failure test is shown in Fig. 2.32. (In Fig. 2.26b, the same curve is shown for values of the vertical load from 0 to 45 kips.)

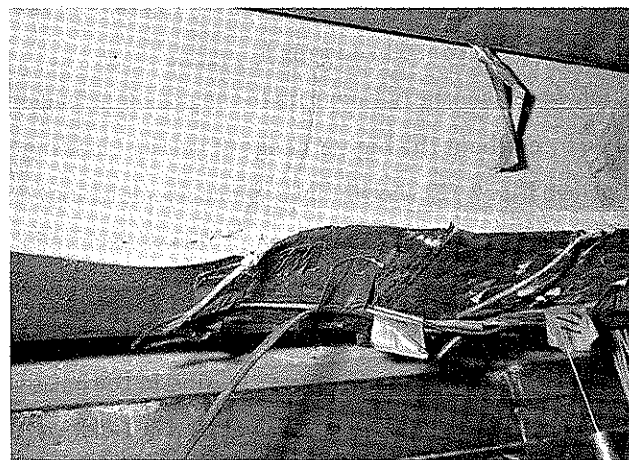
The deflection, which was essentially linear up to the previous load of 43 kips, maintained a smooth curve throughout the higher range of vertical loading. As previously noted, the hold-down force (see Fig. 2.15) was 75 kips. Since no additional deflection occurred when the applied vertical load reached 75 kips, and no uplift was observed at the hold-down, the actual hold-down force was obviously greater than 75 kips. For safety reasons, direct observation of the mockup was limited for vertical loads above 75 kips. Therefore, it was difficult to know exactly when failure began to occur. Yielding in the bottom flange at Section 4 first occurred at a vertical load of 105 kips. At a vertical load of 125 kips, the yield stress was exceeded at Sections 2, 4, and 6 (see Fig. 2.18). The buckling of the flange shown in Figs. 2.31b and c occurred exactly at Section 2 (see Fig. 2.16), 6 in. past the end of the cover plates. The bottom flange strain at Section 2 for the vertical load of 125 kips was



a. RESTRAINED END OF MOCKUP AT FAILURE



b. LOCATION OF FAILURE WITH RESPECT TO ST2.3



c. LOWER BEAM FLANGE AT FAILURE

Fig. 2.31. Photographs of mockup with ST2.3 tested to failure.

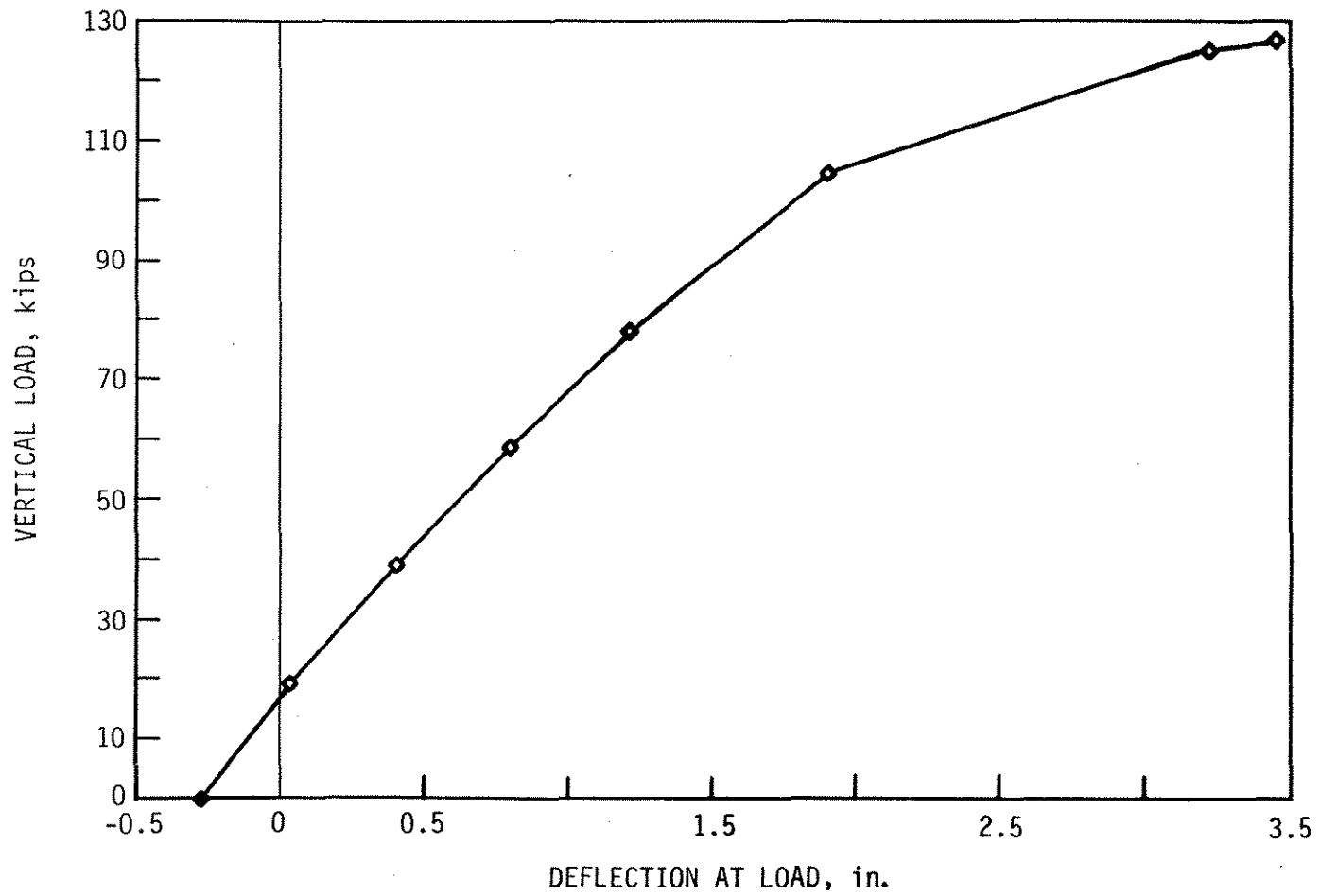


Fig. 2.32. Vertical-load deflection curve for mockup with ST2.3 in place tested to failure.

1446 μ in./in. (41.9 ksi). At Section 4 the bottom and top flange strains were 1833 μ in./in. (53.2 ksi) and 1389 μ in./in. (40.3 ksi), respectively. When the vertical load was increased to 127 kips, the strains at Section 4 increased. However, the strains at Section 2 decreased indicating that the failure occurred at approximately 125 k.

As expected, the test to failure established that the mockup would fail before the strengthening system. For the vertical load of 125 kips, yield stress was not exceeded at any point on the strengthening system. The final compression strut load was 170 kips per tube. This value was approximately 30% above the calculated AISC allowable load for this element assuming a uniform cross-section, pinned ends, and a length of 8 ft-8 7/8 in. The force in the 1 1/4-in.-diameter tendons increased from 130 kips prior to vertical loading to 150 kips at 125 kips of vertical load. The 150-kips force in the tension tendon was 80% of ultimate strength of the tendons. The 5/8-in.-diameter tie bars reached 17.6 kips, which is approximately 40% of their ultimate capacity.

5. SUMMARY AND CONCLUSIONS

5.1. Summary

Part 2 of this report summarizes the research that has been completed in an investigation of the strengthening of continuous, composite bridges by two methods: post-compression of stringers and superimposed trusses within stringers. The research program included reviewing the literature, testing each strengthening scheme on a full-scale mockup of the negative moment region of a bridge stringer, and conducting a finite-element analysis of the laboratory bridge beam mockup for each strengthening scheme.

The literature review involved a search of publications from both the United States and foreign countries. The superimposed truss was researched as an applied strengthening mechanism, which when added to the existing structure "doubled" the structure at some or all locations. Several reports of research involving applied strengthening mechanisms were examined. Post-compression was a relatively unexplored strengthening idea. The engineering literature contained only one example of the strengthening of an existing structure by attaching elements that were subsequently compressed.

The primary purpose of this study was to determine the feasibility of strengthening the negative moment region of continuous composite bridges by two new methods:

1. Post-compression of stringers
2. Superimposed truss within stringers.

Both strengthening schemes were designed to reverse the moments and resulting stresses from service loads.

As part of an earlier research project at ISU, which studied strengthening the negative moment region of continuous composite bridges, a full-size composite beam mockup was constructed in the Structural Engineering Laboratory. This full-scale mockup was used during this research project to test the post-compression strengthening scheme and the superimposed truss-strengthening scheme.

For the superimposed truss, researchers found that this may be accomplished by applying the vertical strengthening force to either the bottom of the bridge deck or the lower flange of the bridge beam: In either case the superimposed truss would cause only positive moment bending when applied. Post-compression is analogous to post-tensioning; however, along with positive moment bending, the post-compression strengthening scheme applies tension to the section rather than compression.

A series of tests were conducted on the full-scale mockup: first with the post-compression strengthening scheme in place, and then with the superimposed truss-strengthening scheme in place. Tests were also performed to establish the strength characteristics of the mockup without any of the strengthening schemes in place. These tests were necessary for determining the amount that stresses and deflections were reduced by each strengthening scheme.

The post-compression strengthening scheme was effective in reducing the bottom flange beam stresses. The top flange beam stresses, however, were actually slightly increased, due to the tension applied to the section. At the design strengthening loads, the post-compression strengthening scheme increased the top flange beam stress 18% and decreased the bottom flange beam stress 36%.

The post-compression tubes and brackets used by the system performed well throughout testing. However, some modifications could be made in order to reduce the potential for bending in the post-compression tubes. Those modifications would consist of a redesigned end condition at the point where force is transferred between the compression tubes and brackets.

The superimposed truss-strengthening scheme was very effective in reducing both the top and bottom flange beam stresses since it applied only positive bending to the full-scale mockup. The superimposed truss (ST2.2), which applied the strengthening force to the bottom of the bridge deck, reduced the top and bottom flange beam stresses by 46% and 48%, respectively. The superimposed truss (ST2.3), which applied the strengthening force to the lower beam flange, reduced both the top and bottom flange beam stresses by 40%.

A test was also conducted on the full-scale mockup with the superimposed truss (ST2.3) in place, in which the system was tested to failure. From that test, the performance of strengthening scheme at high stress levels was evaluated. The test confirmed that failure would occur in the full-scale bridge mockup before it would occur in the applied strengthening mechanism (the superimposed truss).

Although both designs for the superimposed truss performed extremely well, a modification of the end condition for the superimposed truss, which bears against the bottom of the deck (ST2.2), should be considered.

In addition to the experimental laboratory work, finite-element analyses were performed on the full-scale bridge beam mockup with each of the three strengthening schemes applied. The deflections and strains for the finite-element analyses were in good agreement with the experimental results when the concrete deck was in compression.

However, when the concrete deck was in tension, the results of the finite-element analyses did not compare well with the experimental values. This is most likely due to a decrease in the tensile capacity of the concrete deck on the laboratory mockup, resulting from its age, and cracks that developed in the concrete deck during previous strengthening tests.

5.2. Conclusions

The following conclusions were developed as a result of this study.

- (1) Post-compression strengthening (ST2.1), when applied to the negative moment region, caused positive moment and tension in the section. While there was a reduction in bottom flange beam stress, an undesirable increase in top flange beam and deck stress also resulted.
- (2) Superimposed truss strengthening (ST2.2, ST2.3), when applied to the negative moment region, caused only positive moment in the section. Stress reduction in both the top and bottom beam flanges was significant.
- (3) For the superimposed truss, applying the vertical strengthening force to the lower surface of the top beam flange (ST2.2) was more effective than applying it to the lower surface of the bottom beam flange (ST2.3). The difference found in this study, however, was small.
- (4) None of the strengthening schemes (ST2.1, ST2.2, or ST2.3) caused a significant increase in stiffness of the mockup. Similarly, no overall change in behavior of the mockup was found due to their application.
- (5) The superimposed truss-strengthening scheme (ST2.2) has the greatest potential for field application. Fabrication, installation, and maintenance considerations as well as strengthening performance make it the best choice for actual bridge strengthening.

6. RECOMMENDED FURTHER RESEARCH

On the basis of the literature review, mockup testing, and finite-element analysis, it would be logical to continue this strengthening research as follows:

- (1) Strengthening composite bridges of the type investigated in this study with a superimposed truss is feasible; the next logical step is to design and implement superimposed truss strengthening on an actual bridge. The strengthening for the bridge should be initially tested and then monitored for a period of several years to ensure that no unforeseen problems develop.
- (2) If one assumes that the implementation phase of the strengthening is successful, there will be a need for a design procedure for strengthening continuous, composite bridges that is similar to the procedures presented in the manual [8] provided to the Iowa DOT for strengthening simple-span composite bridges using post-tensioning.
- (3) The feasibility of using a post-compression strengthening system similar to ST2.1 in conjunction with post-tensioning should be investigated. If used simultaneously at a critical section, the undesirable axial effects associated with individual use would be minimized, and the desirable positive moment effect could be magnified.

7. BIBLIOGRAPHY

1. Bahkt, Baidar, and L. G. Jaeger, "Bearing Restraint in Slab-on-Girder Bridges," *Journal of Structural Engineering*, 114(12):2724-2740, December 1988.
2. Bathe, K. J., E. L. Wilson, and F. E. Peterson, *SAP IV, A Structural Analysis Program for Static and Dynamic Response of Linear Systems*, Berkeley: College of Engineering, University of California, 1974.
3. Beal, David B., "Failure Test of a Jack-Arch Bridge," Interim Report on Research Project 156-2, Engineering Research and Development Bureau, New York State Department of Transportation, Albany, New York, February 1984.
4. Bjorhovde, Reidar, "Effect of End Restraint on Column Strength--Practical Applications," *Engineering Journal*, 21(1):1-13, 1984.
5. Chen, W. F., "End Restraint and Column Stability," *Journal of the Structural Division*, 106(ST11):2279-2295, November 1985.
6. Dunker, K. F., F. W. Klaiber, B. L. Beck, and W. W. Sanders, Jr., "Strengthening of Existing Single-Span Steel Beam and Concrete Deck Bridges, Final Report--Part II," ERI Project 1536, ISU-ERI-Ames-85231, Ames: Engineering Research Institute, Iowa State University.
7. Dunker, K. F., F. W. Klaiber, F. W. Daoud, W. E. Wiley, and W. W. Sanders, Jr., "Strengthening of Existing Continuous Composite Bridges, Final Report," ERI Project 1846, ISU-ERI-Ames-88007, Ames: Engineering Research Institute, Iowa State University, 1987.
8. Dunker, K. F., F. W. Klaiber, and W. W. Sanders, Jr., "Design Manual for Strengthening Single-Span Composite Bridges by Post-Tensioning, Final Report--Part III," ERI Project 1536, ISU-ERI-Ames-85229, Ames: Engineering Research Institute, Iowa State University, 1985.
9. Dunker, K. F., "Strengthening of Simple Span Composite Bridges by Post-Tensioning," Ph.D. Dissertation, Iowa State University, Ames, Iowa, 1985.
10. El-Metwally, S. E., and W. F. Chen, "Moment-Rotation Modeling of Reinforced Concrete Beam-Column Connections," *American Concrete Institute Structural Journal*, No. 85-S36, 1988.
11. Ferjencik, P., and M. Tochacek, *Die Vorspannung im Stahlbau* (Prestressing in Steel Structures) (in German). Berlin: Wilhelm Ernest & Sohn, 1975.
12. Griffiths, T. M., and A. R. Kukreti, "Simplified Design of 8-Bolt Stiffened Moment End Plates," *American Institute of Steel Construction Engineering Journal*, 25(2):52-53, 1988.
13. Hambly, E. C., and Pennells, E., "Grillage Analysis Applied to Cellular Bridge Decks," *The Structural Engineer*, 267-275, 1975.

14. Jaeger, L. G., and Bahkt, Baidar, "The Grillage Analogy in Bridge Analysis," *Canadian Journal of Civil Engineering*, 9:224-235, 1982.
15. Jones, S. W., P. A. Kirby, and D. A. Nethercot, "Influence of Connection Stiffness on Column Strength," *The Structural Engineer*, 65A(11):399-405, November 1987.
16. Kandall, C., "Increasing the Load-Carrying Capacity of Existing Steel Structures," *Civil Engineering*, 38(10):48-51, October 1968.
19. Kim, J. B., R. J. Brungraber, and J. M. Yadlosky, "Truss Bridge Rehabilitation Using Steel Arches," *Journal of Structural Engineering*, 110(7):1588-1597, July 1984.
20. Klaiber, F. W., D. J. Dedic, K. F. Dunker, and W. W. Sanders, Jr., "Strengthening of Existing Single Span Steel Beam and Concrete Deck Bridges (Phase I)," ERI Project 1536, ISU-ERI-Ames-83185, Ames: Engineering Research Institute, Iowa State University, 1983.
21. Klaiber, F. W., K. F. Dunker, T. J. Wipf, and W. W. Sanders, Jr., "Methods of Strengthening Existing Highway Bridges," National Cooperative Highway Research Program Report 293, Transportation Research Board, 1987.
22. Klaiber, F. W., K. F. Dunker, and W. W. Sanders, Jr., "Feasibility Study of Strengthening Existing Single Span Steel Beam Concrete Deck Bridges, Final Report," ERI Project 1460, ISU-Ames-81251, Ames: Engineering Research Institute, Iowa State University, 1981.
23. Krishnamurthy, Natarajau, Jorng-Te Huang, Paul K. Jeffery, and Louie K. Avery, "Analytical M-Theta Curves for End-Plate Connections," *Journal of the Structural Division*, 105(ST1):133-145, January 1979.
24. Lee, K. K., Duen Ho, and Huang-Wan Chung, "Static and Dynamic Tests of Concrete Bridge," *Journal of Structural Engineering*, 113(1):61-73, January 1987.
25. Lindsey, Stanley D., Socrates A. Ionnides, and Arvind Goverdahn, "LRFD Analysis and Design of Beams with Partially Restricted Connections," *Engineering Journal*, 22(4):157-162, 1985.
26. Lui, E. M., and W. F. Chen, "End Restraint and Column Design Using LRFD," *Engineering Journal*, 20(1):29-39, 1983.
27. Mazroi, Ali, Leon Ru-Liang Wang, and Thomas M. Murray, "Effective Coefficient of Friction of Steel Bridge Bearings," *Transportation Research Record 903*, 1983.
28. Moulton, Lyle K., "Observations of Highway Bridge Movements and Their Effects on Joints and Bearings," *Transportation Record 903*, 1983.
29. Mueller, T., "Umbau der Strassenbruecke ueber die Aare in Aarwangen," (Alteration of the Highway Bridge over the Aare River in Aarwangen) (in German), *Schweizerische Bauzeitung*, 87(11):199-203, March 13, 1969.

30. Murray, Thomas M., and Anant R. Kukreti, "Design of 8-Bolt Stiffened Moment End Plates," *American Institute of Steel Construction Engineering Journal*, 25(2):45-52, 1988.
31. Reiffenstuhl, H., "Eine Bruecke mit Druckspannbewehrung-Konstruktion, Berechnung, Baudurchfuehrung, Messungen," (A Bridge with Compression-Stressed Reinforcing-System, Computation, Construction, Field Measurements) (in German), *Beton-und Stahlbetonbau*, 77(11):273-278, November 1982.
32. Reiffenstuhl, H., "Das Vorspannen von Bewehrung auf Druck: Grundsatzliches and Anwendungsmoeglichkeiten," (Prestressing of Reinforcing in Compression: Fundamentals and Application Possibilities) (in German) *Beton-und Stahlbetonbau*, 77(3):69-73, March 1982.
33. Reiffenstuhl, H., "Verstaerkung eines Sporthallendaches mit Druckspannbewehrung" (Strengthening of an Athletic Building Roof with Compression Stressed Reinforcement), *Beton-und Stahlbetonbau*, 78(6):149-154, June 1983 (German).
34. Sawko, F., "Recent Developments in the Analysis of Steel Bridges Using Electronic Computers," London: British Constructional Steelwork Association Conference on Steel Bridges, 1-10, 1968.
35. Schilling, Charles G., "Moment-Rotation Tests of Steel Bridge Girders," *Journal of Structural Engineering*, 114(1):134-149, January 1988.
36. Vinnakota, Srirmulu, "Planar Strength of Restrained Beam Columns," *Journal of the Structural Division*, 108(ST11):2496-2516, November 1982.
37. Yettram, A. L., and M. H. Husain, "A Grid Framework Method for Plates in Flexure," *Journal of the Engineering Mechanics Division*, 91(Em3): 53-64, 1965.